



Durham E-Theses

The application of ESCA to structure and bonding in selected polymer systems

Thomas, Herbert Ronald

How to cite:

Thomas, Herbert Ronald (1977) *The application of ESCA to structure and bonding in selected polymer systems*, Durham theses, Durham University. Available at Durham E-Theses Online:
<http://etheses.dur.ac.uk/8336/>

Use policy

The full-text may be used and/or reproduced, and given to third parties in any format or medium, without prior permission or charge, for personal research or study, educational, or not-for-profit purposes provided that:

- a full bibliographic reference is made to the original source
- a [link](#) is made to the metadata record in Durham E-Theses
- the full-text is not changed in any way

The full-text must not be sold in any format or medium without the formal permission of the copyright holders.

Please consult the [full Durham E-Theses policy](#) for further details.

UNIVERSITY OF DURHAM

A Thesis Entitled

The Application of ESCA to Structure and
Bonding in Selected Polymer Systems

Submitted by

Herbert Ronald Thomas

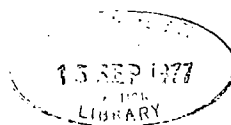
M. Sc.

(Graduate Society)

The copyright of this thesis rests with the author.
No quotation from it should be published without
his prior written consent and information derived
from it should be acknowledged.

A Candidate for the Degree of Doctor of Philosophy

1977



I would like to dedicate this thesis to my wife, May Christine, for her sacrifice, devotion and typing of this manuscript, without whose effort this would not have been possible; to my children, Jason and Morganna, and last, but not least, to my mother, Margaret and step-father, Roland.

ACKNOWLEDGEMENTS

The work described in this thesis was carried out under the supervision of Dr. D. T. Clark and I would like to extend my sincere appreciation for his encouragement and inexhaustible assistance throughout this work, as well as for the friendship we developed. I would also like to thank Professor W. K. R. Musgrave for his support of this work.

I am indebted to Xerox Corporation, Webster, New York for their generous financial support for my family and I, and to the Scientific Research Council for provision of equipment. I wish to thank the following individuals within Xerox Corporation: Dr. C. B. Duke, Dr. J. Goldfrank, Dr. J. O'Malley, Dr. M. Shahin and Dr. M. Smith, without whose efforts this work would not have been possible.

I would also like to thank my friends in the U.S.A. for their support, namely, Bob, Dennis, Carl, Dave and Jim, and their wives, and my fellow students at Durham, Jim, Derek, Dave, Ben, Jiri, Lynn, and especially Alan and his wife Shiela.

ABSTRACT

The core levels of a series of eighty-three homopolymers have been studied by ESCA. Comparisons of the experimentally determined core level binding energies with theoretical calculations within the CNDO/2 SCF MO formalism have been made on the C_{1s} and O_{1s} core levels for the oxygen containing polymers in the series. A comparison of the ground state potential (GPM) and relaxation potential (RPM) models on a series of six model compounds is given. Compilations are given of binding energies of C_{1s} , O_{1s} , N_{1s} , Cl_{2p} , S_{2p} , Si_{2p} and Br_{3d} levels for typical structural features of common occurrence in polymer systems.

Electron mean free paths as a function of kinetic energy have been measured by the substrate-overlayer technique for in-situ polymerized films of polyparaxylylenes. The results are compared with previous estimates of mean free paths available in the literature for organic materials. Comparison is also drawn with corresponding experimental data for typical metals and semi-conductors and it is shown that organic polymers fit into a consistent picture which may be rationalized on the basis of existing theory.

A systematic series of experiments are described on the ESCA examination of 1) a series of [2.2] paracyclophanes, in an attempt to define isomeric differences in the structure and bonding properties of these systems; 2) a series of aliphatic, aromatic and fluorine containing polycarbonates which include theoretical and experimental data pertaining to the absolute and relative binding energies for C_{1s} , O_{1s} and F_{1s} core levels; 3) sample charging phenomena in the ESCA examination of thick insulating samples; 4) polymer/metal interfaces on a series of transition metals: molybdenum, tungsten, niobium and zirconium. Radio frequency plasmas excited in inert gas (argon) and active gas (oxygen) were used to "ablate" and "ash" the polymer overlayers to approach the interface for ESCA investigation of both the carbon type overlayer and metal/metal-oxide substrate; in conclusion 5) a polymeric by-product of the direct fluorination of benzene in an attempt to determine the structure and composition of the polymer.

MEMORANDUM

The work described in this thesis was carried out at Durham University between October 1975 and June 1977. Background information was obtained from work at the University between October 1974 and October 1976.

Part of the work in this thesis has formed the subject matter for the following publications.

- 1) "Some Aspects of Shake-up Phenomena in Some Simple Polymer Systems", D. T. Clark, D. B. Adams, A. Dilks, J. Peeling and H. R. Thomas, *J. of Elect. Spect.* 8, 51 (1976)
- 2) "Application of ESCA to Studies of Structure and Bonding in Polymers", D. T. Clark, A. Dilks, J. Peeling and H. R. Thomas, *Disc. Faraday Soc.* 60, 183 (1975)
- 3) "Some Observations of the Interpretation of ESCA Spectra of Fluorine Containing Polymers and their Relation to the Degree of Crystallinity, to the Surface Tension, and to the Content of Absorbed Gas", D. B. Adams, D. T. Clark, A. Dilks, J. Peeling and H. R. Thomas, *Die Makromolekulare Chemie*, 177, 2139 (1976)
- 4) "A Method to Reduce the Hydrocarbon Contamination of Samples in X-ray Photoelectron Spectroscopy", D. T. Clark, H. R. Thomas, A. Dilks and D. Shuttleworth, *J. of Elect. Spect.* 10, 455 (1977)
- 5) "Polymer Degradation as Studied by ESCA", D. T. Clark, A. Dilks and H. R. Thomas in "Development in Polymer Degradation", Editor, Professor N. Grassie (1977)
- 6) "Electron Mean Free Paths as a Function of Kinetic Energy in Polymeric Films Determined by Means of ESCA", D. T. Clark and H. R. Thomas, *J. Polym. Sci., Polym. Chem. Ed.* 1977 (accepted)
- 7) "A Systematic Study of the Core Levels of Simple Homopolymers", D. T. Clark and H. R. Thomas, *J. Polym. Sci., Polym. Chem. Ed.*, 1977 (accepted)
- 8) "An Investigation Into Sample Charging Phenomena", D. T. Clark, H. R. Thomas and A. Dilks, *J. of Elect. Spect.*, (1977) (submitted)

C O N T E N T S

	<u>Page</u>
<u>CHAPTER 1. Electron Spectroscopy for Chemical Applications (ESCA)</u>	1
(i) Introduction	1
(ii) Processes Involved in ESCA	7
(a) The ESCA Experiment	7
(b) Electronic Relaxation	14
(c) Shake-up and Shake-off	18
(d) Chemical Shifts	21
(1) Equivalent Core Approximation	22
(2) Charge Potential Model	25
(e) Fine Structure	33
(1) Multiplet Splitting	33
(2) Spin-Orbital Splitting	34
(3) Electrostatic Splitting	38
(4) Valence Levels	39
(f) Energy Referencing	43
(g) Signal Intensities	48
(h) Line Shape Analysis	55
(iii) ESCA Instrumentation	61
(a) X-ray Photon Source	61
(b) Sample Chamber	67
(c) Hemispherical Electron Energy Analyser	68
<u>CHAPTER 2. ESCA Applied to Polymers - A Review</u>	71
(i) Introduction	71
(ii) Sample Preparation	72
(a) Powders	72
(b) Solution Cast Films	72
(c) Pressed or Extruded Films	73
(d) 'In-situ' Polymerized Films	73
(iii) Static Studies	76
(a) Chemical Composition	76
(b) Structural Details	80
(c) Fine Structure	91

	<u>Page</u>
(iv) Dynamic Studies on Polymer Systems	99
(a) Surface Treatments	99
(b) Oxidative Degradation of Polymers	102
(c) Absorption at Polymer Surfaces	107
<u>CHAPTER 3. A Systematic Investigation of the Core Levels</u> <u>of Simple Homopolymers</u>	110
(i) Introduction	110
(ii) Experimental	111
(a) Samples	111
(b) Sample Preparation	113
(c) Instrumentation	113
(iii) Theoretical	113
(iv) Results and Discussion	114
(a) Introduction	114
(b) Model Compounds	114
(c) Energy Referencing	120
(d) Results and Discussion	128
(1) Polymers Containing Only Carbon and Hydrogen	129
(2) Polymers Containing Only Carbon, Hydrogen and Oxygen	133
(3) Polymers Containing Only Carbon, Hydrogen, Nitrogen (and Oxygen)	135
(4) Polymers Containing Only Carbon, Hydrogen and Chlorine	138
(5) Miscellaneous Systems Containing Combinations of Carbon, Hydrogen, Oxygen, Sulphur, Silicone, Bromine and Fluorine	140
<u>CHAPTER 4. Electron Mean Free Paths as a Function of Kinetic Energy in Polymeric Films</u>	150
(i) Introduction	150
(ii) Experimental	163
(iii) Results and Discussion	171
(iv) Conclusions	180
<u>CHAPTER 5. An ESCA Investigation of a Series of [2.2] Paracyclophanes</u>	184

	<u>Page</u>
(i) Introduction	184
(ii) Experimental	193
(iii) Theoretical	193
(iv) Results and Discussion	193
(a) Unsubstituted [2.2] PCP	193
(b) Substituted [2.2] PCP's	195
<u>CHAPTER 6. An Investigation into Sample Charging Phenomena</u>	204
(i) Introduction	204
(ii) Experimental	205
(iii) Results and Discussion	207
(a) Equilibrium Charging of Polymers	207
(b) Surface Sensitivity of Sample Charging	210
(c) Sample Charging as a Function of the Operating Parameters of the X-ray Source	215
(d) Time Dependent Studies of Sample Charging	217
(e) Sample Charging as a Function of Surface Modification	219
<u>CHAPTER 7. An ESCA Investigation into a Series of Aliphatic, Aromatic and Fluorine Containing Polycarbonates</u>	222
(i) Introduction	222
(ii) Experimental	222
(a) Samples	222
(b) Sample Preparation	223
(c) Instrumentation	224
(iii) Theoretical	224
(iv) Results and Discussion	224
(a) Model Compounds	224
(1) Experimental	224
(2) Theoretical	227
(b) Aliphatic Polycarbonates	228
(c) Polyglycolcarbonates	232
(d) Fluorocarbonate Polymers	233

	<u>Page</u>
<u>CHAPTER 8. An ESCA Investigation of Polymer-Metal Interfaces</u>	238
(i) Introduction	238
(ii) Background	238
(iii) Experimental	242
(iv) Results and Discussion	245
<u>CHAPTER 9. The Application of ESCA to the Structural Determination of a Fluoropolymer</u>	259
(i) Introduction	259
(ii) Experimental	259
(iii) Discussion of Results	260

REFERENCES

CHAPTER 1

Electron Spectroscopy for Chemical Applications (ESCA)

CHAPTER 1

Electron Spectroscopy for Chemical Applications (ESCA)

i) Introduction

In common with most other spectroscopic methods, ESCA, or X-ray photoelectron spectroscopy, is a technique originally developed by physicists and is now extensively utilized by both inorganic and organic chemists as a tool for investigating structure and bonding.¹

At the beginning of the 20th century Robinson²⁻⁴ (in England) and de Broglie⁵ (in France) investigated the energy distribution of electrons in various elements by the X-ray irradiation of thin foils, producing photoemission via the photoelectric effect. The distribution of electron energies for the transmitted photoelectrons was recorded photographically and analyzed using a homogeneous magnetic field. The electron distributions obtained were characterised by long tails with distinct edges at the high energy end since the radiation source consisted of a continuous spectrum (bremsstrahlung) with the characteristic line spectrum of the anode material superimposed. Measurement of these edge positions gave a determination of the energies of the photoelectrons ejected from the different atomic levels and therefore with a knowledge of the energy of the exciting X-ray line, binding energies were calculated. (In retrospect, it is remarkable that these transmission experiments worked at all owing to the long mean free path for the X-ray photon and the short mean free path for the photoemitted electron.)

Except for a few isolated attempts⁶⁻¹⁰ to extend the work of Robinson and de Broglie, X-ray photoelectron spectroscopy went into a recession until the early 1950's when Siegbahn and co-workers at the University of Upsala, Sweden, developed an iron-free magnetic double-focussing electron spectrometer with high resolution properties.¹¹ In 1954 attempts were made to record high resolution photoelectron spectra excited by X-rays and the observation of a sharp line which could be resolved from the edge of each electron veil changed the course of future development of the technique. The photoelectrons to which this line corresponded had the important property that they did not suffer energy losses and, therefore possessed the binding energy of the atomic level from which they came and could be measured to a precision of a few tenths of an electron volt.¹²



Although core electrons are not explicitly involved in bonding (even though most of the total energy of a molecule resides in the core electrons), the core energy levels of a molecule encode a considerable amount of information concerning the chemical environment of the atom.¹³⁻¹⁴ However, at that time, the chemical effects were difficult to measure accurately and very often difficult to interpret theoretically. Siegbahn and co-workers first studied these chemical effects for copper and its oxides¹⁵ and the value of X-ray photoelectron spectroscopy for measurement of chemical "shifts" became apparent from this work, but its general utility was appreciated only as recently as 1964¹⁶⁻¹⁷ with the publication of the S_{2p} levels in sodium thiosulfate.

Much of the early work of Siegbahn and co-workers was extensively documented in 1968 in "ESCA, Atomic, Molecular and Solid State Structure Studied by Means of Electron Spectroscopy";¹⁸ later work was summarized in 1969 in "ESCA Applied to Free Molecules".¹⁹

In addition to the name ESCA (Electron Spectroscopy for Chemical Application), originally coined by Siegbahn as Electron Spectroscopy for Chemical Analysis, the technique is also known as:

- 1) X-ray Photoelectron Spectroscopy (XPS).
- 2) High Energy Photoelectron Spectroscopy (HEPS).
- 3) Induced Electron Emission Spectroscopy (IEES).
- 4) Photoelectron Spectroscopy of the Inner Shell (PESIS).

The designation ESCA is however, descriptive and aesthetically pleasing and will be used throughout this thesis.

As will become apparent ESCA is an extremely powerful tool with wide ranging applicability particularly in the study of polymeric systems and the principal advantages of the technique may be summarized as follows:

- (1) The sample may be solid, liquid or gas and sample sizes are small being 1 mg. solid, 0.1μ l. liquid and 0.5 cc. (STP) of a gas. (It is important to emphasize that these sample sizes represent a convenient size for sample handling and not the quantity needed for analysis by ESCA.)
- (2) The technique is for all practical purposes nondestructive in that the typical X-ray flux is quite small (0.1 millirad/sec.).²⁰ This is especially advantageous when compared with Auger spectroscopy where the electron beam produces many surface changes, particularly in polymeric systems where cross-linking and degradation can occur.

- (3) The technique is independent of the spin properties of the nucleus and can be used to study any element of the periodic table with the exception of H and He where there is no distinction between the core and valence levels.
- (4) Materials may be studied 'in situ' in their working environments with a minimum of preparation.
- (5) The technique provides a large number of information levels from a single experiment and has a higher sensitivity than most other analytical techniques.
- (6) The data is often complementary to that obtained by other techniques and it has unique capabilities central to the development of a number of important fields.
- (7) For solids, ESCA has the unique capability of differentiating surface from subsurface and bulk phenomena, enabling analytical depth profiling.
- (8) The information obtained is directly related to the molecular structure and bonding, and is applicable to both the inner shells and valence levels of the molecule enabling a quite thorough analysis of the electronic structure of the system.
- (9) The information levels are such that 'ab initio' investigations are feasible and the theoretical basis is well understood resulting in considerable interest to theoreticians.

Having elaborated on the advantages of ESCA it is important to consider also the disadvantages which are surprisingly few. In terms of cost, standard ESCA instrumentation falls in the same league as continuous wave NMR although 'state of the art' instrumentation come somewhat closer to the cost of Fourier transformation NMR spectrometers. In setting up a routine ESCA facility therefore the overall costs are comparable to that for Fourier Transform I.R., Laser Raman and Mass Spectrometers. The vacuum system associated with ESCA instrumentation means that routine sample handling requires provision of vacuum interlocks and also implies that it is not possible to switch the spectrometer on to routinely investigate a sample. In this respect the technique is comparable with mass spectrometry however it does not suffer from the same background problems. A similar criticism may of course be levelled at NMR where the stability of the field is such that there is usually a considerable time lag involved between switching the instrument on and recording

a spectrum. Whilst the technique has superior depth resolution (in the range $\approx 100 \text{ \AA}$) to any other, the spatial resolution is poor and typically an area $\approx 0.25 \text{ cm.}$ is sampled. As a corollary of this of course, unless the outermost $\approx 100 \text{ \AA}$ or so of a thin organic or polymeric film of the sample is representative of the bulk then it is not possible to say anything about the bulk structure by means of ESCA without sectioning the sample.

With conventional unmonochromatized X-ray sources, and slitted designs, two features are of importance in studying thick samples. The first is sample charging arising from a distribution of positive charge over the sample surface under the conditions of X-ray bombardment. The second is that the polychromatic nature of the X-ray source (characteristic lines superimposed on bremsstrahlung) leads to a relatively poor signal/background ratio for the technique. Sample charging for insulating films usually amounts to no more than a few eV shifts in the kinetic energy scale and may readily be corrected for by standard techniques and this phenomena will be discussed in more detail in a subsequent section. The advent of efficient monochromatization schemes and multiple collector assemblies considerably alleviates the signal/background and signal/noise ratios, however sample charging can be much more severe a problem for thick insulating films and needs careful consideration. Since the composite linewidths for C_{1s} levels for organic and polymeric materials studied by means of unmonochromatized X-rays are largely dominated by the inherent width of the X-ray source there is a considerable overall improvement in linewidths on going to instrumentation employing monochromatization schemes. It is still the case however that the overall shift to linewidth ratio for C_{1s} levels as a function of electronic environment are poor compared with say ^{13}C NMR. A particularly interesting case is that for C_{1s} levels appropriate to hydrocarbons in which carbon is formally in sp^3 , sp^2 and sp hybridization whilst for the core levels the shift to linewidth ratio might typically be ≈ 1 with an efficient monochromatization scheme, the corresponding ratio for ^{13}C is $\approx 10^3$.

Finally, to take full advantage of the technique often requires a relatively high level of theoretical competence. However one of the interesting features about the technique is its capability for exploitation at many levels. Thus the technique lends itself not only to

routine trouble shooting problems where often only a straightforward comparison is required without any attempt being made to understand the problem at a fundamental level and on the other hand the technique provides a powerful tool for the investigation of phenomena of considerable interest to a chemical physicist. We may note in this connection that the technique is quite competitive in terms of time taken to record a spectrum (typically ≈ 10 minutes) and with developments already in hand the technique should lend itself to real time applications.

The hierarchy of information levels available in ESCA is shown in Table 1.1. It is the composite nature of these information levels which endows ESCA with such wide ranging capabilities and has seen the technique emerge into one of the most powerful tools available to chemists and physicists today. The way in which ESCA may be exploited will become apparent in the ensuing sections.

Table 1.1

Hierarchy of Information Levels Available in ESCA

- (1) Absolute binding energies, relative peak intensities, shifts in binding energies. Element mapping for solids, analytical depth profiling, identification of structural features, etc.
- (2) Shake-up, shake-off satellites. Monopole excited states; energy separation with respect to direct photoionization peaks and relative intensities of components of "singlet" and "triplet" origin. Short and longer range effects directly (Analogue of U.V.).
- (3) Multiplet effects. For paramagnetic systems, spin state, distribution of unpaired electrons (Analogue E.S.R.).
- (4) Valence energy levels, longer range effects directly.
- (5) Angular dependent studies. For solids with fixed arrangement of analyzer and X-ray source, varying take off angle between sample and analyzer provides means of differentiating surface and sub-surface and bulk effects. Variable angle between analyzer and X-ray source angular dependence of cross sections, asymmetry parameter β , symmetries of levels.

The great advantages of ESCA as a technique, in being able to study in principle the core and valence levels of any element (regardless of nuclear properties such as magnetic or electric quadrupole moments), coupled with the low sample requirements and the ability to study involatile insoluble solids, is nowhere more apposite than in the study of polymers. In applying the technique to the investigation of polymer structures there are several distinct aspects about which one would hope to gain information (Table 1.2).

Table 1.2

ESCA Applied to Polymers

- A. Aspects of Structure and Bonding (Static Studies)
 - (i) Gross chemical compositions
 - (a) elemental compositions,
 - (b) % incorporation of comonomers in copolymers,
 - (c) polymeric films produced at surfaces.
 - (ii) Gross structural information
 - e.g. for copolymers, block, alternating or random nature.
 - Domain structure in block copolymers.
 - (iii) Finer details of structure
 - (a) structural isomerisms,
 - (b) experimental charge distributions in polymers.
 - (iv) Valence bands of polymers
 - (v) Identification of polymers, structural elucidation.
 - (vi) Monopole excited states.
- B. Aspects of Structure and Bonding (Dynamic Studies)
 - (i) Surface treatments e.g. CASING, plasma modification.
 - (ii) Thermal, photochemical degradation.
 - (iii) Polymeric films produced at surfaces by chemical reaction e.g. fluorination (including the use of ESCA for depth profiling and quantitative measurement of film thickness).
 - (iv) Chemical degradation of polymers, e.g. oxidation, nitration, etc.
- C. Electrical Properties
 - (i) Mean free paths of electrons as a function of kinetic energy.
 - (ii) Photoconductivity of polymers.
 - (iii) Statics and dynamics of sample charging.
 - (iv) Triboelectric phenomena.

The topics contained in this thesis are given below:

- Chapter 1 - Fundamental processes involved in electron spectroscopy and ESCA instrumentation.
- Chapter 2 - A review of the current literature on the application of ESCA to structure and bonding in polymers and including an appraisal of the objectives of the experimental portion of this thesis.
- Chapter 3 - A systematic investigation of the core levels of simple homopolymers from both a theoretical and experimental standpoint.
- Chapter 4 - An ESCA study on the direct determination of electron mean free paths in polymeric films as a function of kinetic energy.
- Chapter 5 - An investigation into a series of unsubstituted and substituted [2.2]paracyclophanes and polyparaxylylenes from a theoretical and experimental standpoint.
- Chapter 6 - Surface charging of polymers during the ESCA experiment including charging and discharging.
- Chapter 7 - An ESCA investigation into a series of polycarbonates including the charge potential model calculations to confirm core level assignments.
- Chapter 8 - A study of polymer-metal interfaces using the R-F plasma 'ashing' technique to expose the interface for ESCA investigation.
- Chapter 9 - The application of ESCA to the repeat unit structural analysis of the polymeric by-product of the commercial fluorination of benzene.

ii) Processes Involved in ESCA

a) The ESCA Experiment

The interaction of a monoenergetic beam of soft X-rays with an atom in a molecule results in the photoejection of electrons with given kinetic energies¹⁸. De-excitation of the hole state can occur via both fluorescence and Auger processes, for elements of low atomic number the latter being more probable¹⁸. These fundamental processes are shown schematically in Fig. 1.1. The most commonly employed X-ray sources utilized in ESCA are $Al_{K_{\alpha 1,2}}$ and $Mg_{K_{\alpha 1,2}}$ with corresponding photon

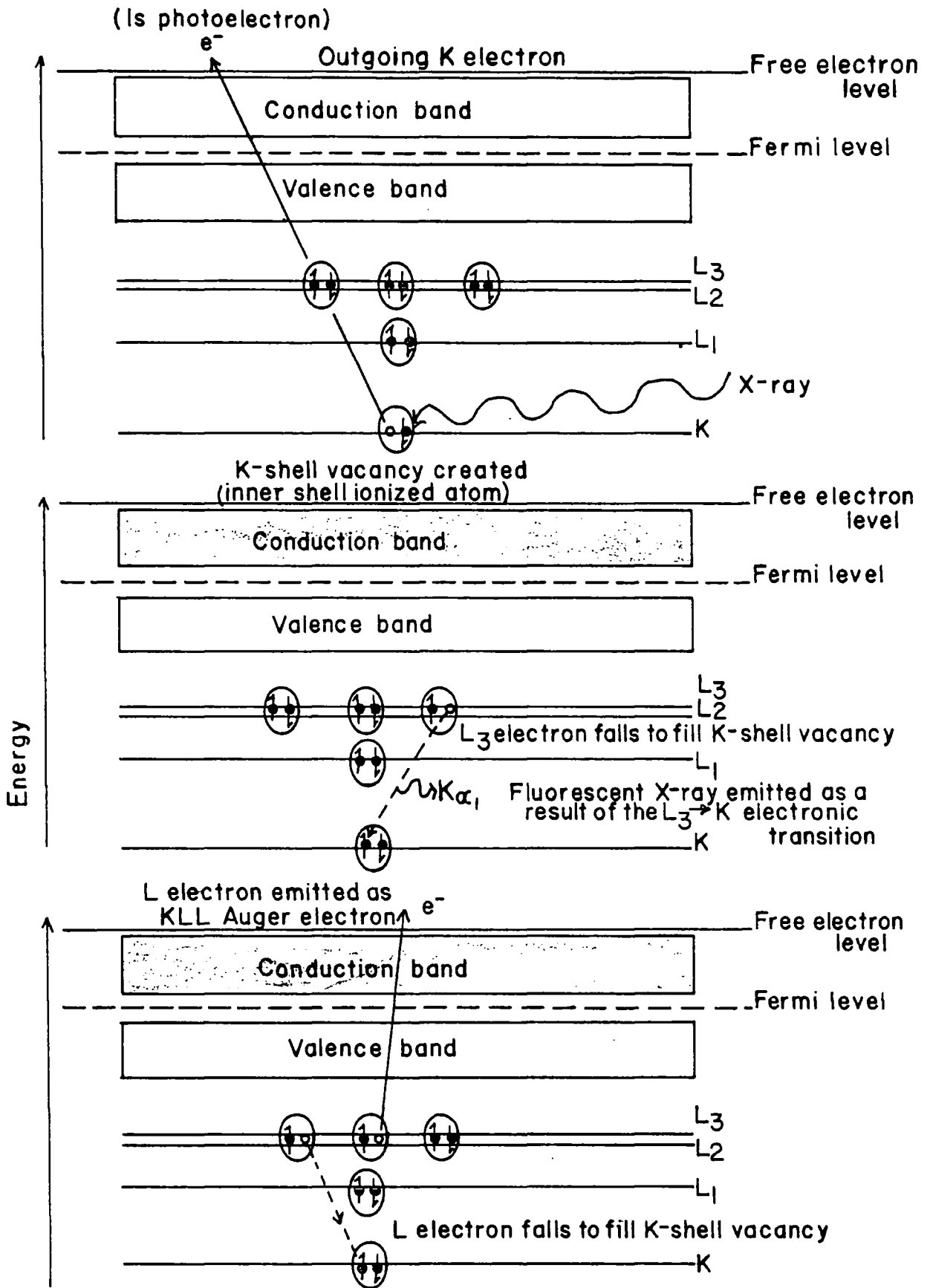


FIGURE 1.1

Fundamental processes encountered in ESCA

energies of 1486.6 eV and 1253.7 eV respectively. With a knowledge of the photon energy and the measurement of the kinetic energy of the photoemitted electrons, ESCA provides a technique for the determination of the binding energies of, in principle, all electrons from the core to the valence levels. The lifetimes of the core hole states are typically in the range 10^{-13} - 10^{-15} sec.²¹ emphasizing the extremely short time scales involved in ESCA compared with most other spectroscopic techniques.

The total kinetic energy of an emitted photoelectron (KE, which may include the contributions from the vibrational, rotational and translational motions as well as electronic) is given by the equation

$$KE = h\nu - BE - E_r \quad (1.1)$$

where $h\nu$ is the energy of the incident photon, h is Planck's constant and ν is the frequency of the X-ray radiation, B.E. is the binding energy of the photoemitted electron which is defined as the positive energy required to remove an electron to infinity with zero kinetic energy, and E_r is the recoil energy of the atom. Siegbahn and co-workers¹⁸ have calculated that the recoil energy of atoms decreases with increasing atomic number e.g. H = 0.9 eV, Li = 0.1 eV, Na = 0.04 eV, K = 0.02 eV and Rb = 0.01 eV. Therefore it is evident that the E_r term only has significance for the lighter elements, when compared with the instrumental linewidths obtained with the present study of elements from carbon upwards in the periodic table. For solids the predominate emphasis is in the direct investigation of the various electronic states of the ionized system, however, recent high resolution gas phase studies have revealed vibrational fine structure accompanying core ionization²²⁻²⁴. This complements the extensive tabulation of data on vibrational excitations accompanying valence ionization which have been compiled over the past decade by means of ultraviolet photoelectron spectroscopy (UPS)²⁵. Indeed for valence ionization in general the lifetimes of the states involved and the inherent width of the exciting radiation are such that in appropriate cases even rotational fine structure may be resolved.²⁶ The predominant emphasis in this work however has been in the investigation of the core and valence levels of polymeric systems and as such any vibrational and rotational fine structures are effectively masked by other considerations. ESCA is primarily concerned, therefore, with the various electronic states of the atom.

Therein, the equation for a free molecule reduces to

$$KE = h\nu - BE \quad (1.2)$$

It is important to understand the relationship that exists between the binding energies observed experimentally by ESCA on solids versus free molecules when compared with values calculated theoretically by ab initio and semi-empirical LCAO-MO-SCF treatments.

The most convenient reference level for a conducting sample is the Fermi level and in a metal this level, sometimes referred to as the 'electron chemical potential', is defined as the highest occupied level.

The work function, Φ_s , for a solid is defined as the energy gap between the free electron level and the Fermi level in the solid. The vacuum levels for the solid sample and the spectrometer may however, be different and the electron will experience either a retarding or accelerating potential equal to $\Phi_s - \Phi_{spec}$ where Φ_{spec} is the spectrometer work function¹⁸. In ESCA it is the kinetic energy of the electron when it enters the analyzer that is measured and taking zero binding energy to be the Fermi level of the sample the following equation results,

$$BE = h\nu = KE - \Phi_{spec} \quad (1.3)$$

Therefore, the binding energy, when referred to the Fermi level does not vary for samples, but only depends upon the Φ_{spec} and this remains a constant for all levels. Although theoretical calculations inevitably refer to isolated molecules in the gas phase with the vacuum level as reference, the theoretical definition of the Fermi level poses some difficulties in polymer systems and it is only with the accurate calibration of the energy scale from a reference, such as the C_{1s} core levels at 285.0 eV, that the theory can be correlated with the experiment. Despite the difficulties associated with defining an analytical expression for the Fermi level of an insulator the use of the Fermi level as an energy reference is operationally convenient. If the work function of the insulator is known then we may also calculate the binding energy with respect to the vacuum level. However, in polymer systems, accurate values for the work function are generally not available and binding energies are calculated relative to the reference material.

It is evident that for conducting samples in electrical contact with the spectrometer the Fermi level serves as a convenient reference level. For insulating samples, such as polymers, the Fermi level is not so well defined theoretically and lies somewhere between the filled

valence levels and the empty conduction band¹⁸.

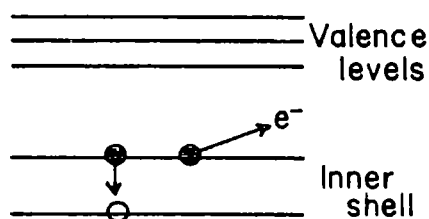
Equation (1.3) assumes equilibrium conditions during the ejection of an electron, which may or may not occur when the resistance of the sample is high compared with the electrical currents needed to replace the electron vacancies due to photoemission.

Several investigations have shown that the primary photoelectrons are rapidly slowed down by the interaction with matter and can generate intense currents of slow 'secondary' electron clouds at the surface of the sample²⁷⁻²⁹. These secondaries play an important role in establishing the electrical equilibrium at the surface of the sample.

However, in practice, the problem of extracting absolute binding energies is circumvented by the use of reference standards for calibration of the binding energy scale. This will be dealt with in more detail in the subsequent section on energy referencing.

Auger emission may be viewed as a two step process involving the ejection of an electron from an inner shell by a photon followed by an electron dropping down from a higher level to the vacancy in the inner shell with the simultaneous emission of a second electron (Fig. 1.1)^{30a-d}. When the electron drops from a valence shell to fill the inner shell vacancy the chemical shifts involved are related to both outer and inner shells and in a few suitable cases information can be gained on the binding energies of both shells.

Where the electronic vacancy in the inner shell is filled by an electron from another inner shell the Auger spectra is useful for analysis of inner shell transitions. Transitions of this type, referred to as Coster-Kronig transitions, are very efficient and lead to very short lifetimes with well resolved spectra^{30e,f}.



Because of the overlap of the wavefunctions, Coster-Kronig transitions are more than an order of magnitude larger than normal Auger processes. Whether a Coster-Kronig transition will occur depends on

whether the differences in the subshell binding energies are sufficient to eject an electron from an orbital in the next higher shell. For example, Coster-Kronig transitions will take place only for elements whose atomic number is less than 40.

For a general Auger transition which involves any set of levels KLM, a peak should appear at:

$$E(Z) = E_K - E_L - E_M (Z + \Delta) - \Phi_A \quad (1.4)$$

where: Z is the atomic number

$\Delta = 1$ (due to the extra positive charge from the loss of an electron)

Φ_A is the work function of the analyzer

E_K is the energy from a K level transition

E_L is the energy from an L level transition

E_M is the energy from an M level transition

Equation (1.4) can, however, lead to errors in some cases because the final state of the double ionized atom must be defined. The additional definition is needed because the energies involved in the transitions in the Auger process are governed by the coupling scheme amongst electronic wavefunctions in the initial (single ionization) as well as the final (double ionization) electronic configuration. LS coupling dominates for light elements and jj coupling for heavy elements.

Essentially, there are three types of chemical information which may in principle be obtained from Auger spectra. (However, it should be pointed out that the extraction of this information is by no means straightforward since differences in energy levels are involved). The first is the chemical shift due to the shifts of the inner shell energy levels arising from changes in valence electron distributions. The second type of information pertains to the valence levels themselves. The valence band spectra are usually quite pronounced due to the redistribution (relaxation) of electrons upon formation of a new electronic configuration. The third type of information that is obtained is much more vague and is referred to as 'molecular orbital energy spectra' and is, of course, also involved with part of the valence levels. If the molecular orbitals are known for a specific compound then the valence energy levels can be compared. This technique, although it has the limitation that to-date molecular orbitals cannot be assigned to specific energy levels, the symmetry of its component wave functions can be used to 'infer' point group symmetry of an atom in a crystal to

locate it within a unit cell.

Wagner has recently³¹ recognized that Auger lines frequently exhibit far larger chemical shifts than the primary photoelectron lines and has led to his ingenious development of the so called "Auger Parameter", the difference in kinetic energy between an Auger line and a photoelectron line. Since it is a difference between the position of two lines the surface charge corrections cancel. This quantity is unique for each compound³² and can be measured more accurately than absolute line position (kinetic energy) which must be corrected for surface charging effects. Changes in the Auger parameters are due principally to changes in extra-atomic relaxation or polarization energy. As the Auger parameter is more developed it will become increasingly important in the hierarchy of information levels available from the ESCA experiment.

Auger Electron Spectroscopy (AES) as conventionally applied is based on the analysis of the energy of electrons that are ejected from a sample as a consequence of excitation by primary electron beams typically ≈ 2 kV, rather than X-ray photons. This technique is truly a surface analysis technique in that the penetration depth for the exciting electrons is only about 5 atomic layers³³.

Under ideal conditions minute amounts of surface atoms have been detected, down to the range of 10^6 atoms/cm.³ at the surface. However, recent evidence has shown that the surfaces of materials studied are altered due to radiation damage from the electron beam.

Coad and co-workers have shown³⁴ that AES can only provide an analysis of a virgin surface without appreciable beam interaction effects at primary beam current densities of about 0.03 A^{-2} (allowing 600 seconds for analysis and choosing a total charge density lower by a factor of ten than that shown to have serious effects on the analysis). Beam damage was demonstrated on such systems as chrome and stainless steels whereas on an organic polymer system we can expect a significantly greater damaging effect from the electron beam. At reduced beam conditions where damage to the polymer surface would be avoided, the advantages of conventional AES or ESCA of speed of analysis and spatial resolution disappear.

The emission of X-rays instead of electrons leads to X-ray fluorescence (secondary-emission analysis) and is an excellent means of qualitative analysis for constituents of atomic number greater than eight(8).

Concentrations down to 0.1% for most elements and 0.01% for elements around Fe, Co, Ni have been detected. X-ray emission tables exist³⁵ which enable a particular element to be observed at a position of its strongest lines, after which all of its lines can be identified in the spectrum once its presence is known.

The decrease in X-ray fluorescence with decreasing energy is due to the fact that it is an electromagnetic (dipole) process and depends mostly on the acceleration of the orbiting electron. The Auger process, however is dependent upon the electrostatic forces accompanied by a vacancy in the inner shell.

Fig. 1.2 is a plot of the X-ray fluorescence yield and Auger electron yields in the X-shell as a function of atomic number (Z)

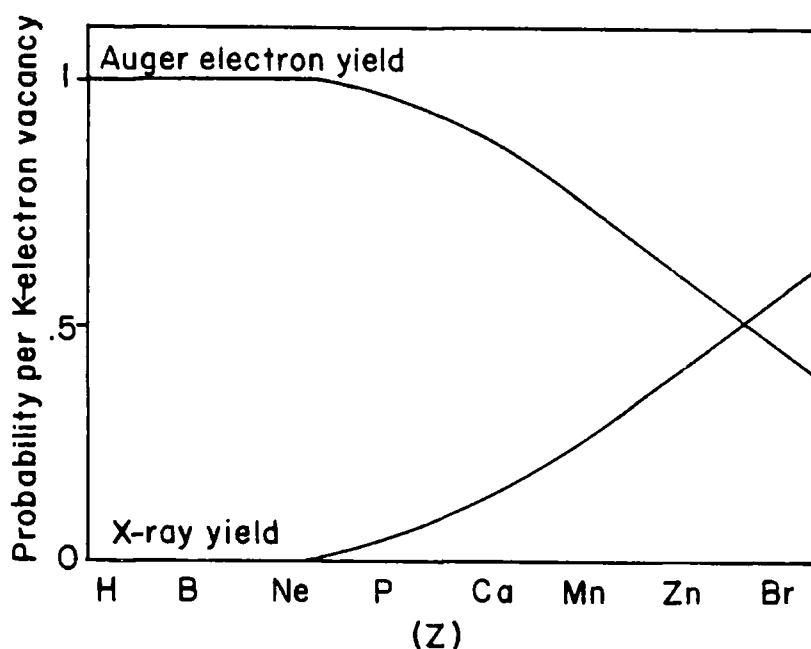


FIGURE 1.2

X-ray fluorescence and Auger electron yields in the K-shell as a function of atomic number

for the light elements in the periodic table¹⁸.

The relative sensitivities of these techniques, together with other familiar analytical methods are shown in Table 1.3

b) Electronic Relaxation

It is well established that photoionization of core electrons is accompanied by substantial electronic reorganization (referred to as electronic relaxation), predominantly associated with the valence electrons³⁶⁻³⁸. Experimental and theoretical studies have indicated that for a given core level the magnitude of relaxation energy (RE) is a sensitive function of the electronic structure³⁹⁻⁴³.

Table 1.3

Sensitivities of Various Analytical Techniques

Technique	Surface	Bulk	Minimum Detectable Quantity (g.)
(a) Infrared		x	10^{-6}
(b) Atomic absorption		x	$10^{-9} \rightarrow 10^{-12}$
(c) Vapor phase chromatography		x	$10^{-3} \rightarrow 10^{-7}$
(d) High pressure liquid chromatography		x	$10^{-6} \rightarrow 10^{-9}$
(e) ESCA	x		10^{-10}
(f) Mass spectroscopy		x	$10^{-10} \rightarrow 10^{-15}$
(g) Neutron activation	x		10^{-12}
(h) Ion-scattering spectrometry	x		10^{-15}
(i) X-ray fluorescence	x		10^{-7}
(j) Auger spectroscopy	x		10^{-14}
(k) Secondary ion scattering spectrometry	x		10^{-13}

Both absolute and relative binding energies and relaxation energies may be calculated with the Hartree-Fock formalism⁴³⁻⁴⁶ if non-empirical calculations of the requisite quality are available for both the neutral molecule and core ionized species. Unfortunately, such calculations are extremely computer intensive and as such are only practicable for systems of relatively modest size. Use has often been made, therefore, of Koopmans' Theorem⁴⁷ which equates binding energy to the negative of the relevant Fock eigenvalue. Unfortunately, since it is implicit in this approach that relaxation phenomena is neglected, Koopmans' theorem not only predicts binding energies incorrectly, but in some cases if relaxation energies are sufficiently different, may also produce an incorrect ordering of energy levels. The relationship between the experimental, Koopmans' Δ SCF binding energy is schematically shown in Fig. 1.3

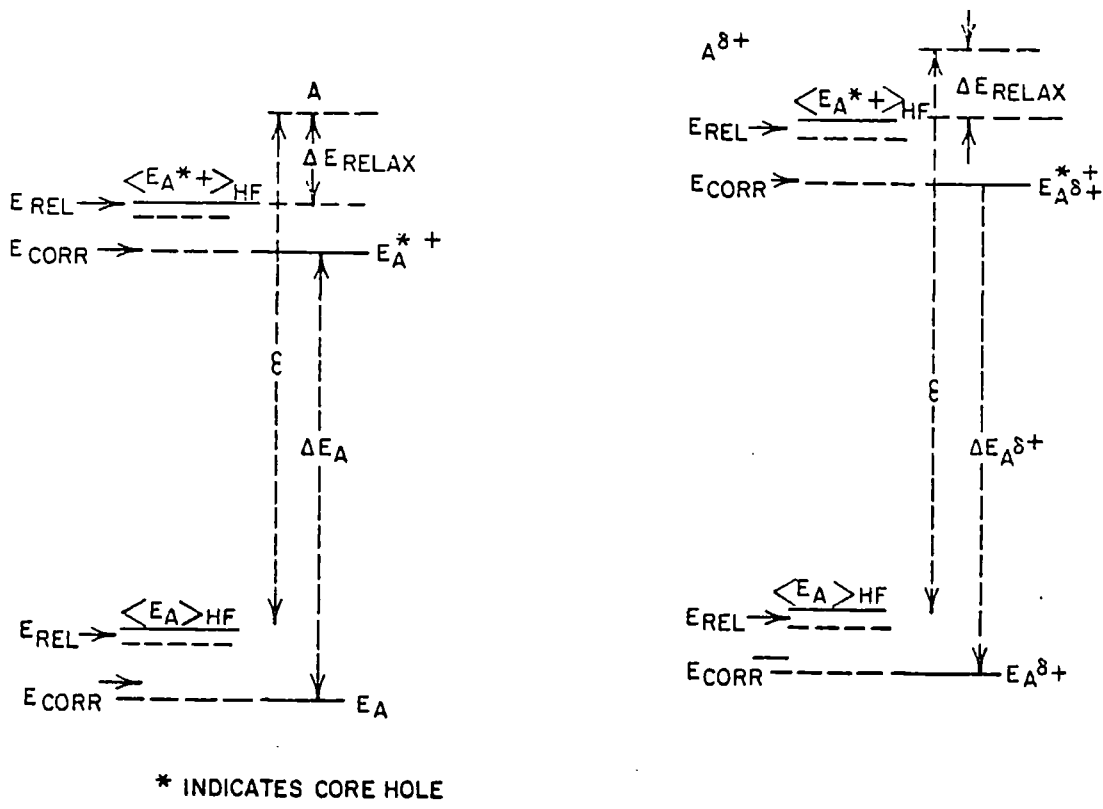


FIGURE 1.3

Schematic relationship between the experimental, Koopmans' Theorem and SCF binding energies

$$RE = -(BE)_{\text{Koopmans'}} - (BE)_{\text{SCF}} \quad (1.5)$$

where:

- E_{CORR} = electron correlation energy
- R_{REL} = relativistic energy

both of which are ignored by Koopmans' and SCF methods.

Hartman and Clementi⁴⁹ have shown in calculations on argon, that most of the relativistic correction is associated with the core electrons and that for argon the 1s contribution in its ions is essentially the same as in the atom. (In the extreme case of Ar^{10+} the correction changes by only 0.72eV compared with the atom). These data⁴⁹ verify the assumption of Scherr and co-workers⁵⁰ that the relativistic contribution of any subshell is independent of the number of electrons in the outer shells. Thus, differences in relativistic corrections to shifts in core electron binding energies between a particular core level for atoms in different chemical environments are small⁵¹. From an analysis of atomic data for first row atoms it is also known that the magnitudes

of the correlation energies of the $1s$ electrons are very similar and intra shell correlation energies small ⁵².

Thus, to a good approximation correlation energy corrections will remain reasonably constant for core levels (which are essentially localized and atomic in nature) and play little or no part in shifts in core electron binding energies. In a detailed study of the ionized states of the CH_4 molecule with a basis set approaching the Hartree-Fock limit, Clementi and Popkie⁴⁴ have demonstrated that for the $1s$ hole state the correlation energy is the same as for the neutral molecule. From the above discussion the relativistic and correlation energy corrections to the binding energies are relatively small and almost complete cancellation of these effects will occur when calculating shifts in core electron binding energies between molecules.

Not only does Koopmans' theorem neglect relativistic and correlation energy contributions to the binding energy but also the relaxation energy associated with the reorganization of electrons which occurs on photoionization.

Relaxation energies are by no means negligible even for valence levels and for carbon atoms with approximate core binding energies of ≈ 300 eV they have values of ≈ 13 eV⁵³⁻⁵⁴. A physical interpretation of relaxation energies is made clear from the following consideration. If an electron is ejected from a core or a valence level, the remaining electrons will experience an increased potential at the nucleus and relax (reorganize) to minimize the energy. This relaxation process changes the spatial distribution of the remaining $n-1$ electrons which is taken into account in the ΔSCF method but not in Koopmans' theorem. A change in potential at the nucleus will be much larger if a core rather than a valence electron is ionized because core electrons have a larger screening coefficient. This is reflected in the value of relaxation energies which are usually smaller by a factor of ten for valence as compared with core electrons. For example, values of RE's for the C_{1s} and the 1π orbitals in CO calculated within the ΔSCF formalism are 11.4 eV and 1.8 eV respectively⁵⁴⁻⁵⁵.

The differences in relaxation energies for closely related molecules are small and therefore make only minor contributions to shifts in binding energies. This is consistent with the tendency of Koopmans' theorem and ΔSCF calculations to give the same estimates of shift despite the fact that Koopmans' theorem neglects the effect of electronic relaxation⁵⁵.

c) Shake-up and Shake-off

The removal of a core electron (which is almost completely shielding as far as the valence electrons are concerned) is accompanied by substantial reorganization (relaxation) of the valence electrons in response to the effective increase in nuclear charge as discussed above. As well as the relaxation process, this perturbation also gives rise to a finite probability for photoionization to be accompanied by simultaneous excitation of a valence electron from an occupied to an unoccupied level (shake-up) and ionization of a valence electron (shake-off) as shown in Fig. 1.4. These relaxation processes result in excited states of the core ionized species.

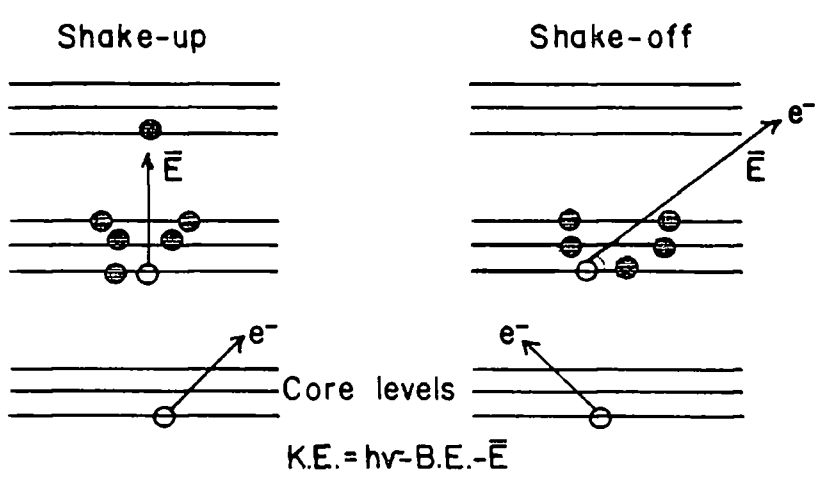


FIGURE 1.4

Schematic representation of shake-up and shake-off processes

These processes, deriving their energy from the single electron process, will lower the K.E. of the primary photoelectron. Therefore, a revision is needed to equation (1.2) to account for these multi-electron processes:

$$KE = h\nu - BE - \bar{E} \tag{1.6}$$

where \bar{E} is the energy of the multi-electron process.

It may be shown that excitations to these states follow monopole selection rules, $J = L = S = M_J = M_L = M_S = 0$, as indicated in equations

$$\Psi_i = \sum_{u=1}^n C_{u_i} \phi_u \tag{1.7}$$

$$\Psi_f = \sum_{v=1}^n k_{v_f} \phi'_v \tag{1.8}$$

$$P_{f \leftarrow i} = N \left| \sum_{u=1}^n k_{u_f} C_{u_i} \langle \phi'_u | \phi_u \rangle \right|^2 \tag{1.9}$$

In the sudden approximation, transition intensities are directly related to the sums of one center overlap terms involving the occupied orbitals of the initial system and virtual orbitals of the hole state species⁵⁶. These monopole excited states are analogues of the more familiar dipole allowed excited states of the neutral molecule studied in conventional electronic spectroscopy. There are subtle differences however, and this can be readily appreciated by the schematic in Fig. 1.5.

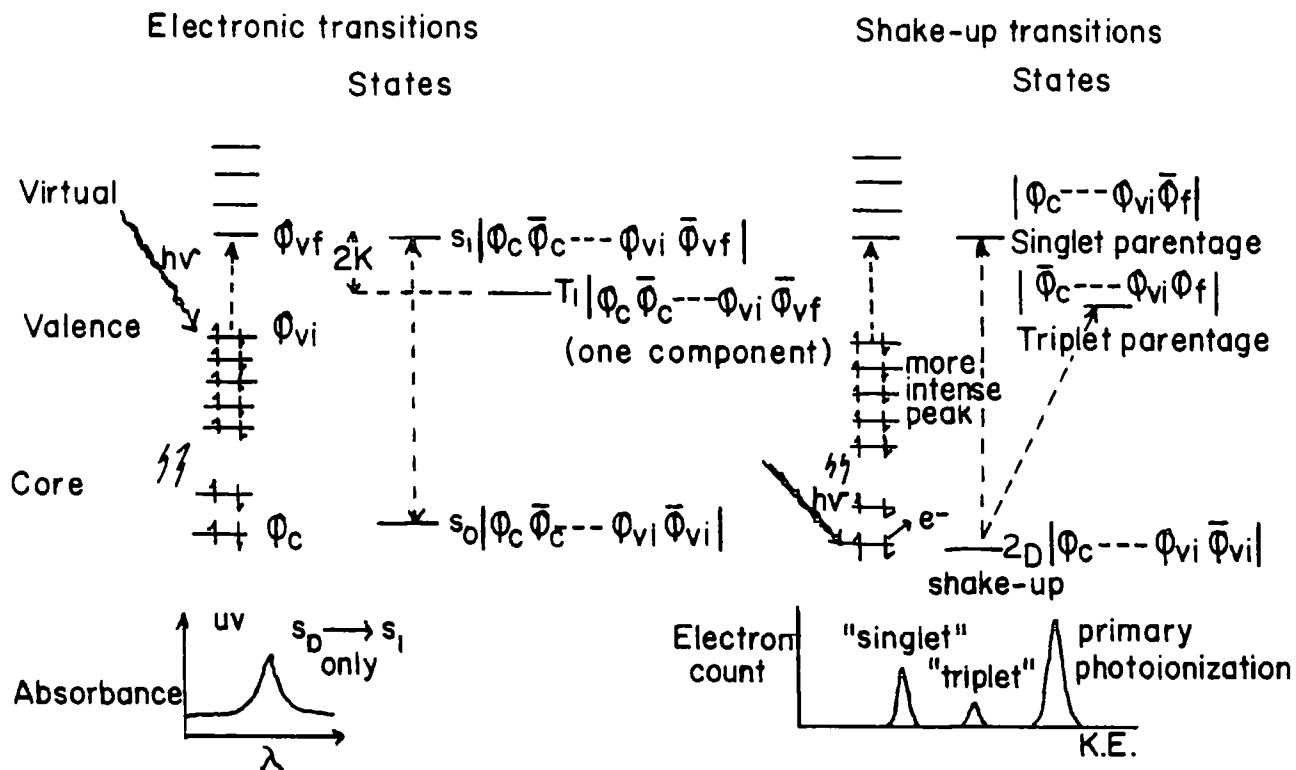


FIGURE 1.5

Comparison of electronic transitions in the neutral molecule with shake-up transitions in the hole state species

If we consider electronic transitions for a closed shell system as depicted on the left hand side of Fig. 1.5 in a simple orbital model we may generate a singlet and triplet state from the same excitation configuration, the latter being lower in energy than the former, the energy gap being given by twice the exchange integral. Except under special conditions, the only transitions observed with substantial intensities are the dipole allowed singlet to singlet transitions. Consider now excitation involving a core hole state in the doublet manifold as depicted on the right hand side of Fig. 1.5 where two possibilities for a given excitation configuration exists. Firstly, if we consider the shake-up

transition to be such that the unpaired electron in the valence level and that excited to the virtual orbital have opposite spins we may consider this doublet state to be of 'singlet origin' by analogy with the excited singlet state of a given excitation configuration, previously discussed. However, we may also generate a doublet state by having the electrons in the valence level and that promoted to the virtual orbital with the same spin whilst the remaining core electron has opposite spin. This by analogy corresponds to the shake-up state of triplet origin. Again, the 'triplet' state is lower in energy than that of singlet origin, however, since both represent doublet states, transitions from the ground state of the core hole state may be viewed as both being allowed. In principle, therefore, we should have as experimental observables the energy separations and intensities for the components of the shake-up states of given excitation configuration. It might be anticipated naively that the shake-up state of singlet origin would be the more intense and in the following discussion this will largely be implicit. The detailed theoretical treatment of shake-up states in general is by no means as simple as has been portrayed, however the simplistic model presented here is conceptually very useful and forms a good starting point for more sophisticated treatments⁵⁷. Fortunately, as will become apparent if we restrict ourselves to the interpretation of trends and differences particularly of shake-up intensities, a rather good description may be obtained at relatively modest computational expense^{57,58}. As has been previously discussed relaxation energies are also characteristic of a given core level and also vary within narrow limits as a function of the bonding environment of the atom on which the core level is located⁵³. For C_{1s} levels for neutral systems for example, binding energies measured with respect to the fermi level as energy reference, fall in the range 285-295 eV whilst relaxation energies might typically fall in the range 12 ± 2 eV⁵⁴. The direct relationship between shake-up and shake-off processes and relaxation energies may be readily understood from theoretical relationships first established by Manne and Åberg⁵⁹. They showed that the weighted average over the direct photoionization and shake-up and shake-off peaks corresponds to the binding energy appropriate to the unrelaxed systems and this is shown schematically in Fig. 1.6. Since relaxation energies fall within such a narrow range for a given core level it is clear that shake-up and shake-off are perfectly general phenomena which are present in every system, the feature which changes

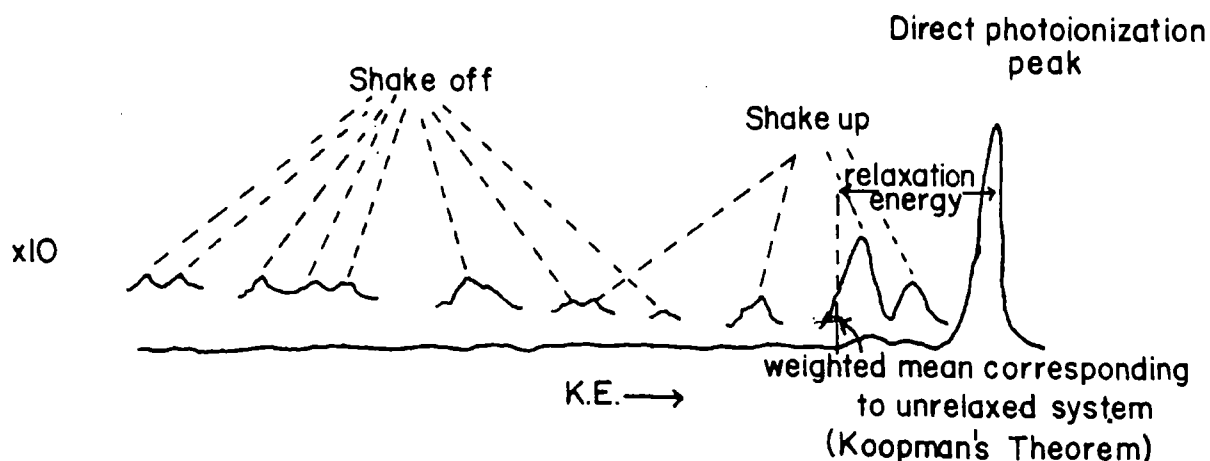


FIGURE 1.6

Relationship between relaxation energies, Koopman's theorem and the relative intensities of direct photoionization and shake-up and shake-off transitions

from one system to another being the weighting coefficients (probabilities) for each transition. It is clear that transition probabilities for high energy shake-off processes should be relatively small and that transitions of highest probability should fall reasonably close to the centroid. In principle, relaxation energies should be available from experiments, provided all of the relevant shake-up and shake-off processes can be estimated in terms of energies and intensities. In practise, this is not a feasible proposition particularly for solids since the overall situation is considerably complicated by the presence of the general inelastic tail (arising from photoemission from a given core level followed by energy loss by a variety of scattering processes discussed in more detail in Chapter 3) which provides a broad energy distribution usually peaking for organic systems ≈ 20 eV below the direct photoionization peaks. This generally obscures any underlying high energy shake-off processes such that it is only for systems exhibiting relatively high intensity low energy shake-up peaks that information derived from this source can conveniently be exploited.

d) Chemical Shifts

Core levels are essentially localized on atoms, their energies are characteristic for a given element and are sensitive to the electronic environment of an atom¹. Thus for a given core level of a given element while the absolute binding energy for that level is characteristic for the element, (Table 1.4) differences in electronic environment of a given

Table 1.4

Approximate core binding energies for 1st and 2nd row elements (in eV)

	Li	Be	B	C	N	O	F	Ne
1s	55	111	188	284	399	532	686	867
	Na	Mg	Al	Si	P	S	Cl	Ar
1s	1072	1305	1560	1839	2149	2472	2823	3203
2s	63	89	118	149	189	229	270	320
2p _{1/2}	31	52	74	100	136	165	202	247
2p _{3/2}			73	99	135	164	200	245

atom in a molecule give rise to a small range of binding energies (i.e. 'chemical shifts') often representative of a particular structural feature.

The quantitative interpretation of chemical shift data has been investigated theoretically by five distinct approaches.

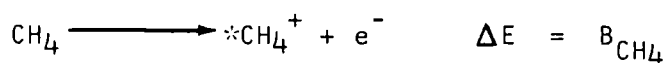
- 1) Koopmans' theorem.
- 2) Core hole state calculations (Δ SCF).
- 3) Equivalent cores approach.
- 4) Madelung charge potential model.
- 5) Quantum mechanical potential model (at the nucleus).

The application of Koopmans' theorem and the core hole state approach (Δ SCF) to the calculation of the absolute binding energy has been discussed in section b). The bulk of this section will, therefore, concentrate on an evaluation of the equivalent cores method and the Madelung charge potential model. The quantum mechanical potential model is of lesser importance and a comparison of experimental results with the other theoretically derived models is discussed in detail elsewhere⁶⁰⁻⁶².

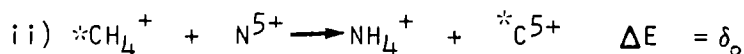
1) Equivalent Cores Approximation

The equivalent cores approximation was developed by Jolly and Hendrickson⁶³ to calculate shifts in core electron binding energies from ground state thermodynamic data, and states, "When a core electron is removed from an atom in a molecule or ion, the valence electrons relax as if the nuclear charge on the atom had increased by one unit". Thus, atomic cores that have the same charge are considered to be chemically equivalent. The following example illustrates how this principle may be used to estimate the gas phase shift in C_{1s} binding energy between the carbon atoms in methane and fluoromethane.

i) The carbon 1s electron binding energy in methane B_{CH_4} is given by the energy of the process

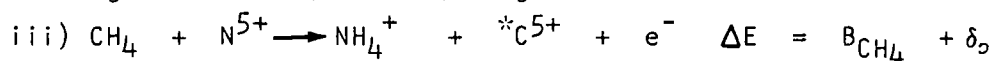


where * indicates a vacancy in a core level (C_{1s} in this case)

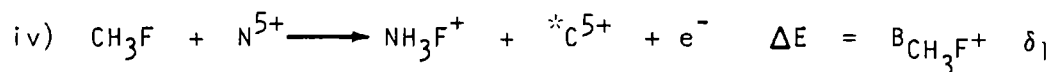


This reaction is the exchange of the $* \text{C}^{5+}$ core and the equivalent N^{5+} core. According to the principle of equivalent cores the energy of this reaction, δ_0 , is zero.

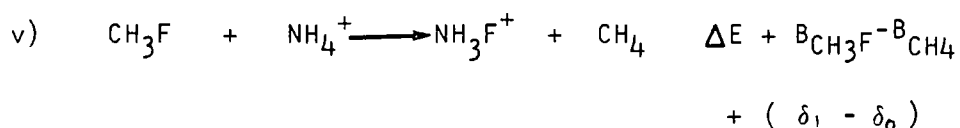
Summing reactions (i) and (ii) gives



A similar reaction may be written for CH_3F , or any other compound containing a carbon atom



The difference of reactions (iii) and (iv) gives



The strong form of the equivalent cores approximation given above states that $\delta_1 = \delta_0 = 0$ and hence, the difference in C_{1s} binding energies between methane and fluoromethane is given by the energy of reaction (v). However, reaction (v) still gives the shifts in binding energy if $\delta_1 = \delta_0$ i.e. if the energy of core exchange is independent of the molecular environment (this is known as the weak form of the equivalent cores approximation). Some typical gas phase data are shown in Table 1.5 and in general indicate good agreement between experimental and thermodynamic shifts.⁶⁴ The main restriction to the use of the equivalent cores method is the lack of and/or inaccuracy of thermodynamic data especially with regard to the positive ions involved in the reactions. The theoretical validity however, of the equivalent cores concept has been well documented by Clark and co-workers on their studies on simple molecules⁶⁵⁻⁶⁶.

However, the heats of reaction may be obtained from SCF calculations on the molecules and ions in their ground states. Pople and co-workers^{67,68} have shown that for reactions involving closed shell

Table 1.5

Experimental and Thermodynamic Binding Energy Shifts

<u>Atomic level</u>	<u>Compound</u>	<u>Experimental Shift</u>	<u>Chemical Reaction Energy</u>
N _{1s}	NH ₃	0	0
N _{1s}	(CH ₃) ₂ NH	-0.7	-0.7
N _{1s}	(CH ₃)NH ₂	-0.3	-0.4
N _{1s}	HCN	1.2	0.95
N _{1s}	<u>N</u> NO	3.2	2.6
N _{1s}	N ₂	4.35	3.5
N _{1s}	NO	5.5	4.4
N _{1s}	N ₂ F ₂	6.8	6.3
N _{1s}	NO ₂	7.3	6.8
C _{1s}	CH ₄	0	0
C _{1s}	CO	5.4	4.1
C _{1s}	CO ₂	6.8	6.9
C _{1s}	CF ₄	11.0	12.3
Xe 3d _{5/2}	Xe	0	0
Xe 3d _{5/2}	XeF ₂	2.95	2.7
Xe 3d _{5/2}	XeF ₄	5.5	5.4
Xe 3d _{5/2}	XeOF ₄	7.0	6.3
Xe 3d _{5/2}	XeF ₆	7.9	7.85

species even minimal basis set (STO 3.G) calculations, which are computationally relatively inexpensive, can reliably reproduce heats of reaction. Particularly accurate results are obtained in the case of reactions in which the number and type (i.e. single, double, etc.) of bonds are the same in both reactants and products since correlation energy changes are very small. Such processes have been designated "isodesmic reactions" and it is exactly this type of reaction which is involved in the equivalent cores method of calculating shifts. Since heats of reaction are involved there is also the possibility that semi-empirical calculations, which are also computationally inexpensive, may be used to predict, at least qualitatively, the required shifts. Thermodynamic

data refer to the isoelectronic cations with their nuclei in the equilibrium positions but since photoionization is a rapid process compared with nuclear motion^{51,69} it is more realistic to consider the cations to have the same geometry as the parent calculations. Also, by using the same geometry for the molecules and isoelectronic cations in ab initio calculations, many of the two electron integrals may be retained and this greatly reduces the amount of computing time required.

2) Charge Potential Model

The charge potential model relates core electron binding energies with the charge on the atom from which the core ionization takes place and the potential from the charges in the remainder of the molecule. Although the model developed by Siegbahn¹⁸ and co-workers was from intuitive observations on systems a non rigorous derivation of the equation relating binding energies to charge distributions may be made, starting from Koopmans' Theorem⁴⁷.

The crucial feature in the derivation of the charge potential equation is the constancy with varying electronic environments of many of the terms which arise (cf. Table 1.6).

Table 1.6

Relevant terms in varying electronic environments for C_{1s} core levels

Molecule	Atom	q	$\langle \Psi_r -1/2\nabla_1^2 \Psi_r \rangle$ AU	$\langle 1/R \rangle$	Koopmans' Shift
H-C≡C-F	H-C	-0.061	16.0168	5.6559	0.33 eV
	F-C	+0.112	16.0181	5.6563	2.96 eV
H-C≡C-Cl	H-C	-0.136	16.0189	5.65.5	0.24 eV
	Cl-C	-0.078	16.0175	5.6515	1.60 eV

The orbital energy of the core orbital Ψ localized on atom m is given by Equation (1.10)

$$\begin{aligned}
 \epsilon_r &= \langle \psi_r | -\frac{1}{2}\nabla_1^2 - \sum_n \frac{Z_n}{r_{n1}} | \psi_r \rangle + \sum_{s=a}^k (2J_{rs} - K_{rs}) = \\
 &= \langle \psi_r | -\frac{1}{2}\nabla_1^2 - \frac{Z_m}{r_{m1}} | \psi_r \rangle + J_{rr} + \langle \psi_r | - \\
 &\quad - \sum_{n \neq m} \frac{Z_n}{r_{n1}} | \psi_r \rangle + \sum_{s \neq r}^k (2J_{rs} - K_{rs}). \tag{1.10}
 \end{aligned}$$

The terms $\langle \psi_r | -\frac{1}{2}\nabla_1^2 - (Z_m/r_{m1}) | \psi_r \rangle$ and J_{rr} (the Coulomb integral) are constants essentially independent of valence electron distribution. Grouping the constant terms into E_0 and neglecting the K_{rs} (exchange integrals, ψ_s orbitals on other atoms in molecule) in Equation (1.10), this transforms to Equation (1.11).

$$\varepsilon_r = E_0 + \langle \psi_r | - \sum_{n \neq r} \frac{Z_n}{r_{n1}} | \psi_r \rangle + \sum_{s \neq r}^k 2J_{rs}. \quad (1.11)$$

The interaction between $|\psi_r|^2$, localized on atom m , and the nuclei of other atoms may be approximated by an interaction between point charges $\sum_{n \neq m} (Z_n/r_{nm})$ and so Equation (1.11) may be transformed into Equation (1.12).

$$\varepsilon_r \approx E_0 + \sum_{n \neq m} -\frac{Z_n}{r_{nm}} + \sum_{s \neq r}^k 2J_{rs}. \quad (1.12)$$

The terms in the last summation including $\psi_j (\neq \psi_r)$, core orbitals on all atoms n , may be approximated by

$$J_{rj} = \langle \psi_r(1) \psi_j(2) | \frac{1}{r_{12}} | \psi_r(1) \psi_j(2) \rangle \approx \frac{1}{r_{nm}}. \quad (1.13)$$

The terms including the valence MO's ψ_i may be written in a LCAO approximation for ψ_i as:

$$J_{ri} = \sum_p c_{ip}^2 \langle \psi_r(1) \phi_p(2) | \frac{1}{r_{12}} | \psi_r(1) \phi_p(2) \rangle. \quad (1.14)$$

They may therefore be divided into two types of terms, whether

- (i) ϕ_p is a valence AO on atom m , or
- (ii) ϕ_p is a valence AO on atom n .

The contribution of the former type of terms to J_{ri} is

$$\sum c_{ip}^2 \langle \psi_r(1) \phi_p(2) | \frac{1}{r_{12}} | \psi_r(1) \phi_p(2) \rangle$$

where the sum is over all ϕ_p on atom m. The remaining terms in J_{ri} may be approximated as

$$\sum_n \sum_{\text{all } \phi_p \text{ on } n} c_{ip}^2 \frac{1}{r_{nm}}$$

so that Equation (1.12) becomes

$$\begin{aligned} \epsilon_r = E_0 + \sum_{n \neq m} -\frac{Z_n}{r_{nm}} + \sum_{n \neq m} \frac{z_n}{r_{nm}} + \sum_{n \neq m} \sum_{\text{all } \phi_p \text{ on } n} \frac{2c_{ip}^2}{r_{nm}} + \\ + \sum_{\text{all } \phi_p \text{ on } n} 2c_{ip}^2 \langle \psi_r(1) \phi_p(2) | \frac{1}{r_{12}} | \psi_r(1) \phi_p(2) \rangle \end{aligned} \quad (1.15)$$

where z_n is the number of core electrons on n.

A diagrammatic representation of core and valence levels is given in Figure 1.7.

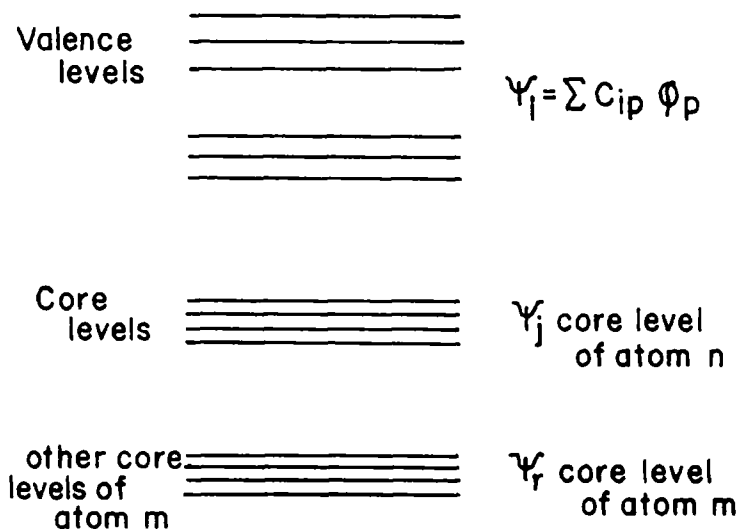


FIGURE 1.7

A diagrammatic representation of core and valence levels

Collecting terms common to each atom and those containing valence orbitals ϕ_p on m , we obtain

$$\begin{aligned} \epsilon_r = E_0 + \sum_{n \neq m} \left\{ \left(-\frac{Z_n}{r_{nm}} + \frac{z_n}{r_{nm}} \right) + \sum_{\text{all } \phi_p \text{ on } n} \frac{2c_{ip}^2}{r_{nm}} \right\} + \\ + \sum_{\text{all } \phi_p \text{ on } n} 2c_{ip}^2 \langle \psi_r(1) \phi_p(2) | \frac{1}{r_{12}} | \psi_r(1) \phi_p(2) \rangle. \end{aligned} \quad (1.16)$$

Remembering that

$$-Z_n + z_n + \sum_{\text{all } \phi_p \text{ on } n} 2c_{ip}^2$$

is the charge q_n on atom n , we get

$$\epsilon_r = E_0 + \sum_{n \neq m} \frac{q_n}{r_{nm}} + \sum_{\text{all } \phi_p \text{ on } m} 2c_{ip}^2 \langle \psi_r(1) \phi_p(2) | \frac{1}{r_{12}} | \psi_r(1) \phi_p(2) \rangle. \quad (1.17)$$

Because $2c_{ip}^2$, the valence electron population on m , is proportional to the charge on m , q_m , we get finally

$$\epsilon_r = E_0 + kq_m + \sum_{n \neq m} \frac{q_n}{r_{nm}}. \quad (1.18)$$

The derivation also shows that k is approximately the one center coulomb repulsion integral between a core and valence electron on a given atom. The charge potential model is of particular importance to organic chemists since it relates charge densities (the theoretical definition of which is inevitably somewhat arbitrary) to binding energies. The third term represents an intramolecular Madelung type potential arising from charges on other atoms in the molecule.

Using all valence electron CNDO/2 SCF MO⁷⁰ calculations, the quantitative discussion of data on quite complex molecules becomes feasible.

For example, the data in Table 1.7 pertaining to the C_{1s} and O_{1s} levels for a series of compounds gives the charge potential correlations shown in Figure 1.8

Absolute Binding Energies for the C_{1s} and O_{1s} Levels of the ModelCompounds from the Charge Potential Model

Molecule	Theoretical Binding Energies in eV			
	<u>-C-O-</u>	<u>C=O</u>	<u>C=O</u>	<u>C-O-</u>
CH_3OH	533.7	-	-	286.5
CH_3CH_2OH	533.6	-	-	286.8
CH_3COCH_3	-	533.2	287.8	-
$CH_3CH_2OCH_2CH_3$	533.2	-	-	286.6
$HCOOCH_2CH_3$	534.4	533.2	289.1	287.4
$CH_3COOCH_2CH_3$	534.2	532.9	289.1	287.2
$CH_3COOCH(CH_3)_2$	534.1	532.9	289.0	287.4
$CH_3COOCH_2CH(CH_3)_2$	534.2	532.9	289.1	287.2
$CH_3COCH_2COOCH_2CH_3$	534.2	532.8	289.1	
		533.1	288.0	287.2

Table 1.7

The correlation is very good and from the slope and intercept, values of k and E° may be established. Since the charge potential model may be related to Koopmans' Theorem which neglects electronic relaxation of the valence electrons (on ejection of a core electron), it must suffer from some of the same deficiencies. Since electronic relaxation will depend on the electronic structure of a molecule it is only for closely related series of molecules that one might expect Koopmans' Theorem to provide a quantitative interpretation of shifts in core binding energies. Similarly for the charge potential model we might expect different values of k and E° for different series of closely related compounds. This is indeed the case. Some values appropriate to series of organic molecules are given in Fig. 1.9 where it is evident that with charges computed from CNDO/2 calculations the value of k clusters around 25.0 eV for C_{1s} levels. Similar correlations may be made for other levels e.g. F_{1s} , Cl_{2p} , N_{1s} , etc.

It is worth considering the relationship between shifts in core binding energies and organic chemists intuitive ideas concerning 'charge distribution'. Since valence electron distributions in molecules are continuous functions the assignment of 'charges' to atoms within a molecule is somewhat arbitrary and depends on how the overlap density is partitioned between atoms. As such, theoretically calculated charge

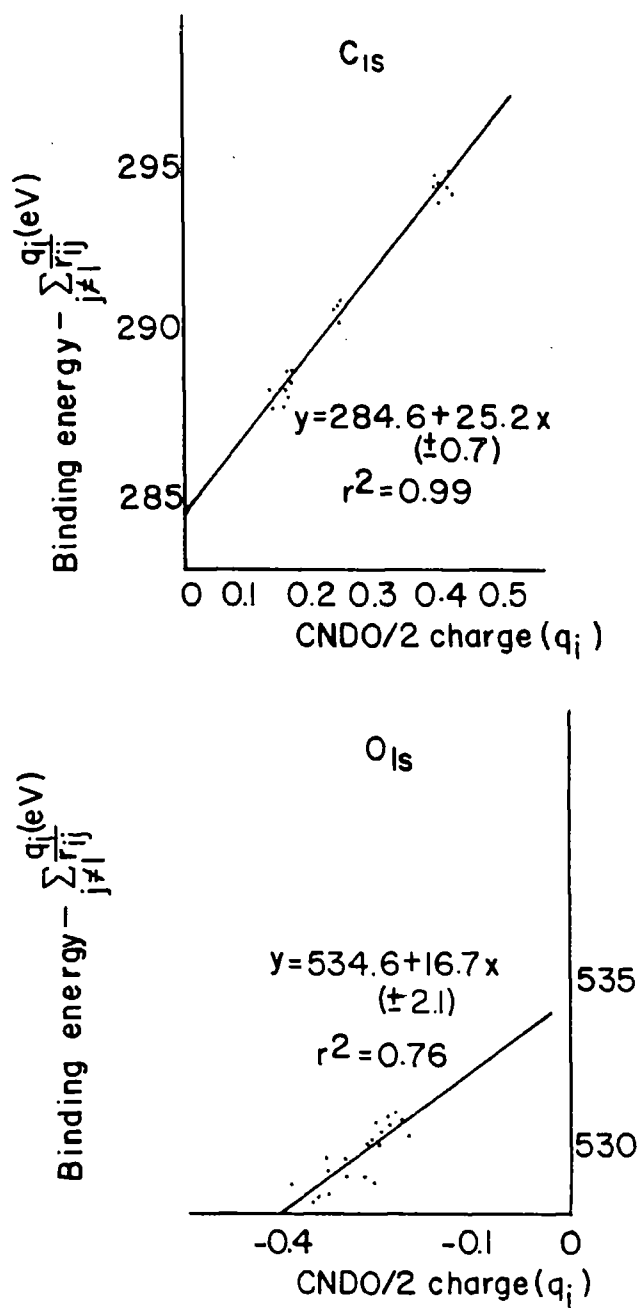


FIGURE 1.8

Charge potential correlations for the C_{1s} and O_{1s} levels of model compounds

densities are only crude guides to the electron density about an atom. Nevertheless, the idea of charge distributions in molecules, within its limitations, is a useful concept.

Charge Potential Model

C_{1s} levels

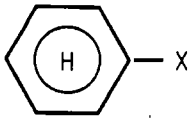
Series	k
	24.6
Alcohols, Ethers, Esters and Carbonyl compounds	25.2
$\underline{C}Cl_3-X, \underline{C}Cl_2 H-X$	28.7
$\underline{C}H_3 \underline{C}OX$	25.0
Aromatics perhydro perfluoro	25.0
Six membered ring heterocycles per H per F per Cl	22.4
Fluorobenzenes	23.5
Five membered ring heterocycles	25.4

FIGURE 1.9

Values of k appropriate to selected series of organic molecules

Inversion of the Charge Potential Model

The uses of the charge potential model in studies of structure and bonding in organic molecules is illustrated in Fig. 1.10. Starting

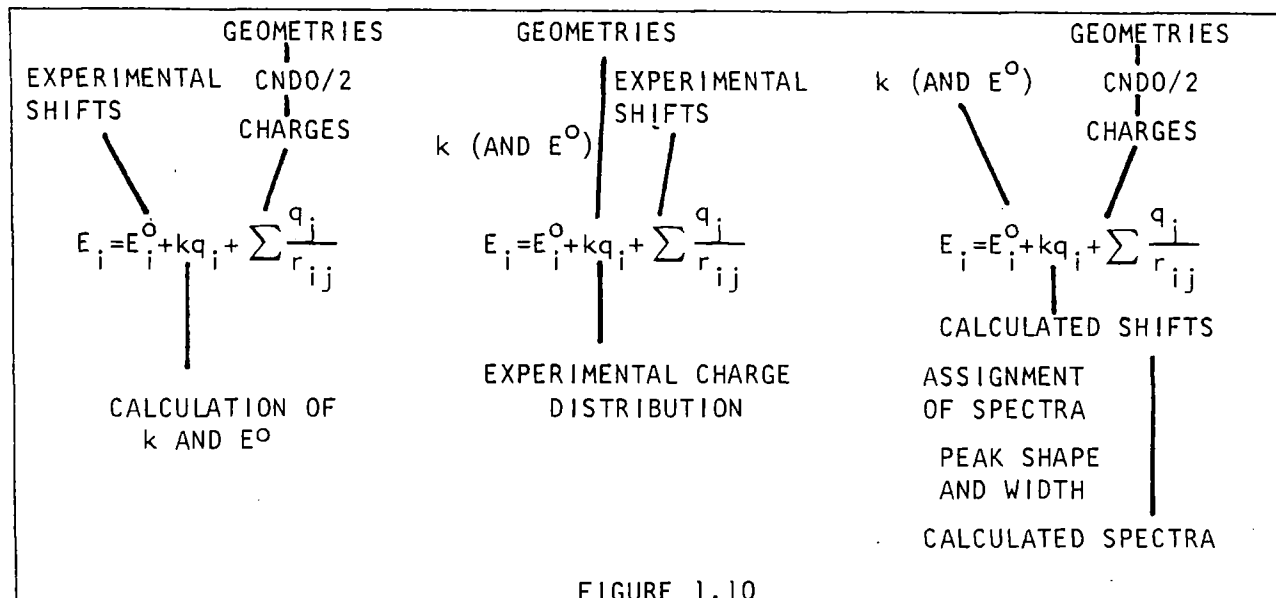
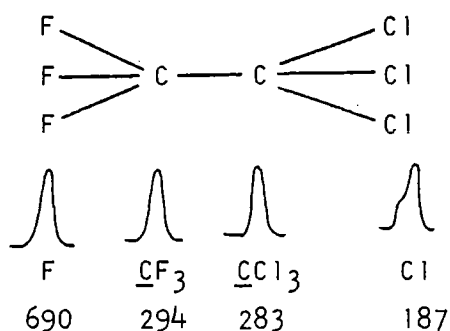


FIGURE 1.10

Uses of the charge potential model in studies of structure and bonding in organic molecules

on the left hand side, if we have geometries and appropriate charge distributions (e.g. CNDO/2), we may use the experimental shifts to obtain values of k and E° for a given level of a given element.

We are now in a position to invert the charge potential model by feeding in the geometry, appropriate values of k and E° (as determined from studies on related systems), the measured BE's may be used to obtain 'experimental' charge distributions. An example is shown in Fig. 1.11 on the application of the inverted model to a simple halocarbon.



Experimentally Determined	Known	Required
E^F	E_o^F k^F	q^F
E^{CF_3}	E_o^C k^C	q^{CF_3}
E^{CCl_3}	E_o^{Cl} k^{Cl}	q^{CCl_3}
E^{Cl}	Molecular Geometry (e.g. bond angles and lengths)	q^{Cl}

FIGURE 1.11

Application of the inverted charge potential model to simple hydrocarbon

Schematically the equations for F_{1s} , C_{1s} , and Cl_{2p} levels are as follows

$$\begin{array}{l}
 E_{1s} \quad E^F \\
 \vdots \\
 \vdots
 \end{array}
 = E_o^F + k^F q_F + \frac{2q_F}{r_{C-F}} + \frac{3q_{Cl}}{r_{FCl}} + \frac{q_{CF_3}}{r_{F-CF_3}} + \frac{q_{CCl_3}}{r_{F-CCl_3}} \quad (1.19)$$

$$\begin{array}{c} \vdots \\ \underline{C1s} E_{CF_3}^C = E_O^C + kq_{CF_3} + \frac{3q_F}{r_{C-F}} + \frac{3q_{C1}}{r_{C-C1}} + \frac{q_{CC13}}{r_{C-C}} \end{array} \quad (1.20)$$

$$\begin{array}{c} \vdots \\ \underline{C12p} E^{C1} = E_O^{C1} + kq_{C1} + \frac{3q_F}{r_{C1-F}} + \frac{2q_{C1}}{r_{C1-C1}} + \frac{q_{CF3}}{r_{C1-C1}} + \frac{q_{CC13}}{r_{C1-C2}} \end{array} \quad (1.21)$$

$$\begin{array}{c} \vdots \\ \text{Also } 3q_F + 3q_{C1} + q_{CF_3} + q_{CC13} = 0 \end{array}$$

A thorough discussion on the application of the charge potential model to predict absolute binding energies in polymeric systems by the use of CNDO/2 SCF MO calculations is presented in Chapter 3.

e) Fine Structure

1) Multiplet Splitting

The chemical shifts in binding energies discussed in previous sections can be attributed to differences in the electronic environments of the relevant atoms. Multiplet splittings on the other hand arises for paramagnetic systems and indeed the phenomenon of multiplet splittings accompanying core ionization was predicted for transition metal ions by Watson and Freeman⁷¹ (in advance of the experimental observations by Fadley and co-workers)⁷² for the 3s level in some fluorides and oxides of manganese and iron which contain unpaired 3d electrons. The interpretation is relatively straightforward only for s-hole states. The following discussion considers s-hole states and is based on van Vleck's vector coupling model which was originally conceived for atoms⁷³. This gives the following results for s-hole states where S is the total spin of the 1ⁿ configuration in the ground state. The two possible final states have a total spin of S[±] 1/2. The splitting ΔE (i.e. the energy difference between the states S + 1/2 and S - 1/2) is proportional to the multiplicity of the ground state

$$\Delta E = (2S + 1)K$$

where K is the exchange integral between the core (c) and valence (v) electrons under consideration and is defined by

$$K = \langle \phi_v(1) \phi_c(2) \left| \frac{1}{r_{12}} \right| \phi_v(2) \phi_c(1) \rangle \quad (1.22)$$

The intensities of the peaks are proportional to the degeneracies of the final spin states

$$\text{i.e. } (2(S + 1/2)+1) : (2(S-1/2)+1) = (2S+2) : 2S \quad (1.23)$$

The magnitudes of multiplet splittings are independent of sample charging effects and reference level. Multiplet splittings in photoelectron spectra have recently been discussed in some detail by Fadley⁷⁴. The magnitude of the splitting for a given ion (or atom) can give valuable information concerning the localization or delocalization of the unpaired valence electrons in compounds^{18,75,76} since the greater the spin density on an atom the greater the splitting. If the total population of unpaired electrons can be assigned among the atoms with a fraction f_i assigned to the i^{th} atom, then the multiplet splitting on the i^{th} atom ΔE^i is approximated by⁷⁵.

$$\Delta E = f_i (2S + 1) K_i. \quad (1.24)$$

A simple example is provided by Siegbahn¹⁹ on NO and O₂. In their study on N₂, NO and O₂ molecules in the gas phase, they found that the N₂ molecule did not possess core level splitting since the core level (1s) after photoemission was degenerate with respect to spin. Whereby NO and O₂ core levels were split, e.g. upon photoemission from a core level in oxygen or nitrogen in NO the molecular ion NO⁺ was left in either a triplet or singlet state respectively. The splitting observed in the 1s spectrum can be attributed to the exchange interaction between the core electrons and the two unpaired 2π electrons having different energies. The O₂ molecule has a similar molecular orbital structure, but has two unpaired electrons in its outer π-type orbital. Figure 1.12a describes the orbital levels in N₂, NO and O₂ and Figure 1.12b the ESCA 1s levels of the molecules.

2) Spin-Orbital Splitting

If photoionization occurs from an orbital which has an orbital quantum number (l) greater than 1 (i.e. p, d and f) then a doublet structure is observed in the ESCA spectrum¹⁸. This doublet occurs from a coupling of the two magnetic moments of the spin

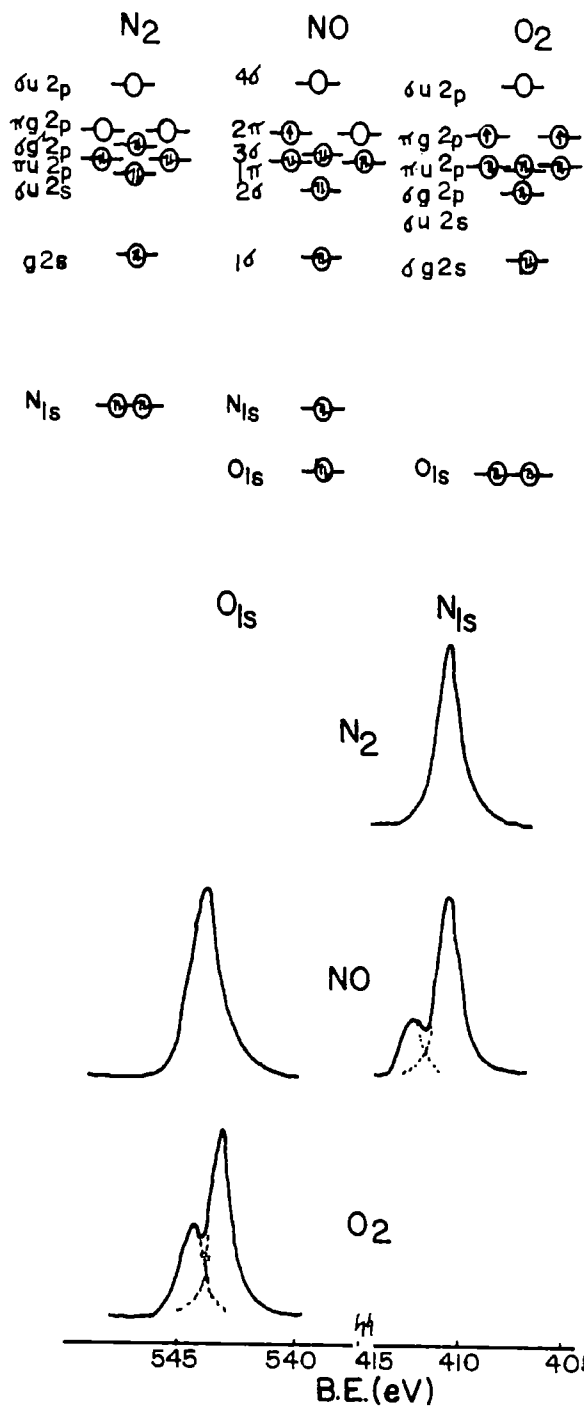


FIGURE 1.12

Diagram of orbital levels in N₂, NO and O₂

(S) and the orbital angular momenta (L) of the electrons to yield a total momenta (J). When spin-orbit coupling is weak, compared to electrostatic interactions, the orbital angular momenta will couple to give a resultant L instead of coupling to the spin angular momenta. A system of coupling where all the individual spin momenta (S) are coupled, and all the individual orbital momenta (L) are coupled and the resulting momenta coupled is known as a Russell-Saunders coupling scheme ($L + S = J$)⁷⁷. The other case where spin-orbit coupling energy is large with respect to the electrostatic energy is the orbital and spin momenta of the individual electrons will couple into a resultant j_1 or j_2 . The coupling of the j_1 and j_2 with electrostatic interaction will yield a final J. This situation where orbital and spin momenta are individually coupled and the resultants coupled is known as the jj couple scheme⁷⁷.

It can be shown that the Russell-Saunders coupling scheme dominates for the lighter elements, up to approximately the lanthanides, and the jj coupling scheme for the heavier elements⁷⁸.

The hamiltonian operator for the spin-orbit interaction may be written

$$\hat{H}_{so} = \xi(r) \hat{s} \hat{l} \quad (1.25)$$

$$\xi(r) = - (e/2m^2c^2) \left(\frac{1}{r} \frac{dV}{dr} \right) \quad (1.26)$$

The radial average of $\xi(r)\hbar^2$ is a useful quantity and is called the spin-orbit coupling constant, ζ_{ni} :

$$\hbar^2 \zeta_{ni} = \langle nlm | \xi(r) | nlm \rangle \quad (1.27)$$

The intensities of the signals in the doublet structure observed are proportional to the ratio of the degeneracies of the states which is quantum mechanically defined by the $(2J + 1)$ rule.

The relative signal intensities of the J states for the s, p, d and f levels are shown in Table 1.8.

In Fig. 1.13 examples of the $s(C_{1s})$, $p(Cl_{2p})$, $d(Ag_{3d})$ and $f(Au_{4f})$ levels are shown as observed in the ESCA experiment.

Table 1.8
Intensity Ratios for Different Levels

Orbital quantum number	Total quantum number $J = (l \pm s)$	Intensity Ratio $(2J + 1)/(2J + 1)$
s	1/2	No splitting
p	1/2 3/2	1:2
d	3/2 5/2	2:3
f	5/2 7/2	3:4

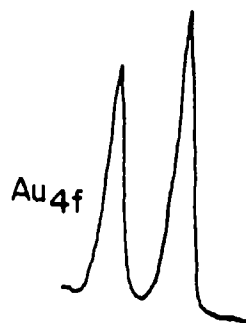
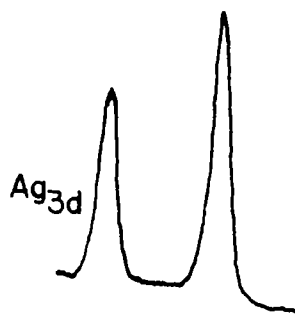
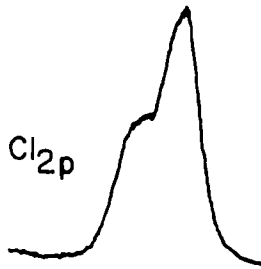
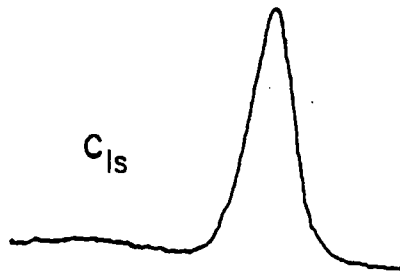


FIGURE 1.13

Examples of spin-orbit splitting in the p, d and f levels

Table 1.8
Intensity Ratios for Different Levels

Orbital quantum number	Total quantum number $J = (l \pm s)$	Intensity Ratio $(2J + 1)/(2J + 1)$
s	1/2	No splitting
p	1/2 3/2	1:2
d	3/2 5/2	2:3
f	5/2 7/2	3:4

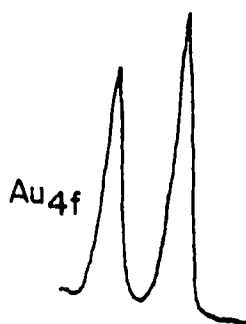
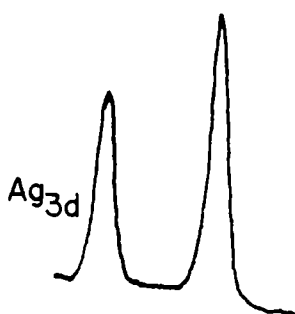
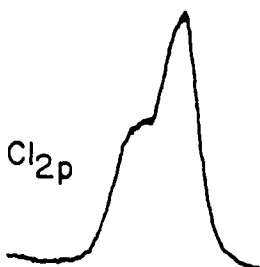
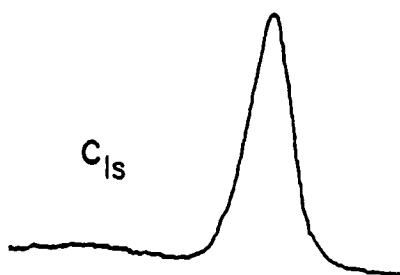


FIGURE 1.13

Examples of spin-orbit splitting in the p, d and f levels

Table 1.8
Intensity Ratios for Different Levels

Orbital quantum number	Total quantum number $J = (l \pm s)$	Intensity Ratio $(2J + 1)/(2J + 1)$
s	0	No splitting
p	$1/2$ $3/2$	1:2
d	$3/2$ $5/2$	2:3
f	$5/2$ $7/2$	3:4

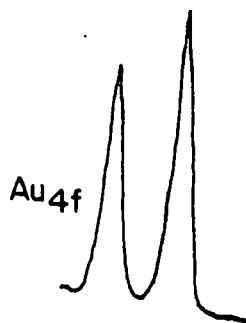
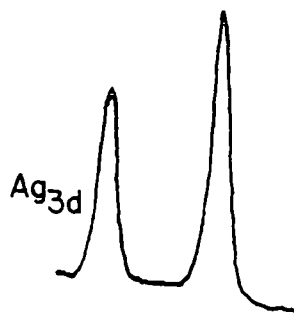
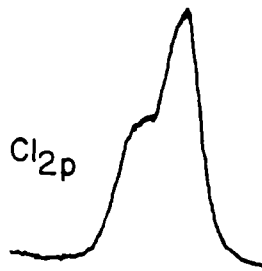
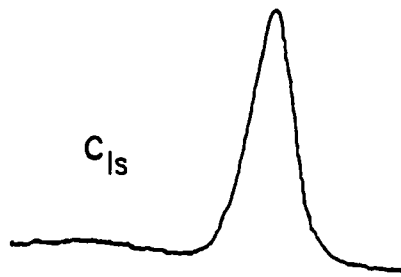


FIGURE 1.13

Examples of spin-orbit splitting in the p, d and f levels

3) Electrostatic Splitting

Splittings in the $5p_{3/2}$ levels of uranium (Fig 1.14) and

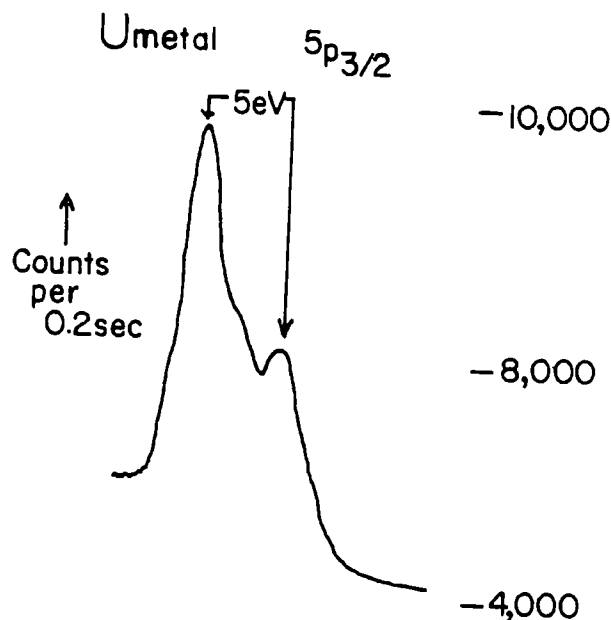


FIGURE 1.14

Electrostatic splitting in the $5p_{3/2}$ levels of U metal

thorium metals and their compounds, and in some compounds of gold have been observed^{79, 80}. These were interpreted as arising from the differential interaction of the internal electrostatic field with the $M = \pm 1/2$ and $M = \pm 3/2$ sub-states of the $5p_{3/2}$ electrons, and a definite correlation was found between this type of splitting obtained by photoelectron spectroscopy, and the quadropole splittings obtained from Mossbauer spectroscopy⁸¹ which arise from the interaction of the nuclear quadropole moment with an inhomogenous electric field. Novakov⁸² has also observed the known 2 eV crystal field splitting of the valence 3d levels in CoSO_4 in ESCA spectra and crystal field splittings should be observable in other systems⁸³.

Electrostatic splitting was also observed by Bancroft and co-workers⁸⁴ on nonconducting organometallic tin compounds in the solid phase. There was a general trend observed between the Sn_{3d} linewidths and the ^{119}Sn nuclear quadropole splitting as

measured by Mossbauer spectroscopy for both solid and gas phase samples. Their computations indicated that the ESCA linewidth was a very insensitive measure of any splitting; with the Mg anode used, where an increase in linewidth of 0.15 eV corresponded to an actual splitting of the $3d_{3/2}$ level of $\sim .4$ eV. With the use of a narrower linewidth source, say $\sim .2$ eV, the overall splitting in the Sn3d widths would be ~ 0.7 eV.

In this work presented in this thesis on polymeric materials, since only 1st and 2nd row elements are incorporated in the system, there will be no electrostatic phenomena observed in the ESCA spectra.

A summary of the types of splitting phenomena observed in ESCA is shown in Fig. 1.15.

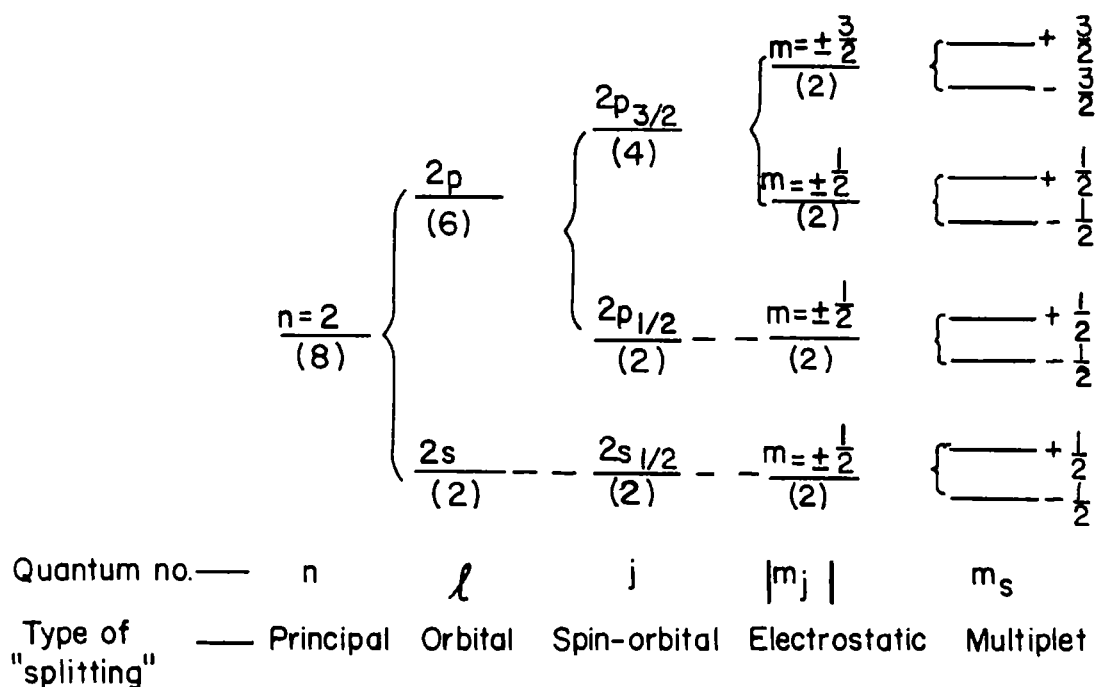


FIGURE 1.15

Summary of types of splitting phenomena observed in ESCA

4) Valence Levels

Information concerning structure and bonding can be largely inferred from shifts in core binding energies which reflect differences in valence electron distributions. The direct investigation of the valence levels in polymers is also relevant to the detailed interpretation of the electrical properties of the material.

The valence energy levels of simple molecules have been extensively studied in the gas phase by low energy photoelectron spectroscopy²⁵. The inherent widths of the exciting radiations which are most commonly used, He(I) and He(II) (photon energies ≈ 21 eV and ≈ 40 eV respectively) are such that in favorable cases vibrational progressions may be resolved which considerably aids assignment. Although the development of ultraviolet photoelectron spectroscopy, (UPS) as the technique has come to be known, has primarily been in the hands of chemists, the application to the study of the valence bands of solids has primarily been the province of the physicist (the technique often being referred to as u.v. photoemission) and has dealt mainly with metals studied as evaporated films under UHV conditions. The study of the valence bands of polymers by UPS is still in its infancy, primarily due to experimental difficulties.

In the case of simple molecules, the study of the valence energy levels by ESCA has two distinct disadvantages compared with the corresponding UPS measurements. (It should be emphasized however, that comparison between the two is very valuable since differential changes in cross sections with photon energy are useful for assigning the symmetries of occupied orbitals.) Firstly, cross sections for photoionization are generally lower than for the longer wavelength photon sources used in UPS, and secondly, the resolution is much poorer, (viz. photon linewidths He(I) ≈ 5 meV²⁵, MgK $\alpha_{1,2}$ ≈ 800 meV¹⁸). A typical spectrum of the carbon monoxide valence levels observed by He(I) and monochromatized ALK $\alpha_{1,2}$ radiation sources respectively, is shown in Fig. 1.16

In studying involative materials such as polymers however, these disadvantages are considerably offset. Thus, since there are so many vibrational modes possible, resolution of ESCA valence signals becomes less of a problem since even with a He(I) source only broad unresolved bands are obtained.

There are three obvious advantages of employing X-ray compared with U.V. photon sources in the study of valence levels in the solid state.

Firstly, with a low energy photon source, not all of the valence energy levels may be studied, only the higher occupied

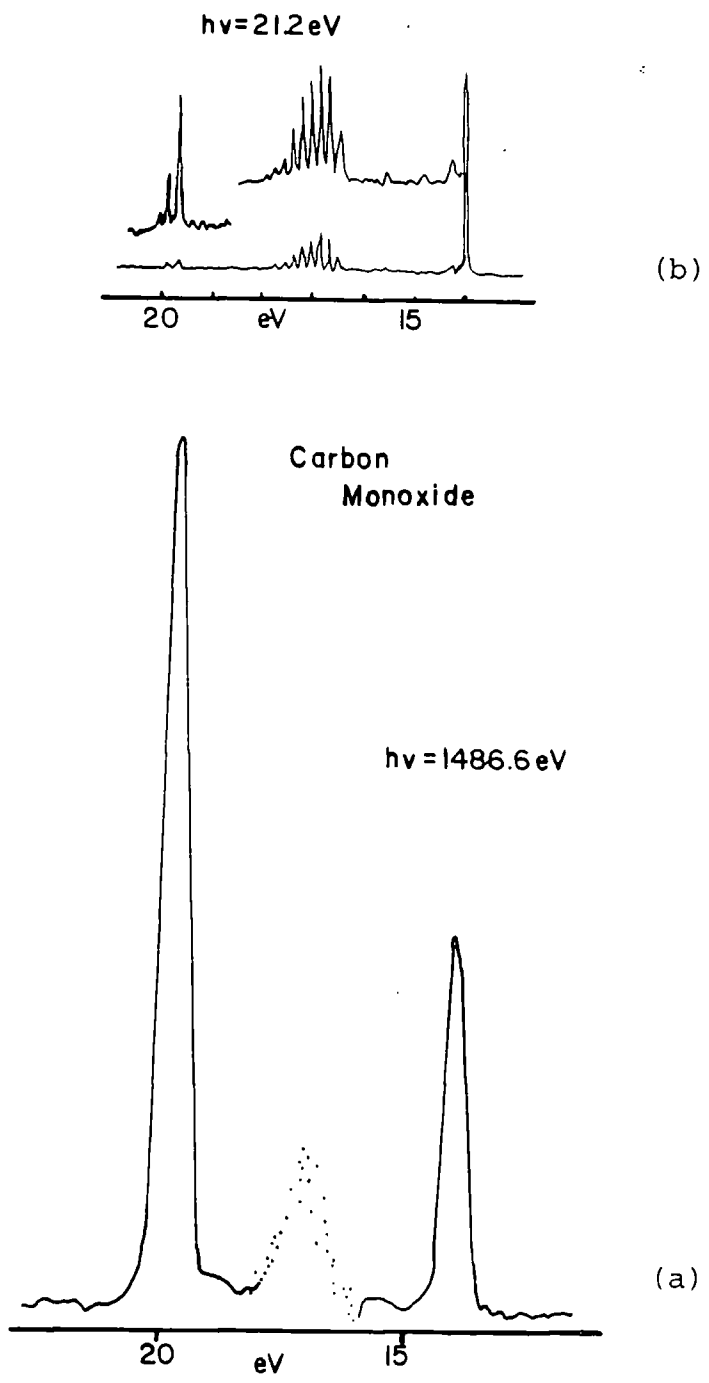


FIGURE 1.16
Typical spectrum of CO valence levels observed by
He(I) and AL_{Kd1,2} sources

levels. Secondly, since the kinetic energy range for electrons will typically be in the range 0-21 eV (HeI), 0-40 eV (HeII) it will become clear in a subsequent section that this is a region of rapidly varying mean free paths for the photoemitted electrons. This

causes difficulties in interpreting the UPS data, whereas this difficulty does not arise in ESCA since the electron mean free paths are virtually constant across the valence band. Thirdly, in studying metals the use of a high-energy photon source also minimizes the modulation arising from final state effects and hence gives a close experimental measure of the density of states.

Typical data which may be obtained is shown in Fig. 1.17

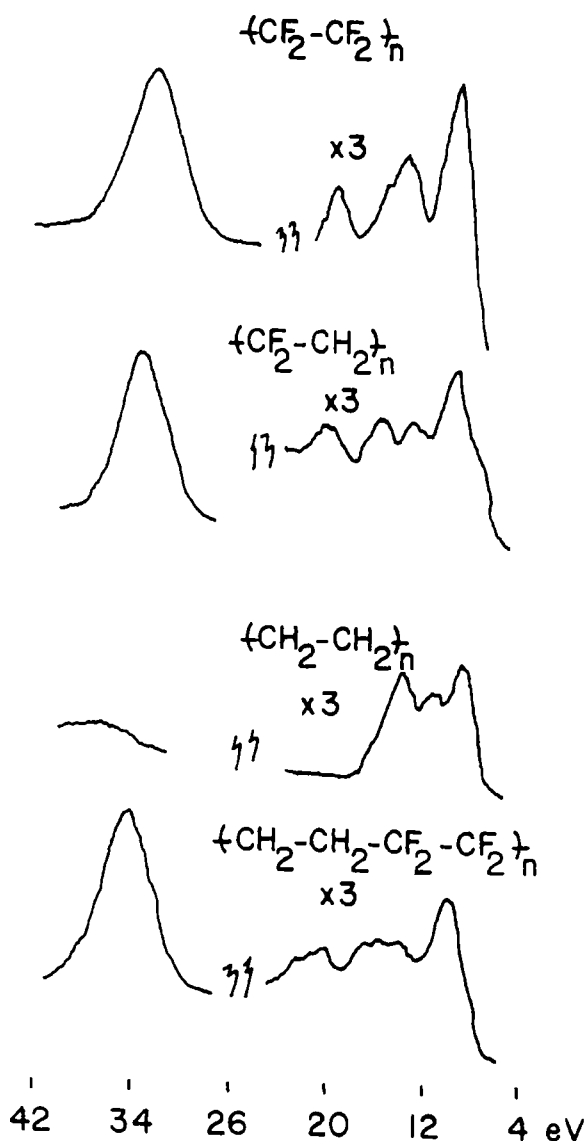


FIGURE 1.17

Typical valence band spectra for simple polymers of polyethylene, polyvinylidene fluoride and polytetrafluoroethylene

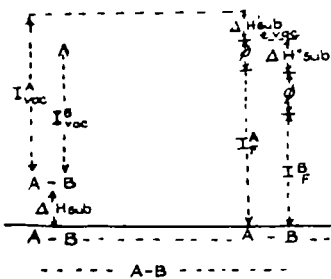
for PTFE, polyvinylidene fluoride, and polyethylene. The theoretical interpretation of the valence band structure is not as straightforward as that of core levels¹. The particular case of polyethylene has received considerable attention and has recently been discussed in detail^{85,86}. For the spectra shown in Fig. 1.17 a reasonable assignment can be made as follows. The large peak at highest binding energy clearly evident in the fluorinated polymers arises from molecular orbitals essentially F_{2s} in character. The prominent peak at lowest binding energy for PTFE which is also clearly evident in polyvinylidene fluoride is assigned to M.O.'s corresponding essentially to fluorine 2p lone pairs. The shoulder at lower binding energy in polyvinylidene fluoride which has its counterpart in polyethylene may then be assigned to carbon hydrogen bonding orbitals (essentially $C_{2p}H_{1s}$). The assignments for the remaining peaks are then essentially C-F and C-C (2s) bonding orbitals. With an appropriate correction for work function (≈ 5 eV) the binding energies correspond to those obtained from UPS studies of simple systems containing the essential structural features²⁵.

For comparison purposes the valence band for the ethylene-tetrafluoroethylene of composition close to 50-50 is also included. This bears a striking resemblance to that for polyvinylidene fluoride as one might expect on the basis of its largely alternating structure.

A number of recent publications on the band structure of polymers has appeared over the past few years and include wave-mechanical studies on polyethylenes and fluoroethylenes correlated with ESCA chemical shifts⁸⁵⁻⁸⁹.

f) Energy Referencing

Theoretical calculations inevitably refer to isolated molecules in the gas phase with the vacuum level as energy reference. The measurements, on the other hand, refer to the condensed phase with the Fermi level as energy reference. The question then arises, under what circumstance will the direct comparison of the two be valid? For covalent solids in which there are no appreciable long range interactions (such as hydrogen bonding for example) the comparison is most readily seen from an appropriate Born cycle and the associated equations schematically presented in Fig. 1.18. The terms are largely self explanatory and it



For organic molecules
Typical values

$$I^{cis} \sim 290 \text{ eV}$$

$$\phi^{vac} \sim 5 \text{ eV}$$

$$\Delta H_{sub} \sim 0.5 \text{ eV}$$

Shift in BE

$$\Delta = (I_A - I_B)_{vac} = (I_A - I_B)_F + (\Delta H_{sub}^0 = \Delta H_{sub}^{''})$$

Shift in BE for different samples

$$\Delta = (I_A - I_X)_{vac} = (I_A - I_X)_F + (\phi_A - \phi_X) + (\delta_A - \delta_X) + (\Delta H_X - \Delta H_A) + (\Delta H_A^i - \Delta H_X^i)$$

For closely related materials in contact with spectrometer

$$(\phi_A - \phi_X) \approx 0$$

$$(\delta_A - \delta_X) = 0$$

$$(\Delta H_X - \Delta H_A) + (\Delta H_A^i - \Delta H_X^i) \approx 0$$

$$(I_A - I_X)_{vac} \equiv (I_A - I_X)_F$$

∴ can understand shifts in terms of isolated molecules (excluding strong intermolecular interactions e.g. H bonding)

FIGURE 1.18

Relationship between energy levels of gaseous and solid samples

can be seen that if the work function of the samples are closely similar and if there is no sample charging then the comparison between theoretical calculations on isolated molecules and measurements on thin films should be valid.

For samples studied as solids, three situations may clearly be distinguished. In the first the sample is in electrical contact with the spectrometer. This is usually the case for thin films deposited in-situ on a conducting substrate in the spectrometer source. Since the

path length for the incident X-ray beam is very large¹⁸, $\approx 10,000\text{\AA}$, depending on the conditions, it is possible for films of the order of 1000\AA , to have sufficient charge carriers to remain in electrical contact with the spectrometer. This can most readily be shown to be the case by applying a D.C. bias voltage to the sample probe. If the sample is in electrical contact the apparent shift in energy scale will exactly follow the magnitude of the D.C. bias. The application of a significant negative voltage to the samples will shift the position of the true zero of the kinetic energy scale and the secondary electron energy distribution (SEED) can then be observed, since the electrons near zero kinetic energy without biasing now have enough kinetic energy to overcome the surface potential barrier due to the photoelectron flux*. Ascarelli and Missoni⁹⁰ have demonstrated that the determination of the sample vacuum level for direct energy referencing can be accomplished by this technique. If the sample has been deposited on a substrate such as gold, and is in electrical contact it is possible to measure the core levels of the sample whilst monitoring the $\text{Au}_{4f7/2}$ core level (84 eV) and this provides a very convenient means of energy referencing¹.

The second situation which arises is for thick insulating samples. Thus it is often convenient to study samples mounted on double sided 'Scotch' tape either as powders or as discrete films. In this circumstance, there is only a fortuitous possibility that the sample will be in electrical contact with the spectrometer and in general it will be 'floating' at some potential due to surface charging and indeed this charging process may be time dependent. If care is taken in the measurements, the charge built up on a sample and its time dependence may be used to investigate electrical and chemical characteristics of samples and a discussion of this particular aspect will be given in a subsequent Chapter (6). The most reliable method of energy referencing for polymers is to follow the slow build of hydrocarbon contamination at the surface. With a base pressure of $\sim 10^{-8}$ torr the partial pressure of extraneous hydrocarbon material is such that taken in conjunction with the low sticking coefficient for most organic and polymeric

* This topic (sample charging) will be discussed in detail in Chapter 6.

systems it normally takes several hours before any signal arising from hydrocarbon (binding energy 285 eV*) is apparent¹⁸. It is, of course, possible to deliberately leak in straight, hydrocarbon material to follow the build up at the surface. Such material almost always goes down in uniform coverage and at submonolayer coverage acquires the same surface potential as the sample⁹¹.

(A short investigation into the origin of the hydrocarbon contamination encountered during analysis of samples by ESCA has revealed that the major contribution arises from the cap covering the standard X-ray gun. The cap was found to become relatively hot and a method of cooling the cap, which results in the substantial reduction of the rate of build-up of hydrocarbon on samples is described in detail in Chapter 3.)

This is not necessarily the situation with regard to metals deposited on the surface since there is a marked tendency for gold (the common reference metal) vapor that is deposited onto a polymer surface to proceed, initially, by way of a nucleation process which results in islands of electrically isolated gold on the surface⁹². Although, generally speaking, the gold islands follow the surface charge and do not react with the polymer, exceptions to both cases have been documented in the literature. Betteridge and co-workers⁹³ have shown that in some particular systems the width and position of the gold signals can change with time, temperature and substrate material and Ginnard and Riggs⁹⁴ have demonstrated that for gold vapor deposited on polyethylene and polytetrafluoroethylene the absolute shift for the gold signal increases as the gold layer increases in thickness, probably due, (as will be discussed later in Chapter 6) to the higher photoelectron flux from the gold, a phenomenon referred to as differential sample charging. In addition, since gold is normally evaporated from a filament the possibility of surface damage, reaction or evaporation of substrate during deposition cannot be discounted. The use of the so-called 'gold decoration' technique is, therefore, not recommended for organic and polymeric materials⁹⁵. Since the factors which determine both absolute and relative binding energies of core levels may be shown to be very short range in nature¹, it is often possible to study smaller molecules which contain the

*This must, of course, be independently established for a given spectrometer. It almost certainly arises from long chain hydrocarbon material.

appropriate structural features as thin films in electrical contact with the spectrometer which may be straightforwardly referenced. Comparison may then be drawn between this model and the insulating sample in question and thus allow direct correction for sample charging. A further possibility which has received considerable attention of recent years is the use of electron 'flood guns'⁹⁶; the prime motivation being the very large sample charging for thick insulating samples in spectrometers employing monochromatic X-ray sources. The removal of bremsstrahlung as a source of secondaries can lead to shifts in the kinetic energy scale in the hundred eV range and can be compensated by flooding the sample with low energy electrons. Samples can become negatively charged, however, and the method needs great care to achieve an accuracy comparable with that for the other methods. An alternative source of low energy electrons is to illuminate the sample region with U.V. radiation from a low pressure, low power mercury lamp via a quartz viewing port in the source region of the spectrometer⁹⁵. Sufficient secondaries are generated from photoemission from the metal surfaces that sample charging is reduced to a low level.

The third situation which can arise is for thick films ~ 1 micron which have been built up by deposition on a conducting substrate. Such films behave as 'leaky' capacitors in that they exhibit rather striking time dependent charging and discharging characteristics and follow an applied bias potential in a particular manner^{cf. 95, 97}. Since the dynamic equilibrium which is established under X-ray irradiation invariably produces an overall positive charge on the sample, the application of a positive bias voltage causes a smaller shift in the kinetic energy scale than the applied voltage whereas a negative bias voltage produces a larger shift in the kinetic energy scale than the applied voltage. From a study of these effects and from the secondary electron distribution the energy referencing may readily be established. The investigation of such effects as a function of the film thickness in the range 1 - 100 micron provides an interesting insight into the electrical characteristics of polymer samples and the typical behavior which is observed is shown in Fig. 1.19⁹⁷.

The energy reference in each case for the measurements described above is the Fermi level and although the exact location of this level in relation to the valence and conduction bands is generally unknown for polymers, under the conditions of X-ray irradiation it is possible

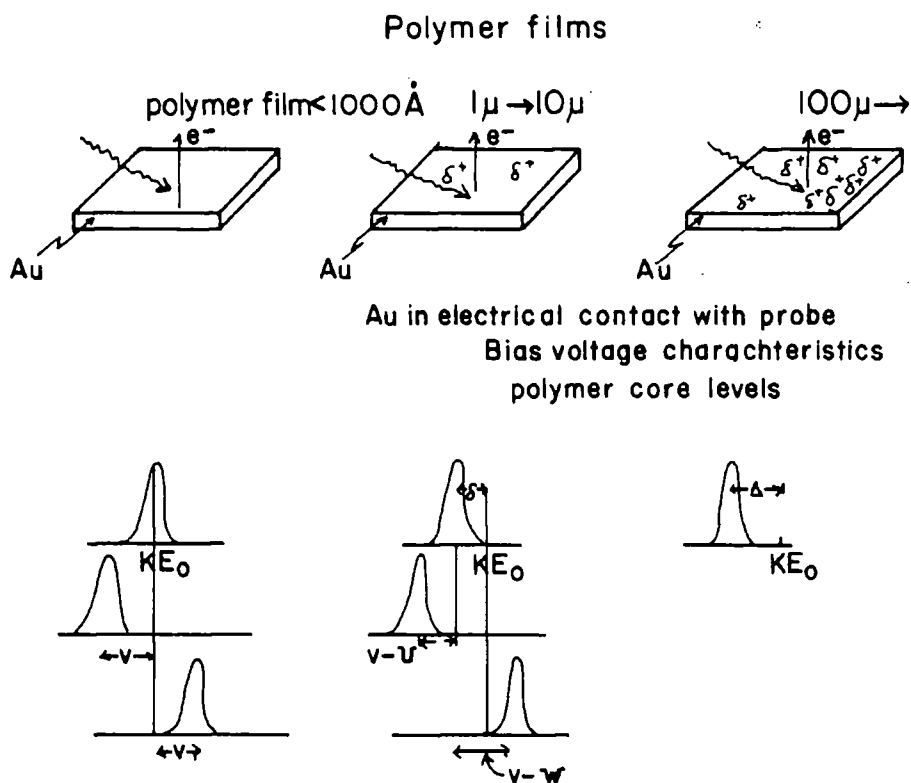


FIGURE 1.19

Typical sample charging characteristics for polymer films

for an 'insulator' to be in electrical contact with the spectrometer i.e. their Fermi level are the same¹. Despite the difficulties associated with defining an analytical expression for the Fermi level of an insulator, the use of the Fermi level as energy reference is operationally convenient. If the work function of the insulator is known we may calculate the binding energy with respect to the vacuum level.

Although sample charging has been widely regarded as somewhat of a nuisance which must be circumvented, the study of sample charging is of interest in its own right. Thus the study of the phenomena provides an interesting means of studying photoconductivity in polymeric films and will be discussed in detail in Chapter 6 on surface charging phenomena.

g) Signal Intensities

For an 'infinitely' thick homogeneous sample the intensity of the elastic (no-energy loss) peak for photoemission from a core level, i , may be expressed as equation^{98,99}

$$dI_i = F\alpha_i N_i k_i e^{-x/\lambda_i} dx \quad (1.13)$$

where: I_i is the intensity arising from core level, i

F is the X-ray flux, essentially unattenuated over the sampling depth

α_i is the cross section for photoionization of core level i

N_i is the number of atoms per unit volume on which the core level, i , is localized

k_i is a spectrometer factor

λ_i is the electron mean free path

This equation may be recast into the integrated form

$$I_i = \int_0^{\infty} F\alpha_i N_i k_i e^{-x/\lambda_i} dx \quad (1.14)$$

$$= F\alpha_i N_i k_i \lambda_i \quad (1.15)$$

For a full understanding of the factors governing the intensity of a given signal in ESCA, it is important to discuss them individually and to elaborate on the parameters on which they themselves are dependent.

Fig. 1.20 shows a schematic of the general geometry of the ESCA experiment

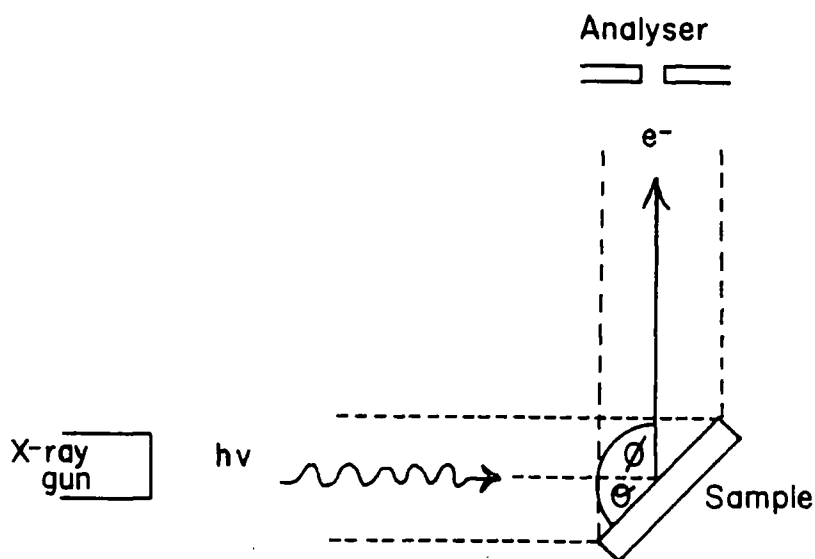


FIGURE 1.20

Schematic of the geometry of the ESCA experiment in the AEI ES 200 B instrument

using the Mg anode with a flat solid sample. $h\nu$ represents the incident X-rays and e^- the fraction of the photoemitted electrons which enter the analyzer. ϕ is the angle between the X-ray source and the analyzer entrance slit and θ describes the angle of the sample in relation to the analyzer. Low values of θ ($\sim 0^\circ$) correspond to grazing incidence of the X-rays and high values of θ ($\sim 90^\circ$) correspond to grazing exit from the sample of the photoemitted electrons which are analyzed. (It should be noted here that Fig. 1.20 describes only the relative positions of the sample to the photon source and analyzer when the Mg anode is used. The monochromatic AL source is not at an angle of 90° to the analyzer slits but at an angle of 60° . Although the angle ϕ is reduced, θ corresponds to the angle of the sample with respect to the analyzer slits and remains defined as such with either anode.) These parameters will be referred to in the ensuing discussion.

The X-ray flux in the sample, F , is primarily determined by the power applied to and efficiency of the X-ray gun. At low values of θ it has been shown, theoretically and experimentally by Henke^{100,101}, that refraction of collimated X-rays in the outermost surface layers of the sample causes an effective increase in flux in the sampling region as seen by ESCA, resulting in an enhancement of the signal intensity. However, in practice this phenomenon is rarely experienced since samples are seldom optically flat X-ray beams, are not collimated, and the angles, θ , for which this applies are very small, which due to other factors involved in conventional spectrometers results in a very low signal intensity.

The cross section for photoionization of core level, i , σ_i is a parameter which describes the probability of the core level being ionized when irradiated by a photon¹⁰², but only includes the fraction of the total number of electrons photoemitted within the angle of acceptance of the analyzer focussing lens. σ_i is a function of the core level to which it relates and of the energy of the incident photon. σ_i may be calculated from the fundamental properties of the atom^{102,103} or determined experimentally from gas phase ESCA experiments¹⁹. The radial distribution of electrons photoemitted from an atom, however, is not uniform and it has been shown experimentally and theoretically that σ_i is a function of θ (Fig 1.21), the angle of detection with respect to the incident photons⁹⁸. It is well established that the cross section, in the dipole moment approximation, for randomly oriented

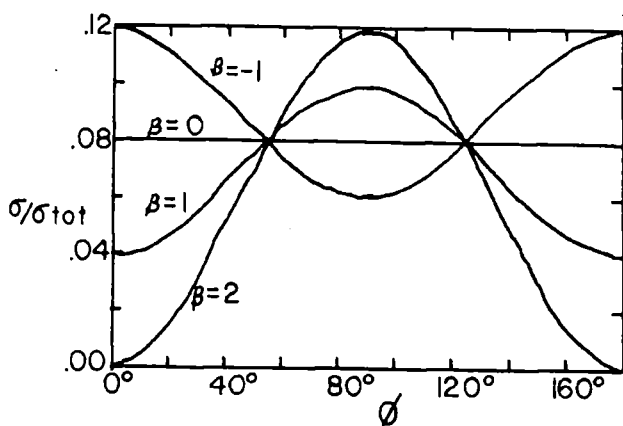


FIGURE 1.21

Plot of σ/σ_{TOT} versus ϕ indicating the asymmetry parameter, β , for the core levels

polyatomic molecules and unpolarized light is of the form¹⁰³;

$$\sigma_i = \sigma_i^{TOT} / 4\pi \left[1 - 1/4\beta_i (3 \cos^2 \phi - 1) \right] \quad (1.16)$$

where β_i is the asymmetry parameter¹⁰⁴ of the core level and σ_i^{TOT} is the total cross section of the level. The angle at which the measured relative σ_i 's are independent of β and equal to $(TOT/4\pi)$ occurs at the so called 'magic angle' of $\phi = \cos^{-1} (1/3) = 54^\circ 44'$ or $125^\circ 16'$ ¹⁰⁴. (It should be noted that for S orbitals $\beta = 0$)

With the use of conventional spectrometers σ_i may be considered as a constant for any given set of experiments employing the same X-ray photon energy since the angle between the X-ray source and the analyzer entrance slit, ϕ , is usually fixed.

With $Mg_{K\alpha_{1,2}}$ and $Al_{K\alpha_{1,2}}$ the cross section for photoionization for

core levels of most elements of the periodic table are within two orders of magnitude of that for the C_{1s} levels, therefore ESCA has a convenient sensitivity range for all elements. The cross sections for core levels are generally considerably higher than for valence levels and this, taken in conjunction with the fact that core orbitals are essentially localized on atoms, and therefore have binding energies characteristic of a given element means that in ESCA the predominant emphasis is on

the study of core levels.

The electron mean free path, (sometimes referred to as the escape depth for the photoemitted electrons), λ_i is defined as the distance in the solid through which the photoemitted electrons will travel before 1/e of them have not suffered energy loss through inelastic collision. Chapter 4 will be concerned with the experimental determination of electron mean free paths for photoemitted electrons in polymers and their usefulness in analytical depth profiling will become apparent throughout this thesis. The main point in this section is that λ_i is a function of the kinetic energy of the photoemitted electron and typically ranges in magnitude from 4 Å for electrons of about 80 eV kinetic energy to 30 Å for electrons of about 1500 eV.

The term 'sampling depth' is often confused with electron mean free path, and the terms in some cases have been used synonymously. To clarify the meanings, however, if the sampling depth is defined as the depth from which 99 % of the signal, arising from a given core level, derives, then it is related to the electron mean free path by;

$$\text{sample depth} = -\lambda \ln 0.01$$

As an example, for carbon 1s levels studied by a Mg_{Kα_{1,2}} X-ray source the kinetic energy of the photoemitted electrons is ≈ 960 eV and the mean free path of the electron is ≈ 15 Å. 50% of the signal seen by ESCA derives from the outermost about 10 Å of the sample and 99% from the outermost 70 Å of the sample.

The final factor to be discussed is the number of atoms per unit volume in the sample on which the core level is localized, N_i . Although N_i is not directly related to the density of the sample it is generally the case that for similar materials of differing density the ESCA signal for a given core level will be more intense for the higher density material (e.g. high density polyethylene vs. low density polyethylene)⁹⁵. The most important consequence of N_i is that the relative signal intensities for the core levels of various atoms in a homogeneous (assuming the surface is representative of the bulk) sample are directly related to the overall stoichiometries of the atoms in the sample, due to the fact that the peak intensity from a given core level is directly proportional to the number per unit volume of the atom in the sample.

$$\frac{I_i}{I_j} = \frac{F\alpha_i N_i k_i \lambda_i}{F\alpha_j N_j k_j \lambda_j} \quad (1.17)$$

where I_i is the signal intensity for core level i and I_j is the signal intensity for the core level j

$$\frac{I_i}{I_j} = \frac{\alpha_i N_i k_i \lambda_i}{\alpha_j N_j k_j \lambda_j} \quad (1.18)$$

If i and j are the same core level in differing chemical environments (e.g. C_{1s} in $\underline{C}H_3 - \underline{C}F_3$) then $k_i \alpha_i \lambda_i = k_j \alpha_j \lambda_j$

and

$$\frac{N_i}{N_j} = \frac{I_i}{I_j} \quad (1.19)$$

If i and j are different core levels then $k_i \alpha_i \lambda_i \neq k_j \alpha_j \lambda_j$ and

$$\frac{N_i}{N_j} = \frac{I_i k_j \alpha_j \lambda_j}{I_j k_i \alpha_i \lambda_i} \quad (1.20)$$

The ratio $\frac{k_j \alpha_j \lambda_j}{k_i \alpha_i \lambda_i}$ may be determined experimentally from standard

samples of known stoichiometry containing i and j . Since k_i and k_j vary from one spectrometer to another and also the angle between the X-ray source and the analyzer, ratios of the type $\frac{k_j \alpha_j \lambda_j}{k_i \alpha_i \lambda_i}$ must be determined for the

particular spectrometer.

As an example, Fig. 1.22 shows the C_{1s} spectrum of polyisopropylacrylate. The signal intensities relative to the total integrated C_{1s} signal are 16.7%, 16.7% and 66.7% for the $\underline{C} = 0$, $\underline{C} - 0$ and $CH C_{1s}$

levels and 28.3% and 28.3% for the $C - \underline{O}$ and $C = \underline{O}$, O_{1s} levels, (not shown). This corresponds to a stoichiometry of 1:1:4:1:1 for these levels respectively since

$$\frac{k_{O_{1s}} \alpha_{O_{1s}} \lambda_{O_{1s}}}{k_{C_{1s}} \alpha_{C_{1s}} \lambda_{C_{1s}}} = 1.67$$

for our particular spectrometer geometry. These stoichiometries are precisely as are found in the polyisopropylacrylate repeat unit.

and a beam which is broader than the width of the sample, w . For the narrow beam the total flux which hits the same is not affected by varying θ within limits. However, for the broader beam the total flux hitting the sample varies as $\omega \sin \theta$ ¹⁰⁵. Therefore, as θ is increased this effect tends to increase the signal intensity. (This effect also applies for the narrow beam when θ is very small). The second effect is concerned with the electrons which are photoemitted in the direction of the analyzer. For a given value of θ the entrance slit of the analyser 'sees' a sample area proportional to $\omega \cos \theta$. Therefore as θ is increased this effect tends to decrease the signal intensity.

The convolution of these two effects, acting in the opposite sense produces an overall function of θ , $f_i(\theta)$ for a core level i , which exhibits a maximum value. This maximum value occurs at a value of θ which is dependent on the core level under investigation, although this phenomena is not clearly understood.

Equation 1.15 therefore may be replaced by equation

$$I_i = f_i(\theta) F \alpha_i N_i k_i \lambda_i \quad (1.21)$$

where $f_i(\theta)$ can be determined empirically¹⁰⁵. Investigations of these angular phenomena are presented in later Chapters.

h) Line Shape Analysis

The need for line shape analysis arises from the unfavorable ratio of chemical shift to line width ratio which is one of the major weaknesses of ESCA compared to, say, NMR or NQR¹. The dominant contribution to the linewidths with most commercial instrumentation is the inherent width of the polychromatic X-ray source.

The measured linewidths for core levels (after taking into account spin orbit splittings, if these are not resolved) may be expressed as

$$(\Delta E_M)^2 = (\Delta E_X)^2 + (\Delta E_S)^2 + (\Delta E_{C1})^2 \quad (1.22)$$

Where: ΔE_M is the measured width at half height, the so called full width at half maximum (FWHM).

ΔE_X is the FWHM of the X-ray photon source.

ΔE_S is the contribution to the FWHM due to the spectrometer (i.e. the analyzer aberrations).

ΔE_{C1} is the natural width of the core level under investigation. (For solid samples this takes into account the solid state effects not directly associated with the lifetime of the hole state, but rather with

slightly differing binding energy due to differences in lattice environments.)

The contributions to ΔE_M from ΔE_X for the commonly used photon sources (i.e. Mg and Al) are essentially Lorentzian line shapes. The characteristics for the energy distribution^{cf.105} in Al $_{K\alpha}$ radiation are essentially comprised of four major components lines $\alpha_1, \alpha_2, \alpha_3$ and α_4 with positions relative to the α_1 line of -.42, +9.7 and +11.6 eV respectively, with relative intensities of 100, 50, 10.8 and 5.5. While for Mg $_{K\alpha}$ radiation for the $\alpha_1, \alpha_2, \alpha_3,$ and α_4 the relative positions to α_1 are -.33, +8.4 and +10.2 with relative intensities of 100, 50, 12.8 and 6.9^{cf.106}. The α_3 and α_4 lines being significantly removed from the α_1 and α_2 lines manifest themselves as satellite peaks to the high kinetic energy side of the intense primary photoionization signal in the ESCA spectrum.

The contributions to ΔE_M from ΔE_S are considered to be Gaussian line shapes and are primarily due to analyzer, focusing and detector imperfections. Whereas for the ΔE_{C1} the contributions are Lorentzian and are dependent upon the Auger and X-ray fluorescence processes upon photoionization of a core level.

The convolution of these line shapes produce a hybrid shape with a Gaussian distribution dominating the overall line shape and with Lorentzian character tails. (In Equation (1.22) the terms are added in quadrature due to the fact that Gaussian line shapes dominate the convolution, where as when Lorentzian line shapes dominate the terms are simply added. Siegbahn and co-workers¹⁹ have found by comparison with experimental curves the shape to be

$$y = \exp - \frac{2}{\Delta E_M} \ln 2.1 \times 1. \ln \left[\frac{1 + \ln(1 + 2.1 \times 1 / \Delta E_M)}{\ln(1 + \ln 2)} \right] \quad (1.23)$$

as a good approximation. From this equation it can be shown that the use of either pure Gaussian or Lorentzian shapes introduces only small errors in the relative positions of peaks and the observed unresolved spectra.

The methods for resolving complex line shapes in the ESCA spectrum arising from the convolution of several signals fall into two main categories. The first involves mathematical methods of enhancing the resolution of the spectrum whilst the second involves curve fitting procedures, in either analogue or digital fashion.

Derivative spectroscopy is a technique for obtaining first or higher derivatives of a signal with respect to kinetic energy of the electrons¹⁰⁷⁻¹⁰⁹. Among the advantages are more characteristic spectra of materials for use in quantitative analysis and increased resolution of overlapping signals. Martin¹¹⁰ has shown that for some examples the FWHM was reduced by factors of about three and five for second and fourth order derivatives. For the overlap of two equal bands he showed that the use of the second order derivative was sufficient if they were separated by one half width or more. In a treatment by Smith¹¹¹ both Gaussian and Lorentzian line shapes were considered and the resolution of a symmetric doublet was found to be the same for the normal and first derivative curves, but the second derivative curve showed an improvement in resolution of 1.78 times and 1.35 times for the Lorentzian and Gaussian line shapes, respectively.

The drawbacks are in the fact that the increased resolution must of course be at the expense of another parameter involved in the signal. The statistical accuracy of the derivative spectra is reduced (i.e. the signal/noise ratio is smaller) and the relative intensities of the component signals are for all practical purposes lost. Further errors occur which are inherent in the mathematical approximation used to calculate the derivatives. The most useful feature which applies to ESCA is that the second or fourth derivatives of a spectrum provide information on the number of components making up overall line shape and an approximation to their kinetic energies. This information is often essential for the use of curve fitted procedures, and a recent review on the subject has been published by O'Haver and Green¹¹².

The application of Fourier transform techniques to enhance resolution in ESCA has only appeared recently and is very much still in its infancy. Beatham and Orchard¹⁰⁶ have concluded that the deconvolution of spectra excited by polychromatic radiation can, with data to sufficient quality, yield a virtual resolution approaching that which can be achieved with monochromatized radiation. Since the full potential of this technique has not yet been fully exploited for application to ESCA, and no use of it has been made in this theses, no further discussion will appear, although Fourier transform deconvolution may become important in the near future.

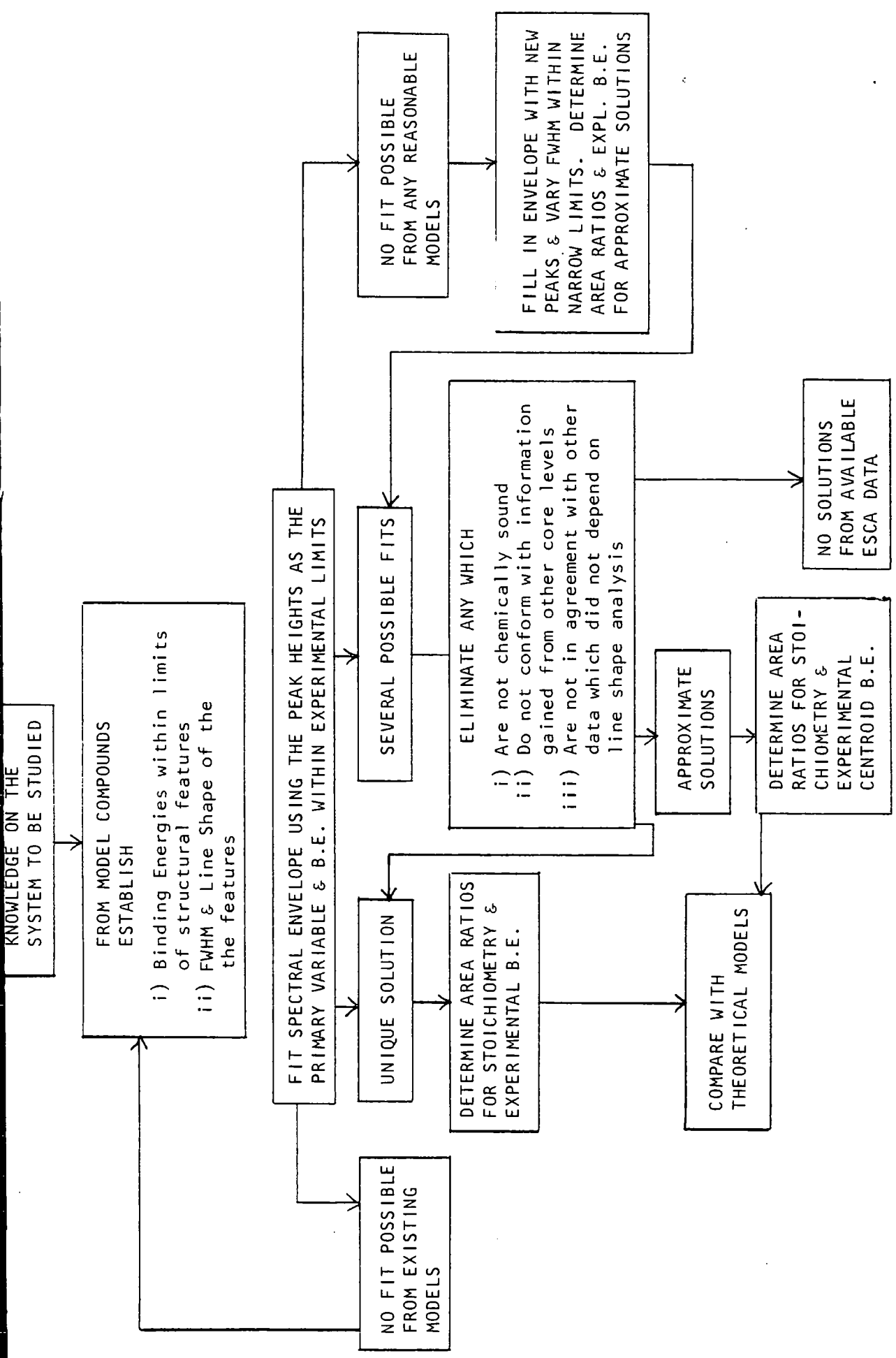


FIGURE 1.24

Block diagram of basic philosophy behind curve fitting technique

The second category for resolving complex line structures involves curve fitting techniques. In general, since one needs to have several variables under close control at any one time an analogue computer analysis is by far more convenient than digital analysis on large computers¹. The basic philosophy behind such an analysis is set out in Figure 1.24.

As examples, consider some separate polymer systems where the 'unique fit' and the 'approximate solutions' apply. Figure 1.25 shows (i) an experimental C_{1s} and Cl_{2p} spectrum of polyvinyl chloride, (ii)

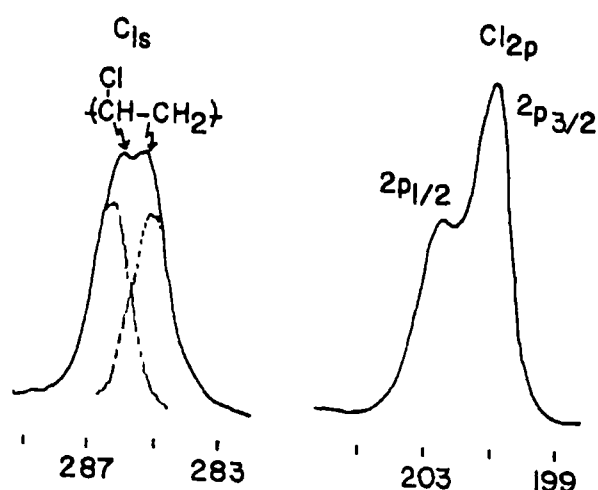


FIGURE 1.25

The C_{1s} and Cl_{2p} core level spectra of polyvinyl chloride

the analogue curve resolution of the two spectra. The repeat unit, $[C-Cl]_n$, contains two types of carbons, one bonded with two hydrogens and one having one hydrogen and one chloride. One would expect, based upon theoretical calculations using the charge potential model previously discussed, to find these two carbons split by approximately 1.4 eV and the curve fitting shows this precisely. The Cl_{2p} is a spin-orbit split doublet arising from the 1/2 and 3/2 degeneracies and, from the previous discussion in section (e), should have an intensity ratio of 1:2, which is shown by curve resolution. The area ratios in the C_{1s} spectrum of 1:1 and the single Cl_{2p} envelope are in agreement with the repeat unit.

From this simple system, consider a slightly more complicated homopolymer; polyethylene terephthalate. Figure 1.26 shows the C_{1s} and O_{1s}

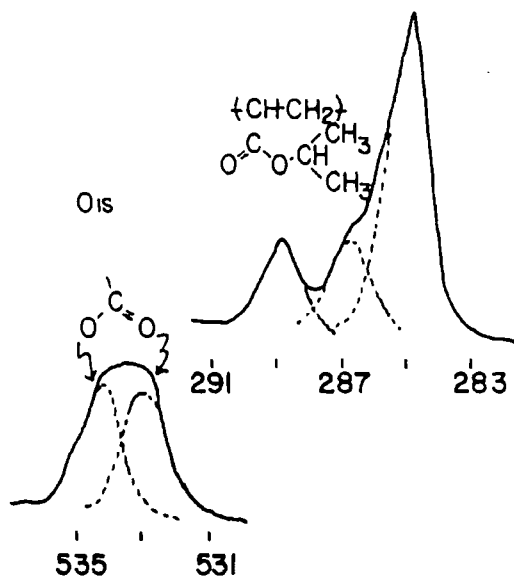
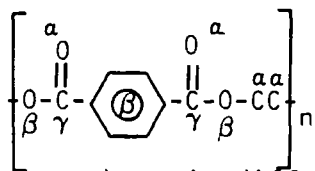


FIGURE 1.26

The C_{1s} and O_{1s} core level spectra of polyethylene terephthalate

core level spectra (i) the experimental and, (ii) the curve resolved envelopes. Consider the repeat unit of the polymer



there are carbons in different types of chemical environment labelled α , β , γ , and oxygens labelled α and β . From a chemist intuitive view, there appear to be 6 carbons on the ring in similar environments and 3 carbons in different ones, with the two oxygens quite different. Curve resolution of the C_{1s} spectrum reveals essentially three separate peaks in a 2:2:6 ratio for the C_{1s} and 1:1 ratio for the O_{1s}. One could, of course, fit any number of peaks under either envelope, but, from Fig. 1.26, we repeat that a general background knowledge helps to eliminate chemically unsound solutions. Theoretical calculations using the charge potential model on a repeat unit of the polymer reveals that the β labelled carbons in the repeat unit having binding energies nearly the same, and within 0.5 eV, will appear essentially under one peak with the present resolution of the instrument. The chemical shifts found for the remaining carbons, α and γ and the oxygens α and β are also predicted well by the

theoretical model.

Having described two rather simple 'unique fit' systems, Fig. 1.27a shows the C_{1s} core level spectra from a sample of polyisobutyl acrylate. An attempt to curve resolve the two core levels indicate that upon close inspection the O_{1s} levels have two unequal components with the $C = \underline{O}$ type at lower binding energy being slightly larger. This inequality of the component peaks in the O_{1s} levels, attributable possibly to surface carbonyl features should also manifest itself in the C_{1s} levels. As a simple model for a system containing both structural features, viz. ketonic carbonyl group and ester group, we may consider ethyl acetoacetate, the C_{1s} levels are shown in Fig. 1.27b, which also details expansion of the C_{1s} levels for isobutyl acetate (c), polyisopropyl acrylate (d), and, for comparison, a film of polyisobutyl acrylate which had been heated in air ($\approx 150^\circ C$ for 30 mins.) whose O_{1s} spectrum also shows evidence for surface oxidation. Considering first the isobutyl acetate and polyisopropyl acrylate spectra, the deconvolution into the component peaks associated with $\overset{O}{\text{C}}-\text{O}$, $\text{O}-\overset{\cdot}{\text{C}}$, and $\overset{\cdot}{\text{C}}$ - structural features with characteristic binding energies developed from model compounds, is straightforward. By comparison, the spectrum of ethyl acetoacetate shows that the carbonyl carbon at 287.2 eV has the effect of 'filling in' the valley between the regions of high and low binding energy. This effect is clearly evident for both the polyisobutyl acrylate and for the polyisopropyl acrylate sample heated in air.

With improvements in instrumentation, e.g. monochromatization of the photo source, for simple systems the need for line shape analysis may well largely disappear and unambiguous analysis of more complex systems become feasible.

iii) ESCA Instrumentation

Since the introduction of the first commercial instrument in 1970, several designs have been placed on the market. This study was performed on both an AEI ES200AA and an updated (monochromatized radiation source) ES200B spectrometer and, therefore, this section on ESCA instrumentation will include only the apparatus appropriate to the AEI spectrometers. (For further information on other apparatus, several reviews have appeared which cover the other areas of instrumentation.)¹¹³⁻¹¹⁹ The essential components of the ES200AA are shown in Fig. 1.28, which include:

- a) X-ray photon source

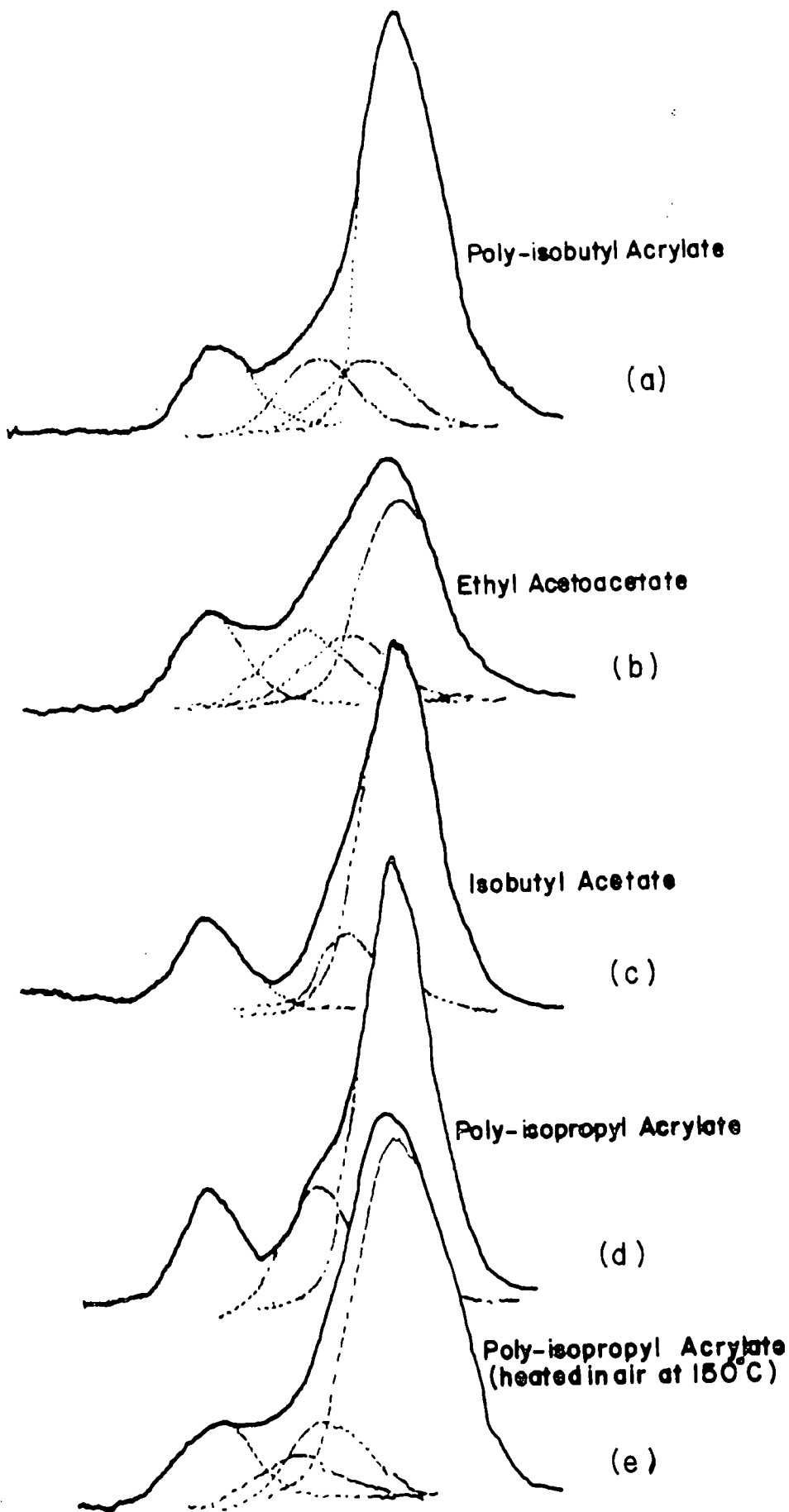


FIGURE 1.27

The C_{1s} core level spectra of polyacrylates and model systems for surface studies of the oxidation of polymers

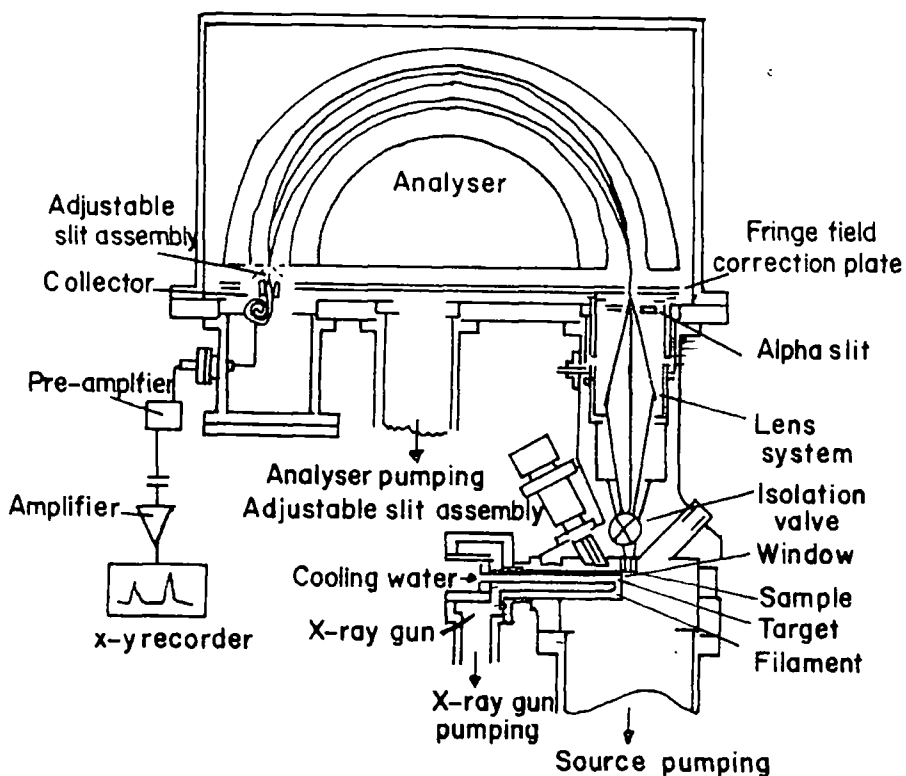


FIGURE 1.28

Diagram of the components of the AEI ES200AA ESCA apparatus

b) Sample chamber

c) Hemispherical electron energy analyzer

and a discussion on each component follows:

a) X-ray photon source

The X-ray gun is of the 'hidden-filament or Henke'¹²⁰ type in which the filament is not directly in front of the target. This reduces the rate of contamination of the target by tungsten evaporated from the filament. The power source to the gun consists of a Marconi-Elliott type GX5 high voltage generator that may be operated in the vacuum region of $\leq 10^{-5}$ torr. The gun is isolated from the sample chamber by means of a thin aluminum window through which the X-rays (and not the electrons) pass from target to sample. The gun filament is earthed and the target operates in the region of +10KV to +15KV, which insures that scattered electrons cannot reach the aluminum window with sufficient energy to excite unwanted X-ray radiation. The

X-ray gun target material is usually magnesium or aluminum and the MgK_{α} or AlK_{α} lines are used to induce photoejections. There are two reasons for using Mg and Al. First, both Mg and Al have relatively narrow natural linewidths, 0.8 and 0.9 (FWHM) respectively - so resolution comparable with this can be obtained ideally in the photoelectron spectrum¹⁸. Secondly, the cross-section for photoionization of various atomic levels is reasonably high for these radiations so that the technique is sensitive for a large number of elements. Both types of targets can be operated at powers up to 500 watts, and both voltage and current supplies are stabilized to 0.1%. Typical conditions, to the Mg anode, for the power input are 12KV and 15ma which produce photon fluxes in the region of ~ 0.1 mill rad/sec.²⁰

Considering first the unmonochromatized sources, a typical X-ray spectra is shown in Fig. 1.29 where it represents the energy content

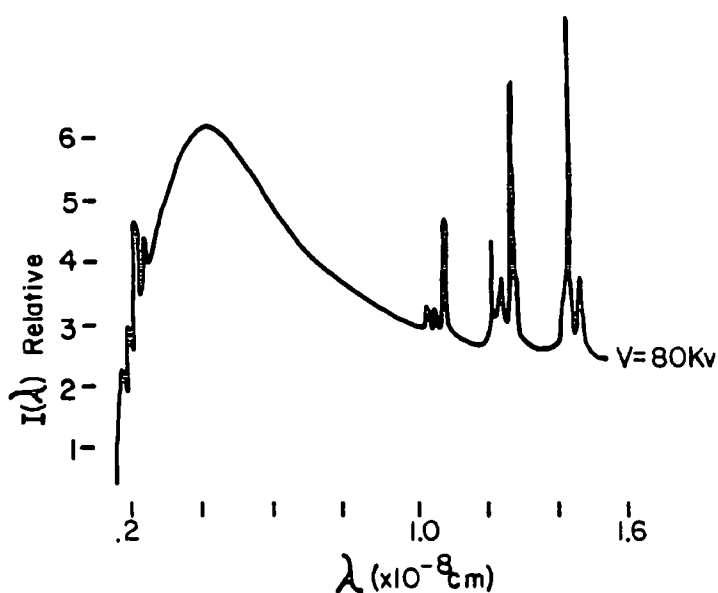


FIGURE 1.29
Typical X-ray spectrum

per unit wavelength emitted by an X-ray tube with a ^{74}W anode¹²¹. It is obvious that the spectrum is composed of a set of sharp lines superimposed on a continuum.

The continuum's shape depends only on the energy of the incident electrons on the anode, not on the nature of the anode and the λ_0 cutoff at short wavelengths is inversely proportional to the electron K.E., and follows the equation:

$$h\nu_0 = E \quad (1.24)$$

where h is Plank's constant. The total X-ray energy per electron, E_T , is proportional to the integral over λ of the continuum and obeys the equation:

$$E_T = kZE^2 \quad (1.25)$$

where $k \approx 0.7 \times 10^{-4}$ for E_T and E in MeV where Z is the atomic number of the anode. The fraction of the electron kinetic energy converted into X-ray energy is:

$$E_T/E = kZE \quad (1.26)$$

For a typical case of $Z = 90$ and $E = 0.05$ MeV, E_T/E is only about 0.3%.

The characteristic line spectra depend only on the atomic number of the anode and not on the incident electrons, however, line spectra are obtained only when the electron K.E. satisfies the relation:

$$(1.27)$$

$$E > E_T = h\nu = hc/\lambda$$

where ν is the frequency and λ the wavelength in question. The total X-ray energy emitted in a particular line increases with incident electron K.E. according to the empirical relation,

$$(1.28)$$

$$I \propto (E - E_T)^n$$

when $n \approx 1.5$.

The line spectra of interest from the Al and Mg anodes normally used in ESCA are from the so-called K series (spectroscopic notation for $n = 1$) transitions and particularly the $K_{\alpha_{1,2}}$ lines. However, the unmonochromatized spectra of the $Mg_{K_{\alpha}}$ radiation contain the continuum and particularly the $k(\alpha_{1,2}, \alpha_3, \alpha_4, \alpha_5, \alpha_6$ and $K\beta$) where the K_{α_3} satellite is 9.5% relative intensity from the primary $K_{\alpha_{1,2}}$ lines (8.4 eV higher K.E.) and the K_{α_4} satellite is 4.5% relative intensity from the primary $K_{\alpha_{1,2}}$ lines (10.1 eV higher K.E.)^{cf. 106}.

$Al_{K_{\alpha}}$ radiation can be monochromatized with a crystal diffraction technique¹⁹, to eliminate the gross satellites (and the continuum) and

be left with the $K_{\alpha_{1,2}}$ lines. (Unfortunately monochromatization of the $Mg_{K_{\alpha}}$ lines is not presently possible with crystal diffraction since no suitable crystal is currently available with the proper lattice spacing!)

For $Al_{K_{\alpha}}$ essentially three techniques are available, (a) 'dispersion-compensation', (b) 'slit-filtering' and (c) fine-focusing, all using crystal diffraction of the X-ray radiation and these techniques will attain ultimate linewidths of 0.2 eV.

Another system described by Gelius¹²² uses a rotating anode (about 5-10,000 r.p.m.) which is characterized by a fine-focusing X-ray line, high power electron gun and several spherically bent quartz crystals for monochromatization of the $Al_{K_{\alpha}}$ radiation. Fig. 1.30 illustrates these

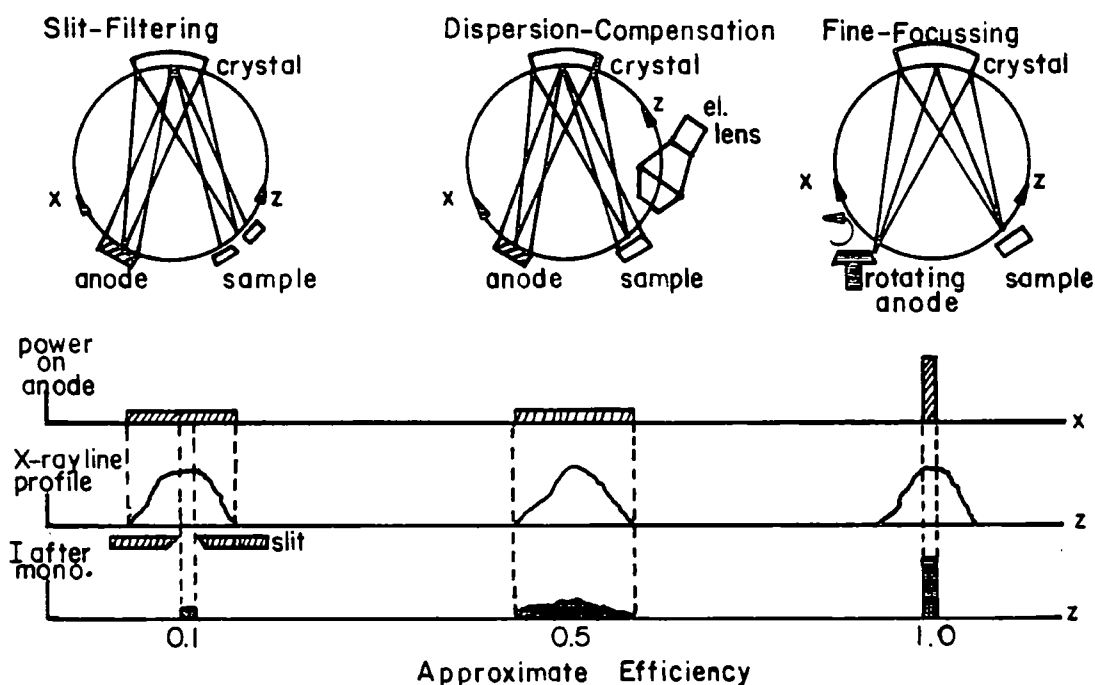


FIGURE 1.30

Techniques for monochromatization of X-rays

techniques, and Fig. 1.31 is a section through the monochromator attached to the ES200B.

The fine-line source of $Al_{K_{\alpha}}$ is produced in the X-ray gun, and the appropriate energy and spread of energy (1486.6 eV and 0.3 eV respectively in the case of $Al_{K_{\alpha}}$) are diffracted by three quartz crystals mounted on a toroidal former. The crystals are cut parallel to the $(10\bar{1}0)$ planes, where the $2d$ spacing is 0.852 nm and the appropriate Bragg

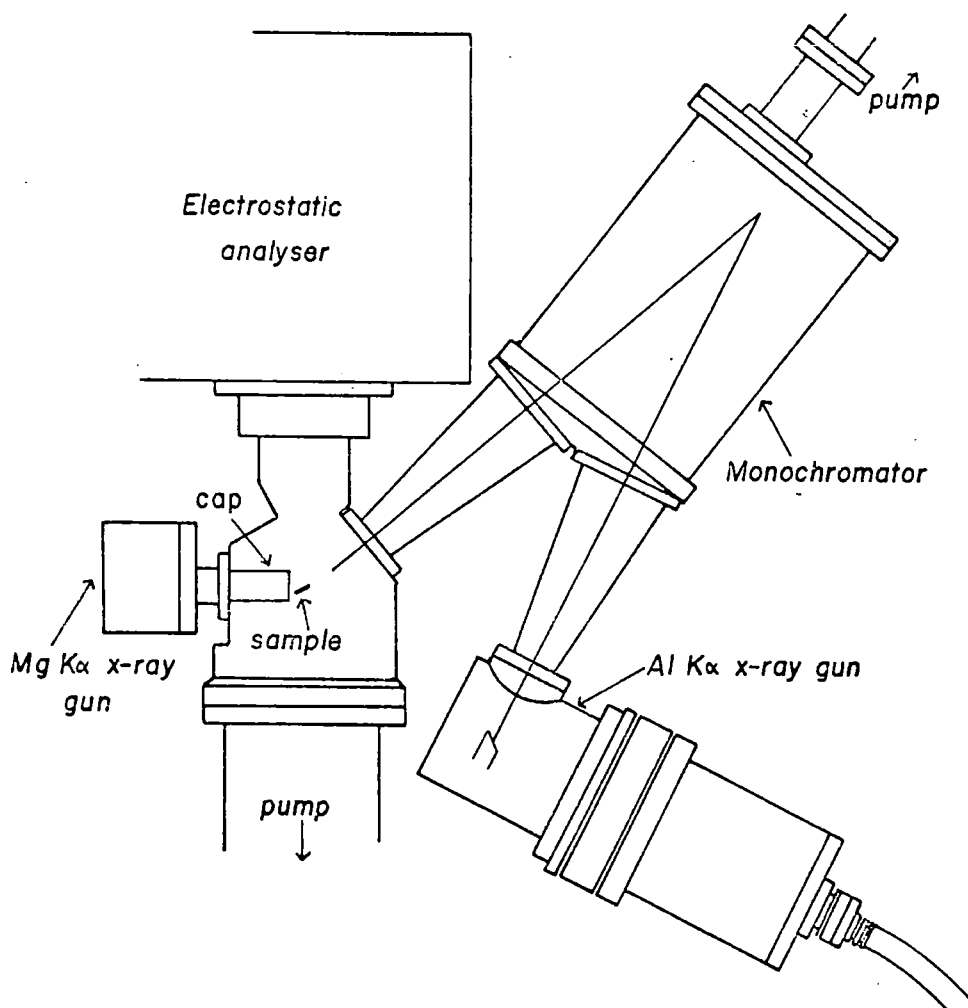


FIGURE 1.31

Cross-section through monochromator attached to the AEI ES200B

angle for Al K_{α} is 78.5° . Quartz was chosen because it bends elastically without affecting its high-quality diffracting ability; it has a high 'reflectivity' for Al K_{α} ($\approx 30-40\%$), and 78.5° is a suitable Bragg angle to work with. Because of the geometry of the system the X-ray flux reaching the specimen is reduced to about a twentieth compared with the normal X-ray gun in the ES200 (compared on a watt-for-watt basis of electron-beam power expended in the respective X-ray guns).

b) Sample chamber

The spectrometer sample chamber contains the X-ray source aperture, seven access ports for sample introduction and various pre- or post-treatments, and a retarding lens system into the analyzer chamber.

The access ports allow for attachment of various sample probes which permit the study of liquids (via a reservoir shaft) volatile

solids (via a direct inlet shaft with vapor condensed on an insertion shaft at low temperatures), gases (via gas valve with studies directly from the gas phase) and non-volatile solids such as films, powders, fibres, etc. (via a plate shaft equipped with heating and cooling temperature control). Typical operating pressures are 10^{-7} torr or better although under ideal conditions better than 10^{-9} torr is attainable.

c) Hemispherical electron energy analyzer

The analyzer on the A.E.I. ES200 is a hemispherical double focusing electrostatic analyzer, which was originally described by Purcell¹²³ in 1938, enclosed within two mu-metal shields for magnetic shielding. The resolution of the hemispherical analyzer is based upon three variables:

- 1) mean radius of the hemispheres, R,
- 2) width of the entrance slit,
- 3) width of the exit slit.

Therefore the resolution, $\Delta E/E$, where E is the energy of the electron is

$$\Delta E/E = R/W \quad (1.30)$$

where W = combined widths of entrance and exit slits.

It is quite easily seen that to improve the resolution three terms can be varied:

- 1) reduce the slit width, which has the effect of reducing the signal intensity,
- 2) increase the hemispherical radius, which increases engineering cost and complexity and pumping requirements,
- 3) retard the electrons before entering the analyzer so as to reduce their K.E.

With reasonable compromises made on the slit width to obtain sufficient signal intensities and the hemispherical sizes to prevent mechanical distortion and high engineering cost and practical vacuum pump sizes the ES200 series retards the electrons before they enter the analyzer by passing them through a lens assembly. This lens system actually serves a double purpose:

- 1) The lens system allows the analyzer to be located at a convenient distance physically from the source chamber which permits a maximum flexibility in sample handling.
- 2) A retarding potential on the electrons allows more flexibility on the resolution requirements of the analyzer¹²⁴.

The electrons passing through the analyzer can be focussed at the collector by either of two methods:

- 1) Electronically scanning the retarding potential applied to the lens while keeping the hemispherical potential constant, or
- 2) Simultaneously scanning the retarding potential applied to the lens and the hemispherical potential and keeping a constant ratio between the two, which is the technique used on this ES200 .

The overall resolution $\Delta E_m/E$, of the system also depends upon contributions from sources other than the analyzer.

- 1) The width of the X-ray radiation line, ΔE_x .
- 2) The natural width of the electron energy distribution in the level being studied, ΔE_1 .
- 3) The line broadening due to spectrometer irregularities, which can vary with electron emission energy, E and slit widths, ΔE_s .
- 4) The line broadening due to solid state effects in the sample, ΔE_{ss} .

Therefore, the overall resolution is given the equation given in section h)

$$(\Delta E_m)^2 = (\Delta E_x)^2 + (\Delta E_1)^2 + (\Delta E_s)^2 + (\Delta E_{ss})^2 \quad (1.22)$$

(This relationship is strictly valid only for Gaussian line-shapes.)

A variable on the ES200 series is the collector slit width which can be adjusted at 0.2, 0.1 or 0.03 inches depending on the resolution and sensitivity desired.

Two modes of scanning the analyzer and lens potentials are available with the ES200. In the first mode the electrons being analyzed are retarded to 5% of their initial kinetic energy before they enter the hemispheres. The line-width contribution of the analyzer is therefore proportional to energy, so that the resolution of the system improves at the low-kinetic-energy end of the spectrum, but at the expense of sensitivity. A fixed potential difference is applied between the two hemispheres in the second mode so that electrons traverse the analyzer with a fixed kinetic energy of 65 eV regardless of their initial kinetic energy. This gives rise to a constant line-width contribution together with enhanced sensitivity at the low-kinetic-energy end of the spectrum. The analyzer and

lens supplies allow electrons with energies up to 4000 eV to be studied, and the stability of the circuitry is such that the energy scale of the spectra is constant to better than ± 50 mV over many hours.

The detector contains a collector aperture (exit slit), described above, which pass the selected K.E. electrons into an electron multiplier. The output pulses from the channel multiplier are amplified and fed into a data handling system. The signals into the data handling system generate the ESCA spectra by one of two methods:

- 1) The continuous scan, where the electrostatic field is increased from the present starting K.E. continuously while the signals from the multiplier are monitored by a rate meter. When the signal to background ratio is sufficiently high a graph of the electron counts per second versus the K. E. of the electrons is plotted directly onto an X-Y recorder.
- 2) The step scans, where the field is increased by preset increments (typically 0.1 eV) and at each increment the (a) counts may be measured for a fixed length of time or (b) a fixed number of counts may be timed. The data obtained from the step scans is stored in a multichannel analyzer and many scans can be made on a sample to average any random fluctuations in background. Using this technique the signal to noise ratio goes up as the square root of the number of scans, although care must be taken to avoid long term sample changes, such as hydrocarbon surface build-up, where the first scans are not typical of the last scans. Wide scans encompassing the entire range from zero K.E. to the K. E. of the X-ray source as well as narrow scan ranges for specific studies are available.

CHAPTER 2

ESCA Applied to Polymers - A Review

CHAPTER 2

ESCA Applied to Polymers - a Review

i) Introduction

From the latter part of 1970 when ESCA investigations into structure and bonding in polymer systems was initiated by Clark at Durham until early in 1974, the emphasis was placed on fluoropolymer systems^{1,125-128}. There were two reasons for the focus of attention on fluoropolymers. Firstly, the large chemical shift in the C_{1s} core levels induced by the substituent fluorine presents the most suitable cases for delineating the information content from the ESCA spectra. Secondly, the importance of the fluoropolymer systems both technologically and academically, and their comparative difficulty of analysis by other common spectroscopic techniques, due to their insolubility and intactability, lend themselves very nicely to investigation by ESCA.

In the development of ESCA as a spectroscopic tool for studying polymers, the logical first step is to study simple, well-characterized homopolymer and copolymer systems. From these simple systems, trends can be drawn and comparisons made with simple monomers. The simplicity of these systems allows for the development of rigorous theoretical models for the quantitative interpretation of the data. These models, in turn, can direct one to the important electronic factors determining shifts in core binding energies; for example, from which theoretically sound, but less rigorous models may be developed to discuss larger systems for which more detailed computations are not feasible. Since 1974 the extension of ESCA into other polymeric systems has been actively pursued and a perusal of the literature confirms the diversity in the current fields of application to structure and bonding in polymers (cf. 1, 86-89, 125-128, 129). There are essentially two main areas that have been investigated and they are briefly outlined below:

A) Static Studies

1) Chemical Compositions

- a) elemental compositions
- b) % comonomers in copolymers

2) Structural Details

- a) structural repeat units in copolymers, e.g. random alternating or block repeat units
- b) domain structures in block copolymers

- 3) Fine Structural Details
 - a) structural isomerism, e.g. cis, trans, etc.
 - b) shake-up studies on unsaturated systems
 - 4) Valence Band Studies on Polymer Systems
- B) Dynamic Studies
- 1) Surface Treatments
 - a) casing
 - b) fluorination
 - c) RF plasma treatments
 - 2) Oxidation of Polymers
 - 3) Adsorption at Polymer Surfaces

Each of these topics will be covered in detail in this chapter, but before discussing the results it is of some importance to consider the methods by which polymer samples may be prepared for ESCA investigation.

ii) Sample Preparation

There are a few methods which have been found to be convenient for preparing samples for examination by ESCA. These are (a) the direct study of suitably mounted powder samples, (b) solution cast films, (c) pressed or extruded films and (d) 'in situ' polymerized films. Each of these techniques will be discussed separately.

(a) Powders

When the polymer sample is available as a powder, which is often the case, it is convenient to examine it by applying the powder to a double sided tape which possesses nominal heat resistance ('Scotch Brand' electrical tape #75, a silicone type polymer, 3M Company), and apply the tape directly to the sample probe. Caution of course must be taken to avoid incomplete coverage of the tape which would result in extraneous signals observed from the tape backing. Samples prepared in this way generally tend to have lower signal/noise ratios than do smooth films and the primary photoionization peaks tend to have broader full width at half maximum (FWHM) than do films.

(b) Solution Cast Films

When the polymers are sufficiently soluble, thin films may be solution cast onto a suitable backing, such as clean gold sheet and mounted onto the sample probe. Conventional dip or bar coating procedures are adequate for the coating process. Care must be taken to use clean coating apparatus and pure solvents to avoid the segregation

of impurities at the surface during evaporation of the solvent. For polymers easily oxidized the coating procedure should be carried out under an inert gas during the evaporation of the solvent, and for systems where hydrogen bonding is a problem, complete removal of extraneous water is imperative.

(c) Pressed or Extruded Films

To eliminate the contaminations possibly introduced by solvent casting for appropriate polymers it is convenient to study them as pressed or extruded films. For polymers with low Tg's, such as elastomers, it is often possible to 'melt' a small amount of polymer onto a suitable substrate and allow it to spread as a thin film. For rubbers, thin slices of the polymer can be attached to the probe with double sided tape. When films are prepared from powders or pellets it is often convenient to press the film between clean aluminum foil at temperatures and pressures appropriate to avoid degradation of the polymer sample, often also done under an inert gas atmosphere to avoid oxidation.

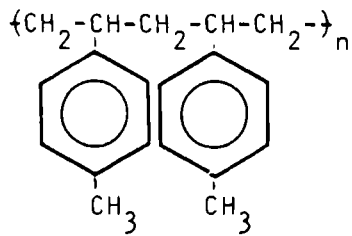
(d) 'In situ' Polymerized Films

A very convenient and often contamination free method of studying polymer films is by direct polymerization onto the tip by various techniques such as U.V. or e^- irradiation, plasma (glow-discharge polymerization) or pyrolysis of appropriate monomers, such as the [2.2]paracyclophane series (cf. Chapter 5).

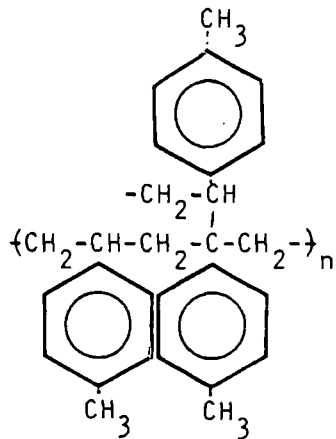
(It is convenient to note here again that since most polymers are inherently good insulators, the thin films studied are, generally speaking, not in electrical contact with the spectrometer. This will result in sample charging, as discussed in Chapter 1, and therefore referencing the energy scale back to the Fermi level becomes necessary.)

The difficulty in the characterization of polymers, particularly in the case of their surfaces, arises from the fact that polymers are not as well-defined as simple non-macromolecular compounds. The gross chemical structure of polymers can be simple as in the case of linear homopolymers, or complex as in the case of branched or cross-linked copolymers. As an example, consider representative systems based on polyvinyl toluene shown in Fig. 2.1.

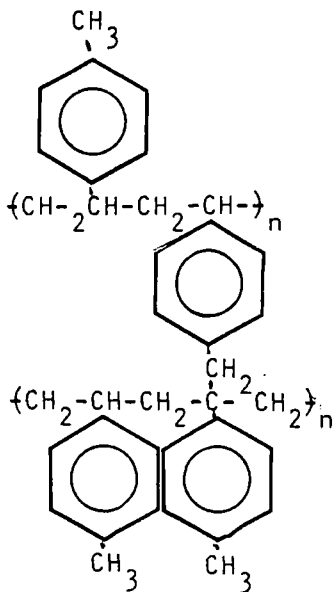
These differences in gross structure, all based on the same basic building block, give rise to a tremendous variation in the physical, chemical, mechanical and electrical properties of the system.



(a) Linear polymer



(b) Branched polymer



(c) Cross-linked polymer

FIGURE 2.1

Structure Assignments to Polyvinyl Toluene

It is often the case that for a given polymer system, the structure of the bulk is substantially different than that of the surface. For example, since solids communicate with the rest of the universe by way of their surfaces it is possible to produce a crosslinked surface while maintaining the integrity of the bulk. A technique which is capable, therefore, of monitoring differences in structure between the surface and the bulk is obviously of considerable relevance in many fields of academic and

technical importance.

Along with gross structural differences in polymers, there are also isomeric differences arising from unsymmetrical monomers and the resultant structures are shown in Fig. 2.2.

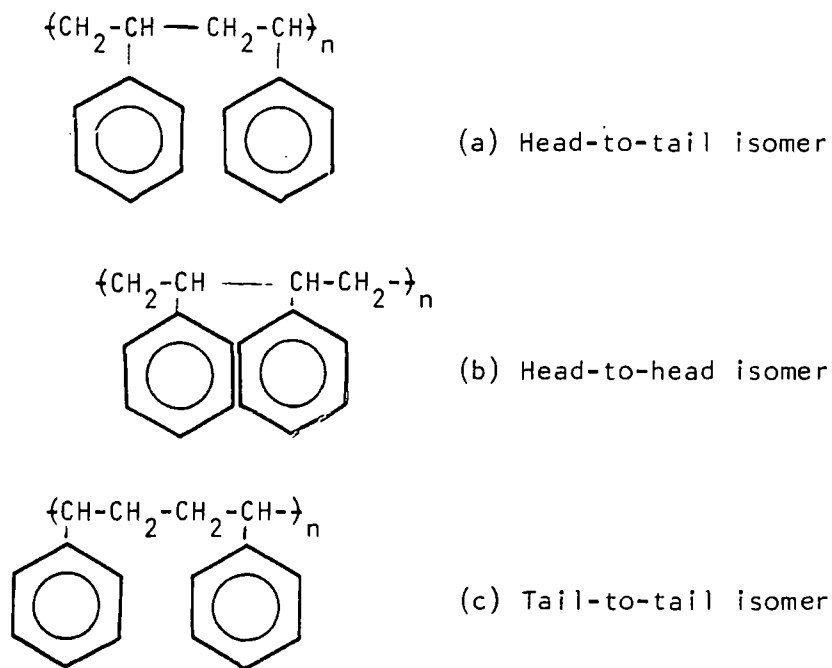


FIGURE 2.2

Isomeric structures of polystyrene

Not only can structural isomerism occur in polymers, but also stereoisomerism (CIS-TRANS) as shown in Fig. 2.3.



FIGURE 2.3

Stereoisomerism of polybutadiene

Tacticity is another type of stereoisomerism and is classified into three categories as shown in Fig. 2.4.

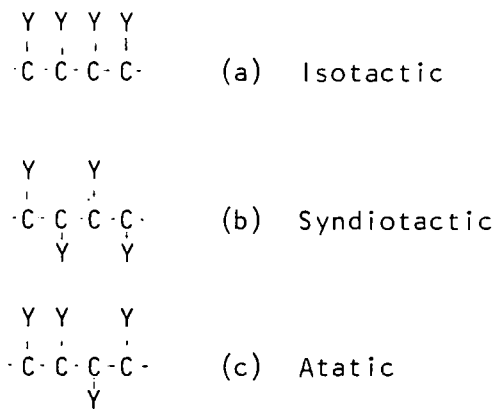


FIGURE 2.4
Representation of tacticity in polymers

Copolymers have other types of structural assignments; for example, such as random, alternating, graft or block copolymers as shown in Fig. 2.5.

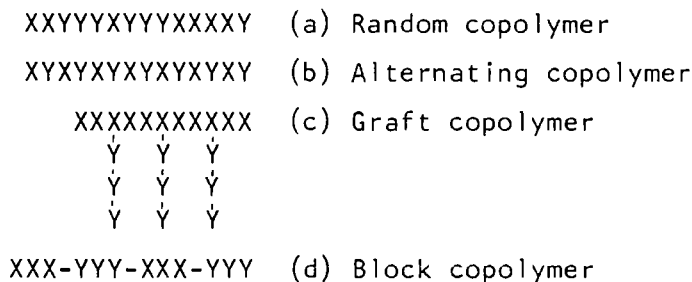


FIGURE 2.5
Structure assignments to copolymers

iii) Static Studies

a) Chemical Compositions

It is quite apparent from the discussions in Chapter 1 that ESCA is capable in principle of being able to study the core and valence levels of any element (with the exceptions of hydrogen and helium) regardless of the nuclear properties, such as magnetic or electric quadrupole moments. This particular feature of the technique makes it very useful for an understanding of surface treatments of polymers such as oxidation, fluorination, ion-bombardment, RF Plasma treatments, etc., which will be discussed in the following sections. A wide scan through the energy spectrum on a sample will, through the use of a calibrated energy reference and the appropriate binding energy reference tables,

allow for an elemental mapping of the surface. As an example, in Fig. 2.6

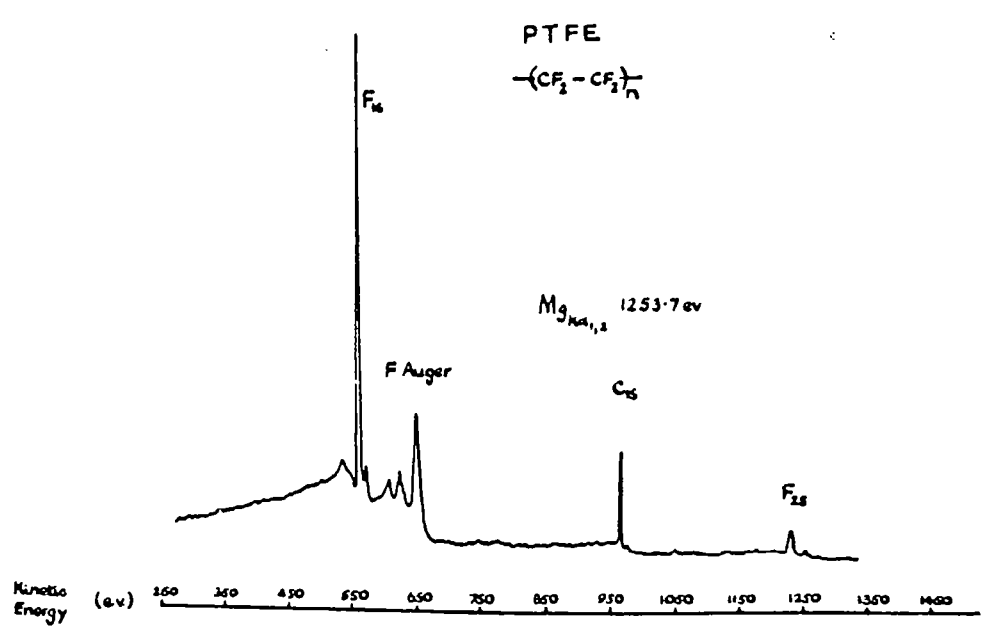


FIGURE 2.6
Wide scan ESCA spectrum of PTFE

is shown a spectrum of polytetrafluoroethylene (PTFE) obtained from a film pressed from PTFE powder between sheets of aluminum foil at the minimum temperature necessary for coalescence of the powder particles into a coherent film ($\approx 200^\circ\text{C}$)¹. When the sample preparation procedure is repeated at higher temperatures ($\approx 300^\circ\text{C}$) films are produced which bulk chemically, by transmission infrared (TIR) and multiple attenuated total reflectance (MATR) measurements appear to be identical to those produced at lower temperatures. The ESCA spectra of the film, however, is quite different from that of films produced at lower temperatures revealing surface contamination, Fig. 2.7. It is clear from the appearance of the oxygen and aluminum core levels that in the high temperature pressing procedure a contamination layer of aluminum (Al_2O_3) is deposited on the PTFE film. The thickness of the layer is almost certainly $< 10\text{\AA}$ and would be undetectable by most spectroscopic techniques (including IR), although evident from the ESCA experiment, this illustrates the extreme surface sensitivity of ESCA.

Another application in chemical compositions by ESCA is in the determination of the percent comonomer in a copolymer, such as the Viton polymers of hexafluoropropane (HFP) and vinyl fluoride (VF_2)¹.

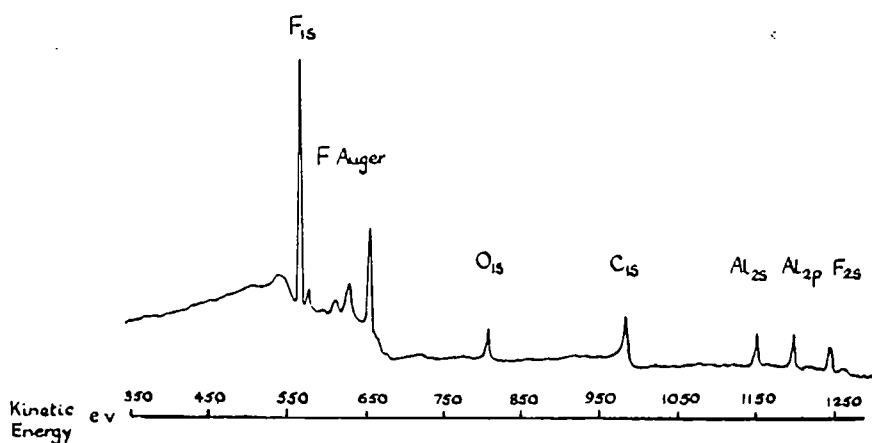


FIGURE 2.7

Wide scan ESCA spectrum of contaminated PTFE

The compositions for such materials may be directly determined by reference to the detailed fine structure of the C_{1s} levels since each distinct chemical environment (e.g. $\underline{C}F_3$, $\underline{C}F_2$, $\underline{C}F$, $\underline{C}H_2$) corresponds to a different absolute binding energy. Since the kinetic energy of the corresponding photoemitted electrons span a narrow range (960-968 eV), the mean free paths are the same and the relative intensities of the component peaks may therefore be utilized to obtain the copolymer compositions directly. If the apparent relative cross sections for the F_{1s} and C_{1s} levels are known, their stoichiometry can also be determined directly from the total intensity ratios for these levels.¹ Since, however, the mean free path for electrons photoemitted from the F_{1s} levels is significantly shorter than for the C_{1s} levels¹³⁰, these two independent methods will only agree for materials which are homogeneous on the ESCA depth sampling scale and an example of this is given below. As an example of the use of the fine structure in the core level spectra for the determination of copolymer compositions, Fig. 2.8 shows the C_{1s} levels of Polyhexafluoropropane, Polyvinylidene fluoride, and two Vitron copolymers.

The procedure as applied by Clark¹ was to measure the area of the $\underline{C}F_3$ peak, the total area of the $(\underline{C}F_2 + \underline{C}F)$ peak and the area of the $\underline{C}H_2$ peak when the spectrum was deconvoluted into its individual components.

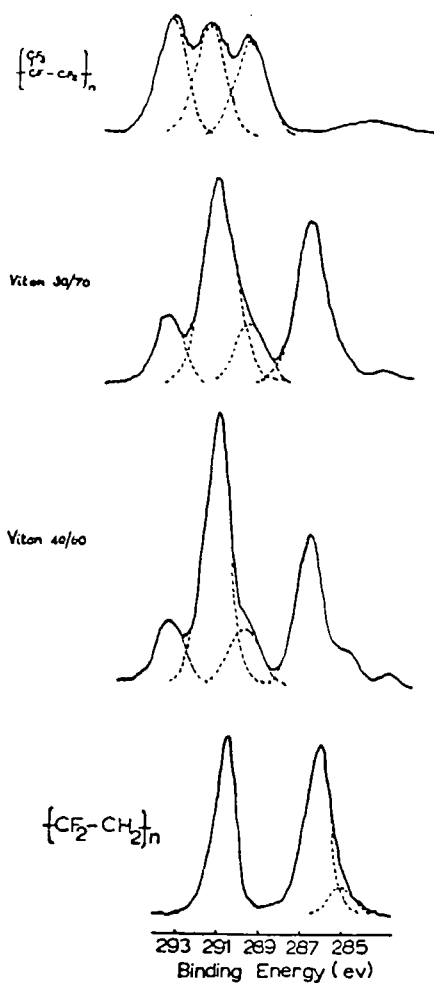


FIGURE 2.8

C_{1s} core level spectra for polyhexafluoropropane, PVF₂
and two 'Viton' copolymers

Three different techniques were used to compute the comonomer ratios as an internal check on the reliability of the methods.

- 1) Based on the stoichiometry of the HFP unit the mole% of HFP must be three times the peak area due to $\underline{\text{CF}}_3$.
- 2) The peak area due to $\underline{\text{CF}}_2$ and $\underline{\text{CF}}$ is made up of half the total C_{1s} peak area due to VF₂ (1/2 VF₂) and two thirds the total C_{1s} peak due to HFP.
- 3) The peak area due to $\underline{\text{CH}}_2$ is half the total area due to $\underline{\text{CF}}_2$, therefore the mole % of HFP is
mole% HFP = 100 - (2X % peak area due to $\underline{\text{CH}}_2$)

Table 2.1 gives the results of the three methods of calculations.

% HFP Incorporation Calculated by Three Methods

	Method of Calculation		
	(i)	(ii)	(iii)
Sample 40/60	39	42	40
Sample 30/70	33	30	32

Table 2.1

The internal consistency is good to within 3% and the values obtained were in good agreement with the compositions quoted for these Viton polymers.

The composition of thin polymer films prepared in an electrodeless RF discharge has been determined by ESCA for some fluorocarbon systems¹³¹⁻¹³⁴. O'Kane and Rice¹³³ have prepared polymers from tetrafluoroethylene monomer and characterized them by ESCA, IR absorption and surface wettability. The films were homogeneous and consisted of \underline{CF}_2 and \underline{CF}_3 functional groups with an increase in the complexity of the polymer chemistry as the plasma reaction zone was approached. The C_{1s} binding energies were compared to calculated values based upon established chemical shifts for specific C-F type environments within the electrostatic potential model.

Clark and Shuttleworth¹³⁴ have recently carried out similar, but more detailed studies on electrodeless RF discharge polymerization of vinylidene fluoride monomer. The surface composition, based upon C_{1s} and F_{1s} energy references and instrumental sensitivity for these levels were established as well as the determination of the electron mean free paths for the F_{1s} core level electrons at kinetic energy of ~ 560 eV. Contact angle measurements were made on the various films to confirm differences in surface compositions.

b) Structural Details

1) Before proceeding to a discussion on structural details in complicated polymer structures, a brief discussion on the qualitative and quantitative nature of the substituent effect on core binding energy in polymers must be treated. In chapter 1 we considered the quantitative interpretation of chemical shift data from several theoretical

treatments, here we consider the experimental determination of substituent effects in a series of fluoropolymers.

The simplest system to begin with, of course, is the simple homopolymers of the fluoroethylenes, for which the complications due to branching, end groups and structural abnormalities are minimal.

The measurement of the core levels of a polymer typically take about 1/2 hour whereas, under normal operating condition, hydrocarbon build-up is noticeable after an extended period of time (See chapter 1). Therefore, as discussed earlier, the reference level of the polymer immediately upon introduction into the spectrometer and then allowing time for hydrocarbon build-up, the spectrum is recorded to observe the appearance of the extra peak, as shown in Fig. 2.9. (Note that the peak

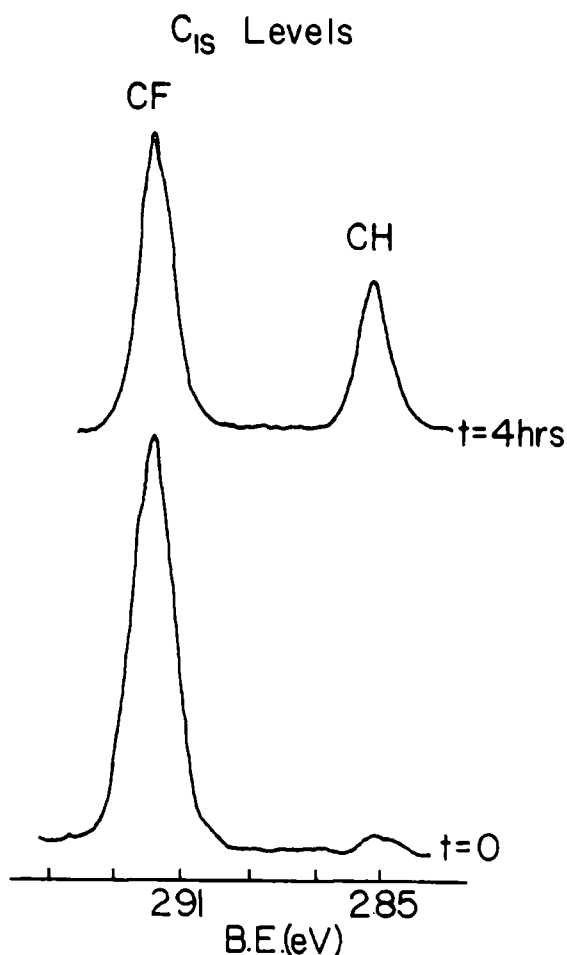


FIGURE 2.9

C_{1s} core level spectra of hydrocarbon build-up on PTFE

at 285 eV on $t = 0$ is a satellite peak from the main photoionization peak at 292 eV due to the excitation from the $MgK_{3\beta}$ photon line and not the C_{1s} level of a hydrocarbon layer. This can also be confirmed by angular dependent studies which will be discussed in more detail in Chapter 4.)

In a series of polymers studied by Clark¹, et al, the binding energies for the C_{1s} and F_{1s} levels were identified and Table 2.2

Binding Energies of the Homopolymers of Ethylene and the Fluoroethylenes

	C_{1s}	$\Delta(C_{1s})$	F_{1s}	$\Delta(F_{1s})$
$(CH_2-CH_2)_n$	285.0	(0)	-	-
$(CFH-CH_2)_n$	- <u>CFH</u> - 288.0	3.0	689.3	(0)
	- <u>CH₂</u> - 285.9	0.9	-	-
$(CFH-CFH)_n$	288.4	3.4	689.3	(0)
$(CH_2-CH_2)_n$	- <u>CF₂</u> - 290.8	5.8	689.6	0.3
	- <u>CH₂</u> - 286.3	1.3	-	-
$(CF_2-CFH)_n$	- <u>CF₂</u> - 291.6	6.6	690.1	0.8
	- <u>CFH</u> - 289.3	4.3	690.1	0.8
$(CF_2-CF_2)_n$	292.2	7.2	690.2	0.9

Table 2.2

list the data pertaining to the polymers and Fig. 2.10 illustrates the substituent effect in the C_{1s} levels of the homopolymers studied.

By taking the appropriate pairs of polymers it was possible to assign structural features to the peaks in the spectrum and investigate the primary and secondary effects of hydrogen replacement, and it was shown that there is a rapid fall off in the C_{1s} B.E. as a function of the fluorine substituted.

It is important also, (as has been previously noted), to determine the intensity ratios for the core levels in the simple homopolymer systems due to the differences in the cross-section for the different core levels being studied. This is most readily accomplished on simple compounds and the values substantiated on the homopolymer systems before proceeding to analyze the more complicated copolymer quantitatively.

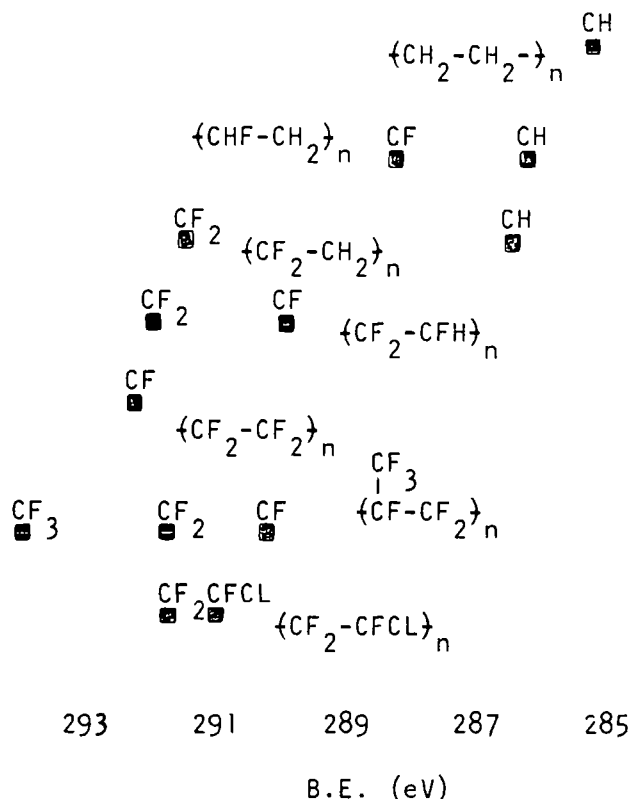


FIGURE 2.10

Illustration of substituent effects in the C_{1s} core levels of selected homopolymers containing fluorine

2) The use of ESCA in the determination of the structural details of a polymer is best illustrated by the application to the copolymer of ethylene/tetrafluorethylene¹³⁵. A series of the copolymers was studied and the C_{1s} and F_{1s} levels of the copolymers are shown in Fig. 2.11

From the ESCA data the copolymer compositions may be calculated from the relative ratios of the high to low B.E. peaks in the C_{1s} levels (attributed to \underline{CF}_2 and \underline{CH}_2 , respectively) and also from the overall C_{1s}/F_{1s} intensity ratios, using data from homopolymers as discussed in the previous section.

It was shown that using these two methods of calculating the composition that they are in good agreement with bulk analytical methods (C and F elemental analysis) and also demonstrated that the samples were homogeneous in the surface region since the two independent ESCA methods are in excellent overall agreement.

Once the compositions are established, structural details are the next order of assignment. The studies on the homopolymers of fluorinated ethylenes revealed that structural information is most

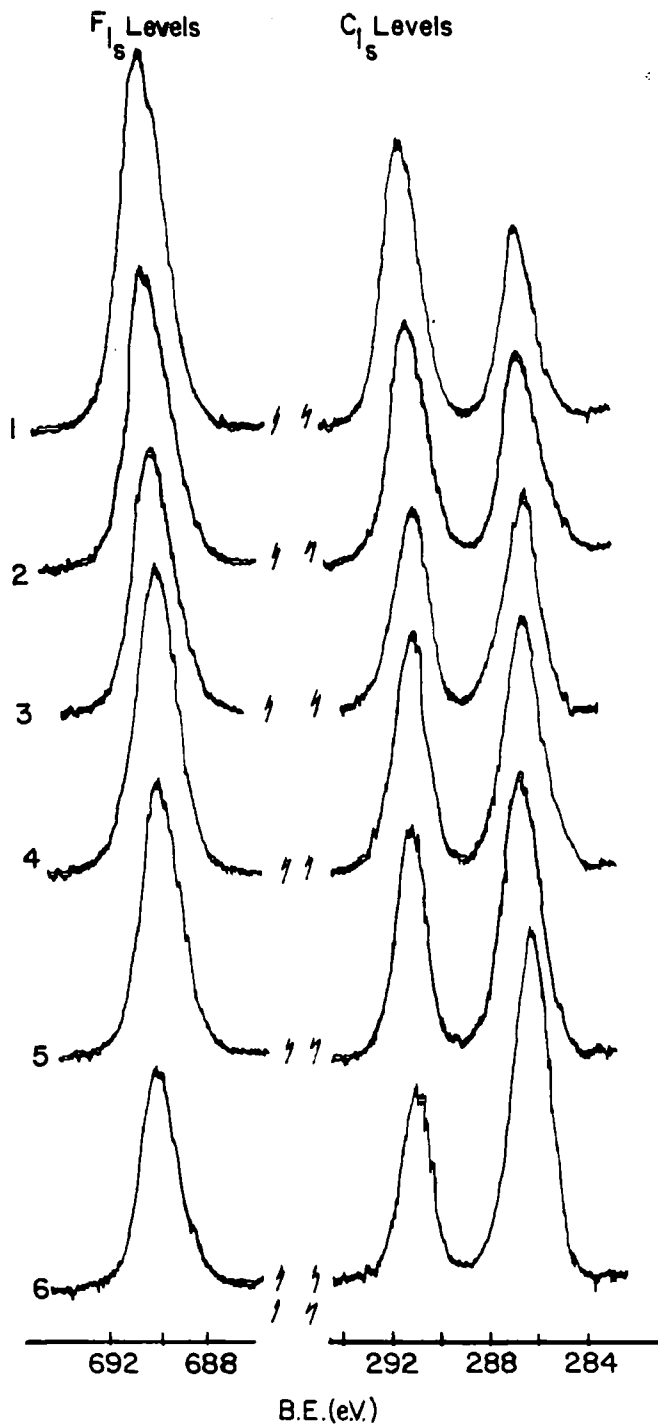


FIGURE 2.11

C_{1s} and F_{1s} core level spectra for the series of ethylene/
tetrafluoroethylene copolymers

readily obtained from the absolute B.E.'s and chemical shifts in the C_{1s} core levels. The chemical shift on the C_{1s} levels is understood qualitatively in terms of the charge potential model discussed in the first chapter and will be further discussed in this chapter on the charge

distribution in polymers. The chemical shifts lead to a clear distinction between the extreme cases of block sequence of ethylene and tetrafluoroethylene from the C_{1s} B.E.'s observed for the PVF_2 based on substituent effects and the calculation with the charge potential model on simple systems would predict the B.E.'s unique for this system.

Therefore, if either the block or the alternating structure predominate the C_{1s} levels would show this and as Fig. 2.11 clearly demonstrates an alternating structure was found due to the expected chemical shift of ~ 4.7 eV versus a shift of ~ 7.2 eV expected for a block structure.

Further examination of the spectra revealed two features where the total linewidths (FWHM) were greater than the (FWHM) for the respective homopolymers (2.0 eV - vs. 1.3 eV ± 0.1 eV) and where the peak shapes were asymmetric. These two observations indicated that the spectra were envelopes of a number of overlapping peaks arising from different molecular environments. With a complex deconvolution of the spectra, theoretical calculations on expected B.E.'s from a series of model compounds using pentad sequences of the two monomers and assignments of triads for the monomer from the pentad sequence calculations, Clark was able to obtain good agreement between the physical and general spectroscopic properties of the ethylene/tetrafluoroethylene copolymer.

3) The surface structure found in AB block copolymers of dimethylsiloxane and styrene was investigated¹³⁶ by comparing the intensities of elastic peaks corresponding to photoionizations from core levels without energy loss for polydimethylsiloxane and polystyrene with those for the block copolymers. By a consideration of shake-up phenomena specific to the polystyrene component, an estimate of the thickness of the polydimethylsiloxane outer layer was obtained.

AB block copolymers frequently exhibit phase separation which typically gives rise to a dispersed phase consisting of one block type in a continuous matrix of the second block type. The detailed morphology of the domain structure of the block copolymers depends upon such factors as the relative proportions of the two components, the molecular weights, the thermal and physical history of the polymers; and the solvent-cast films, upon the solvent and the temperature.

While such techniques as contact angle measurements can clearly

provide some indication of the immediate surface composition of the polymer films, provided relevant standards are available for direct comparison, ESCA offers the possibility of obtaining quantitative information on compositions and structure and bonding in not only the immediate surface, but also the subsurface typically to a depth of $\sim 50 \text{ \AA}$. The analytical depth profiling capability of the technique arises from the strong dependence on kinetic energy of the mean free path for photoemitted electrons corresponding to the elastic peaks in the ESCA spectrum, as was discussed in Chapter 1. The intensity I of the signal from a given core level arising from a surface layer of thickness d is given by

$$I = I_{\infty}(1 - e^{-d/\lambda})$$

where I_{∞} is the intensity observed for an infinitely thick layer and λ is the escape depth of the photoemitted electron. Similarly, the intensity of a signal arising from the bulk of a sample under a surface layer of thickness d is

$$I = I_{\infty}e^{-d/\lambda}$$

These equations form the basis for determination of the surface structure by ESCA, and will be covered in greater detail in Chapter IV on the mean free paths of electrons in polymer films.

The primary sources of ESCA data which have been routinely utilized in the application of the technique to polymers are absolute and relative binding energies and relative peak areas¹. It is becoming increasingly apparent, however, that the observation of shake-up satellites accompanying core ionizations can considerably increase the scope of the technique in many applications⁵⁸.

These considerations are readily apparent from the spectra in Fig. 2.12. For the homopolymers it is clear that whereas polystyrene (Fig. 2.12a) has a well-developed, relatively intense shake-up structure in the region corresponding to transition energies $\sim 10 \text{ eV}$, polydimethylsiloxane (Fig. 2.12d) does not exhibit such a structure, although the binding energies and full width at half maximum (FWHM) are similar for the C_{1s} direct photoionization peaks for both polymers. It is clear, therefore, that the observation of shake-up structure of the appropriate

transition energy provides data specific to the polystyrene component of a block copolymer of PS and PDMS (Figs. 2.12b and c).

Through a consideration of the primary sources of ESCA data, it was shown from the measured intensity ratios and with confirmation from contact angle measurements, and shake-up satellite intensities, that the domain structure in the surface of an AB block copolymer can differ considerably from the bulk.

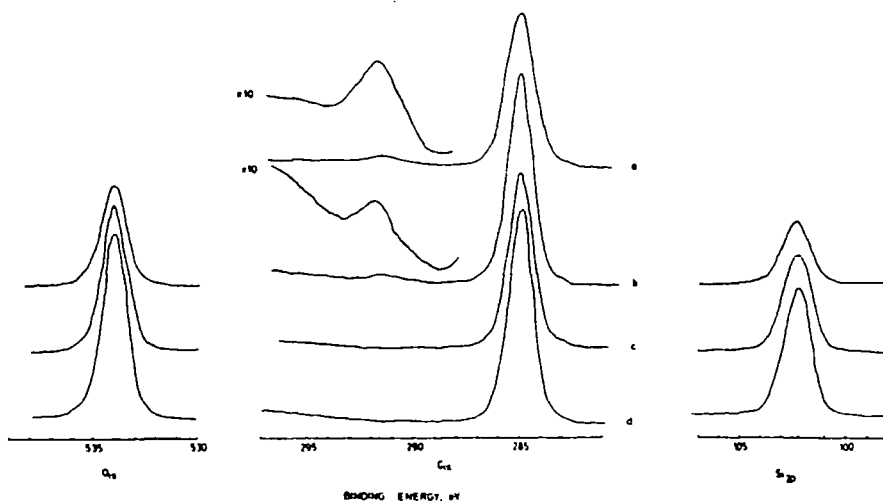


FIGURE 2.12

C_{1s}, O_{1s}, and F_{1s} core level spectra for homopolymers of styrene (a) and dimethylsiloxane (d) and block copolymers (b,c)

4) Another application to the structure and bonding in polymer systems as studied by ESCA, was shown in a study on a series of poly-alkylacrylates¹³⁷. As a preliminary to a detailed investigation of the polyacrylates, it was necessary to study a series of simple molecules as model systems to provide a firm basis for the interpretation of the data. Direct measurements of the relative area ratios for the O_{1s} and C_{1s} levels of homogeneous thick films of the condensed model compounds plotted against the stoichiometric ratios provided an excellent straight line (Fig. 2.13) correlation, the slope being 1.65 ± 0.009 ($r^2 = .99$). This, therefore, provided the required sensitivity factors for the C_{1s} with respect to O_{1s} core levels, these factors of course being instrument dependent since they depend not only on the relative cross sections for photoionization, but also on spectrometer factors such as sensitivity of the detector for electrons of different kinetic energy, etc.

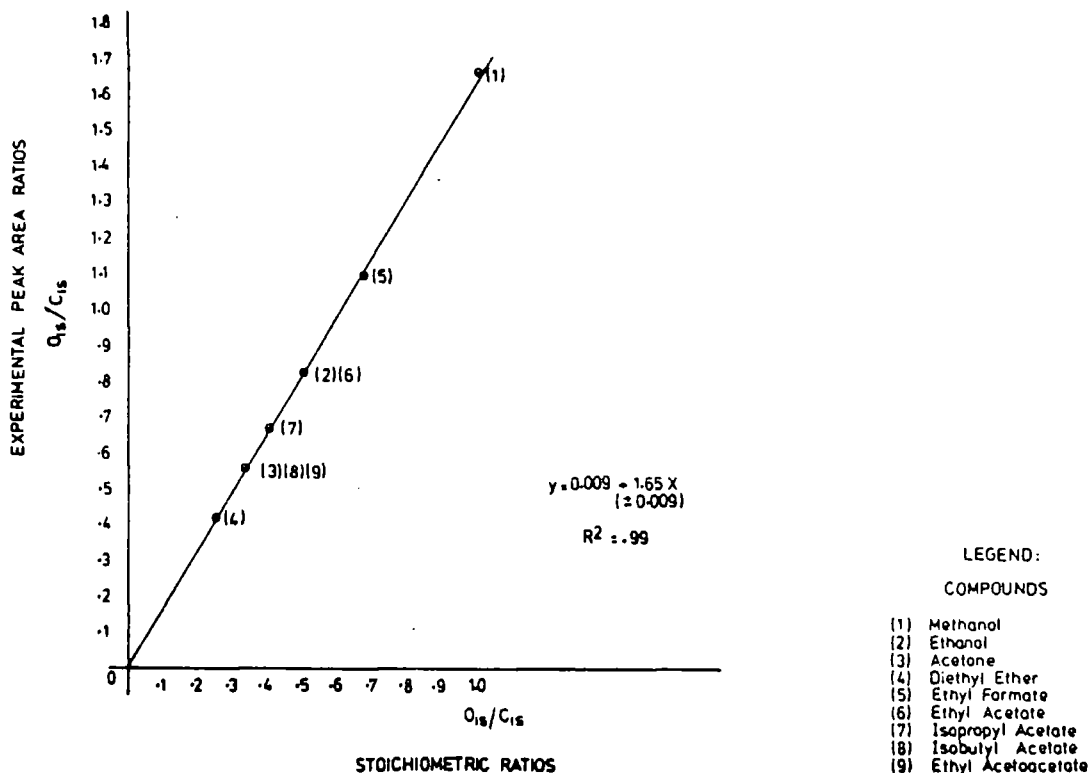


FIGURE 2.13
Model compounds
relative peak area ratios
(experimental-vs-theoretical)

Well resolved spectra were obtained in all cases and by careful calibration of linewidth, (FWHM) and lineshape, incompletely resolved peaks were unambiguously deconvoluted within very narrow error limits (typically ± 0.2 eV). In each case core levels corresponding to carbon atoms not directly bonded to oxygen had binding energies centered ~ 285.0 eV and were taken as the energy reference. It is clear that the shift in binding energy for a given carbon is characteristic of the chemical environment. For carbon atoms singly bonded to oxygen (e.g. alcohols, ethers and simple esters) the binding energies and shifts are highly characteristic, being 286.6 ± 0.1 eV and 1.6 ± 0.1 eV, respectively. The carbon atoms doubly bonded to oxygen fall into two classes, namely simple carbonyl compounds and esters, the binding energies and shifts for the former being significantly lower than for the latter

($287.9 \text{ eV} \pm 0.2 \text{ eV}$, $2.9 \text{ eV} \pm 0.2 \text{ eV}$ and $289.1 \pm 0.2 \text{ eV}$ and $4.1 \pm 0.2 \text{ eV}$, respectively). The overall shifts in binding energies, therefore, are sufficiently large to allow a ready means of identification of a particular structural feature.

For the O_{1s} levels the binding energies for the simple carbonyl compounds, alcohol and ether are essentially the same. By comparison, in the esters the singly and doubly bonded oxygen exhibit a substantial shift ($1.2 \pm 0.2 \text{ eV}$) and theoretical analysis unambiguously assigned the higher binding energy component as arising from the singly bonded oxygen. The core level spectra for a series of polyacrylates is shown in Fig. 2.14.

In other studies on polymeric systems, it was shown that the substantial differences in escape depth dependence for deep lying valence levels which are core like in character (viz. F_{2s}) with respect to tightly bound core levels, may usefully be employed for analytical depth profiling¹³⁰. In the present context it is clear from the published data in the literature on model compounds that it is only for the deep lying O_{2s} valence levels which are readily identifiable that this possibility for analytical depth profiling is a feasible proposition. (This is, of course, in addition to the depth profiling capability arising from differences in escape depth dependence for the O_{1s} and C_{1s} levels. For systems containing relatively large alkyl groups it is also clear from the literature that the region of the spectra corresponding to photoionization from orbitals essentially derived from linear combinations of C_{2s} levels span a considerable energy range making a direct integration of their overall intensities for comparison with that of the core levels somewhat difficult¹³⁸. In utilizing the valence energy region for information, with regard to composition as a function of depth, restrictions were made to using the O_{2s} levels, although it became clear that the overall band profile for the valence levels as a whole constitutes a 'fingerprint' for the system. For example, the measured valence energy levels for a series of isomeric polybutyl acrylates, where the core levels spectra are identical, are shown in Fig. 2.15. Through comparison with appropriate model systems the valence levels of the polymeric isomers allowed for unambiguous assignment of particular structural isomers.

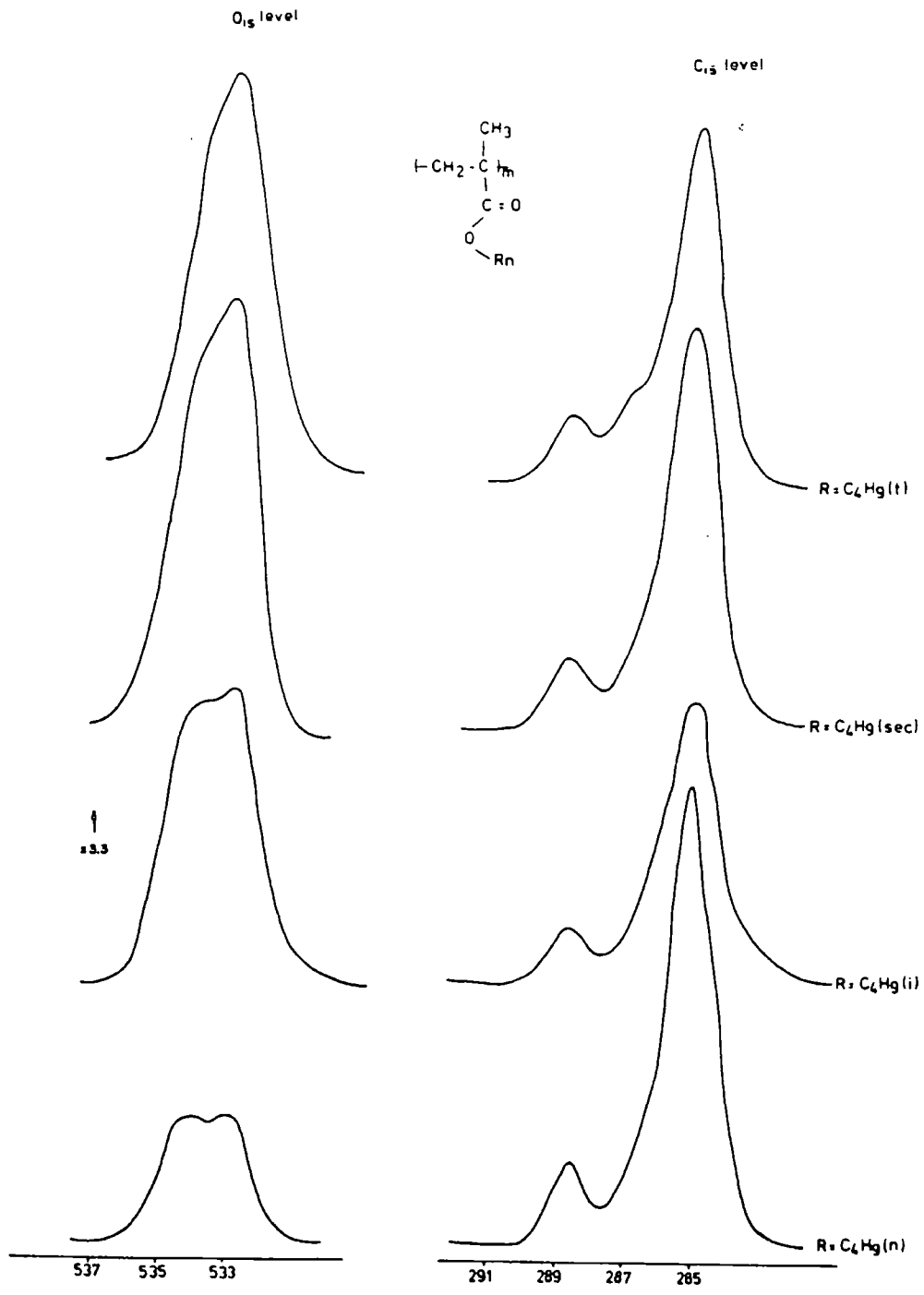


FIGURE 2.14

C_{1s} and O_{1s} core level spectra for a series of polyacrylates

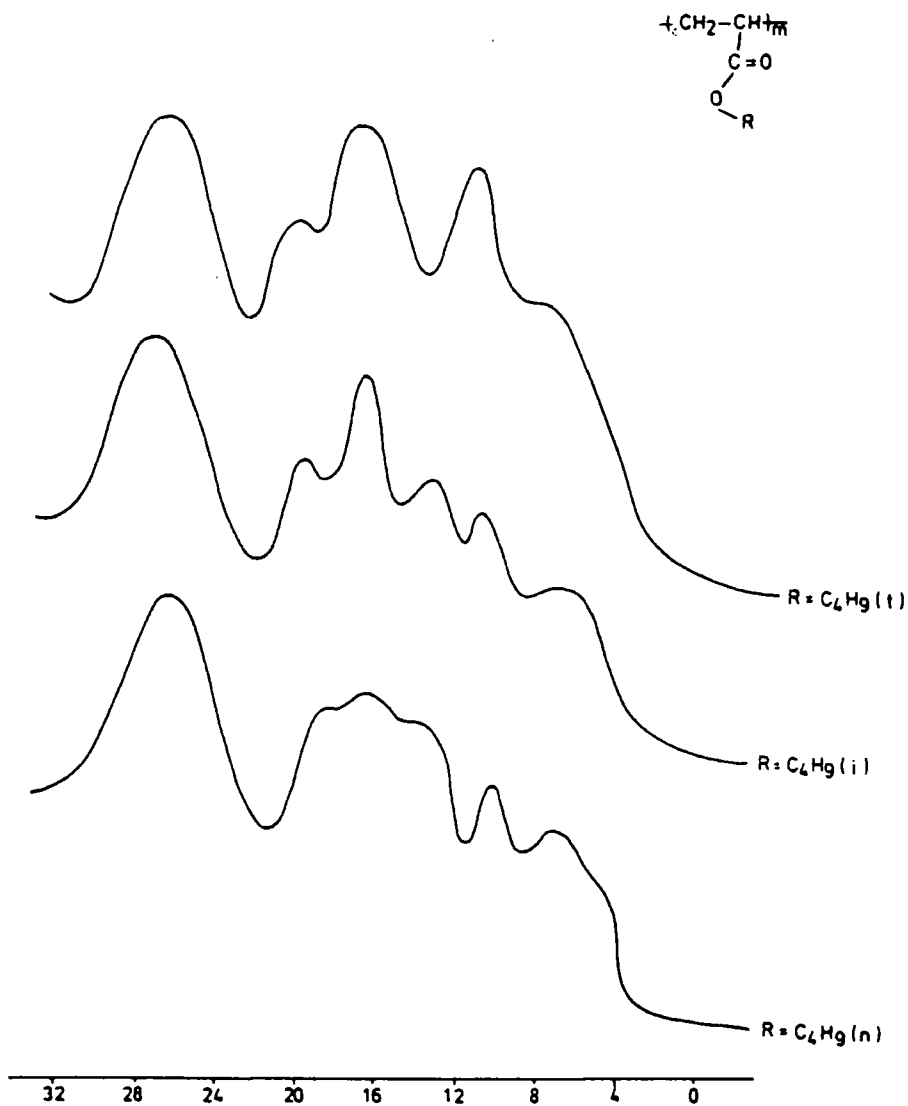
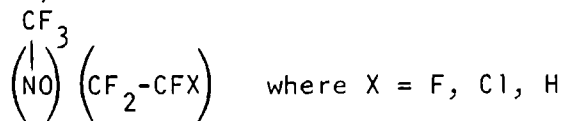


FIGURE 2.15

Measured valence energy levels of various isomers of polybutyl acrylate

c) Fine Structure

1) The complex analysis of the structural isomerism in a nitroso rubber copolymer



was carried out¹³⁹ and the C_{1s} levels for three of the rubbers are shown in Fig. 2.16.

The assignments of the peaks, based on previous knowledge from homopolymer and copolymer systems, is straightforward, and the chemical

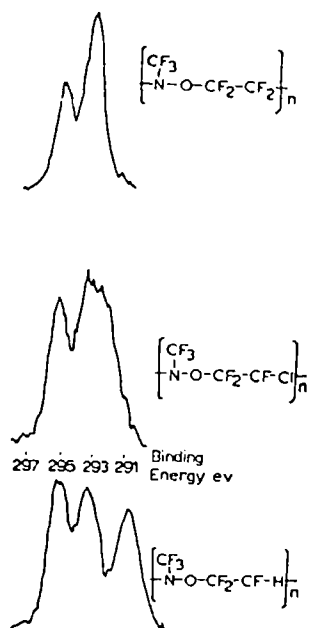


FIGURE 2.16

C_{1s} levels for copolymers of CF₃NO with CF₂=CF₂, CF₂=CFCL and CF₂=CFH

shifts assigned in terms of the simple substituent effect. Once the alternating sequence of the copolymer was identified, by methods discussed previously, an investigation into the possibility of detecting structural isomerism was made. By the application of simple compounds with the charge potential model and complex deconvolutions of the spectra, assignments were made on the structural isomerism.

2) The shake-up phenomena in a series of para-substituted polystyrenes and simple polymer systems was investigated⁵⁸ and has been compared with other spectroscopic data, with theoretical calculations within the sudden approximation equivalent cores model and, CNDO SCF MO formalism identifying the shake-up arising from $\pi \rightarrow \pi^*$ transitions involving the highest occupied and lowest unoccupied orbitals of the pendant aromatic systems. The polymers studied, with their core level spectra shown in Fig. 2.17, included polystyrene, polydiphenylsiloxane, poly-1-vinylnaphthalene, poly-2-vinylnaphthalene, polyacenaphthalene, and polyvinylcarbazole and it was shown that the shake-up structure was characteristic of a given pendant group. Although the simple model calculations have a tendency to predict transition probabilities lower than

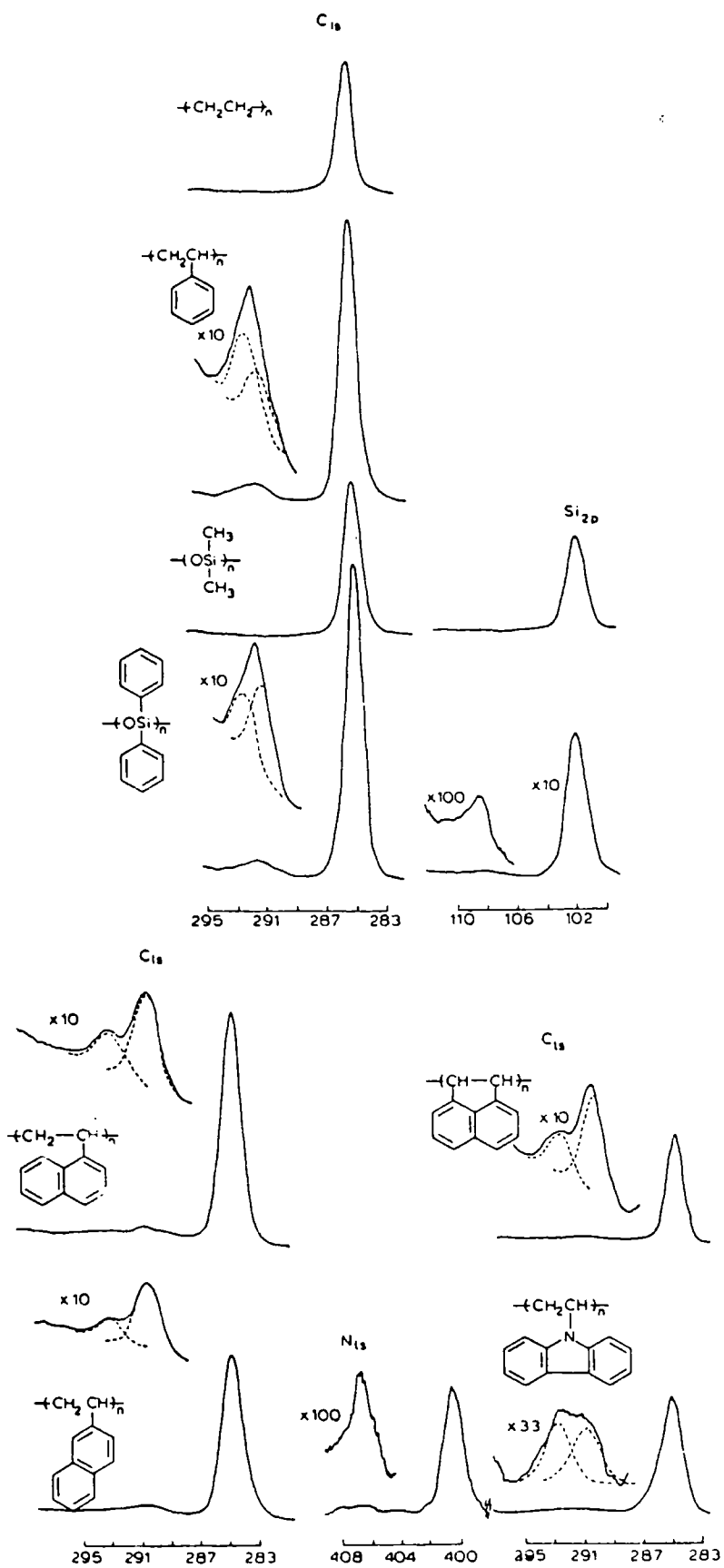
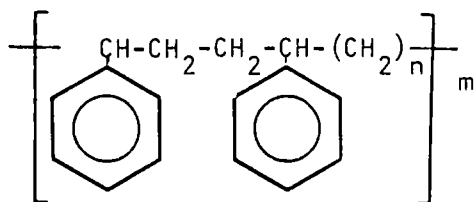


FIGURE 2.17

Core level spectra for various aromatic polymers

found experimentally, the success of the models in predicting trends and arriving semi-quantitatively at results on substituent effects in the substituted polystyrenes provided a firm basis for extension of the work.

The unique application of the shake-up phenomena in the study of a series of alkane-styrene copolymers further demonstrated the potential utility of this method of analysis¹⁴⁰. The study of copolymers



where $n = 0, 1, 3, 5, 6, 10,$

provided evidence that a trend existed between the shake-up intensity and the chain length of the alkane component, and that the structure of the shake-up satellites and the energy separation remained essentially constant. Fig. 2.18 illustrates the effect of decreasing

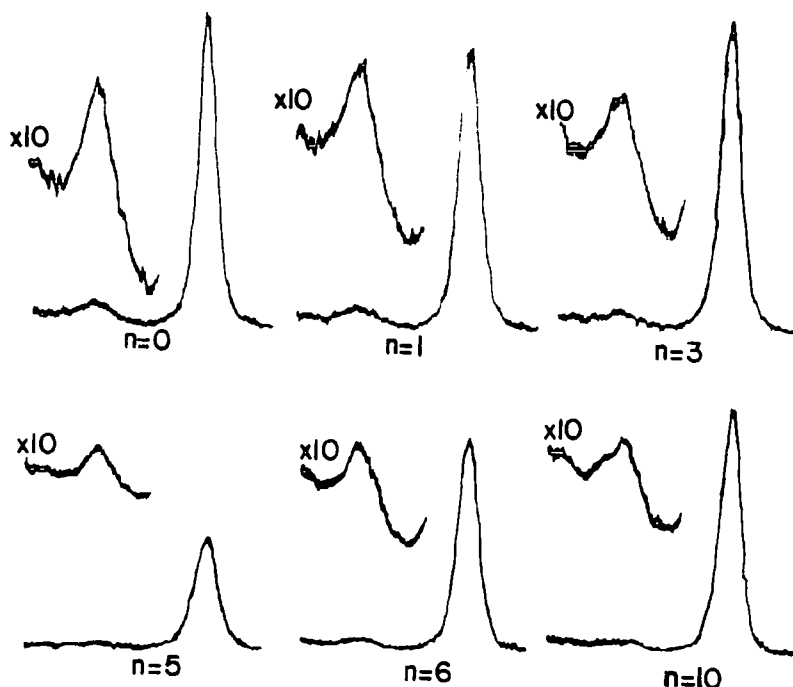


FIGURE 2.18

Illustration of effects of decreasing shake-up intensity with increasing alkane chain length in styrene/alkane copolymers

shake-up intensity with increasing alkane chain length. Because the shake-up intensities are additive in nature, a comparison of the relative area ratios gave a direct measure of the copolymer compositions.

3) The charge potential model, as discussed in Chapter 1, can be applied to polymers when the parameters k and E^0 are established for all the relevant core levels of the polymer systems being studied. It is possible to invert the model to obtain the experimental charge distributions within a polymer system. This method has the obvious application of being able to calculate the charge distributions in large models that are impracticable for conventional molecular orbital calculations and comparing it to experimentally found B.E.'s.

Having established the charge potential parameters E^0 and k for the core levels of the model systems an investigation can be made on both absolute and relative binding energies for models of the polymers.

As an example of an unsymmetrical vinyl monomer, shown in Fig. 2.19, the possibility exists for structural isomerism (viz. head to tail vs. head to head and tail to tail bonding). Also, for a given structural isomer the relative conformation of the pendant groups namely, the carbonyl and ester functions, are of some interest¹³⁷. It has been shown that the factors which determine differences in binding energies are relatively short range in nature and may, therefore, be quantitatively described by calculations on model systems incorporating a small number of monomer units such that all of the important short range interactions are quantified. In particular cases, (e.g. nitroso rubbers¹³⁹), it was shown that structural isomerisms may be investigated directly by ESCA; however, in general for homopolymers based on simple unsymmetrical vinyl monomers both theory and experiment agree that both absolute and relative binding energies are virtually the same for regular and irregular structures³⁵.

Even at the semi-empirical all valence electron SCF MO CNDO/2 level, computations on model systems for the polymers studied in this work are extremely time consuming. Computing limitations, therefore, dictated that the central monomer unit of the model chains were linked to a single monomer unit at each end. Calculations reported in the literature¹³⁹ show that such a model incorporates all the important short range interactions with respect to the central unit. In the model system chosen for study, polyacrylic acid, in all cases standard bond angles and lengths were employed for the various structural features¹⁴¹.

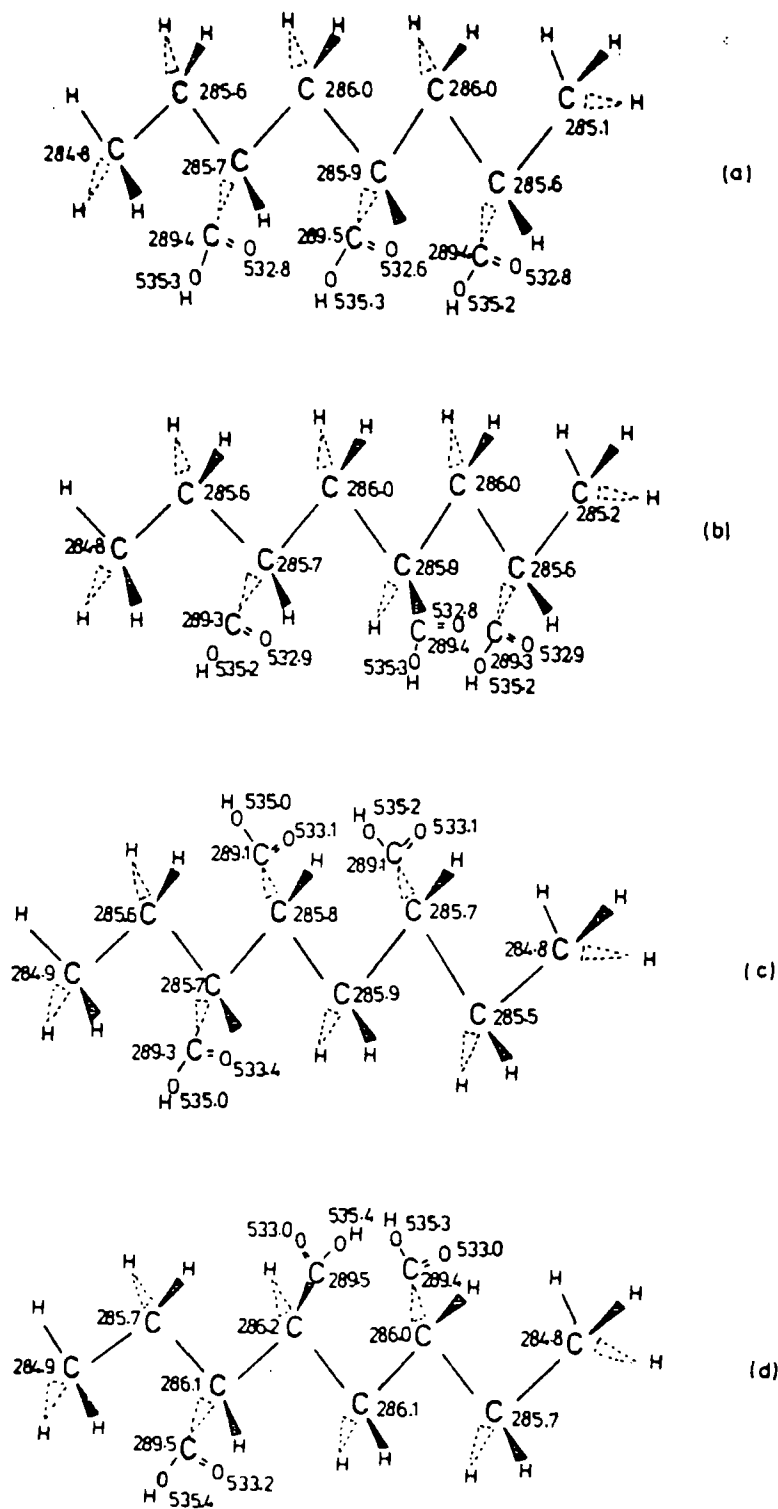


FIGURE 2.19

Conformational models of poly(acrylic acid) with calculated binding energies from the charge potential model shown for (a) HT-HT "isotactic" model; (b) HT-HT "syndotactic" model; (c) HH-HT "isotactic" model; (d) HH-HT "syndotactic" model

For polyacrylic acid the models studied exemplified both structural isomerism and relative conformational preferences for the side chain. For a model system composed of three monomer units the two distinct structural isomers with respect to the central unit may be designated as head to tail (HT) or, head to head (HH) or tail to tail (TT). For the head to tail (regular) arrangement (HT-HT linkages) both the 'isotactic' and syndiotactic' forms were investigated. Calculations on simple model systems such as isopropyl acetate indicated that the most stable conformers involved an eclipsed arrangement for the carbon-oxygen double bond and the adjacent carbon hydrogen bond, and indeed experimental data on related systems supports this conclusion⁵⁶. For the model systems, therefore, the carbonyl group was taken to eclipse the CH bond of the backbone and this is referred to as the π eclipsed arrangement. In particular cases, calculations were also carried out on staggered conformers in which the carbonyl group was rotated through an angle of 60° (with respect to the eclipsed configuration) about an axis through the carbon-carbon bond linking the pendant group and backbone. Without exception, such conformers were calculated to be significantly higher in energy than for those involving a π eclipsed arrangement. For a head to head (irregular) arrangement (HH-HT linkages) the side chains were again taken in the π eclipsed conformations with the pendant groups either all being on the same side of a plane drawn through the backbone or in an alternating arrangement. These are analogous to the isotactic and syndiotactic arrangements in the regular head to tail model system.

The results for the models of polyacrylic acid also are displayed in Fig. 2.19 where the absolute binding energies have been computed using the charge potential parameters derived from the study of simple model systems as described in a previous section. Considering first the regular head to tail arrangement ((a) and (b) Fig. 2.19) it is clear that the factors determining both the absolute and relative binding energies are insensitive to the overall stereochemistry of the system. Comparison with the corresponding data for the staggered (with respect to the carbon-oxygen double bond, conformers reinforces this conclusion since the calculated binding energies are in exact correspondence with those for the eclipsed conformers shown in Fig. 2.19. A comparison of the central monomer units with the adjacent units, effectively demonstrates the short range nature of the factors determining absolute and relative binding energies in these

systems. A comparison with the experimental data revealed the overall adequacy of the theoretical model in respect of both absolute and relative binding energies for both the O_{1s} and C_{1s} levels. For the regular models, the second methylene group in the chain linked directly to the methyl group provides an indication of the likely binding energy for methylene groups appropriate to a tail to tail structural arrangement. This is also apparent from the corresponding irregular HH-HT models ((c) and (d) Fig. 2.19). For the two possibilities considered, it is evident that the calculated binding energies show a small dependence on stereochemistry arising from the significant interaction between carbonyl groups oriented cis to one another on adjacent carbon atoms. For both models, the backbone carbons are predicted to have closely similar binding energies, a feature common to the regular models alluded to previously. The shifts in binding energy for the O_{1s} levels range from 2.7 eV for the HT-HT 'isotactic' model to 1.9 eV for the HH-HT 'isotactic' model. This compares with the experimentally determined value of 1.3 eV. The discrepancy is largely accounted for by the effect of inter and intra chain hydrogen bonding which has somewhat of a levelling effect on the relative charge distribution about the two types of oxygen. This effect has been noted in the literature and is manifest in a distinctly increased linewidth for the individual components of the O_{1s} levels¹.

The application of the charge potential model to an extensive series of homopolymers is described in Chapter 3.

4) The valence levels of polymers are of relevance to the detailed interpretation of the overall electrical properties of polymers. In the case of simple molecules the study of the valence levels by ESCA has the disadvantages, as discussed in Chapter 1, when compared to UPS in that the cross sections are generally lower in ESCA and the resolution is much poorer (see Fig. 1.16).

When studying polymer systems, these disadvantages are offset in that since there are so many vibrational modes possible, resolution becomes less of a problem. Also, with ESCA, all the valence levels can be studied whereas with UPS only the higher occupied levels can be studied and with electron energies of 0 - 21 eV (He I) and 0 - 40 eV (He II). In UPS this is the region of rapidly varying escape depth where surface contamination would be critical, whereas this is much less so with X-ray photon energies. The application of the study of the

valence band to 'fingerprint' different isomers of polymers where the core levels are identical was discussed in section (b) and in Fig. 2.20 is shown the valence band spectra for a series of ethylene and fluoro-ethylene polymers.

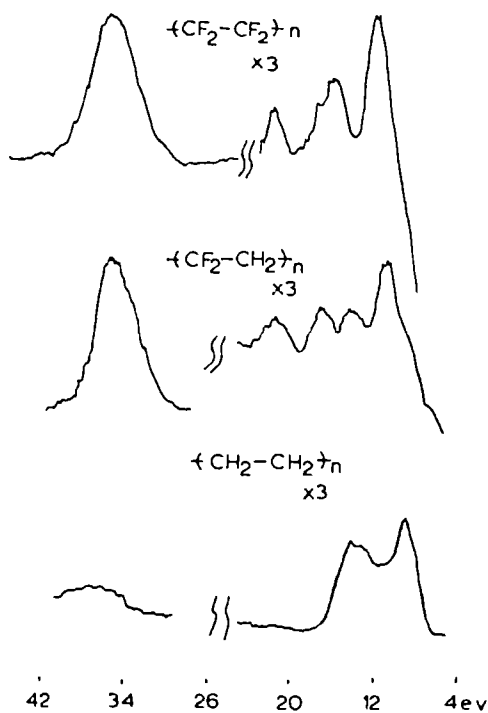


FIGURE 2.20

Valence level spectra for a series of ethylene/fluoroethylene polymers

iv) Dynamic Studies on Polymer Systems

a) Surface Treatments

1) Crosslinking by activated species of inert gases (CASING), where a polymer is exposed to activated species of inert gas is a particularly good application of ESCA to polymer chemistry. Studies have been made on copolymers of ethylene/tetrafluoroethylene where the films were irradiated with a low energy (2 kV) beam of argon ions for successive periods of 5 seconds and the C_{1s} and F_{1s} core levels monitored¹²⁵. Figure 2.21 quite clearly demonstrates the effects on the top surface of the ion bombardment. Possible mechanisms for the process were proposed and the most likely steps chosen based on the ESCA information available.

2) The surface fluorination of polyethylene was examined¹³⁰ and a very detailed analysis of the spectra confirmed the technique to establish a quite complete picture of the early stages of the surface

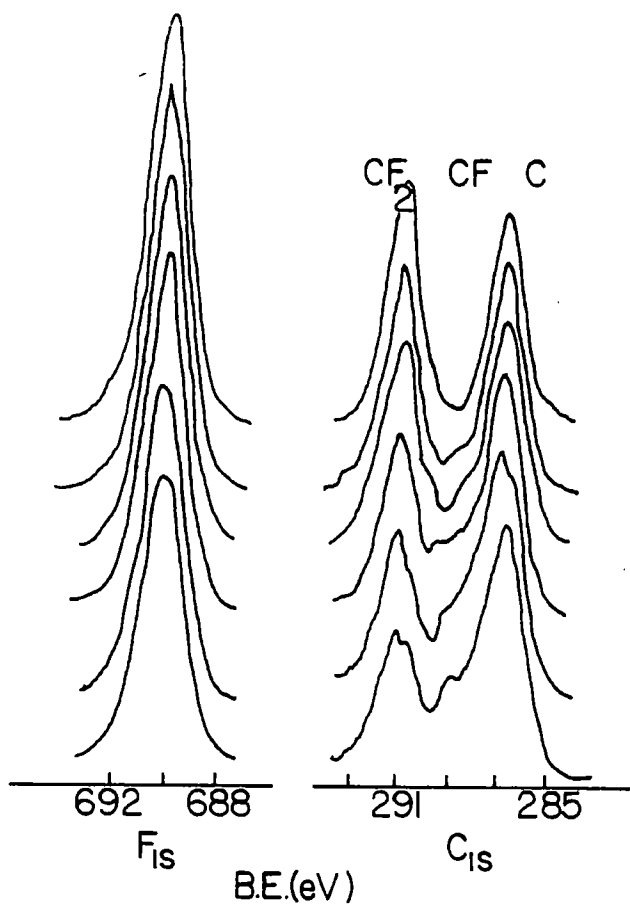


FIGURE 2.21

Effects of ion bombardment on core levels spectra of ethylene/tetrafluoroethylene copolymer

fluorination process.

Although a detailed description of the analysis is beyond the scope of this summary, the results of the investigation were based upon two methods of analysis. The first method was based upon the equation (2.1)

$$\frac{y}{K} - 1 = \frac{y}{K} e^{-d/\lambda_3} - e^{-e/\lambda_1} \quad (2.1)$$

where y = measured area ratios for F_{1s} and F_{2s} peaks from ESCA spectrum.
 K = infinity values for escape depths of infinitely thick films measured from homopolymers.

λ_3 = electron mean free path appropriate to F_{2s} levels

λ_1 = electron mean free path appropriate to F_{1s} levels

where a grid of computed values for the right-hand side of equation (2.1) was prepared to values of \underline{d} in the range 2 - 41 Å at 1 Å intervals and ratio λ_3/λ_1 from 1 to 2 in 0.1 increments. The computations for 40 values of \underline{d} and 11 values for each ratio of λ_3/λ_1 generates 24,200 data points. These tables were used in the analysis of five fluorinated films and fluorinated film thicknesses were computed to be 3.5, 6, 16, 30 and 36 Å, respectively for the five films.

An alternate procedure using the C_{1s} levels determined the depth of fluorination of the film and Table 2.3 illustrates the comparison between the two methods.

Calculated Thickness of Fluorinated Film (d)

Experiment	d, Å		Average
	From C_{1s} spectra	From F_{1s}/F_{2s} spectra	
1	5.5	3.5	4.5
2	9.0	6.0	7.5
3	15.0	16.0	15.5
4	24.0	30.0	27.0
5	46.0	36.0	41.0

Table 2.3

3) RF Plasma Treatments

In recent years a significant amount of research activity has appeared on the application of RF inductively coupled plasmas in inert gas, for the surface modification of polymeric materials to improve adhesive bonding and alter surface properties in general. For plasma excited in Argon, for example, the reactive species are the Argon ions, metastables and electrons¹⁴². In addition, since plasmas are abundant sources of electromagnetic radiation, particularly in the vacuum ultraviolet region, it is clear that modification to the polymer surface could also arise from absorption of short wavelength radiation. With the analytical techniques available in the past, the evidence supported the contention that the modification was dominated by the radiative energy transfer processes to the bulk. With the surface sensitive technique of ESCA it is possible to follow the initial stages of the plasma treatment and to differentiate the surface from subsurface from bulk reactions. In a recent investigation, Clark and Dilks¹⁴² investigated



the relative importance of direct and radiative energy transfer processes in the interaction with an alternating copolymer of ethylene and tetrafluoroethylene (48:52%) treated in a pulsed RF discharge at an average power loading of 0.1 watts. The core level spectra as a function of reaction time are shown in Fig 2.22 where the important features are i) a decrease in intensity of the F_{1s} levels and \underline{CF}_2 component of the C_{1s} levels; (ii) the appearance of structure at intermediate binding energy for the C_{1s} levels appropriate to the production of \underline{CF} structural features; (iii) an overall increase in the total integrated intensity of the C_{1s} levels as a function of reaction time. A detailed analysis using angular studies and other inert gases (He, Ne, Kr) were consistent with an overall picture that a general feature of the inert gas plasma reactions is that the first monolayer or so of a given polymer is dominated by direct energy transfer (e.g. ions, metastables, electrons) processes while for the subsurface and bulk, the dominant mechanism is by radiative transfer predominantly from the vacuum ultraviolet output of the plasma.

b) Oxidative Degradation of Polymers

While for homogeneous samples of polymers sampled by ESCA the outermost few tens of Angstroms correspond to that in the bulk, this is not always the case, as discussed in section (a). For example, Fig. 2.23 shows the ESCA spectra for a series of polyalkyl acrylates¹³⁷.

A distinctive feature clearly evident in all of the spectra is the obvious inequality in intensity of the two component peaks of the O_{1s} levels. Fig. 2.24, for example, shows a plot of the ratio of intensities for the individual components of the O_{1s} levels and also the total O_{1s}/O_{2s} ratios. For comparison purposes the dotted lines indicate the correlations expected for samples which on the ESCA depth profiling scale correspond to a statistical sampling of the appropriate repeat unit in the polymer. It is clear that there are considerable deviations from such correlations in a direction which overall suggests that the samples are oxidized. If we consider the polydecyl acrylate for example, the O_{1s}/O_{2s} ratio is significantly higher than for the reference compounds suggesting that since the mean free path for the O_{1s} levels is considerably shorter than for the O_{2s} level^{125/130} that the oxidation is largely confined to the surface. The absolute binding energies in each case for the O_{1s} component levels which have apparently increased in intensity, corresponds to $\underline{C=O}$ structural features, as is apparent from a comparison with data for the model system. It is interesting to note that high

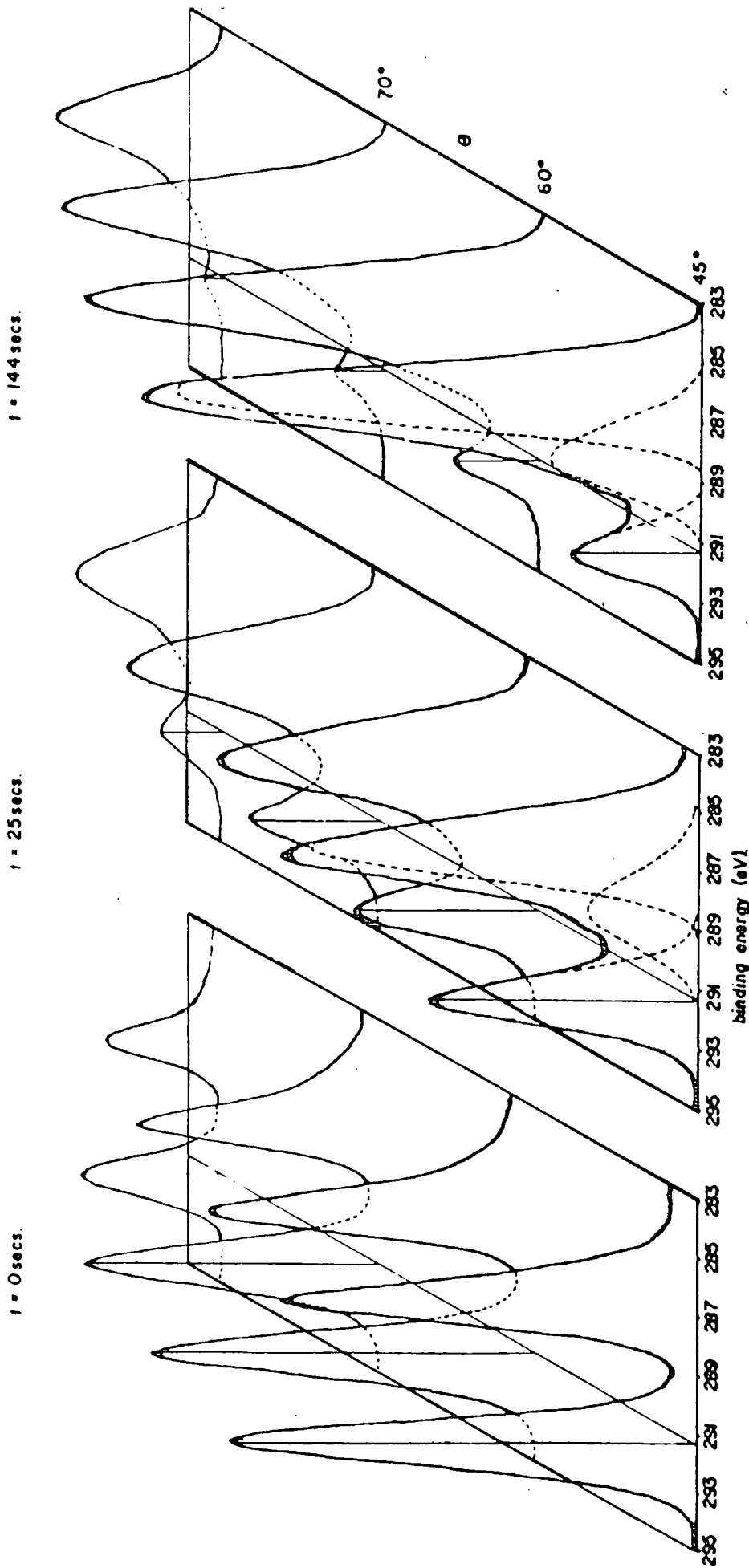


FIGURE 2.22
Core level spectra of ethylene/tetrafluoroethylene copolymer as a
function of time exposed to plasma

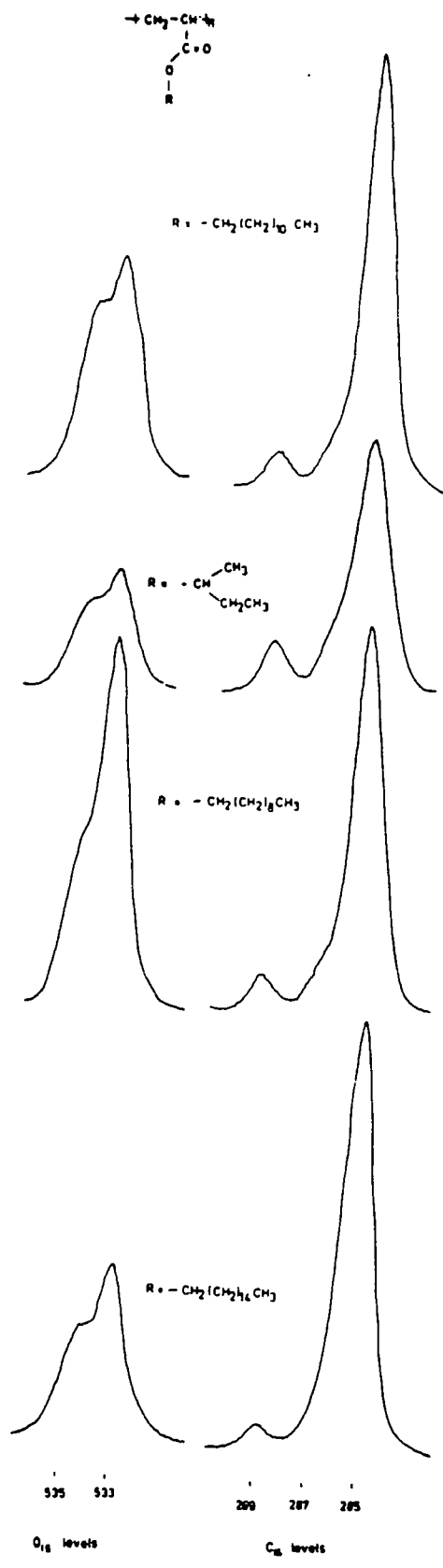


FIGURE 2.23

Core level spectra of oxidized polyalkyl acrylates

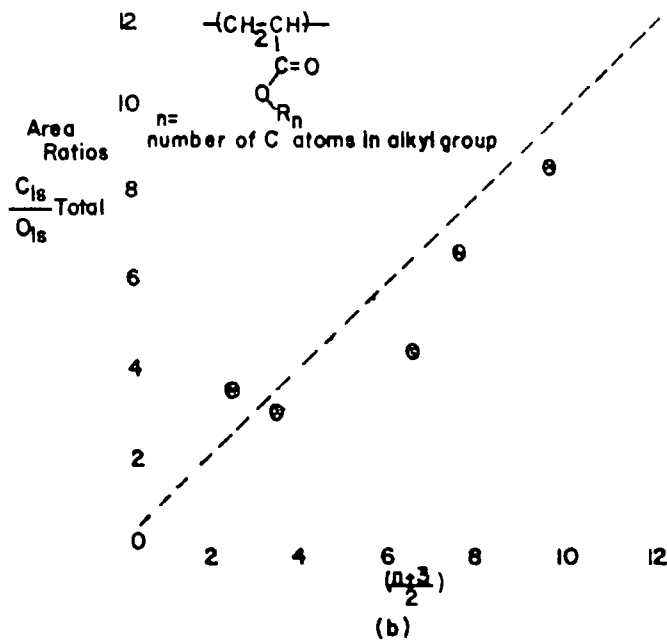
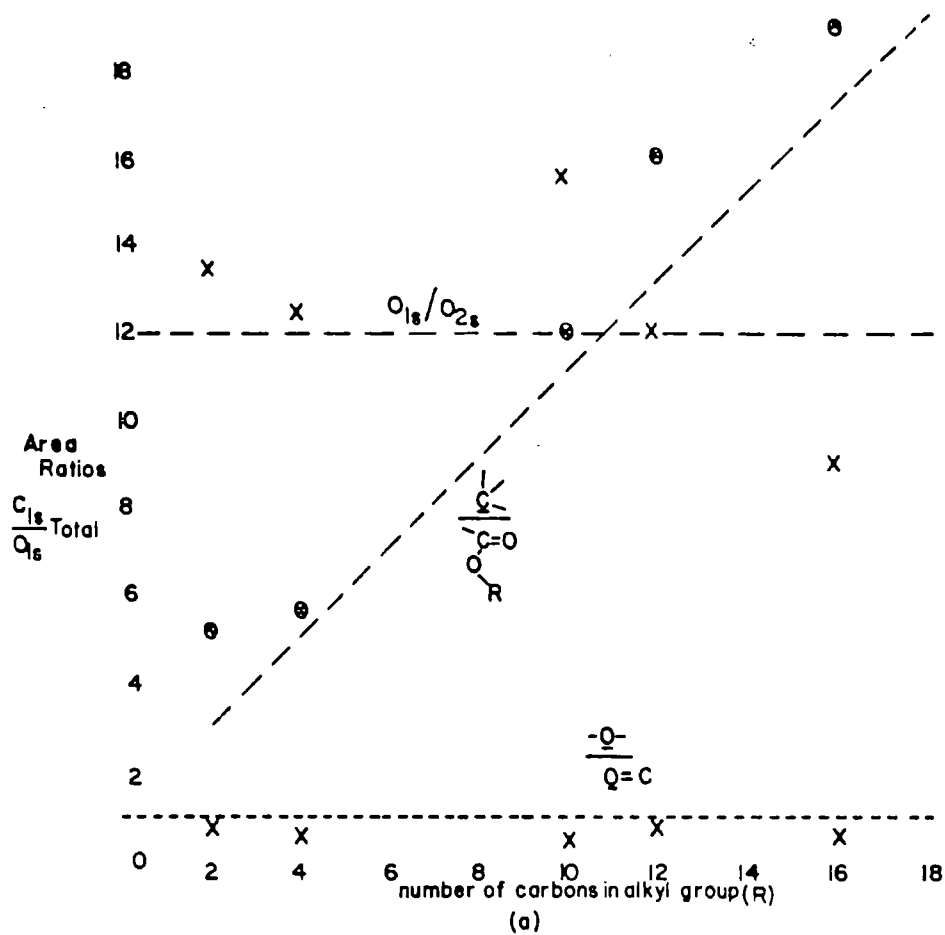


FIGURE 2.24

Plots of (a) intensity ratios for the individual components of the O_{1s} levels and also the O_{1s}/O_{2s} ratios for a series of poly(alkyl-acrylates); (b) the C_{1s} and O_{1s} area ratios vs. the number number of carbons in the alkyl group

resolution infrared studies revealed no major distinction of the type clearly evident from the ESCA spectra and the carbonyl region for all of the samples showed only a single peak in the range $1734 \pm 6 \text{ cm}^{-1}$ consistent with $-\overset{\text{O}}{\text{C}}-\text{O}-\text{R}$ structural features¹⁴³. This is readily understandable since the infrared data pertains essentially to the bulk. Further evidence for the oxidized nature of the poly-n-decyl acrylate surface is provided by the greatly increased wettability with respect to water compared with polyisopropyl acrylate as a representative example of the unoxidized samples. This was immediately apparent from the relative contact angles assessed from the photographs for the two samples. A comparison was also made with poly-2-ethylhexyl and polyoctadecyl acrylates, the latter having a contact angles closely similar to that of polyisopropyl acrylate whilst the former showed a wettability intermediate between that of polyisopropyl acrylate and poly-n-decyl acrylate.

If the surface oxidation inferred from the inequality of the component peaks of the O_{1s} levels is attributable to surface carbonyl features, then this should also be manifest in the carbon $1s$ levels. It should, however, be emphasized that since the escape depth dependence for photoemitted electrons in the energy range considered is such that the mean free path increases with increasing kinetic energy then any surface feature will be relatively more prominent for the more tightly bound O_{1s} levels than for the C_{1s} levels⁴. As a simple model for a system containing both structural features viz. ketonic carbonyl group and ester group, we may consider ethyl acetoacetate. The C_{1s} levels are shown in Chapter 1, Fig. 1.27, which also details expansion of the C_{1s} levels for isobutyl acetate, a polyisopropyl acrylate film which had been heated in air (150°C for 30 mins.) and for comparison purposes a sample of polyisobutyl acrylate whose O_{1s} spectrum also showed evidence for surface oxidation, (Fig. 2.23). Considering firstly the isobutyl acetate and polyisopropyl acrylate spectra the deconvolution into the component peaks associated with $-\overset{\text{O}}{\text{C}}-$, $\text{O}-\overset{\text{O}}{\text{C}}-$ and $-\text{C}-$ structural features with characteristic binding energies is straightforward, as we have previously noted. By comparison, the spectrum of ethyl acetoacetate shows that the carbonyl carbon at 287.2 eV (Table 1.5) has the effect of 'filling in' the valley between the high and low binding energy regions. This effect is clearly evident for both polyisobutyl acrylate and for the polyisopropyl acrylate sample heated in air. A detailed examination

of the C_{1s} spectra for the series of surface oxidized samples, Fig. 2.23, shows that the overall line profiles can only be quantitatively fitted with the addition of a small peak in the C_{1s} spectrum appropriate to isolated carbonyl groups.

c) Adsorption at Polymer Surfaces

Clark, et al, have shown that the great surface sensitivity of ESCA may be used to considerable advantage in studying the hydration of surface features on polymers capable of participation in hydrogen bonding¹²⁵. Such studies are likely to be of some considerable importance in unravelling the complexities of, for example, triboelectric charging and various aspects of tribochemistry. In the particular case of low density polyethylene the adsorption of H_2O on surface carbonyl features manifests itself in terms of the appearance of a shoulder to the high binding energy side of the O_{1s} levels associated with the carbonyl oxygen and attributed to the hydrogen bonded water. Careful double beam infrared studies reveals no evidence for such interactions since they are localized at the surface.

In continuance of this work, Clark and Thomas investigated the interaction of hydrogen bonding species with the surface of polyisopropyl acrylate films, being prototypes for a system which is unoxidized at the surface¹³⁷.

Fig. 2.25 shows the O_{1s} and C_{1s} levels for samples of polyisopropyl acrylate that were exposed to NH_3 , H_2O and HF. These represent an order of increasing hydrogen bond strength and it is clear from the spectra that only in the case of the HF treatment is there any substantial change in the overall spectra. The hydrogen bonding almost certainly involving primarily the carbonyl oxygen of the ester group leads to a sharpening of the O_{1s} levels such that the two components are now more readily apparent without recourse to line shape analysis. The overall signal intensity for the O_{1s} and C_{1s} levels is also attenuated due to the adsorbed HF which is identified by the low absolute binding energy for the F_{1s} levels. The propensity for hydrogen bonding of the carbonyl group of an ester is considerably less than that for a ketonic carbonyl group and, in addition, for these particular polymer samples as the bulk of the alkyl group increases the hydrophilic 'carbonyl region' is increasingly shielded by the hydrophilic portions of the polymer system. In contrast, therefore, to the clear cut detection of surface hydrogen

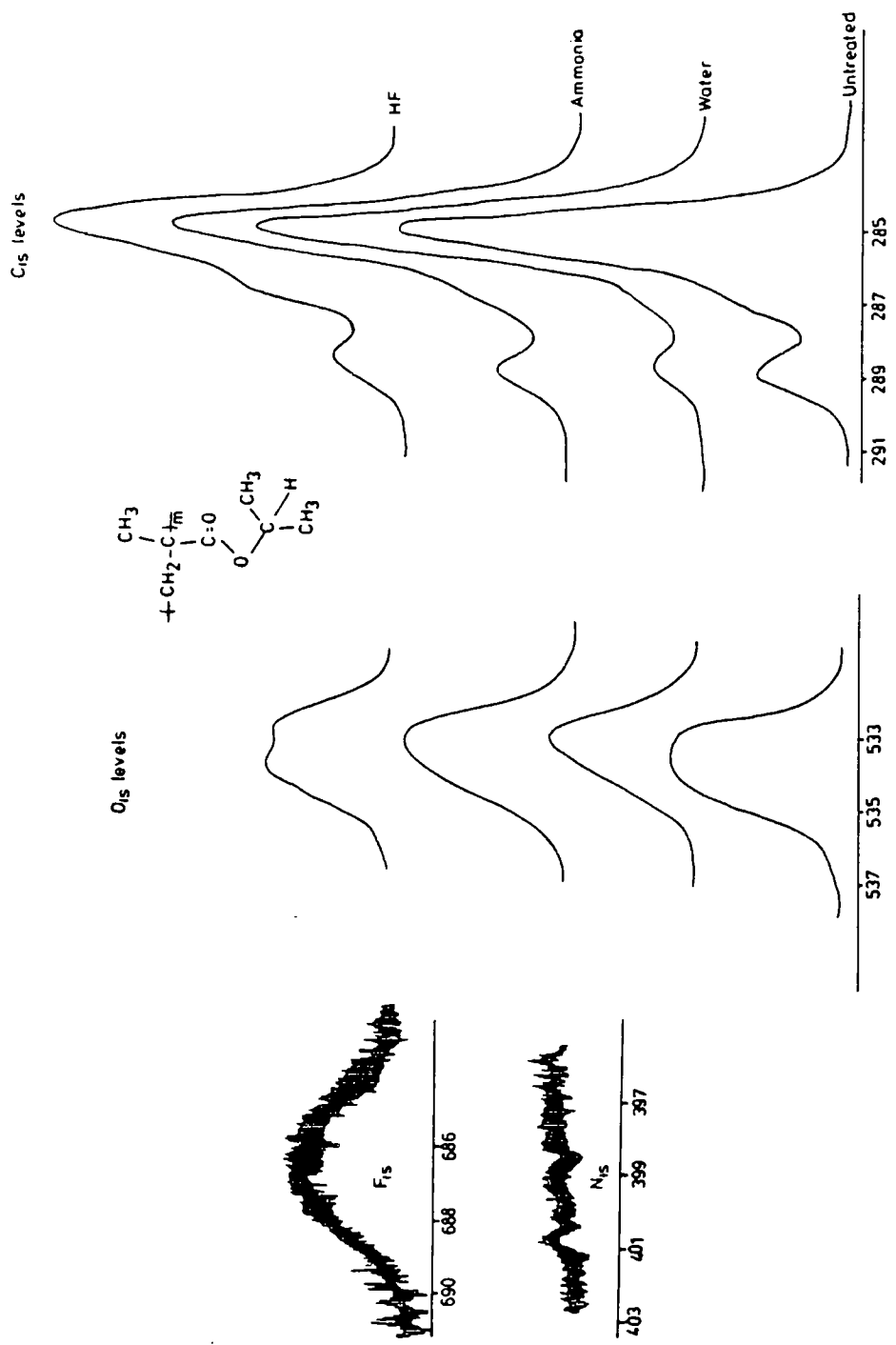


FIGURE 2.25
O_{1s} and C_{1s} core level spectra for samples of polyisopropyl acrylate surface treated with H₂O, NH₃ and HF

bonding to ketonic type carbonyl groups in polyethylene, the net effect of surface treatment of polyisopropyl acrylate with H_2O is a small change in linewidth which can be attributed to a very small degree of hydrogen bonding. It is interesting to note that for NH_3 which might be expected to form the weakest hydrogen bonds, the spectra show little evidence for any interaction since the N_{1s} signal is barely discernable above the background and the overall band profiles for the O_{1s} and C_{1s} levels within the statistical limits of the data are superimposable on those for the untreated sample. The data described here again illustrates the great potential of ESCA for investigating interactions at polymer surfaces.

CHAPTER 3

A Systematic Investigation of the Core Levels
of Simple Homopolymers

CHAPTER 3A Systematic Investigation of the Core Levels of Simple Homopolymersi) Introduction

The first two chapters in this thesis have shown that a detailed analysis of the absolute and relative binding energies and relative peak intensities corresponding to the direct photoionization of core levels can provide data on structure and bonding in polymeric systems. The early work pertaining to fluoropolymers, where the large electronegativity of the fluorine substituents give rise to a substantial range in binding energies for the C_{1s} levels, established the absolute binding energies for the carbons in different electronic environments. For polymer systems that are solely hydrocarbon based and for which the differences in core binding energies are quite small, it has been shown that nonetheless, in particular cases, it is possible to derive information from the study of shake-up transitions, which manifest themselves as satellites to the high binding side of the primary photoionization peak, as discussed in Chapters 1 and 2.

Since many of the important physical, chemical, electrical and mechanical properties of a polymer depend on the structure, bonding and morphology in the outermost few tens of Angstroms of the surface, a technique such as ESCA which can differentiate between the surface, sub-surface and bulk of a polymer is of some considerable importance. It appears that ESCA will become increasingly significant in establishing whether structure, bonding and morphology at the surface of polymers is different from the bulk. In principle, the information levels available from the ESCA experiment are such that the technique may be employed to investigate whether the outermost few tens of Angstroms of a sample are representative in terms of structure and bonding of the bulk, whether in this region the sample is homogeneous and if inhomogeneous, the extent of inhomogeneities in terms of lateral and vertical contributions. An area that has already received considerable interest is in the monitoring of chemical and physical modifications to polymer surfaces such as oxidation¹³⁷, R.F. glow discharge modifications¹⁴², cross-linking by ultra-violet light¹⁴² and direct fluorination of films¹³⁰.

Previous studies of substituent effects on core levels in simple monomeric systems has shown that the effects are short range in nature and are highly characteristic of a given substituent and

moreover tend to follow simple additivity rules^{125,130,135,139,144}. These results have been quantified by extensive nonempirical calculations and the detailed theoretical studies provide a strong basis for extending theoretical models to polymeric systems^{1,127,128}. Whereas large model systems for polymers (i.e. repeat units of, say, ~10 - 15 atoms) would be computationally extremely expensive and time consuming at an ab initio level even with minimal basis sets, computationally less expensive, but theoretically valid models within the semi-empirical all valence electron CNDO/2 SCF formalism⁷⁰ provide a sound basis for quantifying data on polymers since it is feasible to study systems incorporating a substantial number of monomer units such that all of the important interactions which determine both absolute and relative core binding energies are adequately described.

In this chapter a systematic ESCA study on a large number of homopolymers of simple monomers is given to provide a compilation of substituent effects on C_{1s} , O_{1s} , Cl_{2p} , Si_{2p} , F_{1s} , S_{2p} , and Br_{3d} levels. The characteristic nature of many of these substituent effects can now be used as a 'fingerprint' analytical tool in much the same manner as one might use infrared and N.M.R. data. From studies on absolute and relative binding energies and relative peak intensities, the surface composition of these polymers may be established and comparisons drawn with data pertaining to the bulk material based upon a statistically sampled repeat unit. A parallel theoretical investigation on models for quantifying the data pertaining to both the absolute and relative binding energies and confirmation of the core level assignments has also been undertaken. This theoretical investigation also allowed for the evaluation of two models based on the 'ground state potential model' (GPM)¹⁹ and the 'half-ionized or relaxation potential model' (RPM)¹⁴⁵ for a selected number of polymer systems for comparison with experimental data.

ii) Experimental

a) Samples

The polymers, listed in Table 3.1 were commercially available samples (except for the polyparaxylylenes) obtained from Cellomer Associates, Inc. (P.O.Box 311, Webster, N.Y.) and were used directly in preparing samples for the ESCA investigations. Model compounds described elsewhere were used as guides in the interpretation of the data pertaining to the polymer systems^{136,137,144,147}. These previous studies on the core level spectra of model compounds established for

Homopolymers investigated and the physical form studied, where P (powder), F (commercial film), R (rubber), CF (cast film) and N (neat, low Tg)

<u>-C-</u>		<u>C/O continued</u>	
Polyethylene (L.D.)	F	Polyethylene terephthalate	F
Polyethylene (H.D.)	F	Polyacetyl-p-xylylene	F
Polypropylene (isotactic)	F	Polycaprolactone	CF
Polypropylene (Biax oriented)	F	Polycarbonate (aliphatic)	P
Polypropylene (isotactic)	F	Polycarbonate (aromatic)	CF
Polybutadiene (CIS)	R		
Polybutadiene(RandomCIS-TRANS)	R	<u>C/CL</u>	
Polyisobutylene	R		
Poly-1-butene (isotactic)	CF	Polyethylene, chlorinated (25%)	P
Polystyrene (2x10 ³ MW)	P	Polyethylene, chlorinated (36%)	P
Polystyrene (2x10 ⁶ MW)	CF	Polyethylene, chlorinated (42%)	P
Polystyrene (2x10 ⁷ MW)	CF	Polyvinyl benzyl chloride (69/40o/p)	P
Poly-4-methyl Styrene	CF	Polyvinyl chloride	P
Polyvinyl toluene	CF	Polypropylene, chlorinated	P
Polytertbutyl Styrene	CF	Chlorinated rubber	R
Polyacenaphthalene	P	Poly-4-chlorostyrene	P
Poly-1-vinylnaphthalene	P	Polychlorostyrene (mixed isomers)	P
Poly-2-vinylnaphthalene	P	Polychloro-p-xylylene	F
Poly-p-xylylene	F	Polydichloro-p-xylylene	F
Polymethyl-p-xylylene	F		
Polyethyl-p-xylylene	F	<u>C/N/O</u>	
Polybenzyl-p-xylylene	F		
Poly-4-isopropyl Styrene	CF	Poly-2-vinyl pyridine	CF
<u>C/O</u>		Poly-4-vinyl pyridine	CF
Polyvinyl acetate	CF	Poly-4-amino styrene	P
Polyvinyl alcohol	CF	Polyacrylonitrile	P
Polyvinyl methyl ether	CF	Polymethacrylonitrile	P
Polyacrylic acid	P	Poly-N-vinyl carbazole	P
Polymethyl acrylate	N	Polyacrylamide	P
Poly-n-butylacrylate	CF	Polymethacrylamide	P
Poly-n-laurylacrylate	N	Polyvinyl pyrrolidone	P
Polyoctadecylacrylate	N	Polycaprolactam (Nylon 6)	CF
Polymethyl methacrylate	P	Polyhexamethylene adipamide (Nylon6/6)	CF
Poly-n-butyl methacrylate	CF	Polyhexamethylene azelamide (Nylon6/9)	CF
Polylauryl methacrylate	CF	Polyhexamethylene sebacamide (Nylon6/10)	CF
Polyoctadecyl methacrylate	N	Polyhexamethylene dodecanediamide (Nylon6/12)	CF
Polyphenyl methacrylate	P	Polyundecanoamide (Nylon 11)	CF
Polybenzyl methacrylate	P	Polylauryllactam (Nylon 12)	CF
Polyisobornyl methacrylate	P		
Polyacetyl	CF	<u>C/F/O/S/Si/Br</u>	
Polyvinyl cinnamate	P	Polydimethyl siloxane	N
Polyvinyl butyral	P	Polydiphenyl siloxane	P
Polyvinyl-neo-deconoate	N	Polysulfone resin	CF
Polyvinyl stearate	N	Polyphenylene sulfide	P
Polyhexamethylene sebacate	N	Poly-4-bromo styrene	P
Poly-4-methoxy styrene	P	Polybromo-p-xylylene	F
Poly(1,4-cyclohexane dimethyl)		Polyvinyl fluoride	P
terephthalate	CF	Polyvinylidene fluoride	P
Poly(1,4-cyclohexane dimethyl)		Polytrifluoro ethylene	CF
succinate	CF	Polytetrafluoroethylene	F
Poly-m-phenoxylylene	CF	Polycarbonate (fluoro)	P
Polydiallyl-o-phthalate	P		
Polydiallyl-iso-phthalate	P		
Poly-2,6-dimethyl-1,4-phenylene			
oxide	P		
Polyphenylene oxide	P		

TABLE 3.1

the C_{1s} , O_{1s} , F_{1s} , Cl_{2p} , Si_{2p} , S_{2p} and Br_{3d} the absolute binding energies for general substituent effects, relative cross sections for quantifying the data to confirm stoichiometry and provided a basis for line shape analysis for the deconvolution of unresolved peaks.

b) Sample Preparation

The polymers were studied as either fine powders (F) coated onto double sided 'Scotch' tape directly attached to the spectrometer probe; as cast films (CF) onto gold substrates, the gold being attached to the probe by double sided 'Scotch' tape; as neat films (N) where a small sample (normally of low Tg value) was spread on gold and the gold attached as described above; as a film (F) (meaning commercially processed film) attached to the probe with tape as described above. Due care was taken to avoid contamination of the polymers during preparation for the ESCA studies, although the polymers were used as received with no further purifications.

c) Instrumentation

Spectra were recorded with an A.E.I. ES200 AA spectrometer by using $Mg_{K_{\alpha 1,2}}$ exciting radiation. Typical operating conditions were: X-ray gun, 12 kv, 15 mA; pressure in the sample chamber, ca. 10^{-8} torr. Under the experimental conditions employed, the gold $4f_{7/2}$ level at 84 eV used for calibration of the energy scale had a full width at half maximum (FWHM) of 1.2 eV. No evidence was obtained for radiation damage to the samples during the typical time scale involved in these measurements, and indeed, long term irradiation with the relatively low dose rates from the X-ray source revealed no evidence for X-ray damage. Spectra were recorded in the fixed retardation ratio mode.

Overlapping peaks were resolved into their individual components by use of a DuPont 310 curve resolver (an analogue computer). The detailed deconvolutions were based on a knowledge of line widths determined from the model compounds. Previous studies have shown that under the instrumental conditions employed in this work, line shapes for individual components of the core level spectra are well described by gaussians.

iii) Theoretical

The data pertaining to the model compounds for the monomeric systems have been described elsewhere¹³⁷. For the larger polymer model system calculations were carried out within the all valence electron CNDO/2 SCF MO formalism employing the charge potential model. These

computations were carried out on an IBM 360/67 and for a typical convergence limit of 10^{-3} a.u. in the total energy calculations, on the largest model systems studied (50 atoms, 120 basis functions), required about 15 minutes of c.p.u. time and 12 iterations.

iv) Results and Discussion

a) Introduction

Generally speaking, the investigation of a homogeneous material by ESCA is performed in three stages:

1. A wide scan low resolution spectrum is taken to determine an overall crude element map of the material.
2. The accurate measurements of a) the binding energies of the individual core levels allows a fine detail determination of the elements present, b) the measurement of the relative intensities of the signals, allowing for sensitivity factors of the elements determined from model compounds, establishes the experimentally relative abundance of the elements (e.g. stoichiometry).
3. The detailed high resolution spectra of individual core levels to establish absolute binding energies and relative intensities of resolved peaks within a given core level allows deductions to be made concerning finer details of structure and bonding. In this section we discuss in detail these hierarchy of information levels for a large series of homopolymers to establish a firm basis for the detailed analysis of more specific problems in the structure, bonding and morphology in polymer systems.

b) Model Compounds

i) Relative Area Ratios

The factors involved in the signal intensities for the elastic peaks corresponding to direct photoemission from core levels has been discussed in Chapter 1.

As noted previously, since ϕ is fixed for most commercial instruments, at fixed X-ray flux (F) the spectrometer constant k can be determined from measurements on model compounds for specific core levels, (cf Fig. 3.1). In previous studies on other systems^{136, 137, 144, 147} the sensitivity factor, k, for our instrument has been established for the combined value of ϕ and k at fixed flux (F) on several core levels, and the results are shown in Table 3.2.

(It is important to emphasize that these sensitivity factors

are instrument dependent.) These ratios were used in this study to confirm the stoichiometry of the repeat unit in the polymers examined.

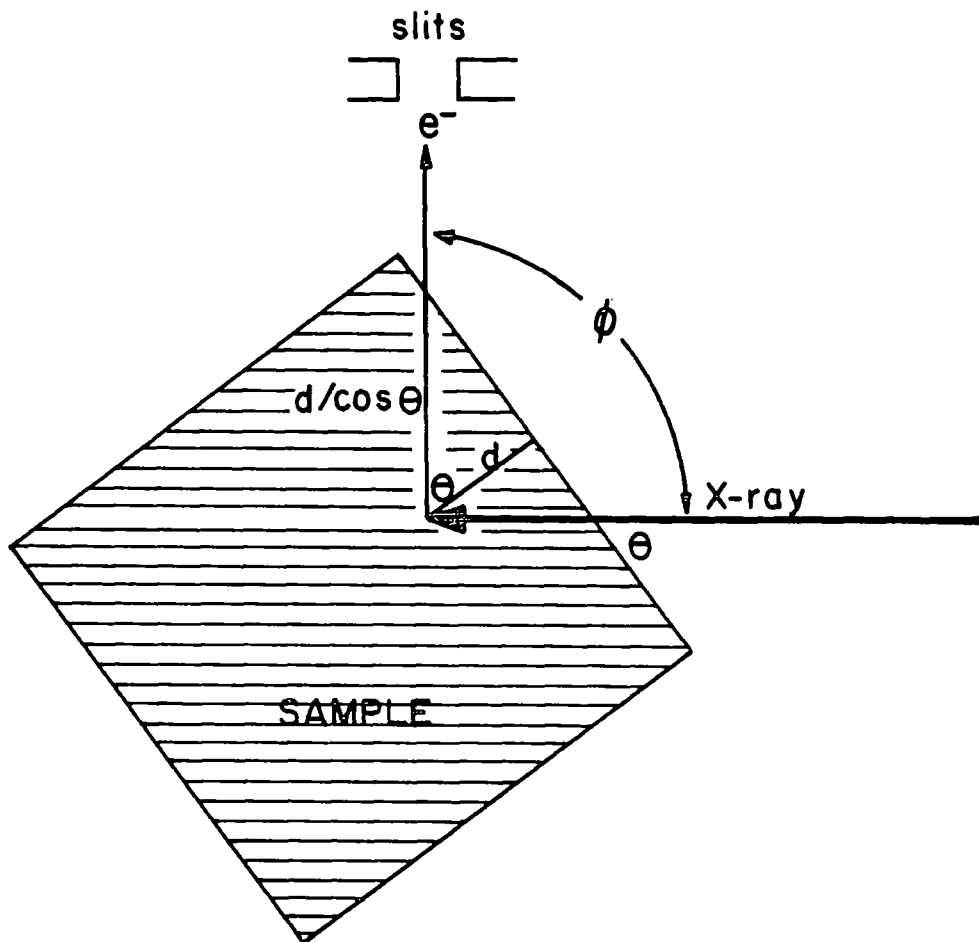


FIGURE 3.1

Sample position relative to the photon source and analyzer
in an AEI ES 200AA and ES200B

ii) Absolute and Relative Binding Energies

One of the primary sources of ESCA data which has been extensively utilized is the absolute and relative binding energy of given core levels. It has been shown that with a careful calibration, with respect to simple model systems, it is possible to quantitatively describe both absolute and relative binding energies for polymer systems^{1,137,144}. The analysis has been based on the charge potential model¹⁹ which may formally be derived from Koopmans' Theorem⁴⁷ in

Instrumental sensitivity ratios at fixed flux (12 kv, 15 ma to anode)
for the ϕ and k parameters studied in the fixed retardation ratio mode
on an AEI ES 200AA and 200B for a series of eleven core levels

<u>Core Level Ratio</u>	<u>Intensity Ratio</u>
C_{1s}/O_{1s}	$.6 \pm .03$
C_{1s}/N_{1s}	$.84 \pm .05$
C_{1s}/F_{1s}	$.52 \pm .009$
C_{1s}/F_{2s}	$3.82 \pm .035$
C_{1s}/S_{2p}	$.53 \pm .05$
C_{1s}/S_{2s}	$.96 \pm .05$
C_{1s}/Si_{2p}	$.83 \pm .03$
F_{1s}/F_{2s}	$7.4 \pm .09$
O_{1s}/O_{2s}	11 ± 1
C_{1s}/Cl_{2p}	$.41 \pm .05$
C_{1s}/Br_{3d}	$.23 \pm .05$

Table 3.2

the zero differential approximation¹, and has been discussed in Chapter 1. The model, relating as it does charge distributions to molecular core-binding energies, is intuitively appealing to chemists and has the distinct advantage that in appropriate cases the model may be inverted enabling charge distributions to be obtained from experimentally determined binding energies⁷⁰.

This model, which is referred to as the ground state potential model (GPM), is related to the charge distribution in the molecule as

$$E_i = E_i^0 + kq_i + \sum_{j=1} (q_j/r_{ij}) \quad (3.1)$$

where E_i is the experimentally determined binding energy for a given core level, E_i^0 is a reference binding energy level, q_i is the charge on atom i on which the core hole is located, and k is a constant (approximately equal to the one-center repulsion integral between a core and valence electron on atom i).

As a pre-requisite in the application of this model to the discussion of the data pertaining to the homopolymers, simple model compounds were studied to confirm the assignment of the core levels and obtain values for the charge potential parameters E^0 and k . The investigation has been limited to the study in particular of the C_{1s} and

O_{1s} core levels since the determination of the charge potential correlation requires a number of compounds where the range in binding energies are large enough to obtain reasonable least-squares analysis of the data. As will be seen in the tabulation of data in later sections, the range in binding energies for the Cl_{2p} , Si_{2p} , F_{1s} and Br_{3d} levels in polymers is quite small and although one can find rather large spans in binding energies for these levels in other organic and inorganic systems (in which the functionality differs) in the polymers studied in this work, which essentially involve covalently single bonded carbon-X bonds, (X = Cl, Br, F, S, Si) the shifts are small and the chemical shifts may, therefore, only be used to confirm overall the general features of structure and bonding involving these atoms. (It should be noted that in this sense sulphur falls into a similar category to oxygen, and the shift range can be quite large even in a simple polymer system.)

Calculations of the requisite charge distributions were accomplished within the all-valence electron CNDO/2 SCF MO formalism as discussed elsewhere¹. By plotting $E_i - \sum(q_j/r_{ij})$ versus $-q_i$, E^0 and k for each core level may be determined as an intercept and slope, respectively. The results of these correlations are discussed in detail elsewhere for a variety of systems and the k values appropriate to these series of organic models are given in references 137 and 147. The k values for C_{1s} levels are all centered about 25 eV/unit charge, with variations with both the different series of molecules and also the substituent on carbon. An interesting feature in the compilation of the k values is found for chlorine containing compounds. Where d orbitals are included on chlorine in the CNDO basis set, the k value is quite high (~ 30.0) whereas if they are ignored the k value approaches the theoretically calculated value, and for the halo-benzenes the value for the fluoro and chloro benzenes are identical within the error limits.

With the usual parametrization of CNDO/2, the contribution of $3d$ orbitals on second row elements is grossly over-estimated and the k value indicates that more realistic estimates of charge distributions are obtained if $3d$ orbitals are neglected¹⁴⁷. The results for the E^0 and k values used in this study are

$$C_{1s} \text{ levels } \begin{aligned} E^0 &= 284.6 \text{ eV} \\ k &= 25.2 \end{aligned}$$

$$\begin{aligned}
 0_{1s} \text{ levels} \quad E^0 &= 534.6 \\
 k &= 16.7
 \end{aligned}$$

In the charge potential model described above a fundamental assumption is made in that the core level binding energy is a function only of the initial (ground) state of the molecule and in this respect neglects the 'relaxation' effects due to the ejection of a core electron from an atom. It has become clear, however, from detailed non-empirical investigations of relaxation phenomena, that in the particular case of C_{1s} levels, there is a strong relationship between relaxation energy and binding energy such that the ground state charge potential model does partly compensate for relaxation phenomena if k and E^0 values are determined experimentally by reference to model systems¹²⁸. The situation with regard to 0_{1s} levels, however, is by no means so straightforward.

Jolly and co-workers¹⁴⁵ have recently proposed a variant of the simple charge potential model in which relaxation effects are explicitly considered by reference to the charge distributions and potentials for the 'half-ionized' system. This is related theoretically to the transition formalism^{148,149} in which a functional, corresponding to the difference in energy between ground state and ionized state is involved rather than the computation of binding energies as energy differences involving two large quantities. It is a straightforward matter to elaborate the relaxation potential model (RPM) within the CNDO/2 formalism since charge distributions in the effective half ionized species are merely obtained as averages for the ground state and for the equivalent cores species^{63,64,150} as a model for the core ionized state. Therefore, a comparison between the one center charge potential parameter k for the C_{1s} and 0_{1s} levels of a series of model compounds for the GPM and RPM formalism is given. For the series of molecules shown in Fig. 3.2 a least squares analysis provides values for k and E_0 for the C_{1s} and 0_{1s} levels, respectively of 24.8, 281.2, 17.7, and 531.1. Whereas, the k values are slightly different from those appropriate to the GPM, the main effect of including relaxation effects is to shift the energy scales (E^0 's) to lower values as might have been anticipated. Since, however, k and E_0 have been determined in each case by least squares analysis of experimental data if the derived values are employed as input to compute absolute and relative binding energies for the core

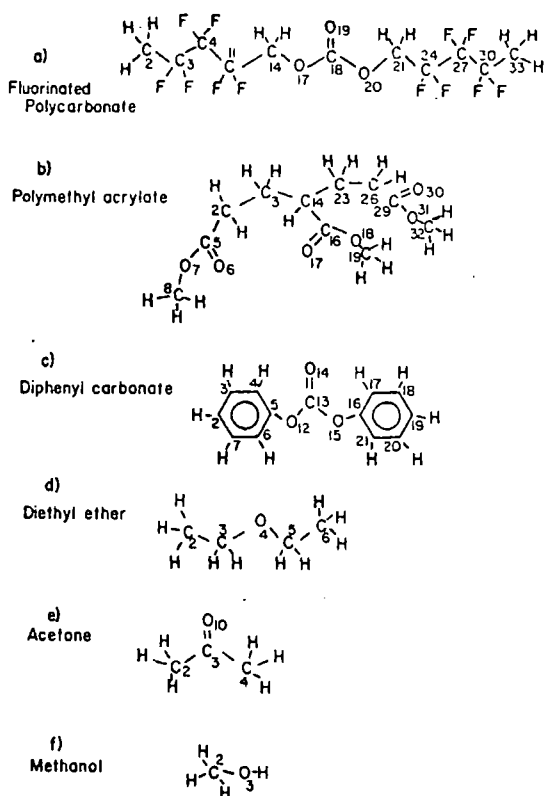


FIGURE 3.2

Series of molecules investigated in comparison of GPM and RPM

levels, the differences between the two models becomes quite small (i.e. since we have two parameters in each case determined by a least squares analysis of experimental data this provides sufficient latitude to compensate for deficiencies inherent in the model). This becomes clear from a comparison of the data in Table 3.3 where both the GPM and RPM models show excellent overall agreement both with one another and with the experimental data. Since the computational expense in employing the RPM is substantially higher than for the GPM, the calculations on model systems of the polymer systems described below have been within the GPM formalism. This overall conclusion is not entirely unexpected

The experimentally determined C_{1s} and O_{1s} absolute core level binding energies on a series of model compounds compared with the theoretically determined values in the GPM and RPM models

<u>Atom Number (from Figure 2)</u>	<u>B.E. GPM</u>	<u>B.E. RPM</u>	<u>B.E. EXP</u>
FLUORINATED POLYCARBONATE			
C_3	291.4	291.5	291.8
C_4	291.5	291.2	291.8
C_{11}	291.5	291.2	291.8
C_{14}	288.0	288.6	288.4
C_{18}	290.7	291.5	291.2
O_{17}	535.2	535.7	535.9
O_{18}	533.5	534.5	534.1
POLYMETHYL ACRYLATE			
C_{14}	285.5	285.9	285.0
C_{16}	288.9	289.7	288.8
C_{19}	286.6	287.3	286.6
O_{17}	533.2	533.8	532.8
O_{18}	524.6	535.0	534.3
DIPHENYL CARBONATE			
C_5	287.2	235.6	286.6
C_{13}	290.7	290.6	290.9
O_{12}	534.8	534.8	535.3
O_{14}	533.1	533.7	533.9
DIETHYL ETHER			
C_2	285.0	286.4	285.0
C_3	286.6	287.1	286.6
O_4	533.2	534.1	533.6
ACETONE			
C_2	285.0	285.7	285.0
C_3	287.3	280.8	287.9
O_{10}	533.2	534.3	533.6
METHANOL			
C_2	286.5	288.1	286.6
O_3	533.7	534.2	533.6

Table 3.3

on the basis of our considerable previous success in applying GPM to the quantification of experimental data pertaining to a wide variety of polymeric systems^{1,127,128}.

c) Energy Referencing

An important consideration in the determination of both the absolute and relative binding energies from experimental data is the establishment of a reference level to calibrate the energy scale^{1,127,128}. In solids, three situations may clearly be distinguished:

- 1) The sample is sufficiently thin such as to be in electrical contact with the spectrometer
- 2) The sample is sufficiently thick such as to be effectively insulated and not in electrical contact with the spectrometer
- 3) and films of intermediate thickness which behave as somewhat 'leaky' capacitors.

These three situations have been discussed in detail in Chapter 1, and for the case of most polymer films studied by ESCA the most common situation is that set out in (2).

In this situation there is only a remote possibility that the sample will be in electrical contact with the spectrometer and in general, it will be floating at some potential due to surface charging from the net loss of photoemitted electrons, where the overall positive charge cannot be neutralized by the flow of electrons from the surroundings. The most reliable method of energy referencing is to follow the slow build-up of hydrocarbon contamination at the surfaces¹²⁷. With a base pressure of $\sim 10^{-8}$ torr the partial pressure of extraneous hydrocarbon material is such that taken in conjunction with the low sticking coefficient for most organic and polymeric systems it normally takes many hours before any signal arising from hydrocarbon is present. (This is approximately an order of magnitude longer than the typical time taken to measure the core level spectra. Such contamination has a highly reproducible binding energy of 285 eV for the C_{1s} level. Although it is generally agreed on the basis of available experimental data that such hydrocarbon contamination deposits on the surfaces of polymers as uniform films in electrical contact with the surface this is not necessarily the situation with regard to metals, such as gold, which have also been proposed for energy referencing purposes and, indeed, available data suggests a marked tendency to 'island' and as such differential surface charging may occur¹⁵¹. This situation has been discussed elsewhere¹²⁷ and suffice it to say the use of the so-called 'gold decoration' technique is not recommended for organic and polymeric materials. In this study the C_{1s} level at 285 eV, arising from carefully controlled build-up of hydrocarbon material on the polymer surface has been used throughout as an energy reference.

Experiments have recently been performed to study polymeric samples, as well as some inorganic samples, with the standard MgK_{α} X-ray source and the monochromatized AlK_{α} X-ray source. It was observed that for samples studied with the AlK_{α} radiation, where the

sample was located in a remote position with respect to the radiation source (cf Fig. 1.31), very little, if any, hydrocarbon contamination was apparent even after a period of many hours. For the same samples studied with the MgK_{α} X-ray gun, significant contamination was observed within a relatively shorter period of time (e.g. 1 hour). This preliminary result was contrary to the popular belief that hydrocarbon contamination is chiefly a result of residual gases from the diffusion pump oil. It was also observed that when a sample was left in the spectrometer source for a relatively long period of time (e.g. overnight) with the X-rays off, subsequent analysis of the C_{1s} levels, revealed very little, or no hydrocarbon contamination.

It was felt that the proximity of the sample to the X-ray source was possibly a factor since the cap covering the MgK_{α} X-ray gun became quite hot when the X-rays were being generated.* In an attempt to demonstrate this an experiment was undertaken in which two polytetrafluoroethylene (PTFE) samples were mounted on opposite faces of a double sided probe tip. The probe was oriented so that one sample was facing the X-ray gun, and could be analyzed, whilst the other sample was out of line of sight of the cap covering the X-ray gun. The spectrum of uncontaminated PTFE is well known and shows a single peak in the C_{1s} region due to $\underline{C}F_2$ type environments. The hydrocarbon contamination on the first sample was continually monitored for 170 mins. by the increase in the signal due to $\underline{C}H_2$ type type environments and decrease in the $\underline{C}F_2$ signal. The probe tip was then rotated through 180° to expose the second PTFE sample for 110 mins. The results are shown in Fig. 3.3. It can clearly be seen that for the first 170 mins. hydrocarbon built-up at a steady rate on the first sample. However, on analysis of the second sample, which had been out of line of sight of the X-ray cap for this period, no hydrocarbon was observed. For the following 110 mins. the hydrocarbon built-up on the second sample at essentially the same rate as it had done on the first. This is strong evidence to demonstrate that the major

*This possibility receives additional support from previous observations using the AEI ES100 spectrometer (the forerunner of the present instrument) which employed a conventional X-ray gun with line of sight between filament and anode, the filament, however, being remote from the X-ray window. In this design, sample contamination under somewhat poorer vacuum conditions occurred on a time scale an order of magnitude or so slower than with the present instrumentation.

INSULATED PTFE

Time Study on Hydrocarbon Build-up

Double sided probe

o - PTFE Sample facing window - 170 minutes
 x - " " on opposite side of probe for 1st - 170 minutes, then rotated for next 110 minutes

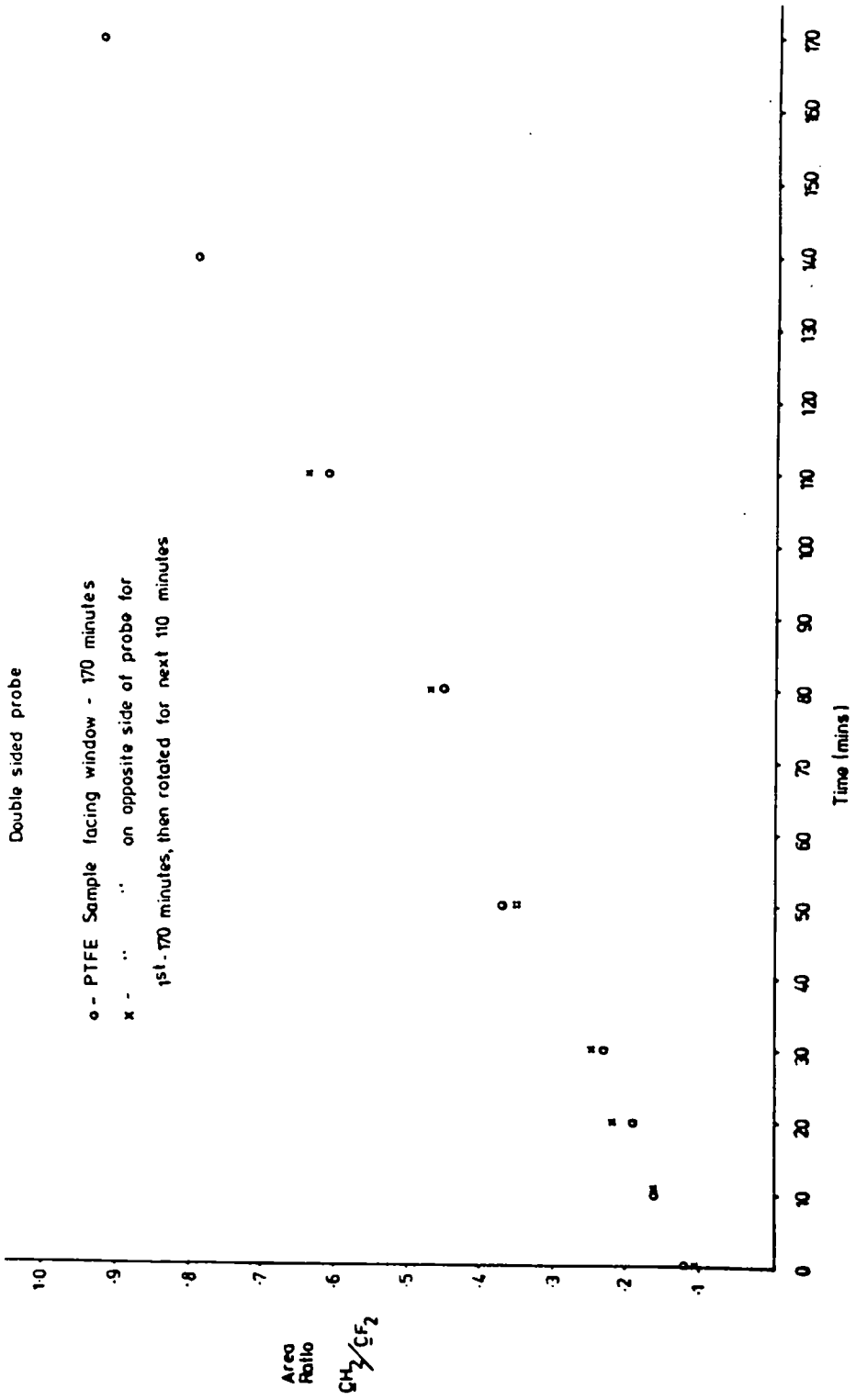


FIGURE 3.3

Hydrocarbon build-up on PTFE sample facing X-ray window for 170 minutes (o) and sample in chamber, not exposed to window for first 170 minutes but exposed for 110 minutes after (x), demonstrating long term build-up of hydrocarbon

contribution to the hydrocarbon contamination in an AEI ES200B spectrometer, and indeed any spectrometer of similar geometry, is not the residual gases in the sample region resulting from diffusion pump oil, but is a direct result of the hydrocarbon 'boiling off' the X-ray cap as a result of heating.

Therefore, a cooling jacket was designed for the X-ray cap, and the design is shown schematically in Fig. 3.4.

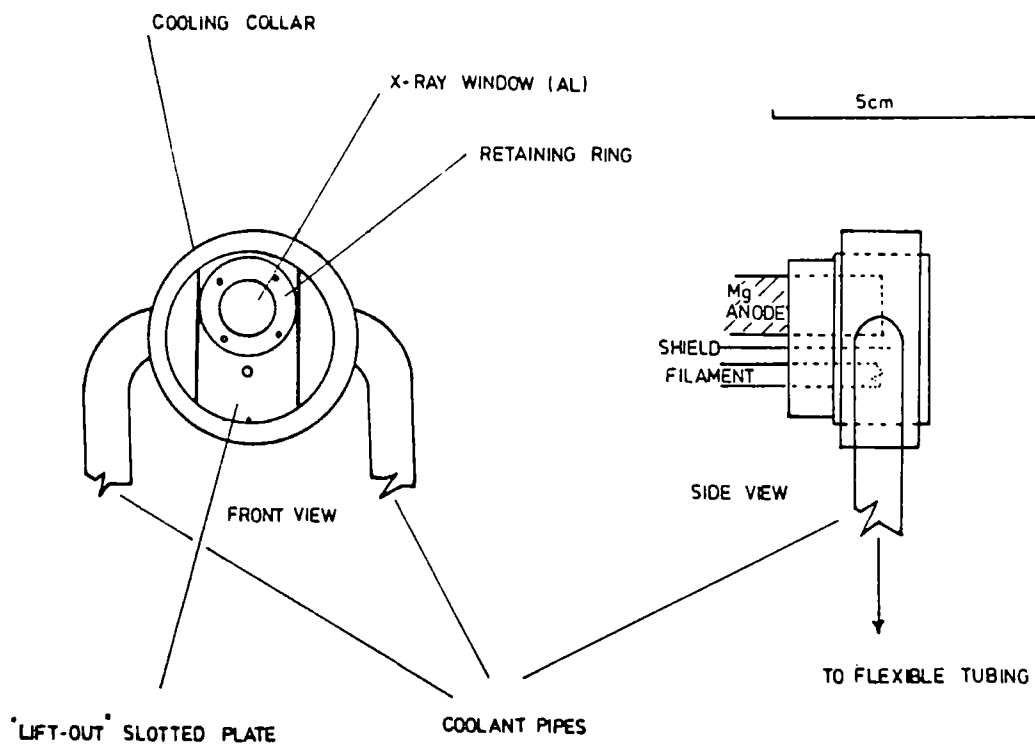


FIGURE 3.4
Diagram of cooling-cap

Three samples were investigated: gold as an example of a reference material, polyethylene oxide powder as an example of a polymeric material and aluminum foil as an example of a more active inorganic

surface. Core levels of the substrate and hydrocarbon contamination were monitored for the three samples over a three hour period under conditions of an uncooled cap, water cooled cap and liquid nitrogen cooled cap. The relevant data is shown graphically in Figures 3.5, 3.6 and 3.7.

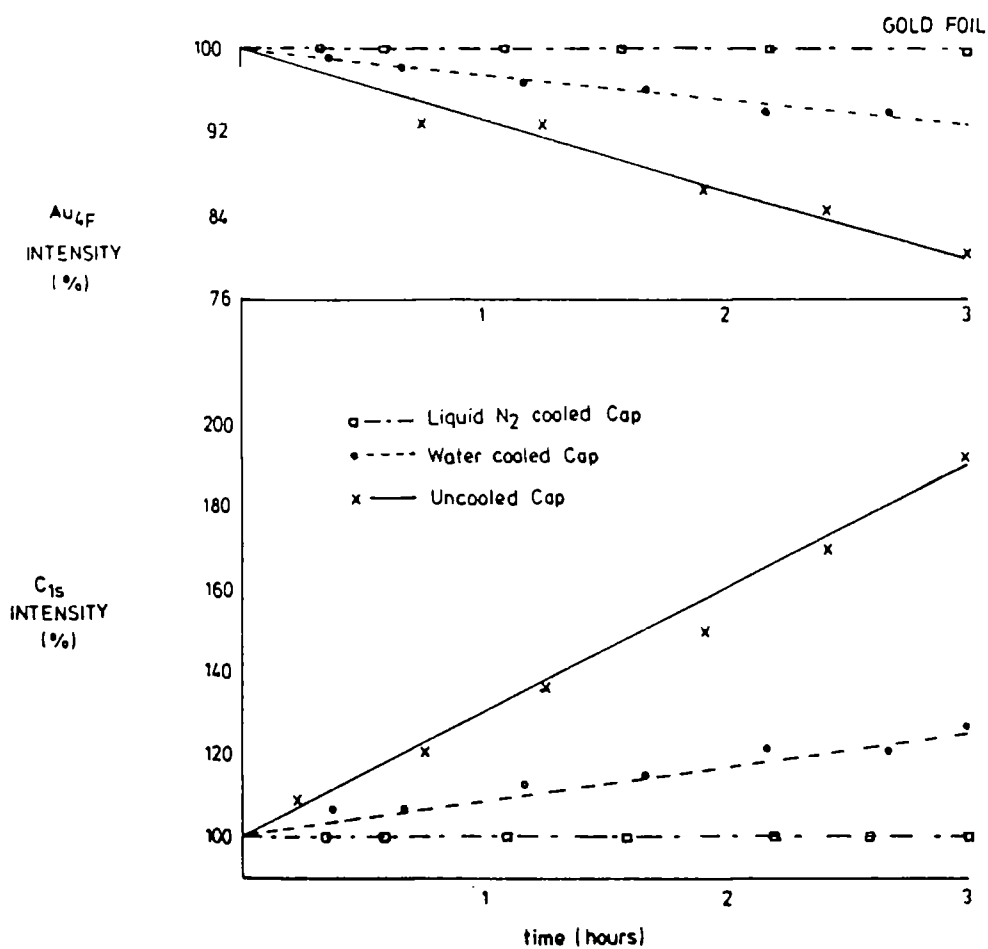


FIGURE 3.5
Hydrocarbon build-up on gold foil

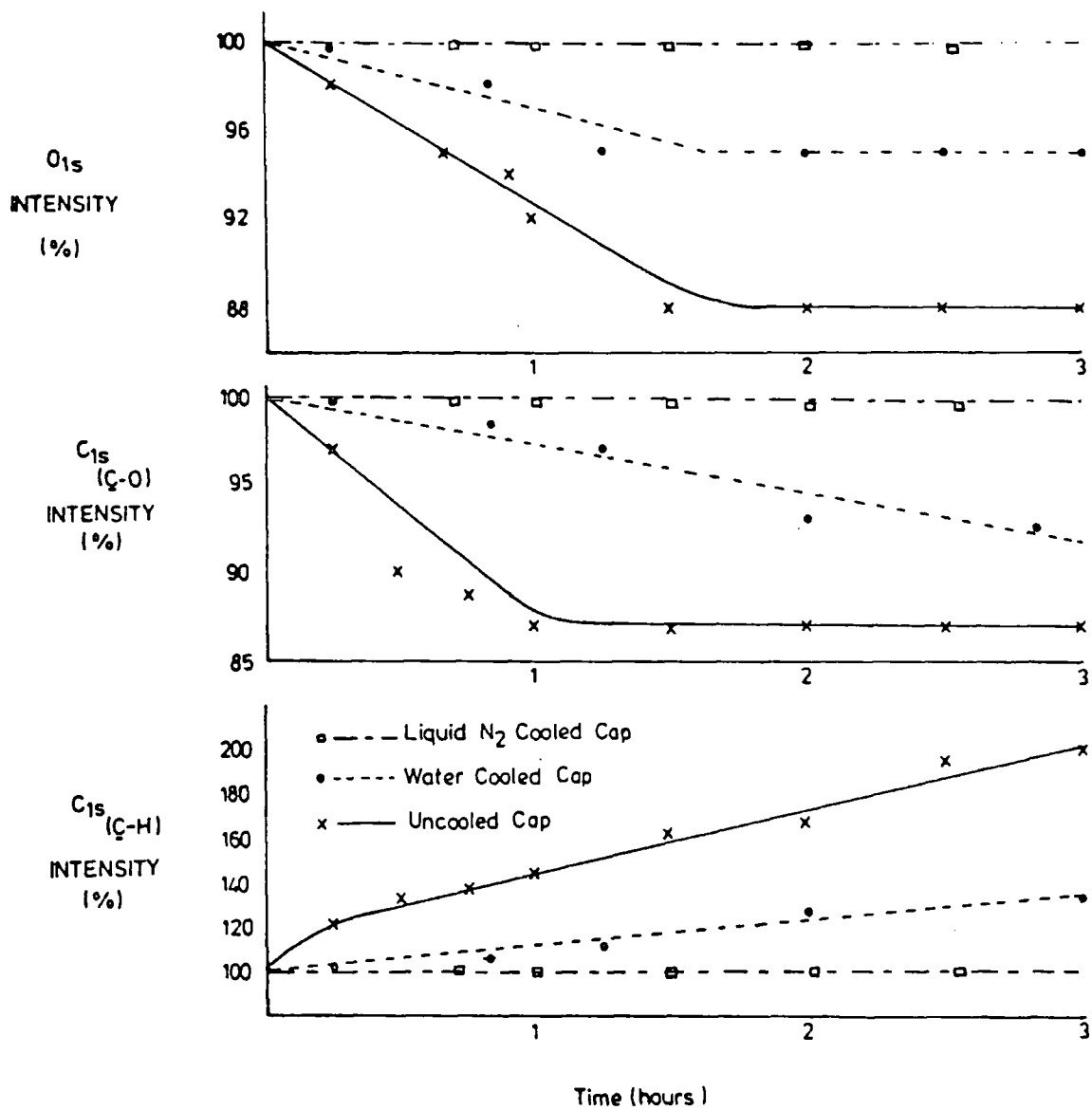


FIGURE 3.6

Hydrocarbon build-up on polyethylene oxide powder

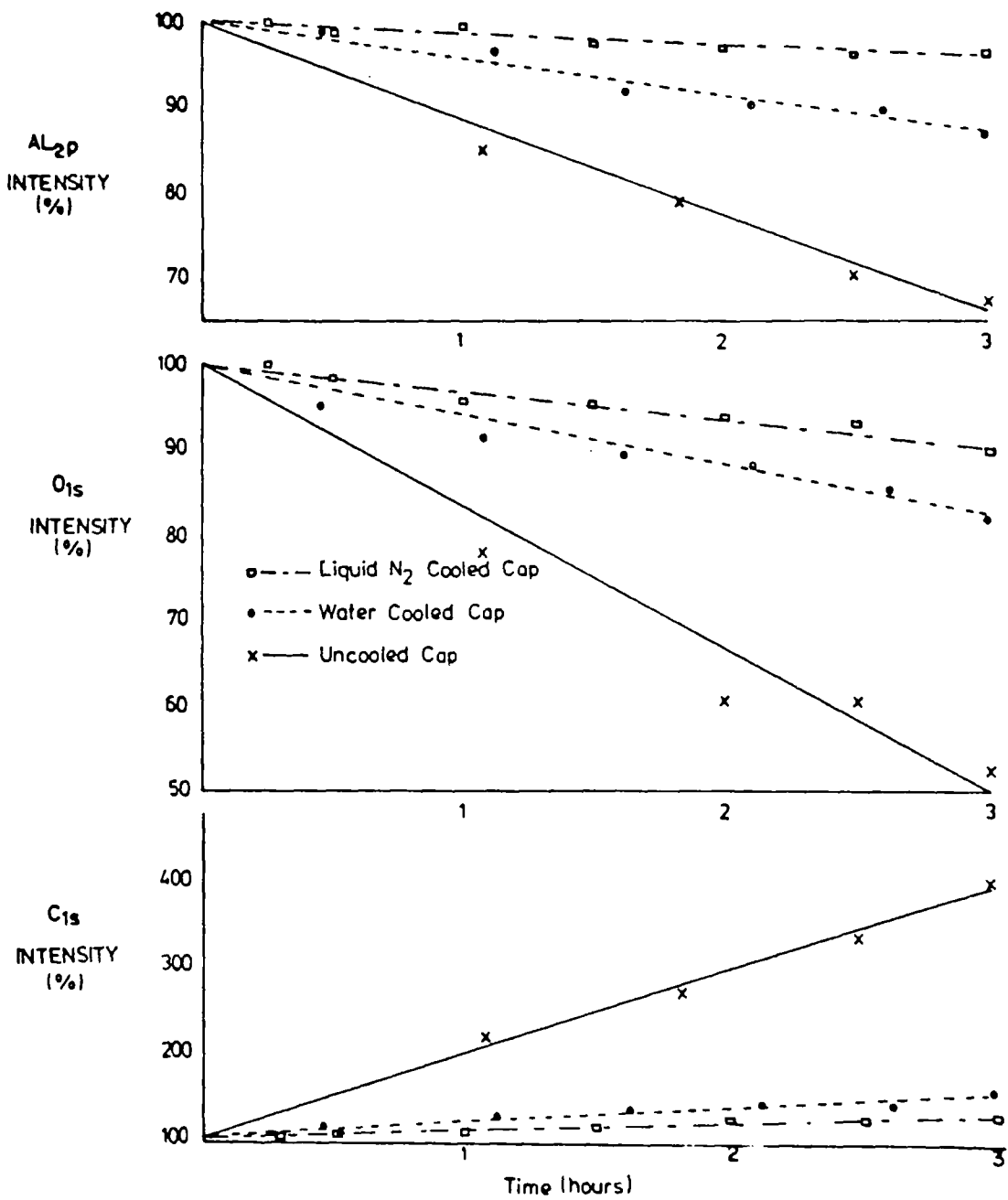


FIGURE 3.7
Hydrocarbon build-up on aluminum foil

The results clearly demonstrate that water cooling of the X-ray cap greatly reduces the accumulation of hydrocarbon contamination on all of the samples, and indeed is completely eliminated (over the three hour time period) for gold and polyethylene oxide samples using liquid nitrogen coolant within the accuracy of the measurements which is estimated to be between 1 and 2%. However, the aluminum foil sample still showed some build-up of hydrocarbon even with the X-ray cap cooled by liquid nitrogen, although the amount is still very significantly reduced. It is apparent from the aluminum foil data that cooling the X-ray cap, in the manner described, does not eliminate all of the hydrocarbon in the sample region of the spectrometer. One can envisage several other sources of residual hydrocarbon, but the data indicates that the design has eliminated the major source.

It is clear that the use of this simple concept can significantly improve surface analysis by ESCA where hydrocarbon contamination has proven a problem in the past. Furthermore, it is demonstrated that it is now possible to perform long term (> 3 hours) studies, under continuous X-ray irradiation with the use of insertion lock systems at pressures in the region of 10^{-8} torr, without the need for ultra high vacuum, 10^{-10} torr, unachievable with insertion locks. This is particularly useful for dynamic studies such as oxidation and reduction of kinetic studies, surface charging and polymer crosslinking where a reaction chamber connected directly via insertion locks to the spectrometer source allows for repeated treatment and ESCA analysis. This application of the cooling cap will be discussed in chapter 6 and 8 in particular.

d) Results and Discussion

In Chapter 2 a detailed discussion on results pertaining to fluoropolymer systems was given, and a considerable understanding has thereby ensued of the factors which determine both absolute and relative binding energies of structural features in polymers. More recently, detailed studies have been made of polyalkylacrylate and methacrylate systems¹³⁷. Considerable data on substituent effects on core levels has thusfar been accumulated on F_{1s} , O_{1s} , and C_{1s} levels and in the succeeding section an extensive tabulation of data pertaining to a wide variety of commercially available polymer systems is presented. The aim has been to produce comprehensive tabulations which may be of use in ESCA applied as a 'fingerprint' spectroscopic tool to the

elaboration of features of structure and bonding in polymers. The tabulation of apparent relative cross-section (cf. Table 3.2 for our particular instrumental configuration) also provides data necessary for the investigation of the compositions of the outermost few tens of Angstroms of polymer surfaces. The homopolymers have been arbitrarily divided into five main categories:

- 1) Polymers containing only carbon and hydrogen.
- 2) Polymers containing only carbon, hydrogen and oxygen.
- 3) Polymers containing only carbon, hydrogen, nitrogen and oxygen.
- 4) Polymers containing only carbon, hydrogen and chlorine.
- 5) A miscellaneous collection of polymers containing combinations of carbon, hydrogen, oxygen, sulphur, silicon, bromine and fluorine.

1) Polymers Containing Only Carbon and Hydrogen

The experimental data together with theoretical computations of absolute binding energies for an extensive series of hydrocarbon based polymers are shown in Fig. 3.8.

It is appropriate at this point to discuss the meaning of the greek lettering used on the structural repeat unit for each polymer as it will apply throughout the remainder of the sections on the homopolymers. The bold horizontal line on the binding energy column refers to the full width half maximum (FWHM) of the primary photoionization peak, with the centroid of the (FWHM) located in the center of the bold line at the experimentally coincident position on the binding energy scale. The vertical lines, on the bold horizontal lines, indicate the binding energy calculated by the GPM and correspond to the α , β , γ , δ sites of the structural repeat unit starting with the vertical line to the extreme right. For example, on polyvinyl toluene there are three vertical lines on the C_{1s} core level line at approximately 284.6 eV, 285.0 eV and 285.5 eV going from right to left. These correspond to the α , β and γ assignments respectively on the structural unit, whereas we have, according to the GPM five atoms with an average binding energy of 284.5 eV, two atoms at 285.0 eV and two at 285.5 eV. (The binding energies from the GPM were rounded off to the nearest 0.5 eV for display as vertical theoretical lines on the experimental data.)*

*(Note, the vertical lines do not correspond to the number of carbon atoms in a particular environment since this would have considerably complicated the diagram.)

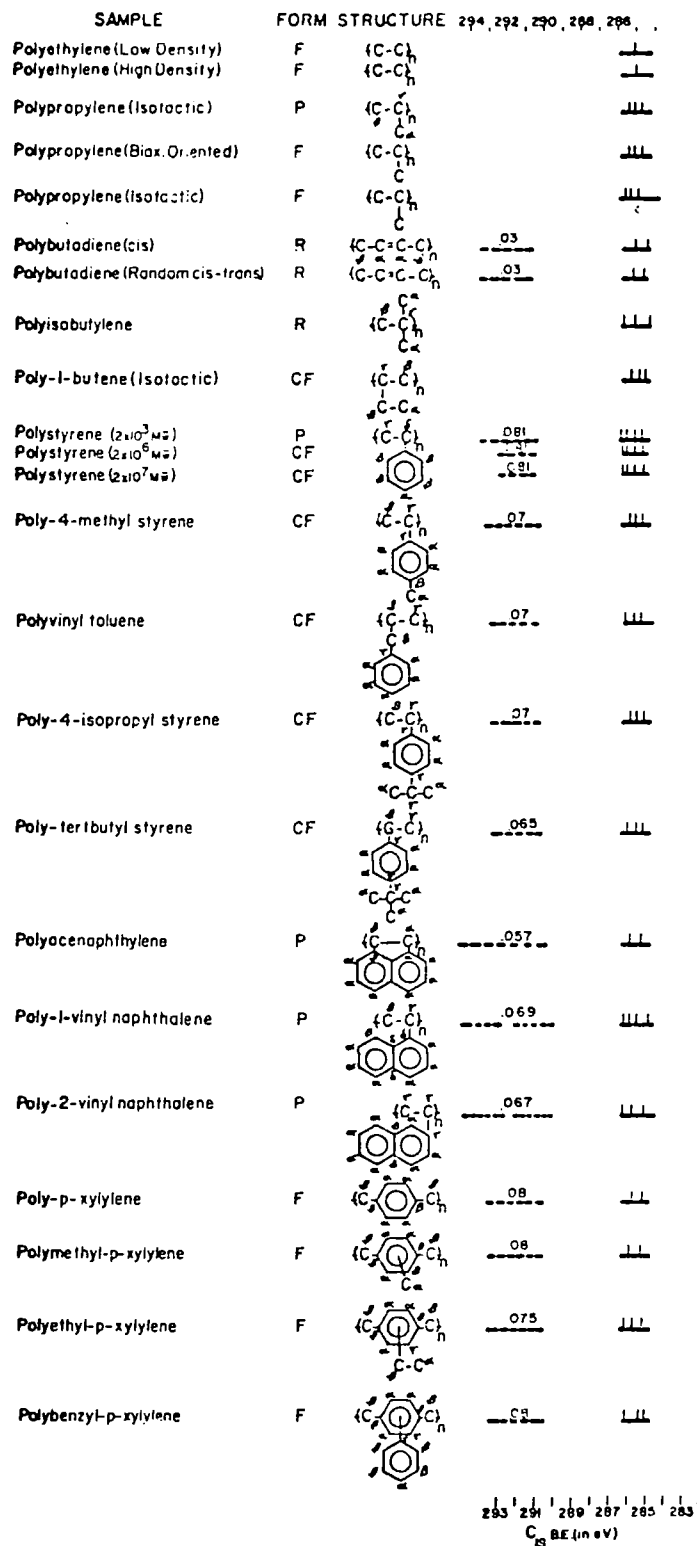


FIGURE 3.8

Tabulation of experimental and theoretical data for polymers containing only carbon and hydrogen

It is evident from Fig. 3.8 that the C_{1s} binding energies of the solely hydrocarbon based polymers all fall within a narrow range and this suggests that the straightforward identification of the polymers from a consideration of absolute and relative binding energies alone would be untenable. It is becoming increasingly apparent, however, that

the data derived from the observation of shake-up satellites accompanying direct core level photoionization can add a new dimension to the application of ESCA where ambiguities in the interpretation arising from the primary data can occur¹⁵².

As was discussed in Chapter 2, the valence band spectra of polymers may often be used as fingerprints for their identification^{1,127,128}. However, the cross sections for the photoionization with the conventionally employed soft X-ray sources are an order of magnitude or so smaller than for the core levels. Since the valence band is a convolution of many overlapping peaks it is often much more convenient to focus attention on the low energy shake-up region since although the shake-up probabilities are typically $\sim 10\%$ of that appropriate to the direct photoionization peak, the selection rules are such that the basic structure of such satellites is quite simple and highly characteristic of the polymer. As typical examples, Fig. 3.9, shows the C_{1s} levels and low energy shake-up region for polybutadiene (cis), polyacenanaphthylene and polypara-xylylene. It is clear that both in terms of transition energies and intensities that ESCA readily distinguishes between them although in terms of absolute binding energy and FWHM the direct photoionization peaks are closely similar. It is not appropriate in this Chapter to discuss the theoretical background to the interpretation of these shake-up transitions or the attempts to establish trends and identify specific transitions, as they have been discussed elsewhere^{58c,d, 140}. However, it is useful to indicate the ratio of the $\pi \rightarrow \pi^*$ shake-up transitions and establish the FWHM and relative binding energy of its centroid with that of the primary photoionization peak. These can be seen as bold dotted lines to higher binding energy on Fig. 3.8 with the corresponding values for the relative intensity of the shake-up peaks with respect to the direct photoionization peaks.

Even with this extra dimension, however, it is evident that for some solely hydrocarbon based polymers it would be possible to effect an identification by studying only the C_{1s} levels and associated low energy shake-up satellites. In such cases high resolution studies of the valence energy regions would be required, which are unfortunately rather time-consuming.

A recent example¹⁴⁰ of the utility of ESCA in elaborating details of structure and bonding in hydrocarbon based polymers is provided by an extensive investigation of styrene-alkane copolymers of

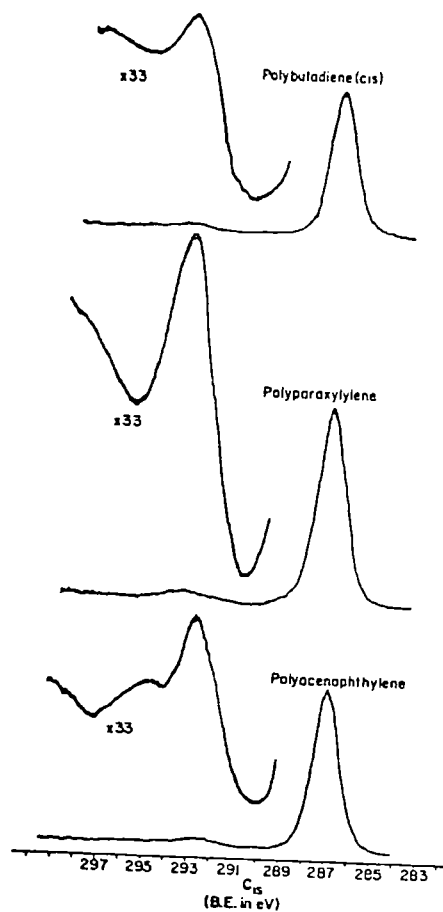
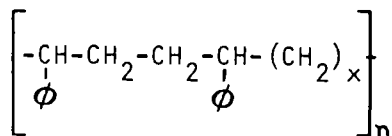


FIGURE 3.9

Typical examples of C_{1s} core levels, and low energy $\pi \rightarrow \pi^*$ shake-up regions for carbon and hydrogen containing polymers

general structure:



which was already discussed in Chapter 2.

It is instructive to note that the FWHM's for the direct photoionization peaks for the polymers in Fig. 3.8 are closely similar and that the GPM provides a good overall account of absolute binding energies in such systems.

2) Polymers Containing Carbon, Hydrogen and Oxygen.

The functional groups encompassed in this study involved oxygen in hydroxyl, ether, carbonyl, carboxyl, and carbonate groups. The relevant data for both C_{1s} and O_{1s} levels are shown in Fig. 3.10. Considering

	SAMPLE	FORM	STRUCTURE		
	Polyvinyl acetate	CP			
	Polyvinyl crotonate	P			
Polyacrylic acid	P				
Poly methyl acrylate	N				
Poly-n-butyl acrylate	CP				
Poly-n-butyl methacrylate	N				
Polyoctadecyl acrylate	N				
Poly methyl methacrylate	P				
Poly-n-butyl methacrylate	CP				
Poly-n-octyl methacrylate	CP				
Polyoctadecyl methacrylate	N				
Polyphenyl methacrylate	P				
Polybenzyl methacrylate	P				
Polyisobornyl methacrylate	P				
	Polyvinyl-iso-decanoate	N			
	Polyvinyl stearate	N			
	Polyhexamethylene sebacate	N			
	Poly(1,4-cyclohexane dimethyl)terephthalate	CP			
	Poly(1,4-cyclohexane dimethyl) succinate	CP			
	Poly(diallyl-o-phthalate)	P			
	Poly(diallyl-iso-phthalate)	P			
	Polyethylene terephthalate	F			
	Polyacetyl-p-styrene	F			
	Polycaprolactone	CP			
	Polycarbonate (Aliphatic)	P			
	Polycarbonate (Aromatic)	CP			

FIGURE 3.10

Tabulation of experimental and theoretical data for polymers containing only carbon, hydrogen and oxygen

firstly carbon singly bonded to oxygen (alcohols, ethers, and esters), the short range nature of substituent effects is manifest in the consistency of the shift in C_{1s} levels compared with a comparable system in

which the singly bonded oxygen is replaced by hydrogen. The characteristic shift is $\sim 1.6 \pm 0.2$ eV and the factors which determine such shifts also lead to simple additivity rules. Thus, in comparing polyacetyl with polyethylene the shift in C_{1s} binding energy associated with having two singly bonded oxygens to a given carbon is ~ 2.8 eV (i.e. approximately twice the effect of a single substituent). In Chapter 2 such additivity effects in fluoropolymer systems were noted. For carbon doubly bonded to oxygen the corresponding shift is ~ 2.6 eV (e.g. for polyacetyl-p-xylylene) and this compares well with that reported previously for simple carbonyl compounds¹³⁷. In going from a carbonyl to a carboxylate group the binding energy shift associated with the additional oxygen singly bonded to a carbon is ~ 1.4 eV giving a total shift of ~ 4.0 eV. The simple additivity picture also extends from a carboxylate to carbonate group the additional shift to higher binding energy associated with the oxygen substituent being ~ 1.4 eV (total shift ~ 5.4 eV). The FWHM and line shapes are sufficiently well-characterized to allow straightforward lineshape analysis for systems which involve incompletely resolved peaks. Indeed, the shift range for the C_{1s} levels for oxygen containing polymers is sufficiently large that lineshape analysis is not normally necessary and the technique provides an unambiguous means of identifying structural features. The fine structure for individual core levels taken in conjunction with relative intensities of the C_{1s} and O_{1s} levels provides a convenient means of investigating structure and bonding in such systems.

The charge potential model in the GPM formalism provides a ready means for quantifying the shift data and provide confirmatory evidence for the assignments.

The oxygen $1s$ levels, as expected, cover a much smaller span in binding energy in going from singly to doubly bonded oxygen. The vertical uprights on the bold horizontal bars are defined in the same way as for the C_{1s} levels in that going from right to left the verticals correspond to the α and β oxygens. The confirmation of the assignment of the O_{1s} core levels has been based on comparison with model systems and by detailed non-empirical LCAO MO SCF computations¹³⁷. We note that for the simple carbonyl (i.e. polyacetyl-p-xylylene), alcohols (i.e. polyvinyl alcohol) and ethers (i.e. polyethylene oxide) the binding energies for the O_{1s} levels are essentially the same. This has previously been noted in experimental studies of simple model systems

and the detailed theoretical interpretation is consistent with the experimental data. By comparison, in the esters (i.e. polyacrylates and methacrylates) the singly and doubly bonded oxygens exhibit a substantial shift (~ 1.5 eV) and the theoretical analysis unambiguously assigns the higher binding energy component as arising from the singly bonded oxygen¹³⁷. Confirmatory evidence for this assignment is available from the O_{1s} levels for the carbonates which consists of a 2:1 doublet, the higher binding energy component, therefore, corresponding unambiguously to the ester type oxygen. The O_{1s} binding energies span a range of ~ 2 eV in going from doubly to singly bonded oxygen and the extremes are, in fact, encompassed by the O_{1s} levels of the carbonates. As representative examples of the shift ranges in oxygen containing polymeric systems, Fig. 3.11 shows the C_{1s} and O_{1s} levels for polymethylene oxide, polyethylene oxide, polyacetyl paraxylylene, polyisopropylacrylate and an aromatic polycarbonate based on bisphenol A. The systems involving aromatic residues for which low energy $\pi \rightarrow \pi^*$ shake-up satellites of considerable intensity arise are readily distinguishable. Thus, for polyacetyl-p-xylylene) the shake-up transitions appear as a broad satellite to the high binding energy side of the C_{1s} levels appropriate to the carbonyl groups. In the particular case of the polycarbonate the shift for the carbonate carbon is sufficiently large that it overlaps with the $\pi \rightarrow \pi^*$ shake-up transitions of the aromatic moiety. The polycarbonates will be discussed in detail in Chapter 7.

3) Polymers Containing Carbon, Hydrogen, Nitrogen, (and Oxygen).

The data for the core levels of the polymers are displayed in Fig. 3.12. Since the shift arising from replacing a carbon or hydrogen by nitrogen directly attached to the atom under consideration is small ~ 1 eV, the C_{1s} levels of the polyvinylpyridines reveal little evidence for chemically shifted carbons directly attached to nitrogen. This is not entirely unexpected on the basis of previous studies of pyridine itself^{58b}. The N_{1s} levels, however, are characteristic and at substantially lower binding energy than those in the poly-4-aminostyrene. In this respect, the amides occupy an intermediate position and in order of increasing binding energy we have



The binding energies for the C_{1s} levels of the amide groups are typically shifted by ~ 2.4 eV from the energy reference (285 eV)

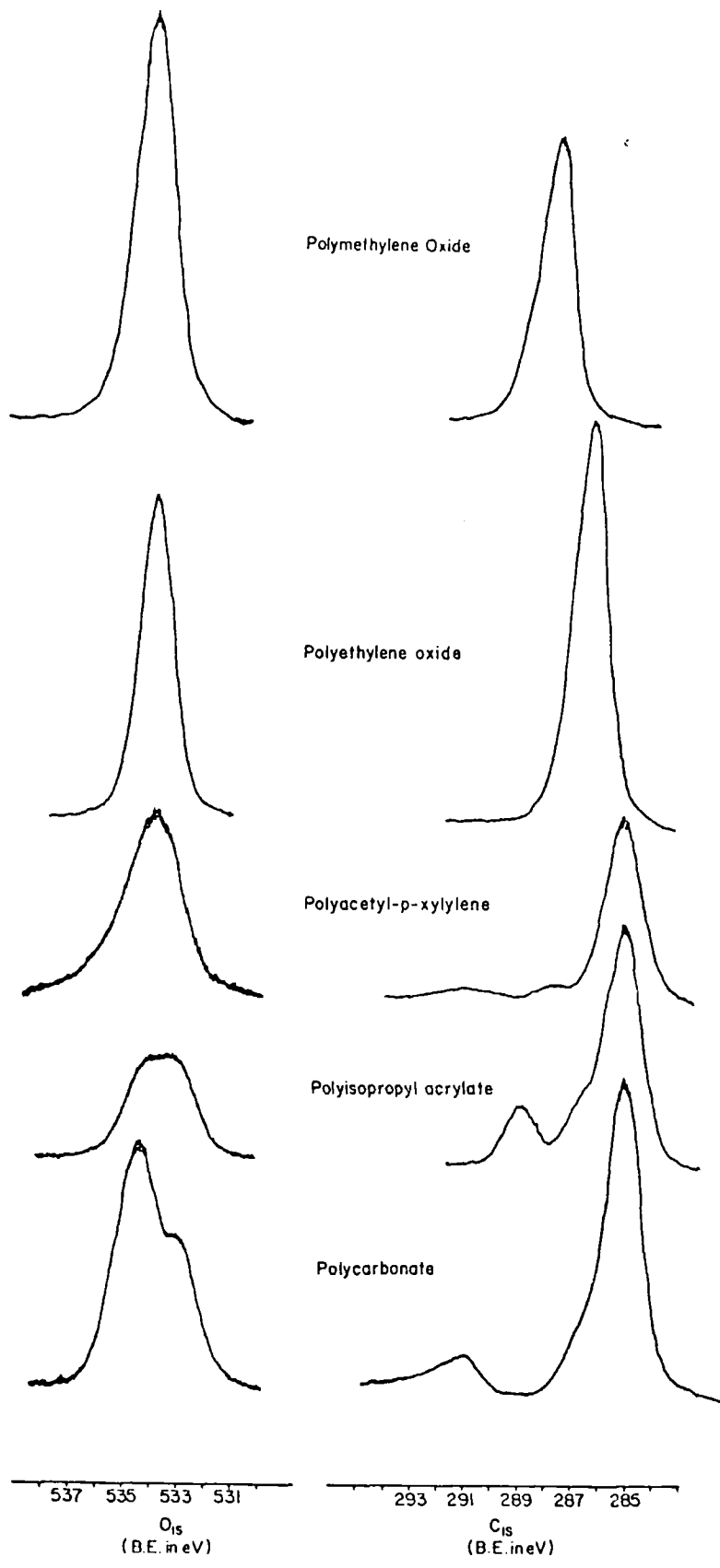


FIGURE 3.11

Typical examples of the C_{1s} and O_{1s} core levels for polymers containing only carbon, hydrogen and oxygen

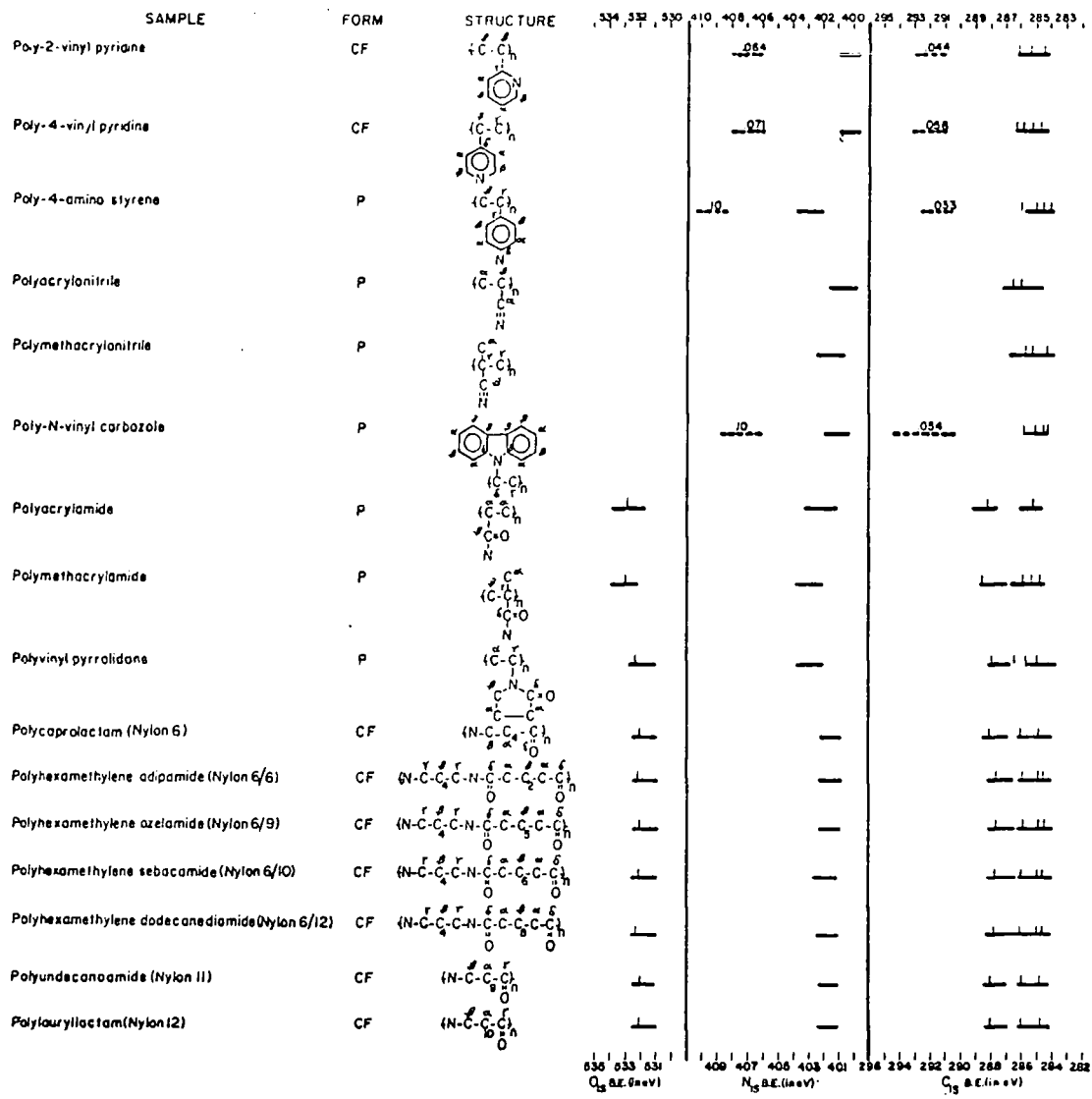


FIGURE 3.12

Tabulation of experimental and theoretical data for polymers containing carbon, hydrogen, nitrogen (and oxygen)

and this is significantly lower than for simple carbonyl compounds (cf. preceding discussion). It is, in fact, interesting to contrast this situation with that in going from a carbonyl compound to an ester where the effect of the singly bonded oxygen is an additional shift of ~ 1.4 eV. The decreased binding energy for the amide group may be attributed to the overall electronic effect of the nitrogen which in comparison with oxygen is a weaker σ electron acceptor but stronger π electron donor. The two features, therefore, of relatively low binding energy C_{1s} levels for the $\underline{C}ONH$ group and relatively high N_{1s} binding energy for the N_{1s} level is highly diagnostic for the presence of amide groups. In support of this simplistic interpretation based

on the electronic effect of the nitrogen we may compare the O_{1s} binding energies for simple carbonyl compounds (ketones) with that for amide groups. It is clear from a comparison of Figures 3.10 and 3.12 that there is a substantial shift to lower binding energy in going from the former to the latter.

It has been previously commented that the shift in C_{1s} levels arising from carbon triply bonded to nitrogen is surprisingly small when due consideration is given to the large degree of charge asymmetry in the system¹⁵³. The C_{1s} binding energy for carbon in cyano groups is little different than for the hydrocarbon reference, it should be noted, however, that theoretical calculations are entirely consistent with the experimental data¹⁵³.

Despite the fact that nitrogen as a substituent has a relatively small influence on C_{1s} binding energies the overall electronic effect is much more marked when we consider shake-up transition. Thus, we have previously commented on the shake-up spectra of poly-2- and -4-vinyl pyridines and poly-4-amino-styrene in discussing the assignment of shake-up transitions in polystyrene^{58c,140}. Comparison has also been drawn between the characteristic shake-up spectra accompanying C_{1s} and N_{1s} photoionization in polyvinyl carbazole and those for the polyvinyl-naphthalenes and polyvinylacenaphthylene^{58d}.

The GPM provides a good overall interpretation and confirmatory assignment of the C_{1s} and O_{1s} levels in these systems.

4) Polymers Containing Carbon, Hydrogen and Chlorine

Clark and coworkers have previously published extensive tabulations of C_{1s} and Cl_{2p} core level binding energies for series of poly-chlorinated aliphatic¹⁵⁴, aromatic¹⁵⁵ and heteroaromatic¹⁵⁶ systems so that the substituent effect of chlorine is well understood both experimentally and theoretically. The effect of replacing hydrogen by chlorine is a shift to higher binding energy of ~ 1.6 eV, the shifts thus being comparable to those appropriate to a single bonded oxygen substituent as might have been anticipated on the basis of the relative electronegativities of chlorine and oxygen. The Cl_{2p} binding energies (spin orbit splitting ≈ 1.6 eV) for covalently bonded chlorocarbon systems fall within a relatively narrow range, with the more highly chlorinated systems corresponding to higher bonding energy¹⁵⁶.

The core level spectra for representative chloropolymers is shown in Fig. 3.13. Integration of the C_{1s} and Cl_{2p} levels reveals that in

each case the repeat unit is statistically sampled by ESCA and that the compositions of the outermost few tens of angstroms is representative of the bulk. The derived apparent sensitivity factors for the Cl_{2p} levels with respect to the C_{1s} levels is shown in Table 3.2.

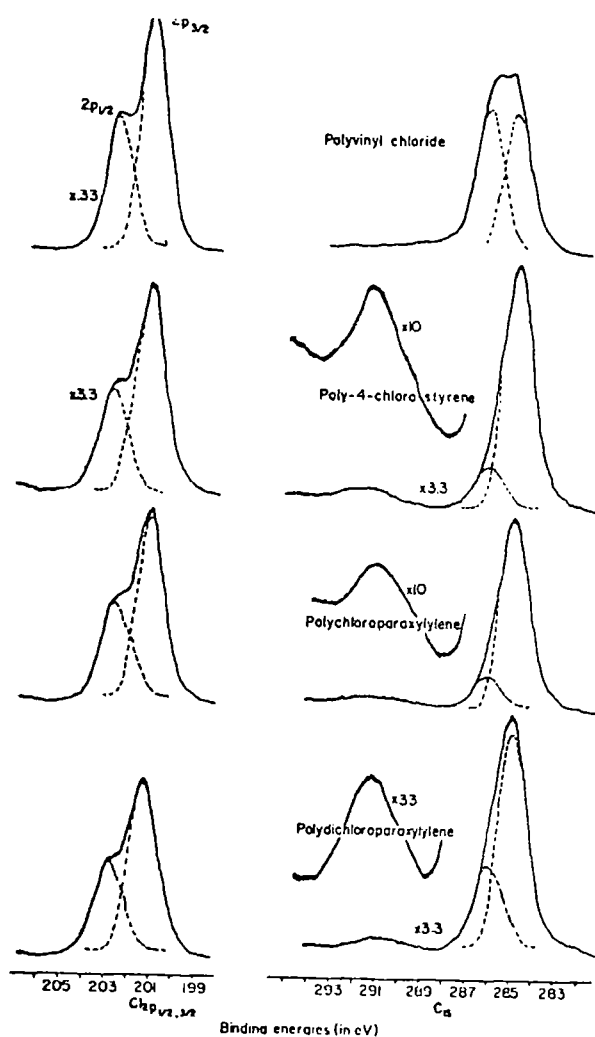


FIGURE 3.13

Typical examples of the C_{1s} and Cl_{2p} core levels for the chloropolymers

The C_{1s} core level spectrum of PVC consists of a flat topped peak characteristic of two components separated approximately by their line widths. The measured shift of ~ 1.2 eV represents the difference between the primary shift of 1.6 eV consequent upon replacing a hydrogen by chlorine $-\underline{CH}_2-$ $-\underline{CH}Cl$ and the secondary shift viz. $-\underline{CH}_2-\underline{CH}_2-$ compared with $-\underline{CH}Cl-\underline{CH}_2-$ where the C_{1s} level under consideration is that associated with the atoms underlined. In the case of the other chlorinated systems in which the repeat unit contains either one or two \underline{CCl} moieties, the carbons directly attached to chlorine appear as shoulders to the high binding energy side of the main peak. Deconvolution of the spectra indicated in Fig. 3.13 reveals the correct overall intensity ratios and the shifts with respect to the centroid of the main C_{1s} peak are in each case ~ 1.4 eV.

The data in Fig. 3.13 reveal the substantial shake-up intensity for two energy $\pi \rightarrow \pi^*$ transitions accompanying core ionization of both the C_{1s} and Cl_{2p} levels, and this is in striking contrast to the situation for PVC which is a prototype for a solely saturated chloropolymer system. The influence of chlorine as a substituent on the intensity of shake-up transitions in the particular case of poly-parasubstituted styrenes has previously been discussed in some detail¹⁴⁰. It is evident, however, that the presence or absence of low energy satellite peaks accompanying core ionization of Cl_{2p} levels and halogens in general, potentially provides a diagnostic tool for differentiating chlorine in saturated and unsaturated environments. It should be possible, therefore, even in the absence of any shift in absolute binding energy, to estimate the proportion of chlorine substituents directly attached to pi systems in polymers.

The data for the complete set of chlorine containing polymers is shown in Fig. 3.14. The lack of theoretical calculations on several of the polymer systems is largely due to the incomplete information on the geometry of the molecule, especially for example, in the chlorinated polyethylenes.

5) Miscellaneous Systems Containing Combinations of Carbon, Hydrogen, Oxygen, Sulphur, Silicon, Bromine, and Fluorine

In this section a miscellaneous collection of routinely available homopolymers which do not conveniently fit into the preceding sections is discussed. Clark and coworkers have discussed the core level spectra and associated shake-up transitions in polydimethyl (PDMS) and polydiphenylsiloxanes (PDPS)^{58c}. From the relative peak area ratios the

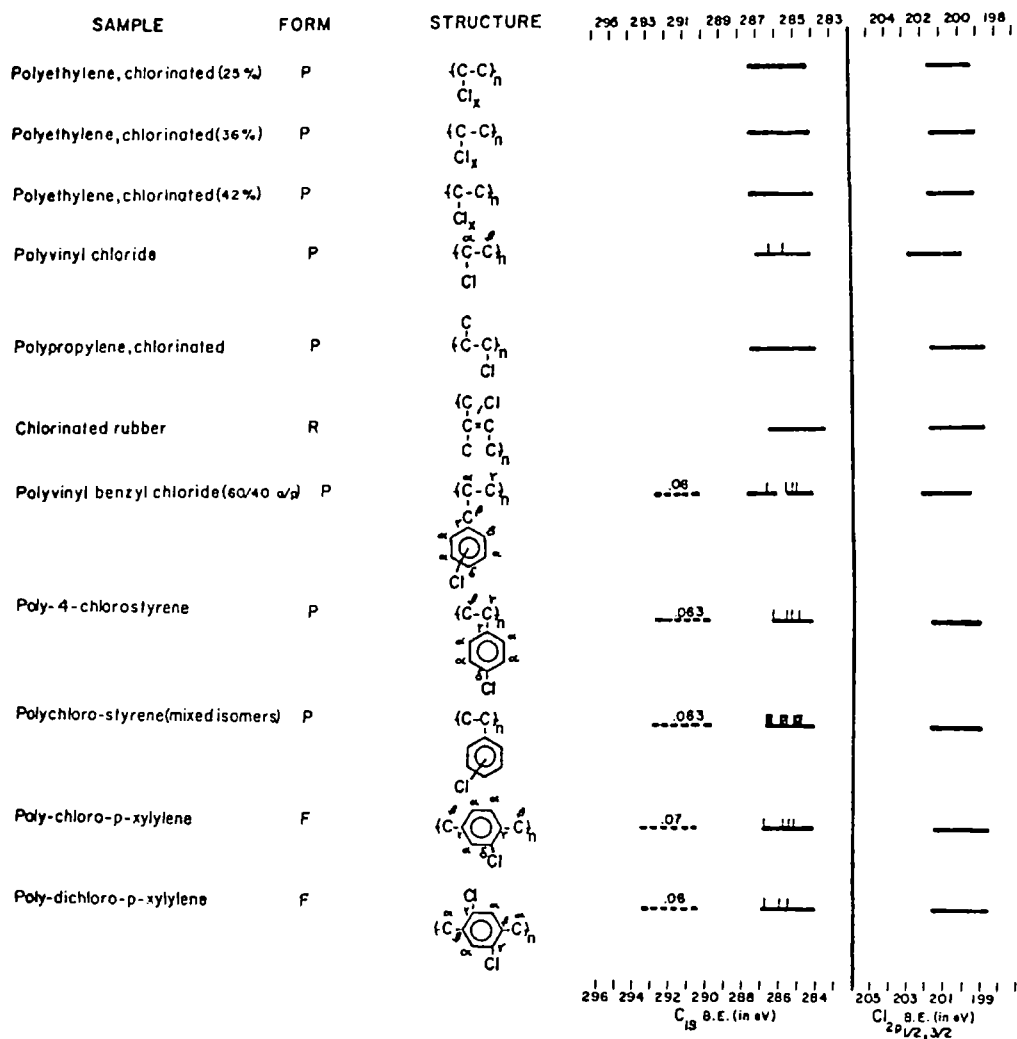


FIGURE 3.14

Tabulation of experimental & theoretical data for polymers containing carbon, hydrogen and chlorine

apparent sensitivity factors may be derived for the C_{1s} and Si_{2p} levels and these are detailed in Table 3.2. The most striking feature of the core level spectra are the presence of low energy shake-up satellites accompanying C_{1s}, Si_{2p}, and O_{1s} photoionization for PDPS but not for PDMS.

The shake-up intensities follow the order $C_{1s} > Si_{2p} > O_{1s}$ and this may readily be understood in terms of low energy $\pi \rightarrow \pi^*$ shake-up transitions. The net effect of having silicon directly attached to oxygen as far as the C_{1s} levels are concerned is extremely small and the absolute binding energies for the peak maxima and the FWHM for the C_{1s} levels are closely similar in PDMS and PDPS. It is instructive to compare the absolute binding energies for the O_{1s} levels in the silicones with those discussed previously for polymethylene and polyethylene oxides. For PDMS and PDPS the O_{1s} binding energies are 533.6 ± 0.2 eV which is within experimental error of the corresponding value of the polymethylene and polyethylene oxides (533.8 ± 0.2 eV). This is not entirely unexpected on the basis of the relative electronegativities of carbon and silicon. It is also of interest to compare the effects on core binding energies of going from carbon (graphite) to polymethylene oxide and silicon compared with the siloxanes as far as the C_{1s} and Si_{2p} levels, respectively, are concerned. The somewhat greater polarity of the carbon oxygen bond is manifest in the substantially larger shift for the C_{1s} levels (≈ 3 eV) compared with ≈ 2 eV for the Si_{2p} levels. The shift for the latter is, in fact, approximately half that in going from silicon (Si) to silica (SiO_2) ≈ 4 eV, where each silicon interacts with four nearest neighbor oxygens¹⁵⁷.

Two bromo-substituted polymers have been studied (viz. poly-4-bromostyrene and polybromo-p-xylylene) and for both deconvolution of the spectra provides a substituent effect on the C_{1s} levels of ~ 1 eV directly comparable with that previously established for simple monomeric systems¹⁵⁴. The integrated intensities for the Br_{3d} and C_{1s} levels provides the apparent sensitivity factors given in Table 2. Clark has previously discussed the electronic effect of a bromine substituent in the case of poly-4-bromostyrene in an investigation of shake-up phenomena in substituted polystyrenes^{58c}. Since in both of the polymer systems studied bromine is directly attached to a conjugated pi system, low energy shake-up satellites accompanying core ionization are apparent not only for the C_{1s} levels, but also for the Br_{3d} levels. The absolute binding energies, therefore, may be used to confirm that the systems contain covalent C-Br bonds and also in the light of the considerable satellite structure accompanying core ionization that in each case the bromine is attached to the aromatic moiety. The total shake-up intensities for the C_{1s} levels, as might have been anticipated, are closely similar for poly-4-bromostyrene

and polybromo-p-xylylene (~6%).

Although extensive studies have been made of simple organo-sulphur containing systems^{18,158,160}, very few studies have previously been reported on organo-sulphur polymers. Indeed, the most extensively studied would appear to be poly(thiocarbonyl fluoride) which has been shown to be one of the few polymer systems to rapidly degrade under the normal conditions for ESCA examination¹²⁶. The previous studies of simple monomers and sulphur containing amino acids and proteins¹⁴⁶ provides sensitivity ratios for C_{1s}/S_{2p} core levels. The only simple organosulphur polymer studied in this work, polyphenylene sulphide, provides from an analysis of the C_{1s}/S_{2p} area ratios a sensitivity factor within experimental error the same as that for simple monomers indicating unambiguously on the ESCA depth sampling scale that the repeat unit is statistically sampled. Low energy shake-up satellites attributable to $\pi \rightarrow \pi^*$ excitations accompanying core ionization are in evidence on both the C_{1s} and S_{2p} core levels. The substituent effect of sulphur on the C_{1s} levels is quite small (~0.4 eV) compared with oxygen (~1.6 eV) as previously outlined. The S_{2p} core binding energy (centroid of spin orbit split doublet) of 163.7 eV is typical for sulphur covalently bonded to carbon.

By way of concluding this Chapter, it is of interest to show how the ESCA data previously described may be used to investigate structure and bonding in more complex systems. As a particular example, consider a typical polysulphone resin where the core level spectra are displayed in Fig. 3.15, and a step-by-step analysis of the ESCA data is given to provide information on structure and bonding in this system.

Ignoring for a moment the fine structure clearly evident for both the O_{1s} and C_{1s} levels, direct integration provides an analysis (assuming for a moment that ESCA statistically samples the likely repeat unit) of C, 76.6%, S, 8.6% and O, 14.8%.* It is difficult to place error limits on these figures, but it is unlikely that these exceed $\pm 0.5\%$. By comparison, the compositions based on the repeat unit shown in Fig. 9 are 77.1%, 7.6% and 15.2% for carbon, sulphur and oxygen, respectively. The analyses in terms of carbon and

*It should be noted that this analysis is based on carbon sulphur and oxygen alone since for hydrogen the 1s level is simultaneously both a core and valence level. In the ESCA spectrum there are no levels specifically characteristic of hydrogen and the hydrogen content must therefore be inferred indirectly (e.g. from shake-up phenomena etc.).

Polysulfone Resin

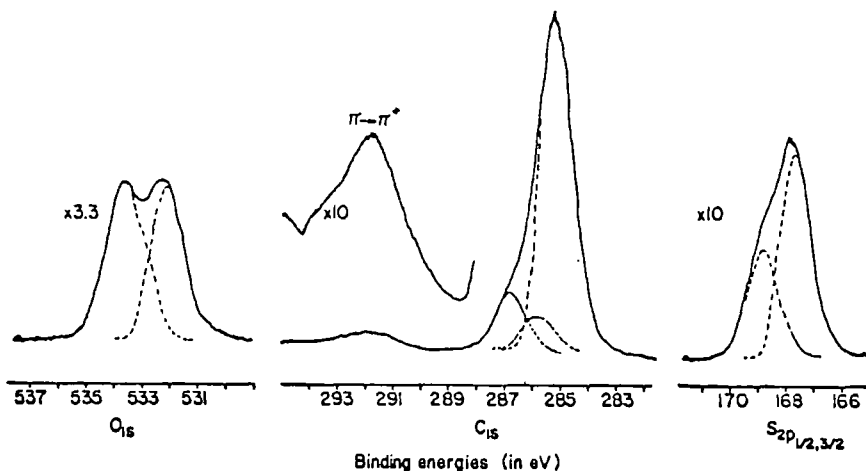
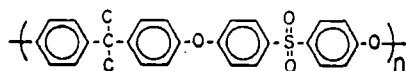


FIGURE 3.15

The C_{1s} , O_{1s} and S_{2p} core level spectra for Polysulfone Resin

oxygen are in strikingly good agreement, however, the ESCA data might tend to suggest that the slightly higher sulphur content from this analysis arises from a preferential orientation of sulphur containing structural features at the surface. Since, however, the sulphur analyses are so close it is not possible to infer more than this. It is interesting to note that the carbon stoichiometry indicates no evidence for any hydrocarbon contamination on the sample which can readily be confirmed by angular dependent studies. Considering now the details of the individual core levels, the S_{2p} levels (binding energy for peak maximum 167.6 eV) are at significantly higher binding energy than for a typical thioether or thiol and the measured shift with respect to polyphenylene sulphide of 3.9 eV is entirely consistent with sulphone groups. This is confirmed by comparison with data for simple organic sulphones and sulfoxides which have previously been studied¹⁶¹. It

is interesting to note that the shift for sulphur with two oxygens attached is somewhat similar to that for carbon with two oxygens attached ($O-C=O$ with respect to C shift ≈ 4 eV).

The O_{1s} levels exhibit a clear cut double structure with the two components of equal intensity being shifted by ~ 1.7 eV with the higher binding energy component being centered ~ 534 eV. This is entirely consistent with oxygens directly bonded to carbons in ether type linkages. The lower binding energy component has substantially lower binding energy than those previously discussed in section (2) and are entirely consistent with oxygens attached to sulphur in sulfone groups. The overall conclusions to be drawn from the absolute and relative binding energies of the O_{1s} and S_{2p} core levels is that both ether type and sulphone linkages are present in equal amounts. The C_{1s} levels exhibit a marked asymmetry and tailing to the low kinetic energy side of the main photoionization peak and line shape analysis reveals two components with relative intensities with respect to the low binding energy component of 11:7:82. The corresponding shifts of ~ 1.6 eV and ~ 0.6 eV are consistent with carbons, with either a single oxygen or sulfone group attached. It is interesting to note that the line shape analysis is equally well described by two components of relative intensity 7:11 with corresponding shifts of 1.8 eV and 1.2 eV, respectively, with respect to the main photoionization peak. Although this is an equally good fit mathematically it is not consistent with the remainder of the data. Thus, a shift of 1.8 eV is reasonable for carbons singly bonded to oxygen, however, a shift of 1.2 eV is too high for carbons directly attached to sulphur since the β effect of oxygen is relatively small. The alternative assignment is even less likely, namely, that carbons singly bonded to oxygen are shifted by 1.2 eV, whilst carbons attached to sulphone residues are shifted by 1.8 eV. The only assignment consistent with all of the available data is, therefore, that based on an intensity ratio of 11:7 for the higher binding energy component, shifted by 1.6 eV and 0.6 eV, respectively. Rounded to the nearest integers the calculated intensity ratios for the C_{1s} levels, based on the statistical sampling of the repeat unit shown in Fig. 3.15, are 11:7:81 in excellent overall agreement with the analysis presented here. The intense low energy shake-up satellite, both in terms of its intensity band shape and separation with respect to the direct photoionization peak is characteristic of a structure

which is predominantly benzoid^{58c}. This fact taken in conjunction with the evidence that although the number of ether type and sulfone type oxygens are the same, but that the number of carbons directly attached to oxygen are different for the two structural features leads straightforwardly to a formulation along the lines of that displayed in Fig. 3.15. Although the ESCA data does not permit an unambiguous assignment of the structure as that shown in Fig. 3.15, there are in fact surprisingly few alternatives which would fit into the overall scheme. Since, in most cases, an educated guess may be made of the likely materials involved in producing such a resin, the alternatives can be ruled out and the ESCA data, therefore, taken in conjunction with a knowledge of the chemistry of sulfone resins provides a means of identifying the basic building block in such systems.

The data for this final class of miscellaneous polymers is shown in Fig. 3.16 and included in the figure are the fluorinated ethylenes which have been discussed in great detail elsewhere^{125,126}, and a fluorinated polycarbonate which will be discussed in detail in Chapter 7.

In conclusion for the two core levels for which the work described in this Chapter provides the most extensive data (viz. C_{1s} and O_{1s} levels) it is of interest to tabulate the data in a manner suitable for ready reference for the identification of particular structural features. The data for C_{1s} levels is shown in Fig. 3.17, where the range of shifts for C_{1s} levels is ~ 10 eV.

The corresponding data for O_{1s} levels are also shown in Fig. 3.17 and in this case, the span in binding energies is ~ 4 eV.

Finally, in Fig. 3.18 is shown the binding energy ranges for the F_{1s} , O_{1s} , N_{1s} , C_{1s} , Cl_{2p} , S_{2p} , Si_{2p} and Br_{3d} core levels from the homopolymers described in this Chapter. It should be noted, however, that for F_{1s} , O_{1s} , C_{1s} , N_{1s} , Cl_{2p} core levels where several different homopolymers were studied in each class and the data can be considered to be a good representation of the range in core level binding energies for those polymers, the data for the S_{2p} , Si_{2p} and Br_{3d} core levels is much less substantial. In fact for those core levels only two polymers were investigated in each case. As more data becomes available for these particular core levels the range in binding energies may well expand.

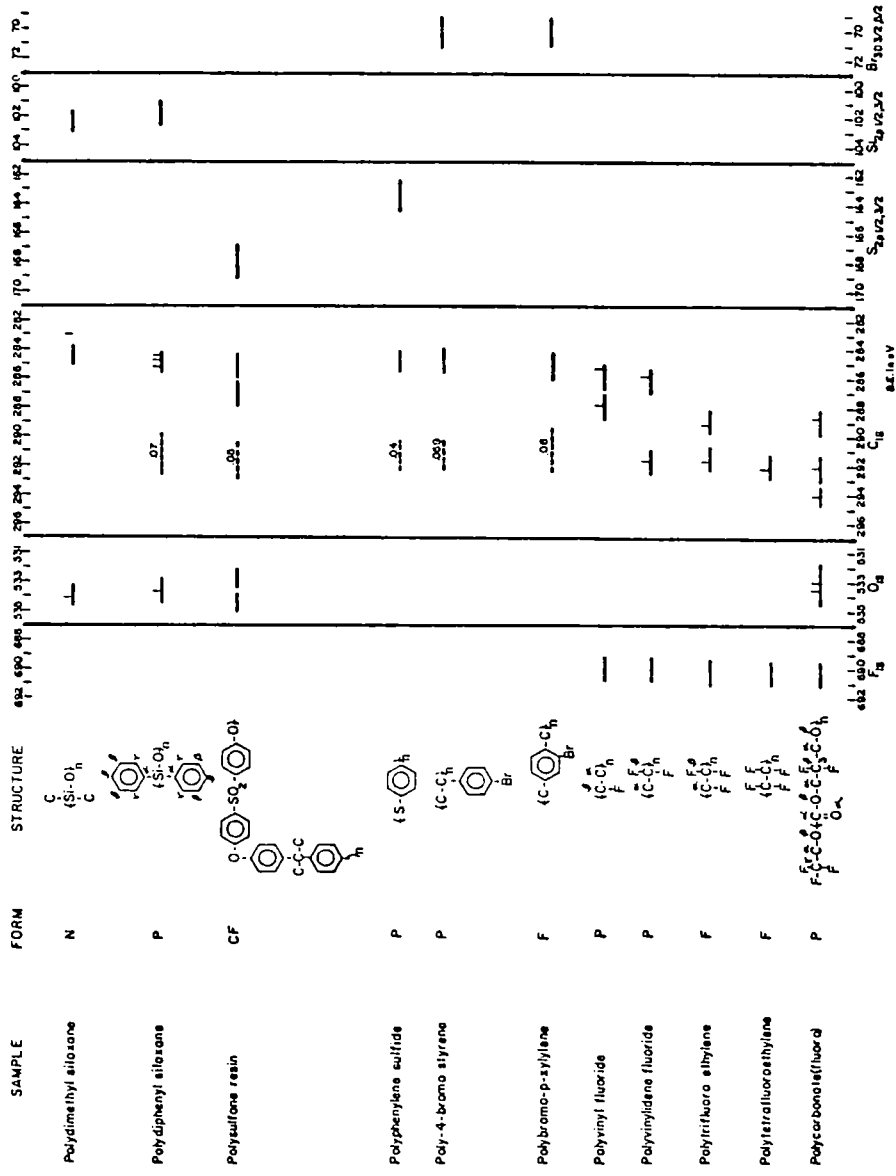


FIGURE 3.16

Tabulation of experimental & theoretical data for polymers containing carbon, hydrogen, silicone, sulphur, bromine and fluorine

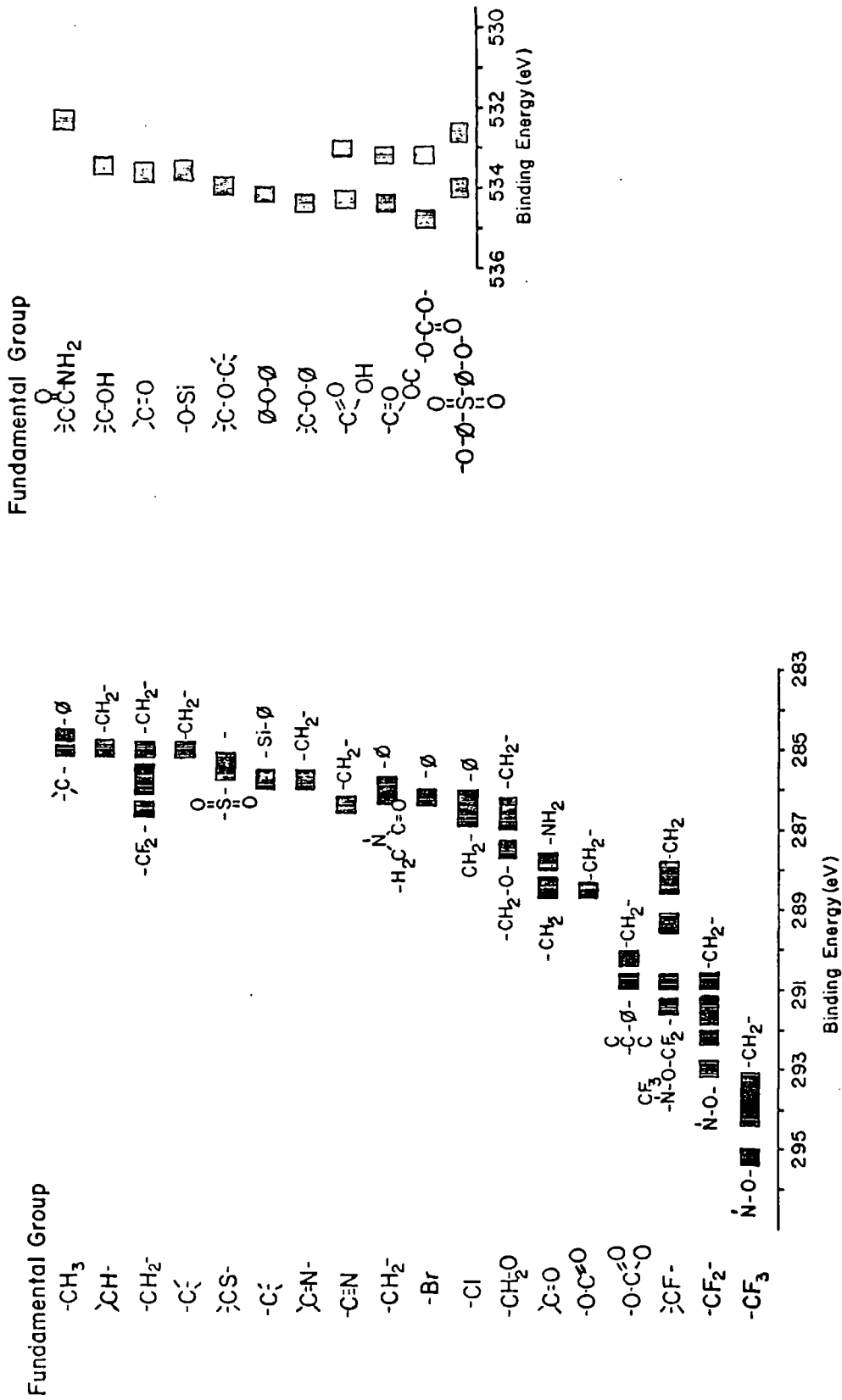


FIGURE 3.17
 Tabulation of experimental chemical shifts for C_{1s} and O_{1s} core levels

CHAPTER 4

Electron Mean Free Paths as a Function of
Kinetic Energy in Polymeric Films

CHAPTER 4

Electron Mean Free Paths as a Function of Kinetic Energy in Polymeric Films

i) Introduction

The development of electron spectroscopy, in general, for the quantitative investigation of structure, bonding and reactivity of solids is dependent to a large degree on an accurate knowledge of the escape depth dependence of electrons as a function of their kinetic energy. The restricted number of core and valence levels available for study for a given element and the limiting nature of the characteristic X-ray sources, means that for even the most well studied cases, the escape depth dependence on kinetic energy has only been studied over selected energy ranges^{18,100,101,120,130,162-194}. In the particular case of the low energy region 0-100 eV, the advent of synchrotron sources have enabled relatively detailed studies in this particular energy range¹⁹⁵. Of more importance, however, in the development of ESCA, is the escape depth dependence in the energy region up to ~ 1500 eV spanned by the commonly used $AlK_{\alpha_{1,2}}$ X-ray sources. Despite the lack of complete investigations encompassing the whole of this energy range, a clear picture emerges as to the general behavior of electron mean free paths as a function of kinetic energy¹⁹⁶⁻¹⁹⁷. Namely, a minimum of the order of a few Angstroms in the region of 80 eV with a roughly square root dependence on energy to the higher kinetic energy side and a steeply increasing mean free path to low kinetic energy such that for electrons of near zero energy escape depths can be in the range of hundreds of Angstroms¹⁹⁵. The increase in mean free path with increasing kinetic energy in the region 100-1500 eV is well documented for a wide range of materials in investigations based on a number of techniques, and has been exploited for semi-quantitative investigation of inhomogeneous samples in the particular case where two levels of the same element corresponding to widely different escape depth dependencies are available for direct comparison (e.g. F_{1s} and F_{2s} and O_{1s} and O_{2s})¹³⁰⁻¹³⁷ (cf. Figures 4.1 and 4.2)

Since the majority of ESCA investigations have been (and will continue to be) carried out with instrumentation involving either or both of $AlK_{\alpha_{1,2}}$ and $MgK_{\alpha_{1,2}}$, it is clear that a necessary pre-requisite

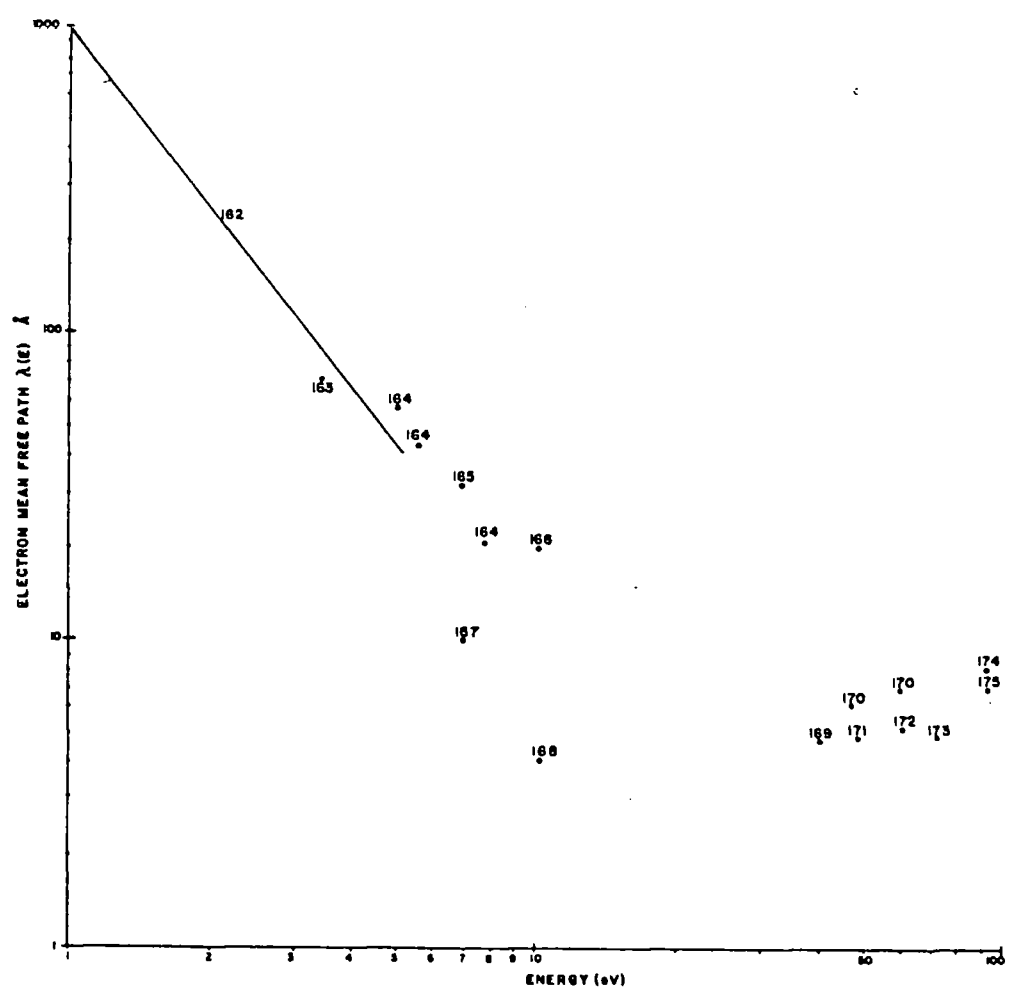


FIGURE 4.1

Experimental data for electron mean free paths in the kinetic energy range from 0 → 100 eV. (Numbers on data points refer to references at the end of thesis)

to the quantitative development of the technique is a knowledge of escape depths for electrons photoemitted from the commonly observed core levels. Although it would be desirable, particularly for comparison with theoretical models to have a detailed knowledge of escape depth as a function of kinetic energy at narrow spaced intervals across the energy range normally encountered for a given material, this does not seem feasible even in the most favorable cases in the near future. The best that can be hoped for at the present time, therefore, are detailed investigations over selected energy ranges.

The available data published up until 1972 and collected together by Tracy¹⁹⁶, seemed to indicate that mean free paths for the materials

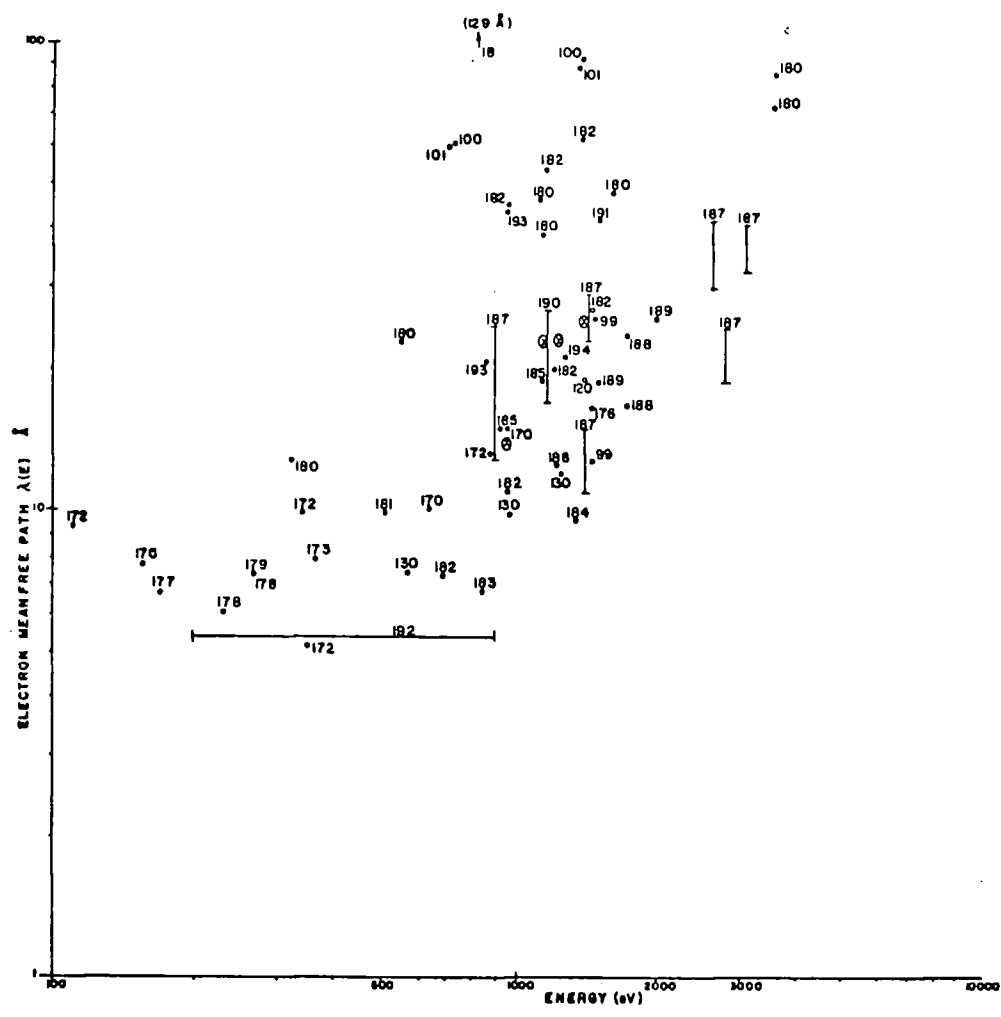


FIGURE 4.2

Experimental data for electron mean free paths in the kinetic energy range 100 → 3000 eV (numbers on data points refer to references at the end of thesis, ⊗ refers to data points from this work.)

which had been studied to that data fitted a generalized curve implying that mean free paths were not too strongly dependent on the material. The extensive review by Powell¹⁹⁷ which included substantially more data, revealed a somewhat greater scatter in values when typical insulators, semi-conductors and metals were included in the same correlation. More recently, Lindau and Spicer¹⁹⁵ have compiled data for 20 different materials in the energy range 0-3000 eV, which again shows that for a given kinetic energy, escape depths can vary from one material to another. However, the striking feature is that even in the most extreme cases, the escape depths fall within a range which is typically

$\pm 50\%$ of the average for a particular kinetic energy. To put this in context it should be emphasized that the experimental difficulties are such that escape depths are typically quoted to an accuracy of $\pm 20\%$ ¹⁹⁵⁻¹⁹⁷. It is gratifying to note that the available theoretical models^{103,197} which have received considerable attention over the past few years, are in good overall agreement with the main details revealed by direct experimental determination of escape depths in that theoretically computed mean free paths are dependent on the electronic structure of a given material, but nonetheless, for a given kinetic energy fall within quite narrow ranges. It is particularly noteworthy, in this respect, that elemental solids as widely disparate in electronic structure as carbon and gold are theoretically predicted to be closely similar in terms of electron mean free paths as a function of kinetic energy¹⁰³.

Investigations of structure, bonding and reactivity of polymers in particular and organic systems in general¹²⁸ have revealed the great surface sensitivity of ESCA, and by taking advantage of the strong dependence of escape depths on the kinetic energy of photoemitted electrons from both core levels of the same and different elements, it has proved possible to provide semi-quantitative information on surface and sub-surface compositions in inhomogeneous samples^{128,130,136,140}. Although the evidence has been somewhat indirect, the strong inference from these wide ranging investigations is that electron mean free paths in organic polymers as a function of kinetic energy are quite similar to those for typical metals and semi-conductors¹²⁸. Thus, from a self consistent computer analysis of data pertaining to the surface fluorination of polyethylene¹³⁰, mean free paths of $\sim 7\text{\AA}$, 10\AA and 12\AA were inferred for electrons of kinetic energies of 560 eV, 969 eV and 1220 eV, respectively. The use of these data in subsequent investigations of surface oxidation¹³⁷, surface structure of AB block copolymers¹³⁶, of fluorographites¹⁹⁸ and of styrene-alkane copolymers¹⁴⁰ lead to eminently reasonable conclusions both on chemical and physical grounds. Comparison with data derived from much less surface sensitive techniques, such as MATR (multiple attenuated internal reflectance infrared spectroscopy) also reveals that in organic materials ESCA with conventional X-ray sources typically samples only the outermost 100\AA . The conclusion of this work, therefore, is that in terms of their behavior as far as electron mean free paths are concerned, organic materials are not significantly different than typical metals and semi-conductors. Much of the data so far published on polymers would be

difficult, if not impossible, to explain on chemical or physical grounds if electron mean free paths in polymers were drastically different than for other classes of materials and, indeed, if mean free paths were an order of magnitude larger than for a typical metal; for example, this should have been readily detectable by careful experiments involving less surface sensitive techniques such as MATR^{130,199}.

There has, in fact, to date, been a considerable divergence of opinion on the relative magnitudes of electron mean free paths in organic materials and to set the work presented in the later sections in proper context, it is worthwhile briefly reviewing the available results prior to this investigation and the methodology involved in their determination.

It is interesting to note that one of the first investigations which revealed the surface sensitivity of ESCA involved a relatively crude study of successively deposited double layers of α -iodo stearic acid by Siegbahn and co-workers¹⁸. By monitoring the intensity of the $I_{3d_{5/2}}$ core levels as a function of double layers deposited it was shown that the signal intensity rapidly reached a plateau value indicative of the fact that the intensity of the elastic peak derives essentially from the surface and immediate sub-surface and a crude estimate of $\sim 100\text{\AA}$ was suggested for the sampling depth.* It is difficult to attempt to make a meaningful estimate of electron mean free paths from this pioneering data since there are many factors which are difficult to quantify. Thus, the importance of investigating intensities as a function of electron take off angle has only been appreciated in the past few years⁹⁸. Control experiment on substrate core levels (chromium oxide) and other core levels of the overlayers are not available and cannot, therefore, be used to investigate the self-consistency of the results (e.g. is the repeat unit for the α -idostearic acid statistically sampled). The difficulties of producing well authenticated, highly oriented Langmuir-Blodgett films are well known and add further complications to any attempt to quantify the analysis²⁰⁰⁻²⁰². Thus, if the films were produced under carefully controlled conditions in which

*It should be noted that there is considerable confusion in the literature since escape depth and sampling depth have often been used in senses which imply they are synonymous which is of course incorrect.

the hydrophilic carboxyl group hydrogen bonds to the similarly hydrophilic chromium surface then with such well ordered films, it becomes imperative to study intensities as a function of take off angle. In his comprehensive review, Powell¹⁹⁷ recognized that specific channelling phenomena for electrons travelling nearly parallel to the long chains of the oriented α -iodo stearic acid molecules could lead to large estimates of mean free paths. Indeed, it becomes apparent that investigations of electron mean free paths involving Langmuir-Blodgett films have consistently yielded mean free paths which are extremely large by comparison with other studies. Thus, Henke¹⁰⁰⁻¹⁰¹, in a study of stearic acid overlayers on Barium Stearate substrates, obtained a mean free path of 60\AA for electrons of kinetic energy of 705 eV. Detailed consideration of the experimental arrangement¹⁰⁰ employed in the work, however, strongly suggests that no angular dependent studies were attempted and that samples were studied at a fixed take off angle normal to the plane of the substrate. This configuration is optimum for channelling and hence, might be expected to give rise to larger mean free paths than for typical organic and polymeric thin film systems with their more random surface morphologies. Powell¹⁹⁷ also reports as a private communication a mean free path of 106\AA obtained by Riggs for 800 eV electrons in erucamide (with a C_{22} chain), although in the intervening period no details or further information have appeared in print. It is almost certain, however, that this value represents an estimate for oriented monolayers deposited on an appropriate substrate. It seems likely that angular dependent studies were not performed and that no attempt was made to check the internal consistency of the results from the investigation of more than one core level which would have indicated whether on the ESCA depth sampling scale the repeat unit of the overlayer was statistically sampled.

It is interesting to note that in a recent review by Swingle and Riggs²⁰³ no mention is made of this work and, indeed, the authors report angular dependent studies of perfluorodecanoic acid by Duch which clearly reveal the surface sensitivity of ESCA in examining organic materials. The authors conclude their article by comparing the depth resolution of various techniques and suggest $10-30\text{\AA}$ for ESCA.

Leaving aside the difficulties mentioned above in obtaining reliable escape depths on organic materials from the study of Langmuir-Blodgett films, one obvious limitation is that points are generated on the attenuation curve at widely spaced intervals (since typically

successive double layers of long chain fatty acids or amines are deposited). In addition, in the published work to date emphasis has been placed on the study of either substrate or overlayer core levels^{18, 100, 101} whilst for internal consistency it is obviously advisable to study both^{128, 130}. The fact remains, however, that the most detailed investigations of escape depth as a function of kinetic energy in materials in general, have employed the substrate overlayer technique since only relative intensities are involved¹⁹⁵⁻¹⁹⁷. The most detailed investigation of carbon containing materials reported to date is that of Steinhardt and co-workers¹⁸⁵ who monitored substrate and overlayer core levels for thin vacuum deposited carbon films (5-60Å) on gold. Film thicknesses were determined with a quartz deposition monitor and although the Varian spectrometer employed in these studies obviated any angular dependent investigations to provide independent evidence for the uniformity of the films, the data overall for both substrate and overlayer strongly support the contention of Steinhardt and co-workers that the films were in fact uniform and that 'islanding' did not occur¹⁸⁵. Mean free paths of 15Å and 18Å were obtained for electrons of kinetic energy ~ 970 eV and ~ 1169 eV, respectively. This provided the first evidence supported by more recent theoretical considerations^{103, 197} that carbon containing materials are not significantly different than typical metals and semi-conductors and raises doubts on the anomalously long mean free paths obtained from the investigation of Langmuir-Blodgett films.

More recently attempts have been made to estimate mean free paths from a knowledge of photoelectron cross sections, the mean free path for electrons of a given kinetic energy for a standard material and a comparison of absolute intensities for core levels of the sample in which mean free paths are required and the standard¹⁹³. In principle, if all the contributing factors are closely controlled the method should be capable of providing information on mean free paths. However, even if we consider silver¹⁸³ and silicon¹⁵⁷ which are relatively easy to produce in optically flat topographically regular films the results do not agree well with those determined by substrate-overlayer techniques. Thus, whilst substrate overlayer techniques employing either Auger or ESCA provide mean free paths of ~ 7Å¹⁵ and 27Å¹⁶ for silver and silicon at kinetic energies of ~ 850 eV and 1386 eV, the corresponding values reported by Cadman¹⁹³ and co-workers on the basis of absolute intensity measurements (an assumed mean free path for the standard

(gold)), are 21\AA and 39\AA , respectively for kinetic energies of 884 eV and 1178 eV. It should be emphasized that the method depends on the determination of the ratios of absolute intensities of different core levels in different samples and this introduces difficulties as will become apparent in the ensuing discussion. By studying pressed films of a number of polymers Evans²⁰⁴ has recently claimed to have measured by this technique mean free paths in the range of $\sim 100\text{\AA}$ for electrons of kinetic energy of $\sim 1000\text{eV}$.

For an infinitely thick homogeneous sample the intensity of the elastic peak for photoemission from core level i may be expressed as Equation (1)^{98,99}.

$$I_i^a = k_i F_i a_i N_i \lambda_i \quad (1)$$

where k_i is a spectrometer dependent function which includes effects due to detector efficiency, transmission characteristics of the analyzer, and geometric factors such as solid angle of acceptance of the analyzer. In the conventional arrangement for instrumentation the X-ray flux F_i is at a fixed angle with respect to the analyzer so that in principle, we do not need to consider variations in cross section a_i arising from the asymmetry parameter (β)⁹⁸. However, the electron take off angle θ (with respect to the sample cf. Fig. 4.3) may be

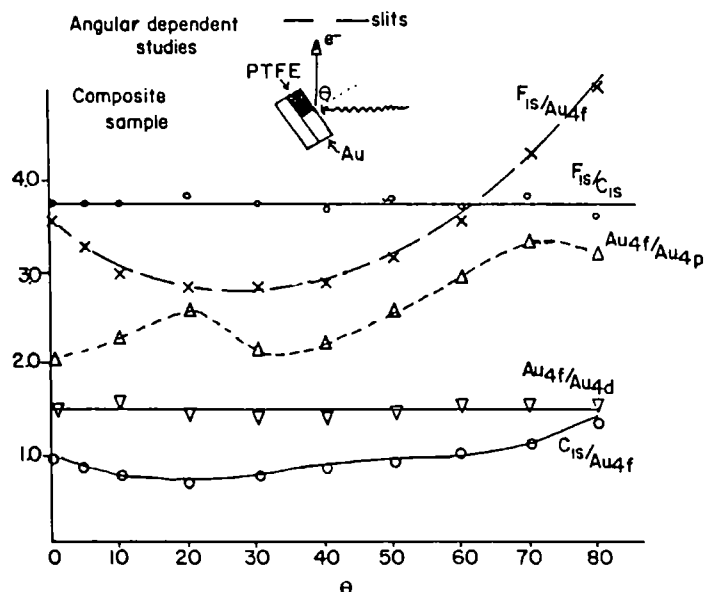


FIGURE 4.3

Core level intensity ratios for a composite sample of gold and PTFE studied as a function of electron take off angle,

varied and the function $f_i(\theta)$ (representing the convolution of effects arising from the effective total flux irradiating the sample (F_i) and the spectrometer function k_i), is strongly dependent on the core level under investigation. Equation (1) may therefore be replaced by (2)

$$I_i = f_i(\theta) N_i \lambda_i \quad (2)$$

where N_i is the number of atoms per unit volume on which core levels i are located λ_i is the mean free path or escape depth. If $f_i(\theta)$ depends on the core level being studied for a given sample, or more importantly, varies from one sample to another (e.g. comparing core levels of a metal and of a polymer) then it is clear that independent angular studies must be made if ratios of absolute intensities for different samples are to be used for estimating escape depths from Equation (2). As a typical example, we may note that for a thick homogeneous sample of gold, the spectrometer function $f_{AU}(\theta)$ is such that the absolute intensity as a function of θ is different than for a typical polymer film. In our particular spectrometer, the fixed angle between X-ray source and analyzer is 90° and Fig. 4.3 shows data on the angular dependence of the ratios of integrated intensities for homogeneous samples of gold and PTFE mounted side by side on the spectrometer probe. It is clear from this that the core levels of PTFE (all of s symmetry) maximize in signal intensity at a different angle than for those of the gold sample. However, whilst the core levels for the polymer maximize in intensity at the same angle, those for the gold sample differ significantly. That this is not an artifact of the sample topographies, may readily be demonstrated since the results are reproducible if samples of gold and PTFE are studied independently and the corresponding ratios are then computed. It is interesting to note that a change in a given ratio of signal intensity as a function of take off angle* when the core levels being studied are such that the numerator data corresponds to a different escape depth than that for the denominator is often taken as evidence of inhomogeneity in the surface structure of a given solid. The inhomogeneity normally alluded to is with respect to the depth co-ordinate into the sample which we refer to as 'vertical inhomogeneity' (e.g. substrate-overlayer). It is clear, however, that

*A take off angle of 90° would, in our definition, correspond to grazing exit for the photoemitted electron.

if ratios of intensities are being employed and separate experiments on the corresponding homogeneous (in both a lateral and vertical sense) materials have not been performed then it is possible to confuse lateral and vertical inhomogeneities. Thus, the mere observation that the $F_{1s}/Au_{4f_{7/2}}$ intensity ratios increase dramatically as the take off angle approaches 90° could, in the absence of the relevant control experiments and a knowledge of the exact nature of the samples, be interpreted as arising from a fluorocarbon overlayer on a gold substrate. However, even without prior knowledge of the samples configuration to which the experimental data in Fig. 4.3 pertain, the data itself provides unambiguous evidence that the samples are vertically homogeneous. Thus the fact that the F_{1s}/C_{1s} intensity ratios are invariant to take off angle provides unambiguous evidence for a homogeneous fluorocarbon film and, indeed, the absolute binding energies and relative intensities could readily be employed to identify this as PTFE. It is clear, therefore, that angular dependent studies (take off angle) are mandatory if comparisons are being made of absolute intensities. Further, if the relevant control experiments have been made, it is possible to clearly differentiate between homogeneous samples on the one hand, and samples which are either laterally or vertically inhomogeneous. It is also possible, by extension, to investigate samples which are both laterally and vertically inhomogeneous as would be the case, for an overlayer which 'islands' on a substrate⁹⁸.

The second major objection to the use of Equation (2) even if angular dependent studies have established the $f_i(\theta)$'s for each core level, is that absolute intensities also depend on surface topography, and on the density of atoms on which the core levels of interest are located. If we consider a typical polymer sample of a given density studied as either a powder (e.g. mounted on double sided Scotch tape) or as a film then the absolute intensities for the core levels of the latter are significantly higher than for the former. Whilst for a film the surface is relatively uniform the surface topography for a powdered samples is irregular and, indeed, these differences are manifest in the observed line widths for the core levels which are significantly narrower for the film¹²⁵. Thus, although both insulating samples exhibit sample charging the surface charge is uniformly distributed for the film, whilst for the powder the topographical irregularities lead to a small spread in binding energies giving rise to

the observed line broadening. It is also possible to fabricate polymer films of differing porosity and since this corresponds to a difference in atom density, this also gives rise to differing intensities for materials of the same bulk composition (cf. Chapter 6). If absolute intensities are to be employed, it is again mandatory, therefore, that samples of identical topography be studied. Whilst these arguments pertain to the structures on the atomic scale, it is also the case that the macroscopic topographical aspects be the same. As a simple example, two identical samples of a polymer film may be mounted on a sample probe such that the films either closely follow (flat) sample mount (e.g. by mounting the sample on a double sided Scotch tape of dimension equal to or greater than that of the sample) or by affixing the sample only over small areas at its corners. The macroscopic topographies are, therefore, not identical and significant differences in absolute intensities are observed for the two samples.

Whilst the objections so far raised to the estimation of mean free paths based on absolute intensity measurements are clearly considerable, a potentially more serious source of error in employing Equation (2) is the relative importance of shake-up and shake-off processes⁹⁸. It is implicit in using a relationship such as (2) (to ratio absolute intensities for different core levels in different materials) that the contributions of shake up and shake off processes (which effectively remove intensity from the elastic peak) are constant proportions of the direct photoionization peaks. Cadman and co-workers are largely dismissive on this point¹⁹³.

Whilst it is to be expected* that the sum total of shake-up and shake-off intensities with respect to the direct photoionization peaks would vary over a relatively narrow range for a given class of related polymers (e.g. organic polymers) this might not be the case in comparing these with typical semi-conductors or metals. In support of their contention that shake-up and shake-off processes may be

*In an extensive series of theoretical studies on prototype systems we have previously shown that whilst relaxation energies vary as a function of electronic environment, such variations are small for related systems compared with the typical range of shifts in core binding energies⁵³⁻⁵⁵. We may infer that the sum total of shake-up and shake-off intensities are closely similar in such systems from the relationships developed by Manne and Åberg⁵⁹.

neglected, Cadman and co-workers cite the consistency of the data on relative intensities of core levels obtained in their measurements with those previously reported in the literature¹⁹³. The error spread in the cross sections reported is considerable and comparison with previous experimental data of Chapman and Lohr²⁰⁵ reveals considerable discrepancies. Thus, whilst Chapman and Lohr's data for C_{1s}, N_{1s} and O_{1s} relative cross sections are in excellent agreement with theory²⁴ the corresponding data obtained by Cadman and co-workers are 4%, 9% and 20% smaller. For the S_{2p}, Cl_{2p}, Ag_{3d_{5/2}} and Au_{4f_{7/2}} levels, however, direct comparison with the recent theoretical tabulations of Scofield²⁰⁶ reveals discrepancies which are 11%, 9%, 12% and 5% larger, respectively. Whilst this does not necessarily invalidate the whole of the arguments put forward by Cadman and co-workers¹⁹³, it highlights the importance of considering all of the factors which contribute to the absolute intensity of a given core level.

Considered here in broad outline are some of the difficulties which arise in attempting to estimate electron mean free paths in materials from a knowledge of photoionization cross sections and the absolute intensities of the elastic peaks. These difficulties account, at least in part, for the discrepancies in mean free paths estimated for organic materials, since the factors elaborated will be particularly important for this class of material. However, before concluding this section, it is worthwhile pointing out that there are logical inconsistencies in the interpretation of the data presented in reference 193, and the resolution of these inconsistencies suggest somewhat shorter mean free paths for organic materials.

The data on absolute measured intensities in Table 1 of reference 193 allow a direct computation of the intensity ratio for unit stoichiometry for photoemission from the Au_{4f_{7/2}} and C_{1s} levels. Thus, from column 5 of Table 1

$$\frac{I_{AU}}{I_C} = \frac{I_{AU}}{I_N} \cdot \frac{I_N}{I_O} \cdot \frac{I_O}{I_C} = 12.6$$

From the relative cross section given for the relevant core levels (for unit stoichiometry), the intensity ratio I_{AU}/I_C may also be calculated from Equation (3) of reference 193 as a function of the ratio of the

Table 4.1

Calculated intensity ratios I_{Au}/I_C^*	Mean free path for electrons (in Å)
5.0	44
22.1	10
12.3	18
13.0	17

*For $Au_{4f_{7/2}}$ and C_{1s} levels using Equation (3) of reference 193 for hypothetical material of unit stoichiometry.

electron mean free paths. The results are displayed in Table 4.1.

Comparison of the data in Table 4.1 with the experimentally derived data therefore provides an estimate of the mean free path in the hypothetical material of unit stoichiometry of 17-18Å. This compares with the assumed value of 20.2Å for gold and the estimate of 44Å for graphite. The inconsistency in this arises largely from two elements of cyclic arguments employed in reference 193. Thus, the relative cross sections calculated in Table 1 of reference 193 are of two types. In column 9 the ratio reported for the solid samples assume that the mean free paths corresponding to photoemission from different levels in both the same and different compounds are identical although the latter analysis using these data are purported to show that this is not, in fact, the case. Further, the data reported in column 10 indicate that the relative escape depths have been 'corrected for kinetic energy' according to the relationship

$$\lambda \propto (E)^{0.5}$$

Analysis of the final data, however, presented in Table 2 of reference 193 shows that there is considerable deviation from a square root dependence of mean free path on kinetic energy.

It should be clear that there is a considerable divergence of opinion on mean free paths in organic materials, in general, and it is the purpose of the succeeding section of this paper to present in detail evidence obtained on the direct measurement of mean free paths in polymers by the substrate overlay technique which resolves some of the ambiguities alluded to in the preceding discussion.

ii) Experimental

Although the substrate-overlayer technique provides, in principle, the most straightforward and reliable methods of measuring electron mean free paths, the experimental difficulties in implementation are considerable¹⁹⁷. Thus, if mean free paths are to be estimated in polymers, we require uniform films of known thickness and structure and an angular dependent study of both substrate and overlayer core levels. For a variety of reasons which will become apparent, the study to be reported here involved the in situ production of poly paraxylylene films by polymerization of paraxylylene precursors generated in a pyrolysis flow system and the direct measurement of film thicknesses by means of a quartz deposition monitor.

A careful consideration of all of the factors which must be controlled in such a study leads to a straightforward selection of the poly paraxylylene system²⁰⁷. Thus, the sublimation and pyrolysis rates for the [2.2] paracyclophanes²⁰⁸ may be precisely controlled providing a convenient deposition rate for the paraxylylenes via various pyrolytic routes has been exhaustively studied in the literature and forms the basis of the commercially available PARYLENE* coatings²⁰⁷. The major advantages of employing the synthetic route involving [2.2] paracyclophane starting materials may be summarized as follows:

- 1) The pyrolysis under appropriate conditions yields quantitative conversion to the polymer with no side reactions²⁰⁷.
- 2) Since the method allows close control of the rate of production and deposition rate of the intermediate paraxylylenes, uniform thin films may readily be produced²⁰⁷.
- 3) The thin films produced in this way as opposed to other methods (e.g. solvent casting) are essentially impurity free (e.g. from solvent impurities, antioxidants, catalysts, filler, antiblocking agents, etc.)²⁰⁷.
- 4) The poly paraxylylene polymers produced by this route have been well characterized in the literature²⁰⁹.
- 5) The films can be prepared in-situ in a sample chamber directly attached to the spectrometer source which obviates any possibility of contamination which might arise if the samples

*Union Carbide Corporation trade mark.

were prepared elsewhere and then transferred to the spectrometer (cf. ref. 185).

- 6) Substituted derivatives of [2.2] paracyclophane have been well characterized and provide a route to the substituted polymer system so that possible variations in mean free path as a function of polymer structure may be investigated^{207c}. (cf. Chapter 5)

A schematic of the synthetic route is shown in Fig. 4.4 where

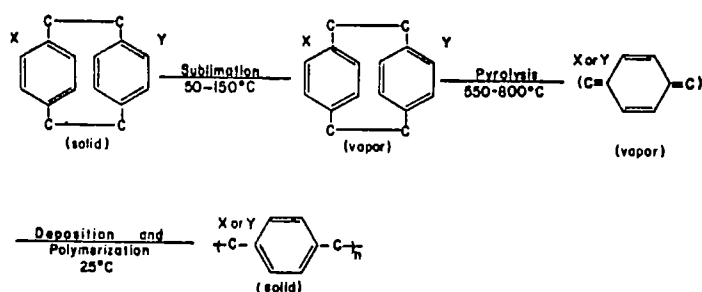


FIGURE 4.4

A schematic of the polymerization process from the [2.2] paracyclophane to the poly paraxylylene

the sublimation and pyrolysis temperatures were optimized for a given paracyclophane precursor and were in the range indicated.

The starting materials [2.2] paracyclophanes were obtained from Union Carbide Corporation, U.S.A. and included the unsubstituted and dichloro 2.2 paracyclophanes (monosubstituted rings). For the latter, the dominant isomer is the pseudo para²⁰⁹, however, the fact that an isomeric mixture was employed is of no significance since pyrolysis leads to the same monochloro paraxylylene intermediate²⁰⁷. Dibromo [2.2]paracyclophane was synthesized according to the literature procedure^{207c} and all starting materials were recrystallized from appropriate solvents, a minimum of three times and characterized by V.P.C., M.Pt. and by U.V. and I. R. spectroscopies. In all cases, the purities were >99.5%. ESCA spectra were recorded on all starting materials

and as an additional check, the constancy of the ratios of shake up intensities in the region ~ 10 eV from the direct photoionization peaks determined*. This provides a good internal check on the polymer overlayers produced and would readily reveal any extraneous contamination. However, in all cases reported here excellent agreement was obtained for the shake up intensities for paracyclophane precursors and the polymers themselves.

The room temperature deposition of the paraxylylenes produce polymer films which have been well characterized and an extensive literature is available on structure, crystallinity, density and linearity of the polymers²⁰⁹. The mechanism of polymerization involving as it does successive addition of paraxylylenes to a growing (linear) polymer chain would suggest a priority that films of closely uniform coverage should be produced by this route with little or no tendency for 'islanding'²⁰⁷. As will become apparent, this is in fact the case**.

The 'initial' sticking probabilities for substituted paraxylylene systems is a strong function of the electronic effect of the substituent and of the substrate and represents the convolution of effects due to the initial interaction between paraxylylene and substrate and the overall rate of the polymerization reaction at the interface²⁰⁷. For a variety of reasons gold was chosen as the substrate. The sticking coefficients for the paraxylylenes involved in this work for a gold substrate provide a very convenient time scale for the initial build up of thin films. The 4f core levels of gold have a sufficiently large cross section that they may still be monitored with considerable statistical accuracy for relatively thick

Since the shake up intensity in this region derives from $\pi \rightarrow \pi^$ transitions accompanying core ionization in the conjugated system, we would anticipate that the shake-up intensity for the precursor would be identical to that for the polymer since they are closely related structurally.

**A further important consideration is that since such polymers are not 'crystalline' in the sense normally employed when discussing single crystals of typical organics, metals and semi conductors, the problem of specific channelling phenomena does not arise. In this sense the results are likely to be particularly useful since the majority of ESCA studies where quantitative data is of use pertains to polycrystalline or amorphous materials.

overlayers. There is also no likelihood of chemical interaction between deposited paraxylylenes and the substrate. Finally, since the thin film thicknesses were measured using a quartz deposition monitor (gold coated), it is important that a substrate is available from which it is relatively straightforward to produce a uniform evaporated overlayer on quartz crystals such that sticking probabilities etc. for the deposition monitor are identical to those for the substrate itself.

As we have noted, the use of a pyrolysis flow system obviates many of the problems and artefacts which might arise if polymer films of known thickness are produced by other means. The final design of the apparatus employed in this work is shown in Fig. 4.5 and utilized

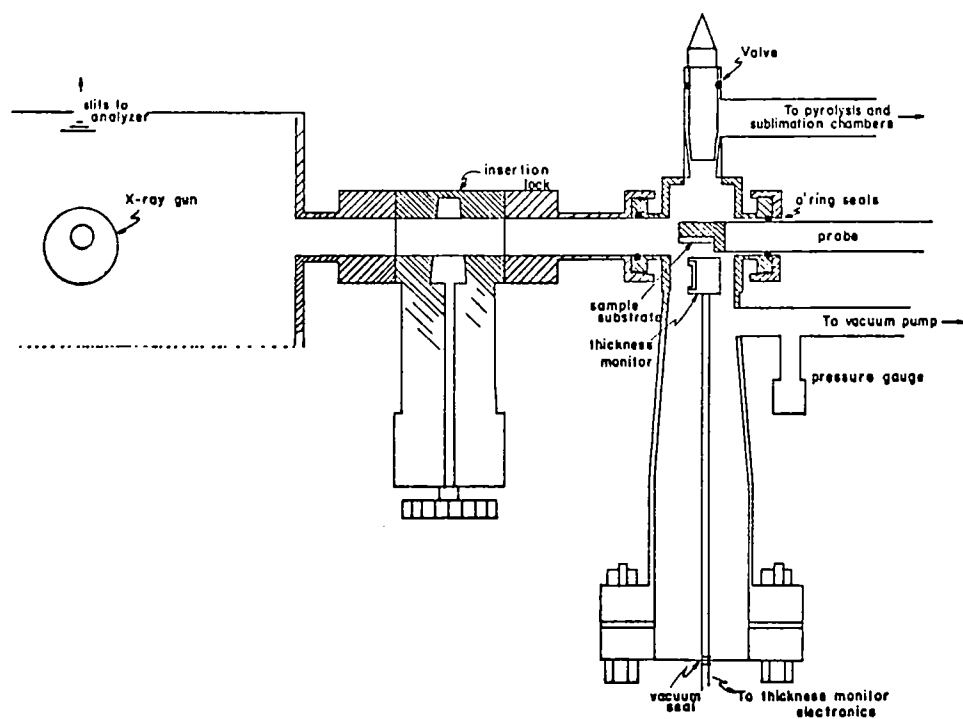


FIGURE 4.5

The apparatus (shown attached to the insertion lock system of the spectrometer) for the controlled deposition of poly paraxylylenes

the flexibility of the insertion lock system of our particular ESCA instrumentation.

The purified [2.2] paracylcophane starting materials were placed in the temperature controlled sublimation end of 1/2" diameter quartz

tubes ~24" in length. The samples ~ 2 gms. were sublimed into the pyrolysis zone which extended over a length of ~12" starting some 6" from the closed end of the tubes. The 'Lindberg' (Type 55035A, Lindberg, Watertown, Wisconsin, U.S.A.) pyrolysis furnace enabled accurate control of the temperature profile over the pyrolysis zone and depending on the [2.2] paracyclophane precursor temperatures in the range 500-650°C were employed. The post pyrolysis zone of the quartz tube was connected via greaseless couplings (Cajon Corporation, Cleveland, Ohio, U.S.A.) to the deposition chamber. The use of vacuum T fittings enabled pressures to be measured at the inlet to the deposition chamber by means of a Hastings DV-6 thermocouple gauge (Teledyne Hastings - Radist, Hampton, Virginia, U.S.A.) which could be isolated from the pyrolysis stream during an actual deposition experiment. The inlet to the deposition chamber from the pyrolysis tube could be isolated by means of a greaseless valve. The deposition chamber was mounted directly onto the spectrometer insertion lock system which in turn was mounted on a 'Goddard' valve (Goddard Valve Corporation, Worcester, Mass., U.S.A.) directly attached to the source of the ESCA spectrometer. Pumping for the system was provided by the two stage rotary pump (Edwards ED50, Edwards High Vacuum, Crawley, England) normally employed for pre-pumping in the insertion locks for the normal mode of introduction of the sample probe into the spectrometer. This arrangement provides considerable flexibility since the deposition chamber and ancillary apparatus may readily be demounted so that the experiments described here could conveniently be interfaced with the normal spectrometer work load. The quartz deposition monitor was attached to the deposition chamber in such a manner that the gold substrate mounted on the sample probe tip and the monitor head (gold coated quartz crystal) were as nearly as possible arranged in a symmetrical relationship to the inlet from the pyrolysis chamber. Independent experiments described below established the relationship between film thickness for polymer films deposited on the gold substrate on the sample probe and on the deposition monitor. The thickness monitor (Kronos Type QM 300, Kronos Corporation, Torrance, California, U.S.A.), employed in this work, measures the change in period of oscillation of the quartz crystal, thereby eliminating the non-linearity resulting from the measurement of changes of frequency²¹⁰. An assumption which must be made, however, is that a deposited film of some given mass per unit area will produce the same effect as a quartz film of the

same mass per unit area, provided that the thickness of the deposited film is small compared to the thickness of the quartz crystal. Sufficient studies have been made to establish the validity of this assumption up to film thicknesses in excess of $100,000\text{\AA}^{211}$. The calibration of the thickness monitor itself for the determination of film thicknesses for the polymer films requires a knowledge of their densities. Detailed studies are, in fact, available in the literature for the bulk polymers and there seems no reason to suspect a priori that the thin polymer films studied in this work would vary significantly in density from the reported data²⁰⁹. Indeed, as will become apparent, the overall agreement with independent estimates of film thicknesses based on ellipsometry and microbalance measurements fully support this contention. In a typical experiment, the apparatus was pumped down to a pressure of $\sim 10^{-2}$ torr and the thickness monitor zeroed. The sublimation heater was then placed over the closed end of the quartz tube containing the relevant [2.2] paracyclophane precursor. With appropriate adjustment of sublimation and pyrolysis temperatures the poly paraxylylenes films were deposited onto both the gold substrate mounted on the spectrometer sample probe tip (mounted on the deposition chamber by means of the insertion lock) and the deposition monitor head. When a film of appropriate thickness as monitored on the digital readout of the apparatus had been deposited, the pyrolysis chamber was valved off from the deposition chamber and the sublimation heater removed. The sample probe was then directly introduced into the spectrometer source by opening the intervening Goddard valve. Our particular instrumentation is equipped with a horizontally mounted unmonochromatized $\text{MgK}_{\alpha_{1,2}}$ X-ray source of Henke design and also a monochromatized $\text{AlK}_{\alpha_{1,2}}$ source produced by dispersion from three toroidally bent quartz discs. This slit filtered monochromatized source is at an angle of 60° to the horizontal in the same vertical plane as the $\text{MgK}_{\alpha_{1,2}}$ source as shown in Fig. 4.6. It thereby proved possible to study samples with both X-ray sources. Since, however, angular dependent studies (which are quite time-consuming) were also performed, in which the electron take off angle with respect to the sample surface was investigated, studies with both X-ray sources were restricted to the parent poly paraxylylene ring system. For similar reasons, only the most intense core levels were investigated; namely, the C_{1s} levels of the polymer overlayer and the Au_{4f} levels for the substrate. Preliminary experiments established a suitable range of film thicknesses and

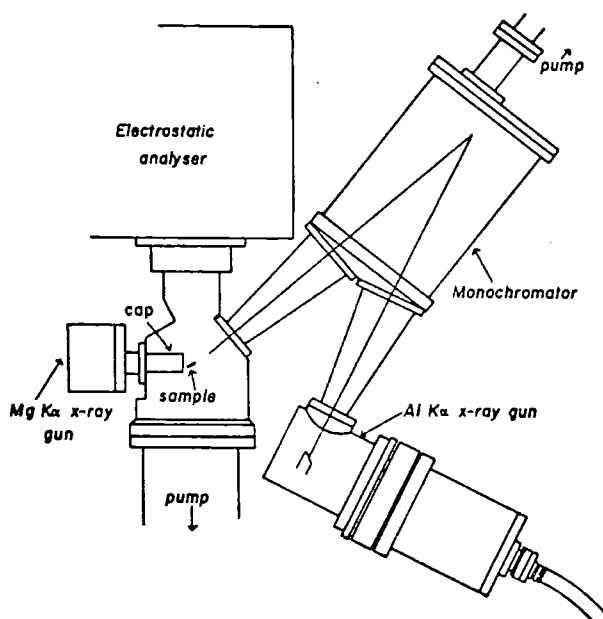


FIGURE 4.6

The AEI ES 200B schematic indicating the relative positions of the Mg and Al X-ray sources with respect to the sample, and the sample with respect to the analyser

convenient time scales for deposition. The preliminary experiments indicated the overall reproducibility of producing films of given thickness and also established that films of the same indicated overall thickness which were either deposited in one run or built-up by successive runs, gave identical results. For the parent polymer system which was subjected to the most detailed scrutiny 20 thicknesses interspersed in the range 5-100 \AA were investigated and repeat runs were entirely reproducible. Area measurements were made using a DuPont 310 Analog curve resolver (E. I. DuPont de Nemours and Co., Instrument Products Division, Wilmington, Delaware, U.S.A.)

The calibration of film thicknesses essentially resolves into two components. Firstly, the calibration of the thickness monitor itself, and secondly the calibration involving the relationship between films deposited on the sample probe tip and on the deposition monitor. For the direct calibration of film thickness polymer films in the thickness range $\sim 10\mu$ were produced which could readily be removed from both the monitor head and the substrate. Direct weighing

of samples of known area by means of capacitance microbalance (Cahn Electrobalance, Model G, Paramount, California, U.S.A.) established that the indicated film thickness on the deposition monitor was within experimental error the same as that obtained by direct weighing, and this indicates that to a high degree of accuracy the density of the films were identical to those reported in the literature²⁰⁹. (For poly paraxylylene density = $1.129 \text{ gm. cm.}^{-3}$)^{209a}. The measurements were highly reproducible indicating that cleavage of the polymer films from the substrate almost certainly left less than a few monolayers of material adhering to the latter (this was confirmed in the case of the gold substrate on the sample probe tip). This operation could readily be effected with no significant change in surface area of the films (i.e. the films did not 'stretch'). Having established the direct correspondence between the indicated and independently measured film thicknesses for the quartz deposition monitor, a correlation was then established for films peeled from the deposition monitor and from the sample probe tip. Repeat measurements on different films in the tens of microns thickness range gave a ratio of film thicknesses for the probe substrate and deposition monitor of 0.75 ± 0.03 . This represents a geometric factor since the probe substrate and monitor head are not in identical positions with respect to the pyrolysis chamber inlet. The dimensions of the apparatus were such as to preclude an absolutely identical arrangement and to avoid the possibility of widely disparate film thicknesses on the two substrates which could arise from streaming effects the arrangement employed was as indicated in Fig. 4.5 with the gold substrate mounted on the sample probe at right angles to the quartz deposition monitor and thus being rotated 180° with respect to the pyrolysis inlet tube. Streaming effects should, thereby, be minimized and if they occur would be expected to produce a somewhat thicker film on the deposition monitor substrate. This is, in fact, the case as has previously been noted (ratio of thicknesses 0.75 ± 0.03).

The calibration of film thicknesses was checked for internal consistency by independent measurements employing ellipsometry. Since these measurements involved preparation of films and then transportation to another laboratory* for the ellipsometry studies, sample thicknesses

*Thanks are due to Dr. I Callaghan, Proctor and Gamble Research Laboratories, Newcastle-upon-Tyne for undertaking these measurements. The requisite refractive index data for the poly paraxylylene films were taken from reference 209a.

were chosen such that any contamination which might arise in handling would be minimized. Films of poly paraxylylene were, therefore, deposited on gold substrates, the indicated film thicknesses on the deposition monitor being 350\AA and 600\AA .

The He/Ne laser (632.8 nm.) employed in the ellipsometry studies provided a sampling area ~ 1 mm. in diameter and measurements were, therefore, made over different areas of the polymer films and the values reported are the average of these in each case. For a given polymer film measurements fell within a narrow range which may be taken as independent evidence, at least on the macroscopic scale that the samples are of uniform thickness. For the 350\AA sample (indicated thickness on the deposition monitor) the ellipsometry measurements gave a thickness of $263\text{\AA} \pm 5\text{\AA}$, whilst for the 600\AA sample the corresponding value was $462 \pm 5\text{\AA}$. This provides ratios of 0.75 and 0.77 for the geometric factor involved in relating film thicknesses for the probe substrate and the deposition monitor head in excellent agreement with that for the thick films.

iii) Results and Discussion

Initial experiments established a convenient range of thicknesses and deposition rates for films and to establish the overall reproducibility of the method studies were carried out on the parent system, poly paraxylylene, using unmonochromatized $\text{MgK}\alpha_{1,2}$ radiation. Samples were studied at a fixed take off angle (θ) of 10° which corresponds to the maximum in signal intensity for the $\text{Au}_{4f_{7/2}}$ levels of the gold substrate with out particular experimental arrangement. The data are displayed in Fig. 4.7 which shows a plot of $\ln I_0/I_0^\infty$ vs. film thickness for the substrate core levels and the corresponding plot of $\ln (1 - I_S/I_S^\infty)$ for the C_{1s} levels of the polymer overlayer. Statistical analysis of the data yields R^2 values of 0.99 for both correlations with derived mean free paths of 20.4\AA and 14.4\AA for electrons of kinetic energy ~ 1170 eV and ~ 969 eV, respectively. Even in the absence of angular dependent investigations the good statistical nature of the data with linear extrapolations provides strong evidence for the absence of any significant 'islanding' effects. Since the quartz deposition monitor actually measures the mass of material deposited, islanding should readily be detectable by deviations from straightforward exponential behavior for the attenuation of core level signals for substrate and overlayer¹⁷². This is readily appreciated in a simplistic fashion,

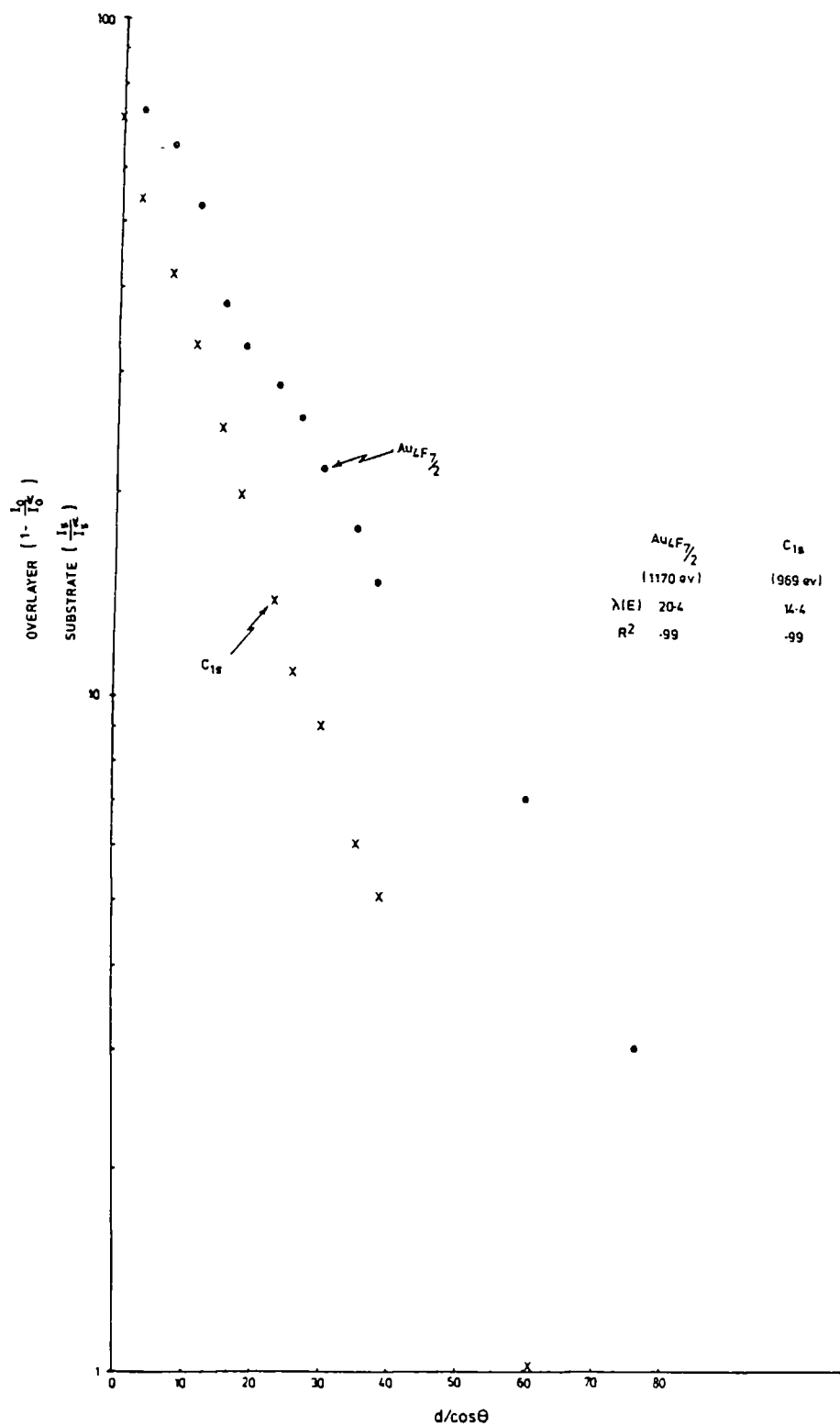


FIGURE 4.7

$\frac{\ln(1 - \frac{I_0}{I_0})}{\frac{I_0}{I_0}}$ for the overlayer and $\ln(\frac{I_s}{I_s})$ for the substrate, versus $d/\cos\theta$,
for a series of thicknesses of poly paraxylylene on a gold substrate,
studied at a constant θ of 10° , with a $MgK_{\alpha 1,2}$ X-ray source.
 (Note the ordinate has been arbitrarily normalized to a ratio of 100
 where $\frac{I_0}{I_0}$ equals 1.)

if we ignore to a first approximation shadowing effects. Thus, for a uniform coverage of thickness d the intensity ratios are of the form:

$$I_s^d = I_s^\infty e^{-d/\lambda_s \cos \theta} \quad (4.3) \quad \text{for substrate (Au}_{4f_{7/2}})$$

$$I_o^d = I_o^\infty (1 - e^{-d/\lambda_o \cos \theta}) \quad (4.4) \quad \text{for overlayer (C}_{1s})$$

If the same mass of material, however, is distributed in 'islands' with fractional surface coverage f then the analogues of (3) and (4) are:

$$I_s^d = (1 - f) I_s^\infty + f I_s^\infty e^{-d/f\lambda_s \cos \theta} \quad (4.5)$$

$$\text{and } I_o^d = f I_o^\infty (1 - e^{-d/f\lambda_o \cos \theta}) \quad (4.6)$$

The manifestation of this behavior would be an exponential dependence for both substrate and overlayer core levels, however, for the former a plateau value would be reached corresponding to the first term in Equation 4.5. The net effect would be that depending on f , an upper bound on mean free paths will be obtained. The nature of the experiments in which films are built up by successive deposition, and the polymerization reactions themselves would make the possibility of islanding seem exceedingly remote. The final confirmation of this, however, comes from the angular dependent studies which have been carried out in a separate series of experiments.

The results are displayed in Fig. 4.8 for poly paraxylylene films studied with unmonochromatized $MgK_{\alpha_{1,2}}$ radiation. Take off angles with respect to a normal sample surface of 0° , 10° , 30° and 50° were investigated and it is clear from the data displayed in Fig. 4.8 that the overall agreement is extremely good for both substrate and overlayer core levels. Statistical analysis of the data points taken for each angle in each case provides R^2 values of 0.99 and the derived mean free paths for the overlayer and substrate core levels show a remarkably small degree of scatter. The derived mean free paths of 10° take off angle of 21.0\AA and 12.6\AA respectively for electrons of kinetic energy of ~ 1170 eV and ~ 969 eV compare favorably with those obtained in the independent study just described (20.4\AA and 14.4\AA).

The scatter in the data in Fig. 4.8 is more apparent than real since the data correspond to the superposition of a series of data

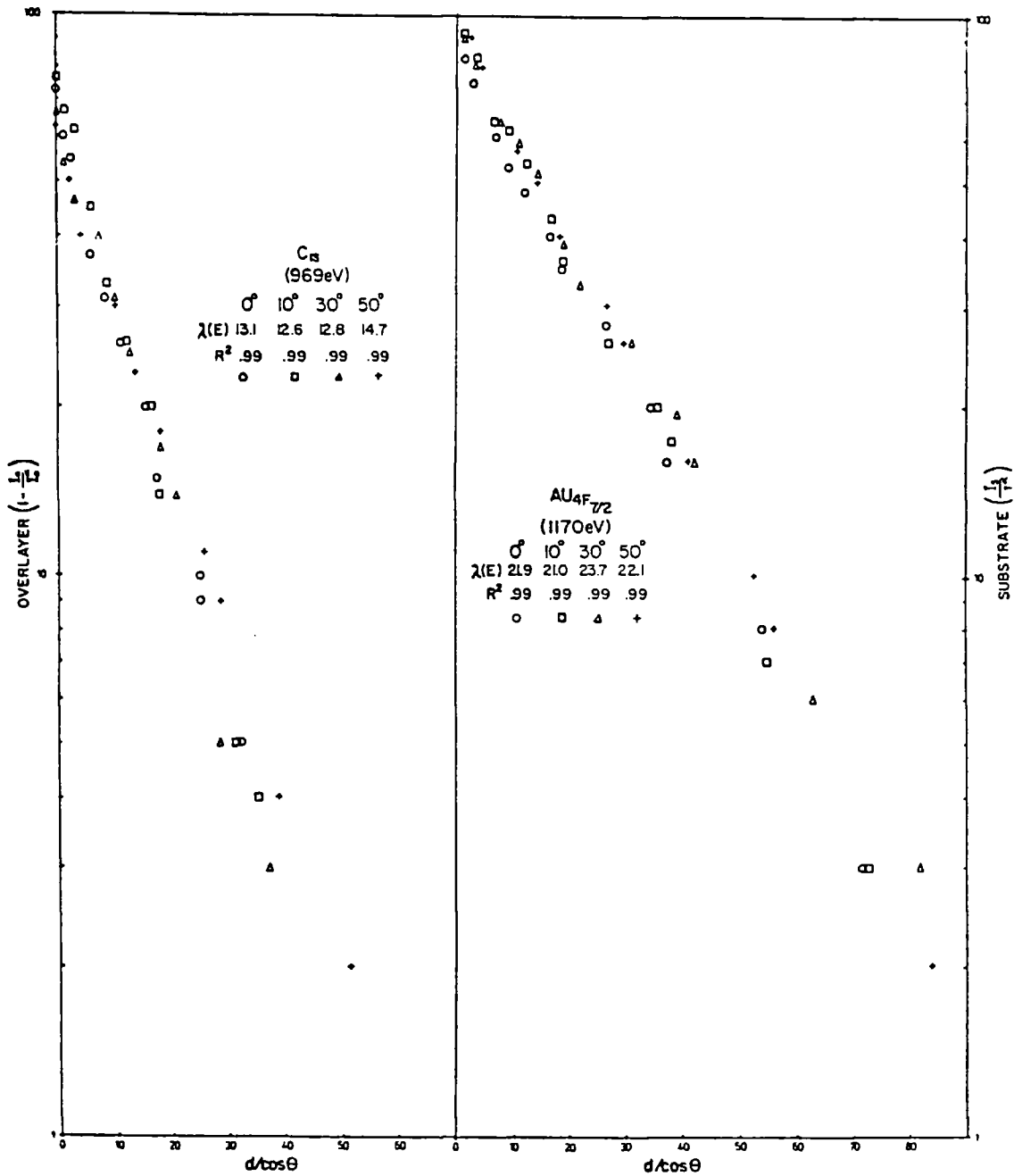


FIGURE 4.8

$\ln(1 - \frac{I}{I_0})$ for the overlayer and $\ln(\frac{I}{I_0})$ for the substrate versus $d/\cos\theta$, for a series of thicknesses of poly paraxylylene on a gold substrate studied as a function of θ , 0° , 10° , 30° , and 50° with a $MgK\alpha_{1,2}$ X-ray source (Note the ordinate has been arbitrarily normalized to a ratio of 100 where $\frac{I}{I_0}$ equals 1)

points describing straight lines with slightly differing origins, i.e. no attempt has been made to adjust intensity ratios to a common origin for a given core level as a function of take-off angle. The important point is, of course, that the mean free paths are determined by the slopes of the least squares defined straight line correlations. In this connection, it might also be noted that some of the initial points on these correlations undoubtedly refer to less than a monolayer coverage of the substrate. As such 'islanding' effects may be significant (i.e. insufficient polymer mass has been deposited to provide uniform coverage). Since, however, such data points are close to the intercept they play a relatively minor role in determining the slope. If, in fact, these initial points (for substrate and overlayer) are plotted on a greatly expanded scale (e.g. in the 0-10 \AA range) it is clear that the projected slopes would correspond to the type of behavior projected from Equation 4.5 and 4.6, and provide exaggerated estimates of the relevant mean free paths. Although a discussion on the absolute magnitudes of the measured mean free paths will appear later on, at this stage note that the values agree well with those previously published by Steinhardt¹³ and are also eminently reasonable in terms of the relative magnitudes as a function of kinetic energy (viz. λ_{1170} eV λ_{969} eV).

To gain further information, angular dependent studies have also been carried out on deposited paraxylylene films using the higher energy monochromatized AlK $\alpha_{1,2}$ photon source ($h\nu = 1486.6$ eV) for which the corresponding kinetic energies for electrons photoemitted from Au $4f_{7/2}$ and C $1s$ levels are ~ 1403 eV and ~ 1202 eV, respectively. The results are displayed in Fig. 4.9. The statistical correlation is again extremely good (R^2 0.98-0.99), however, the distribution of values obtained for the mean free paths (comparing one angle with another) is somewhat greater than for the data obtained with the MgK $\alpha_{1,2}$ photon source. This is partially attributable to the poorer signal/noise ratios both at large (for the substrate core levels) and small (for the overlayer core levels) thicknesses arising from the relatively low flux available with the X-ray monochromator. It is interesting to note, however, that studies of the secondary electron distributions and of the shift in core levels as a function of applied bias voltage, reveals that in all cases sufficient charge carriers are available for the polymer films to be in electrical contact with the spectrometer (i.e. no sample charging was evident for any of these systems, cf. Chapter 6.

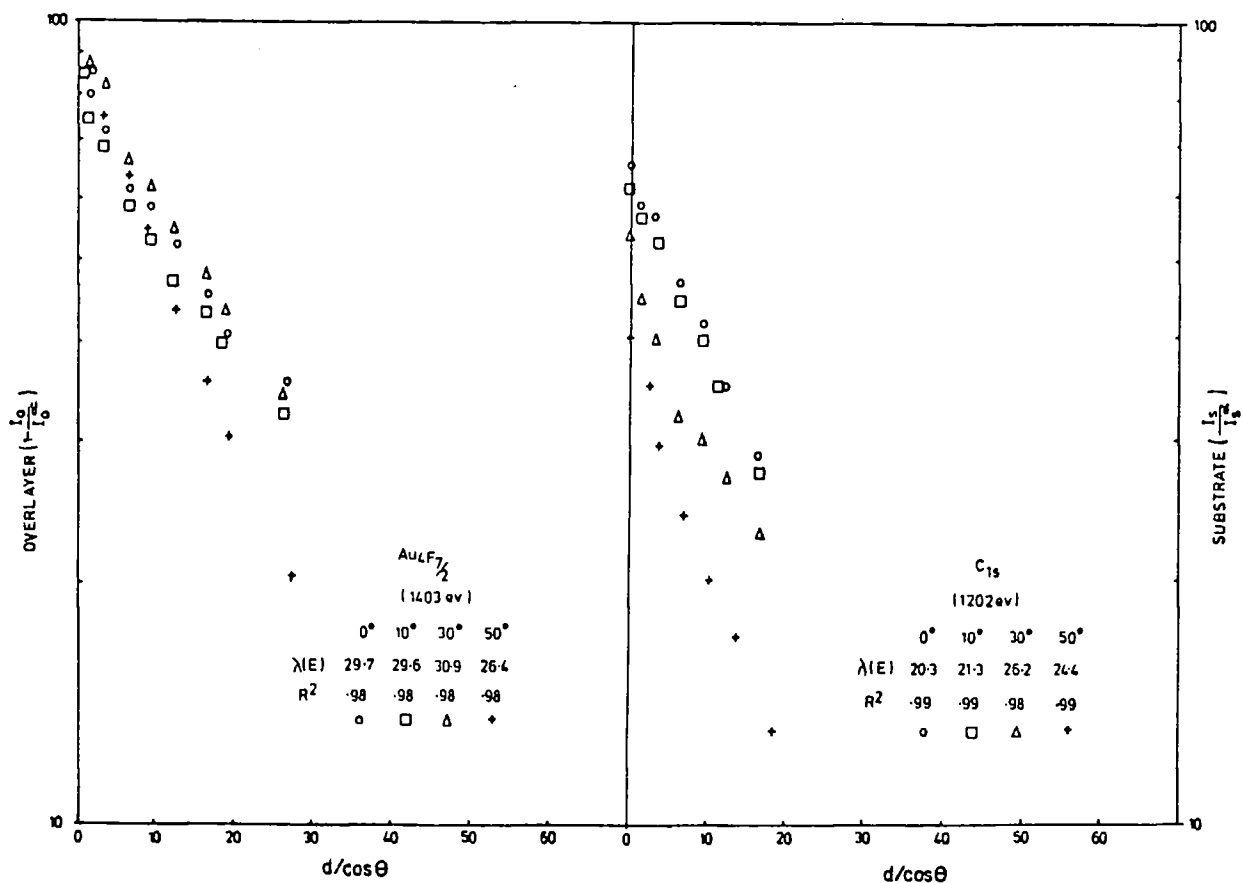


FIGURE 4.9

$\ln\left(1 - \frac{I_o}{I_o^\infty}\right)$ for the overlayer and $\ln\left(\frac{I_s}{I_s^\infty}\right)$ for the substrate versus $d/\cos\theta$, for a series of thicknesses of poly paraxylylene on a gold substrate studied as a function of θ ; 0° , 10° , 30° and 50° with an $AlK_{\alpha 1,2}$ monochromatized X-ray source. (Note the ordinate has been arbitrarily normalized to a ratio of 100 where $\frac{I}{I_o}$ equals 1)

This is not entirely unexpected on the basis of our previously reported studies of thin films of low molecular weight organic monomers generated by controlled deposition from the vapor onto a cryogenic tip¹. A striking feature evident from the data is the excellent overall agreement for the measured mean free paths for electrons of similar kinetic energy obtained by studying the C_{1s} levels of the polymer films using

AlK $\alpha_{1,2}$ radiation and the Au $_{4f_{7/2}}$ levels of the substrate using MgK $\alpha_{1,2}$ radiation, the respective kinetic energies being 1202 eV and 1170 eV (e.g. average of data from Figures 4.8 and 4.9, 23.1 \AA and 22.2 \AA , respectively). The internal consistency is also shown by the mean free paths following the expected trend as a function of kinetic energy^{103, 195-197}. It is difficult to estimate errors for the measurements reported here and the mean free paths quoted are merely to the accuracy of the least squares analysis. A more realistic error limit would seem to be of the order of $\pm 15\%$. The spread in values generated by least squares analysis of data pertaining to different take off angles is certainly well within such limits. The average values for the electron mean free paths as a function of kinetic energy for poly paraxylylene within these error limits are 13 $\pm 2\text{\AA}$, 22 $\pm 3\text{\AA}$, 23 $\pm e\text{\AA}$, and 29 $\pm 4\text{\AA}$ for electrons of kinetic energy 969 eV, 1170 eV, 1202 eV and 1403 eV, respectively. It is interesting to compare these values with those for gold at comparable kinetic energies since the theoretical model recently discussed by Penn¹⁰³ suggests a close similarity between carbon and gold. At 940 eV and 1403 eV for example, the quoted values from the most complete study on gold are 19 $\pm 6\text{\AA}$ and 26 $\pm 3\text{\AA}$, respectively¹⁸⁷.

The theoretical calculations discussed by Penn¹⁰³ suggest mean free paths of $\sim 13\text{\AA}$ and $\sim 17\text{\AA}$ for both carbon and gold at kinetic energies of ~ 950 eV and 1400 eV, respectively. The experimental results for both the polymers and for gold suggest a greater increase in mean free paths as a function of kinetic energy than is evident from the theory. However, considering the overall approximations and difficulties involved in both theory and experiment, the agreement is entirely reasonable. It is interesting to note that Cadman and co-workers¹⁹³ lay considerable emphasis on the validity of their derived value of 44 \AA for the mean free path for ~ 1000 eV electrons in graphite by comparison with the available data for silicon at similar energy (1178 eV) (39 \AA)¹⁸⁰. In this connection, however, it is noteworthy that a recent careful investigation, including angular dependent studies of the mean free path of electrons in silicon by Hill and co-workers¹⁵⁷, suggests a considerably shorter mean free path than that obtained in previous work¹⁸⁰. Thus, for electrons of kinetic energy 1386 eV, a mean free path of 27 $\pm 6\text{\AA}$ is quoted¹⁵⁷ which compares extremely well with that obtained for poly paraxylylene in this work, 29 $\pm 4\text{\AA}$ for 1403 eV electrons. Indeed, the theoretical models^{197, 103} suggest that mean free paths in silicon should, if anything, be

somewhat longer than in carbon. If we consider the range of values, which arise within the likely error limits, for the ratio of mean free paths for silicon and for poly paraxylylene for electrons of ~ 1400 eV, using the experimental data reported in this work and that given by Hill and co-workers¹⁵⁷, these range from λ_{Si}/λ_c 1.3-0.64. The theoretical ratio¹⁰³ by comparison is 1.45, whilst the corresponding ratios elaborated with the most recent value for silicon and an extrapolation of Cadman's¹⁹³ value of 44\AA to a kinetic energy of ~ 1400 eV and assuming a likely error limit of $\pm 15\%$ is 0.73-0.34. Whilst the experimental data presented here could, therefore, be compatible with theory the error limits being such that they encompass the possibility of a longer mean free path in silicon than carbon, the mean free path for carbon derived by Cadman and co-workers¹⁹³ is entirely inconsistent with theory. This strongly supports our previous contention that the analysis of data, presented by Cadman and co-workers is in error and our own re-analysis gives a value of 17\AA for 1000 eV electrons which corresponds quite closely to that reported here for poly paraxylylene.

Since, as we have already pointed out, both theory and experiment tend to suggest that electron mean free paths as a function of kinetic energy are subtly dependent on the material, another surprising conclusion reached by Cadman and co-workers was that their method of estimating mean free paths suggested that the structure of organic films results in mean free paths at a given kinetic energy which can differ by $>100\%$ (cf. quoted values for 1000 eV electrons of 44\AA for graphite and 100\AA for polyethylene, although as we have pointed out, our own analysis of the data presented in reference 193 suggests a mean free path of 17\AA for graphite). The inconsistency of this assertion is evident from a comparison of the data on graphite obtained by Steinhardt and co-workers¹⁸⁵ and that reported here for poly paraxylylene, which are in good agreement, suggest little structural variation on electron mean free paths in materials of a given class. To investigate this point, however, we have studied in some detail electron mean free paths in the chloro- and bromo-substituted poly paraxylylenes.

Considering firstly the polychloro paraxylylene system, the angular dependent data are displayed in Fig. 4.10 where the data refer to the $\text{MgK}_{\alpha 1,2}$ photon source. With the exceptions of the data pertaining to 0° and 10° take off angles for the polymer overlayers, the statistical correlations are extremely good R^2 0.98-0.99. Even for

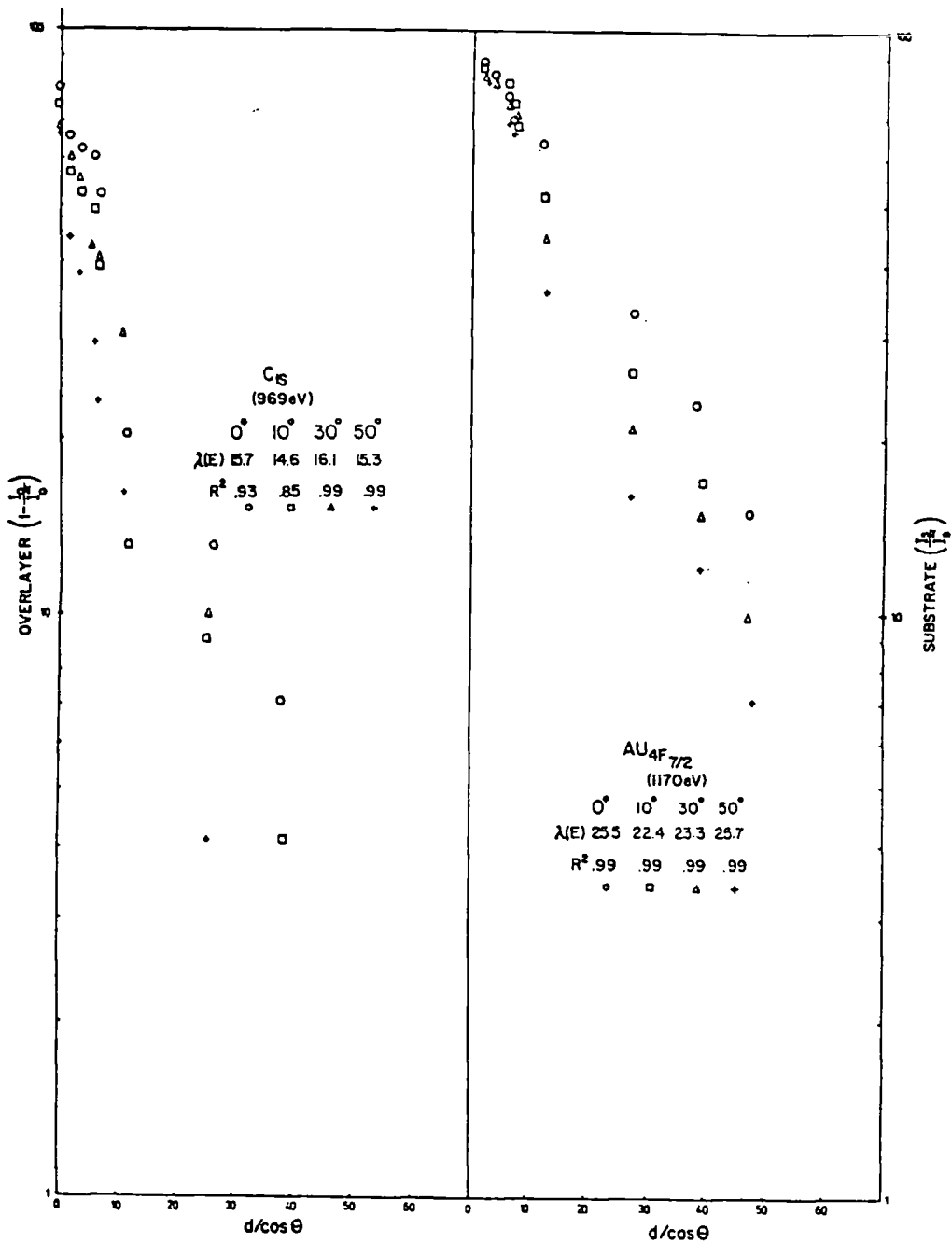


FIGURE 4.10

$\ln\left(\frac{I}{I_0}\right)$ for the overlayer and $\ln\left(\frac{I}{I_0}\right)$ for the substrate, versus $d/\cos\theta$,
 for a series of thicknesses of polychloroparaxylylene on a gold
 substrate studied as a function of θ ; 0° , 10° , 30° and 50° with a
 $MgK\alpha_{1,2}$ X-ray source. (Note the ordinate has been arbitrarily
 normalized to a ratio of 100 where $\frac{I}{I_0}$ equals 1)

these two sets of data, however, the correlations are still statistically significant, in that 93% and 85% of the total variability is accounted for in the direct relationship between ordinate and abscissa. In this connection it should be pointed out that the error bounds for the correlations are well within $\pm 3\text{\AA}$ even for the statistically worst correlation (R^2 0.85). The statistically lower values for the 0° and 10° angles arise partially from the relatively low signal intensities for the overlayer for these angles as compared, for example, with the 30° and 50° spectra. A contributing factor in this respect is that the electronic effect of chlorine gives rise to a significant chemical shift in the C_{1s} core levels and compared with poly paraxylylene itself the spectrum is, therefore, somewhat more extended over the energy scale, cf. Chapter 5). The derived average of the mean free paths for electrons of kinetic energy ~ 969 eV and ~ 1170 eV from the data in Fig. 4.10 for polychloro paraxylylene are $15 \pm 3\text{\AA}$ and $24 \pm 4\text{\AA}$, respectively. Within experimental error these are identical to those for the parent polymer system.

The experiments described thus far are extremely time consuming and since the angular dependent studies for both poly paraxylylene and the chloro derivative are internally self-consistent, studies on the corresponding bromo derivative were limited to a fixed angle (10°) investigation. This was partially dictated by logistics since the convolution of sticking coefficient and reaction rate for the bromo paraxylylene obtained by pyrolysis of the bromo paracyclophane meant that the deposition of polymer films under identical conditions to those employed for the unsubstituted and chloro derivatives required a much longer time scale. The preparation and study of the C_{1s} and $Au_{4f_{7/2}}$ spectra for the requisite number of film thicknesses even at fixed angle, therefore, required a large amount of instrument and operator time. The data presented in Fig. 11, for example, required ~ 50 hrs. of dedicated operator and instrument time. The derived mean free paths for electrons of kinetic energy ~ 969 eV and ~ 1170 eV of $16 \pm 3\text{\AA}$ and $22 \pm 4\text{\AA}$ is in excellent agreement with that for the parent and chloro substituted polymers.

iv) Conclusions

The work reported here goes some considerable way towards the clarification of ambiguities regarding the magnitudes of electron mean

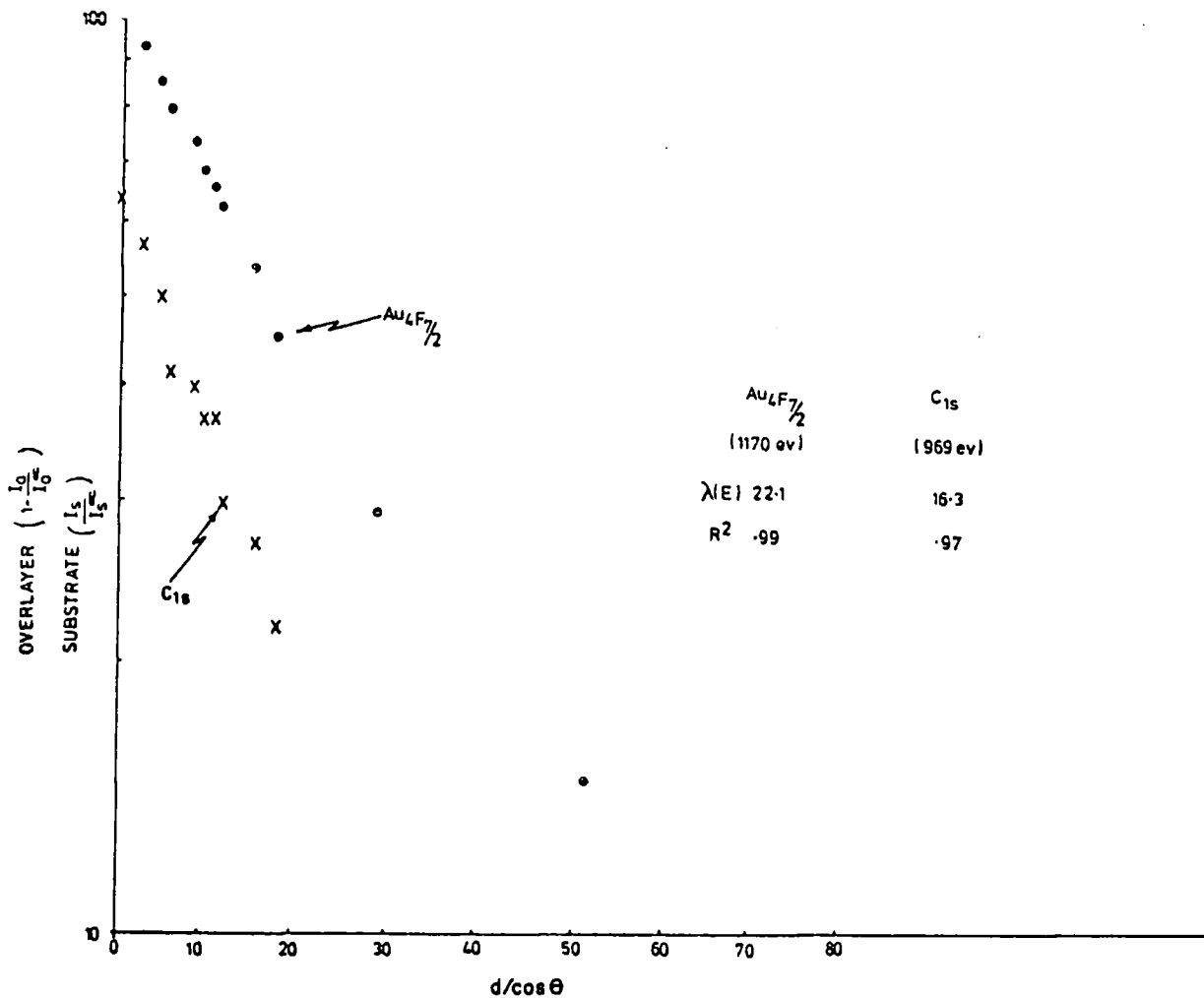


FIGURE 4.11

$\ln(1 - \frac{I_0}{I_0^\infty})$ for the overlayer and $\ln(\frac{I_s}{I_s^\infty})$ for the substrate, versus $d/\cos \theta$,

for a series of thicknesses of polybromoparaxylylene on a gold substrate studied at a constant θ of 10° with a $MgK\alpha_{1,2}$ X-ray source. (Note the ordinate has been arbitrarily normalized to a ratio of 100 where $\frac{I_0}{I_0^\infty}$ equals 1)

free paths as a function of kinetic energy in organic materials as compared to typical metals and semi-conductors¹⁹⁵⁻¹⁹⁷. The data also provides a firm basis for the quantitative development of ESCA to organic and polymeric systems in general. Comparison of the data reported here with the available theoretical models^{103, 197} reveals overall satisfactory

agreement and resolves inconsistencies which were previously apparent. The work also demonstrates the importance of detailed angular dependent studies and highlights the difficulties of obtaining estimates of mean free paths from the study of oriented Langmuir-Blodgett films and from measurements of absolute signal intensities.

The fact that the measured mean free paths in the parent poly paraxylylene and corresponding monochloro and bromo substituted derivatives are within experimental error the same illustrates the overall consistency of the data and supports the contention that mean free paths are only subtly dependent on electronic structure for related materials. The average values for mean free paths as a function of kinetic energy for the polymer systems studied are $\sim 14\text{\AA}$, $\sim 22\text{\AA}$, $\sim 23\text{\AA}$ and $\sim 29\text{\AA}$ for kinetic energies of ~ 969 eV, ~ 1170 eV, ~ 1202 eV, and ~ 1403 eV, respectively, and is shown in Fig. 4.12. Comparison with theory¹⁰³ reveals a much stronger dependence on kinetic energy and this is also apparent from the experimental data on typical metals and semiconductors¹⁹⁵⁻¹⁹⁷.

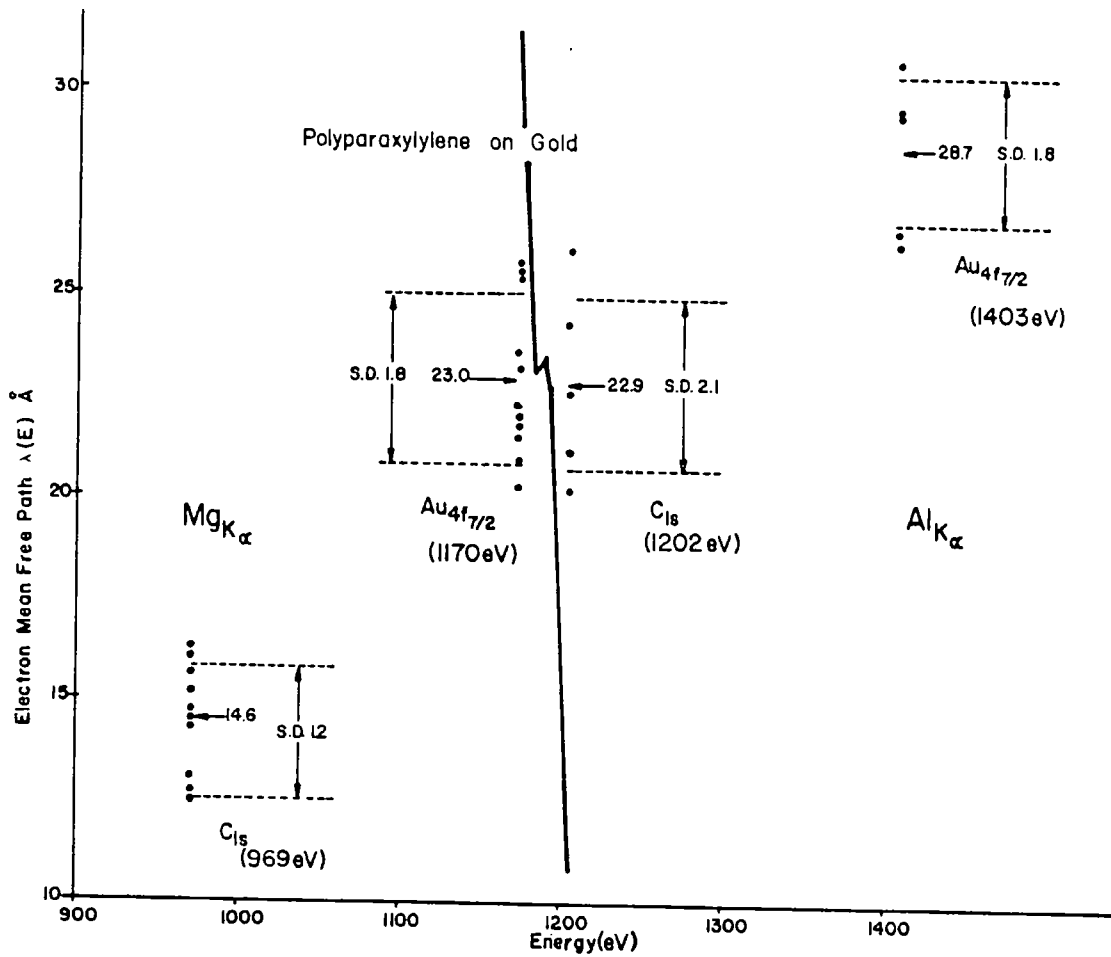


FIGURE 4.12

Electron mean free paths determined from this work

CHAPTER 5

An ESCA Investigation of a Series of [2.2]
Paracyclophanes

CHAPTER 5

An ESCA Investigation of a Series of [2.2] Paracyclophanesi) Introduction

The pyrolysis of p-xylene by Szwarc²¹² at the University of Manchester in 1947 led to a tremendous amount of research over the past thirty years involving reaction by-products of the pyrolysis, polymers from the reaction products and polymers from variations and improvements of Szwarc's method. The reaction conditions of this pyrolysis, being in the temperature range of 800 - 1000°C under a pressure of 2 - 15 mm Hg afforded many pyrolysis products, of which "di-p-xylylene" (tricyclo [8:2:2:2^{4:7}] hexadeca - 4:6:10:12(1):13:15 hexane) was isolated in small quantity²¹². Brown and Farthing's²¹³ extraction of the polymer (prepared by Gill and Ford of Imperial Chemical Industries, Ltd., using the technique described by Szwarc) with chloroform in a Soxhlet apparatus, gave a mixture of many low molecular weight components. The extract contained small amounts of a compound, that when recrystallized from glacial acetic acid had a m.p. of 285°C. Analysis by X-ray intensities from about 300 planes indicated the structure to be that represented in Fig. 5.1 below (for simplicity the hydrogens have been omitted):

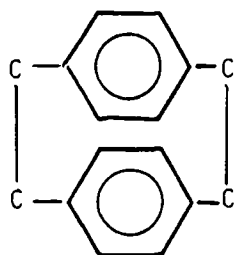
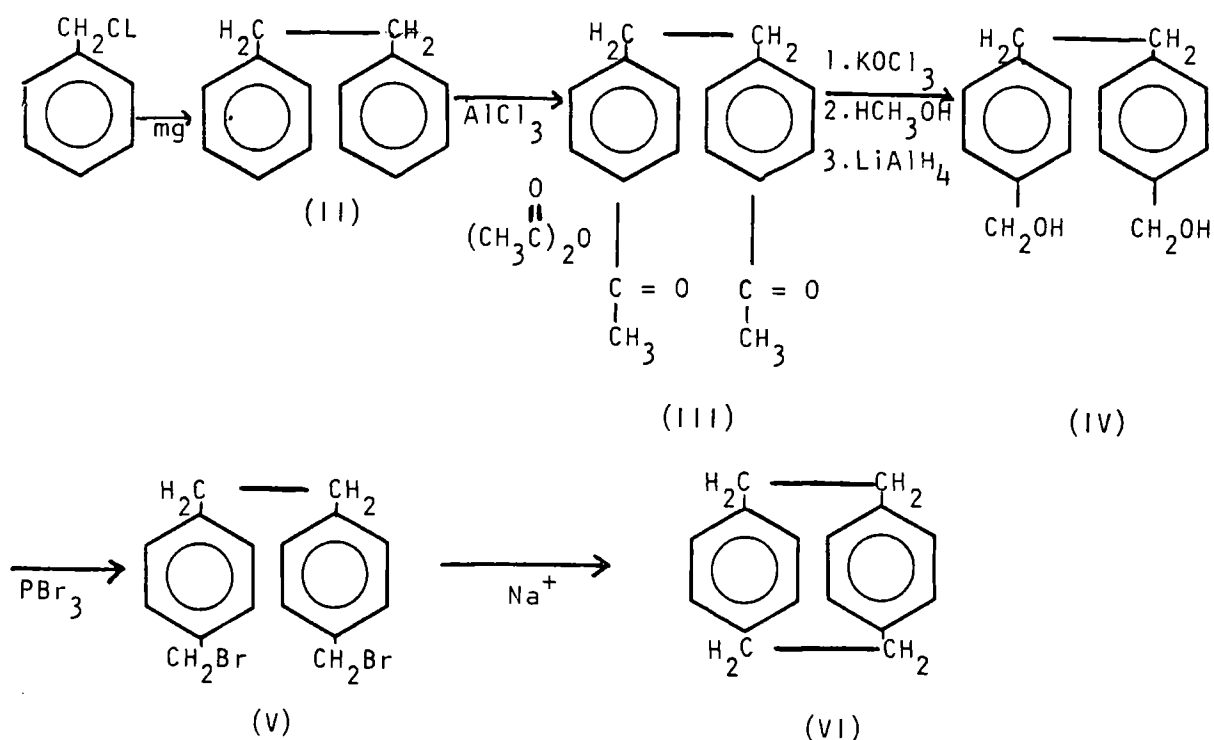


FIGURE 5.1

General structure for [2.2] paracyclophane

The atomic configuration of the molecule proved to be quite interesting in that the two substituted carbon atoms on the benzene ring were displaced from the plane of the remaining four carbons by 0.13Å.

This displacement was attributed to a relieving of the strain in the system. Brown and Farthing's attempts to prepare the "di-p-xylylene" were unsuccessful, however, in 1951, Cram and Steinberg²⁰⁸ successfully synthesized the "di-p-xylylene" and suggested the name of "paracyclophane" (PCP) for the class of compounds. The [2.2] paracyclophane" (the [2.2] refers to the number of carbon bridges joining the para positions of the benzene ring) was prepared by an intermolecular Wurtz reaction with a dibromide, with the reduction and linear polymerization of the bromides occurring as side reactions. Thus (II) was prepared by the action of magnesium on benzyl chloride after which the hydrocarbons were acetylated with $(\text{CH}_3\overset{\text{O}}{\parallel}\text{C})_2\text{O}$ give (III) which in turn was oxidized with KOC1_3 ; the acidic product was esterfied with CH_3OH and the ester was reduced with lithium aluminum hydride to give the alcohol (IV). Reaction of this carbinol with phosphorus tribromide gave the resultant dibromide (V). The dibromide was then added to sodium to give the [2.2] paracyclophane (VI).



Cram and Steinberg characterized the [2.2] paracyclophane by ultra-violet and infrared absorption spectra and compared it with the open chain analog and found evidence for considerable electronic perturbation associated with the fused ring system. This they attributed to the fact that the proximity of the two benzene rings in space was

well within their van der Waals radii, giving rise to an inter-benzoid overlap of the π -orbitals, that are pushed out perpendicularly from the benzene rings. This explanation is substantiated by the X-ray diffraction studies of Brown and Farthing²¹³ mentioned earlier, Fig. 5.2:

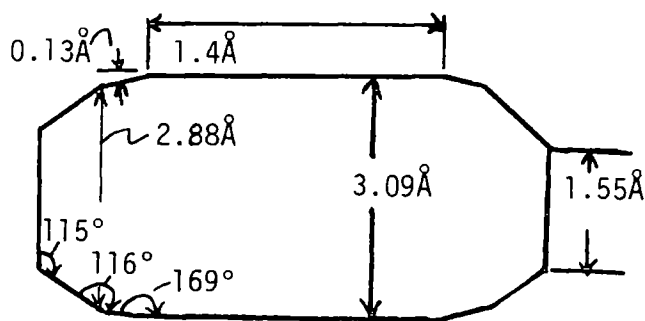


FIGURE 5.2

Interatomic distances and bond angles for carbons in [2.2] paracyclophane

The repulsion of the two benzene rings increases the bond angle between the bridges and the ring from 109° to 115°, thus giving rise to 6° of strain. The other bonds equally share in distribution of the strain which illustrates the principle that in a strained system the distribution of strain between several bonds is energetically favored over the strain in only one bond angle.

Later studies by Lonsdale, Milledge and Rao²¹⁴ reported results which were quite different from Brown and Farthing²¹³. Lonsdale, et al, reported aliphatic C-C bonds of considerably longer length than any known C-C bond and reported variations in length with temperature changes from room temperature to 93°K. They concluded from their study that there existed internal vibrations of large amplitudes in the molecule and described them as "concertina-like motion of the rings toward and away from one another, accompanied by a twisting motion of each benzene ring about its normal, out of parallelism with its opposite member". With

the results reported by Lonsdale, et al, Trueblood²¹⁵ re-examined the structure of the [2.2] paracyclophane. Tale 5.1 compares the different determinations of Brown²¹³, Lonsdale²¹⁴ and Trueblood²¹⁵. Differences in the data of all three investigations is not easily explained and it is clear that better data needs to be obtained in order to determine the exact structure of the [2.2] paracyclophane.

Distances and Angles in [2.2] Paracyclophane
Comparison of Different Determinations and Refinements

<u>Distance or Angle**</u>	<u>Brown</u>	<u>L.S. on Brown's Data</u>	<u>Lonsdale et al.*</u>	<u>L.S. on Trueblood's Diffractometer Data</u>
C(1)-C(1')	1.548 Å	1.563 Å	1.627 Å	1.569 Å
C(1)-C(2)	1.540	1.493	1.546	1.522
C(2)-C(3)	1.390	1.408	1.378	1.384
C(3)-C(3')	1.400	1.343 (sic)	1.421	1.400
C(1)-H(1)	---	0.97	1.12	1.13
C(3)-H(3)	---	0.91	1.03	1.02
C(2)...C(2')	2.83	2.76	2.75	2.786
C(3)...C(3'')	3.09	3.10	3.08	3.10
C(1')-C(1)-C(2)	114.6°		111.2°	113.6°
C(1)-C(2)-C(3)	119.9		119.9	120.6
C(3)-C(2)-C(3a)	118.6		119.7	117.6
C(2)-C(3)-C(3')	120.2		119.1	120.4
	10 1/2°		14°	12.7°
	14		7	10.9

The numbering of the atoms is shown below

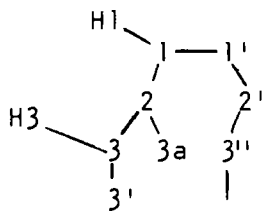


TABLE 5.1

There is a considerable amount of data available concerning the spectra of the [2.2] paracyclophane and a brief presentation of the major characterization methods is presented.

The UV spectrum of the [2.2] paracyclophane revealed several distinct differences compared with prototype benzoid systems and these were discussed by L. L. Ingraham²¹⁶. The most striking feature is the band which occurs at 2600Å for the parent benzene system. The large bending vibrations caused by the more flexible strained system results in stronger interaction between the electronic and vibrational states and tends to "smear out" the fine structure.

Later, Cram and Heigson²¹⁷⁻²¹⁸ substantiated empirically the theoretical treatment of Ingraham by the following conclusion; that the abnormal spectrum was due to transannular electronic effects and the nonplanarity of the rings.

The electronic spectrum studied on single crystals of [2.2] paracyclophane by Ron and Schnepf²¹⁹ utilizing polarized absorption and fluorescence spectra indicated a broad band in the fluorescence spectrum with a maximum at 3500Å. Transannular interactions and ring bending accounted for the position of the band due to the ring separation of only 3Å in the ground state. Later work by Ron and Schnepf²²⁰ indicated that the absorption spectrum allowed, originated in transitions to two different electronic states, being the out-of-phase combinations of the $B_{2\mu}$ and $B_{1\mu}$ benzene states.

The phosphorescence spectrum of the [2.2] paracyclophane was taken by ElSayed²²¹ and was found to be broad (4100 to 5600Å) with a maximum at 4700Å. The lifetime of the blue phosphorescence was 3.3 seconds. Work by Valta²¹², et al, further substantiated the role of intermolecular electronic interactions in this respect.

The proton magnetic resonance (N.M.R.) spectra by Wilson²²³, et al, and J. S. Waugh and R. W. Fessenden²²⁴ consisted of two sharp peaks of equal intensity at 6.96 and 3.70 σ and indicated that both kinds of protons are in regions where the diamagnetic effects are small except for the effect of its own ring. The large chemical shift was reported due to the strain in the system.

The potential energy and thermodynamic functions of the [2.2] paracyclophane have been investigated by Boyd²²⁵ and J. T. S. Andrews²²⁶, et al, and values for the heat capacity measured between 10 and 350°C by adiabatic calorimetry gave a value of 60.31 at 298°K²²⁶. The shape of the curve is normal except near 50°K where a rounded maxima occurs which was postulated by Andrews to be "a weakly cooperative disordering phenomenon". Andrews suggested that NMR and IR in this region

might help explain the maxima. Entropy, enthalpy and Gibbs free energy functions were found to be 63.50, 30.74 and -32.76 cal/mole degrees, respectively at 298°K.

Boyd²²⁷ found the heat of combustion and vapor pressure curve for the [2.2] paracyclophane and used these values to determine the heats of combustion and formation in both the solid and gas. A summary of the thermochemical data at 298°K is shown in Table 5.2.

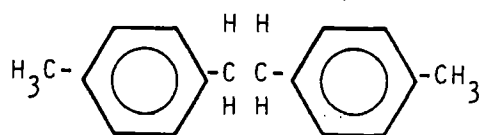
Thermochemical Data

	ΔH_c (kcal mole ⁻¹)	ΔH_v (kcal mole ⁻¹)	ΔH_f° (kcal mole ⁻¹)
solid	-2088.2 [±] 0.9	22.2 [±] 0.2	36.9 [±] 0.9
gas	-2111.2 [±] 1.9	23.0 [±] 1.0	59.9 [±] 1.9

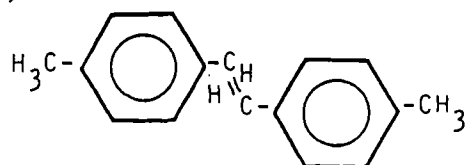
Table 5.2

The [2.2]paracyclophane has been analyzed by VPC and a series of five impurities were identified in trace amounts.

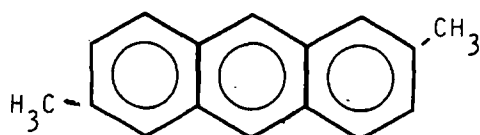
- 1) 1,2-Di-p-tolyloethane (linear dimer)



- 2) 4,4'-trans-dimethylstilbene



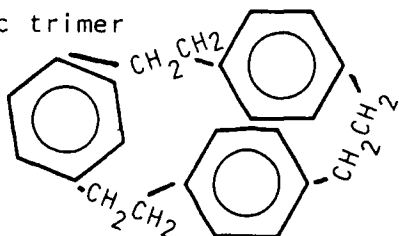
- 3) 2,6-Dimethylantracene



4) Linear trimer



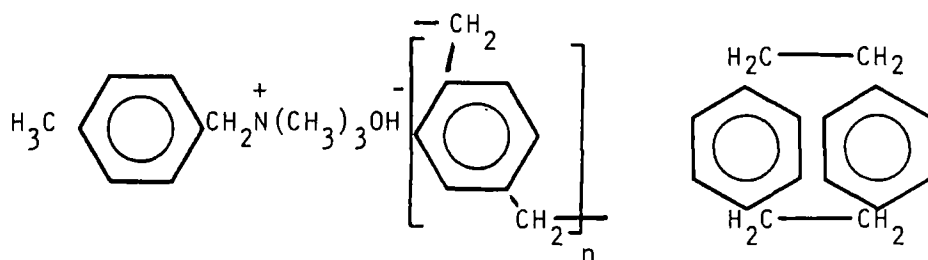
5) Cyclic trimer



The retention time for each compound appears in the order given above with poor resolution on the linear and cyclic trimer. The VPC was run on 1% 20m carbowax on Gas-Chrom D (1 meter columns) at 75°C with programming at 15°C/min. to 225°C. A thermal conductivity detector at 315°C with a helium flow rate of 70 cc/min. was used. Analysis on silicon columns with a flame detector at 2X indicates high purity (99+) after recrystallizing from p-xylene.

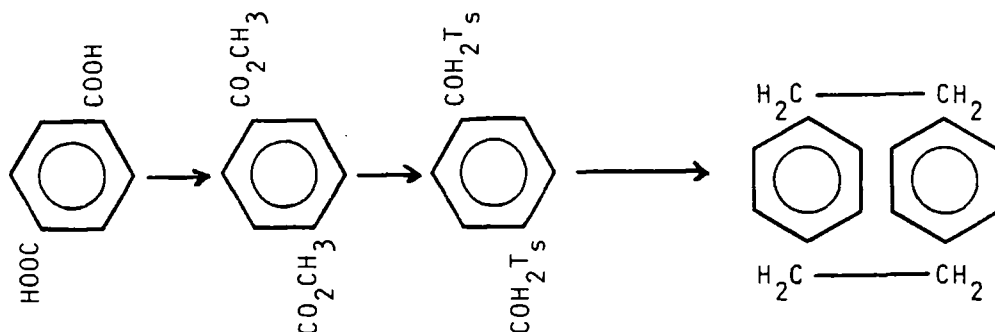
The [2.2] paracyclophane has limited solubility in p-xylene at 135°C of about 10 g/100cc. Its solubility in dichloromethane at 25°C is 1.5%. Cram and Riech²²⁸ found that when [2.2] paracyclophane is heated to about 200°C that the cyclic dimer structure was cleaved to the p,p'-dimethylenebibenzyl diradical. The fate of this diradical species was dependent upon the environment that it was generated in.

After Cram's work on the synthesis of [2.2] paracyclophane, several investigators reported other synthetic routes to the compound. Winberg²²⁹, et al, synthesized the compound by the thermal decomposition of p-methylbenzyltrimethylammonium hydroxide to yield polymer and cyclophane;



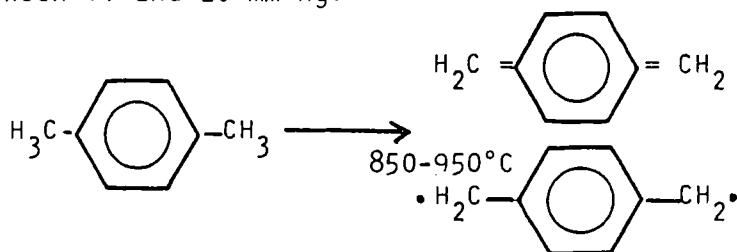
Although the route was not investigated in any detail, it was found that by addition of a free radical polymerization inhibitor, the cyclophane yield was about 17%. Marsh and Young²³⁰ also synthesized the cyclophane by the decomposition of the quaternary halide in hot alkali, this being a simpler route since the halides are commercially available.

Later Brown and Sondheimer²³¹ reported the synthesis of the cyclophane by the Birch reduction of terephthalic acid with sodium in liquid ammonia, which gave the cis-trans mixture of 1,4-dihydroterephthalic acid. Esterification by diazomethane in ether gave the dimethyl ester which when reduced with lithium aluminum hydride gave the diol. Reaction of the diol with p-toluenesulfonyl chloride gave the di-tosylate which was solvated in pyridine to the [2.2] paracyclophane.



Hopf²³² synthesized the cyclophane via a nonaromatic route by the 1,4-cycloaddition to 1,2,4,5-hexatetrane with dimethyl acetylenedicarboxylate. Reduction of the ester with lithium aluminum hydride in THF gave the tetrol and hydrolysis of the -ol with a potassium hydroxide/methanol mixture gave the acid. The tetracarboxylic acid, when cyclized to the anhydride and boiled in glacial acetic acid, decarboxylates to the [2.2] paracyclophane.

The most significant procedure developed, and the one of commercial importance came from Pollart²³³ of Union Carbide. In his process the reactive diradical, p-xylylene is generated by the pyrolysis of para-xylene at high temperatures (850-950°C) and partial pressures of between .1 and 20 mm Hg.



Steam is introduced at atmospheric pressure as a diluent to maintain the partial pressure of p-xylene and also to prevent charring of the p-xylene resulting from overpyrolysis. The diradical vapors are then cooled to between 25 and 150°C and introduced into a fluid medium,

such as p-xylene, where they condense and dimerize to the [2.2] paracyclophane, upon which recrystallization recovers the product.

This procedure is now in commercial use for the production of Parylene N (Union Carbide tradename for [2.2] paracyclophane). Although only 8-10% yields are obtained on each pass, recycling of the mother liquor results in overall yields of better than 60%.²³⁴

Table 5.3 summarizes the data available from the literature sources on [2.2] paracyclophane.

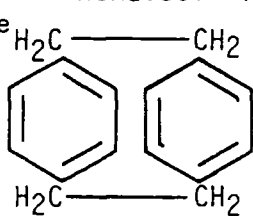
ACS Nomenclature	Tricyclo 8:2:2:2 ^{4:7} hexadeca-4:6:10: 12(1):13:15-hexane
Structure [2.2] Paracyclophane di-p-xylene Union Carbide "Parylene N"	
Melting Point	284°C (decom.)
Density	1.22 gram/cc
Solubilities	p-xylene at 135°C 10 grams/100cc dichloromethane at 25°C 1.5 grams/100cc
Purification Technique	Sublimation (vacuum) Recrystallization: p-xylene glacial acetic acid
UV Spectrum	λ_{max}, μ E 224 25,000 284 250 302 160
IR Spectrum	Strong bands (μ) 13.9, 12.4, 11.3 Medium bands (μ) 10.8, 9.2, 7.1, 6.5, 6.3 Weak bands (μ) 11.8, 8.5, 8.3, 7.4, 5.3, 3.4
H _c	Solid -2088.2 [±] 0.9
H _v	Solid 22.2 [±] 0.2
H _{f0}	Solid 36.9 [±] 0.9
NMR	two peaks, of equal area - 6.96 and 3.70
Typical impurities by VPC analysis	1,2-di-p-tolyethane 4,4'-trans-dimethylstilbene 2,6-dimethylanthracene Linear trimer Cyclic trimer

TABLE 5.3

A series of substituted [2.2] paracyclophanes have also been investigated and include the dichloro, tetrachloro, dimethyldibromo, ethyl, benzyl, acetyl and the linear dimer 1, 2-di-p-tolyethane. Very little information was available on these derivatives in the literature and an ESCA investigation was undertaken in an attempt to define some structure and bonding properties of these substituted [2.2] paracyclophanes.

ii) Experimental

Both the unsubstituted and substituted [2.2] PCP's were obtained from Xerox Corporation, Webster Research Center, Webster, N.Y., U.S.A.* The unsubstituted and substituted dichloro and tetrachloro dimers were commercially available materials from Union Carbide Corp., Bound Brook, N.J., U.S.A., and were recrystallized from p-xylene and glacial acetic acid before use. The remaining substituted dimers were specially prepared according to literature preparations^{207,218,228,233} and were purified by techniques described therein.

The ESCA instrumentation used has been described previously in Chapter 3.

iii) Theoretical

The theoretical models used were based upon the ground state potential model (GPM) within the all-valence electron (CNDO/2 SCF MO formalism, also previously described in detail in Chapter 3. The bond angles and bond lengths used as input to the MO programs were obtained from the crystallographic data where available²¹³⁻²¹⁵, and standard bond angles and lengths were used where it was not.

iv) Results and Discussion

a) Unsubstituted [2.2] PCP

The crystallographic data on the [2.2] PCP is described in the introduction²¹³⁻²¹⁵ and an attempt was made to vary the intermolecular distance between benzene rings using the GPM model to determine whether the carbon 1s core levels B.E.'s would significantly change to be detected by ESCA. The models varied the transannular distance from the crystallographically determined 3.09Å for a minimum value of 2.89Å to a maximum value of 3.29Å by varying the interatomic distance between

*The author is indebted to Dr. C. B. Duke for approval to use these specially prepared [2.2] PCP's for this work.

aliphatic bridging carbons (cf. Fig. 5.2). This increased strain (2.89\AA) and decreased strain (3.29\AA) relative to the experimentally determined 3.09\AA might be expected to effect C_{1s} B.E.'s, and if they are affected, could be potentially identified by ESCA.

The results of the GPM's, along with the C_{1s} core level spectra are shown in Fig. 5.3 and it can be readily seen that the very small

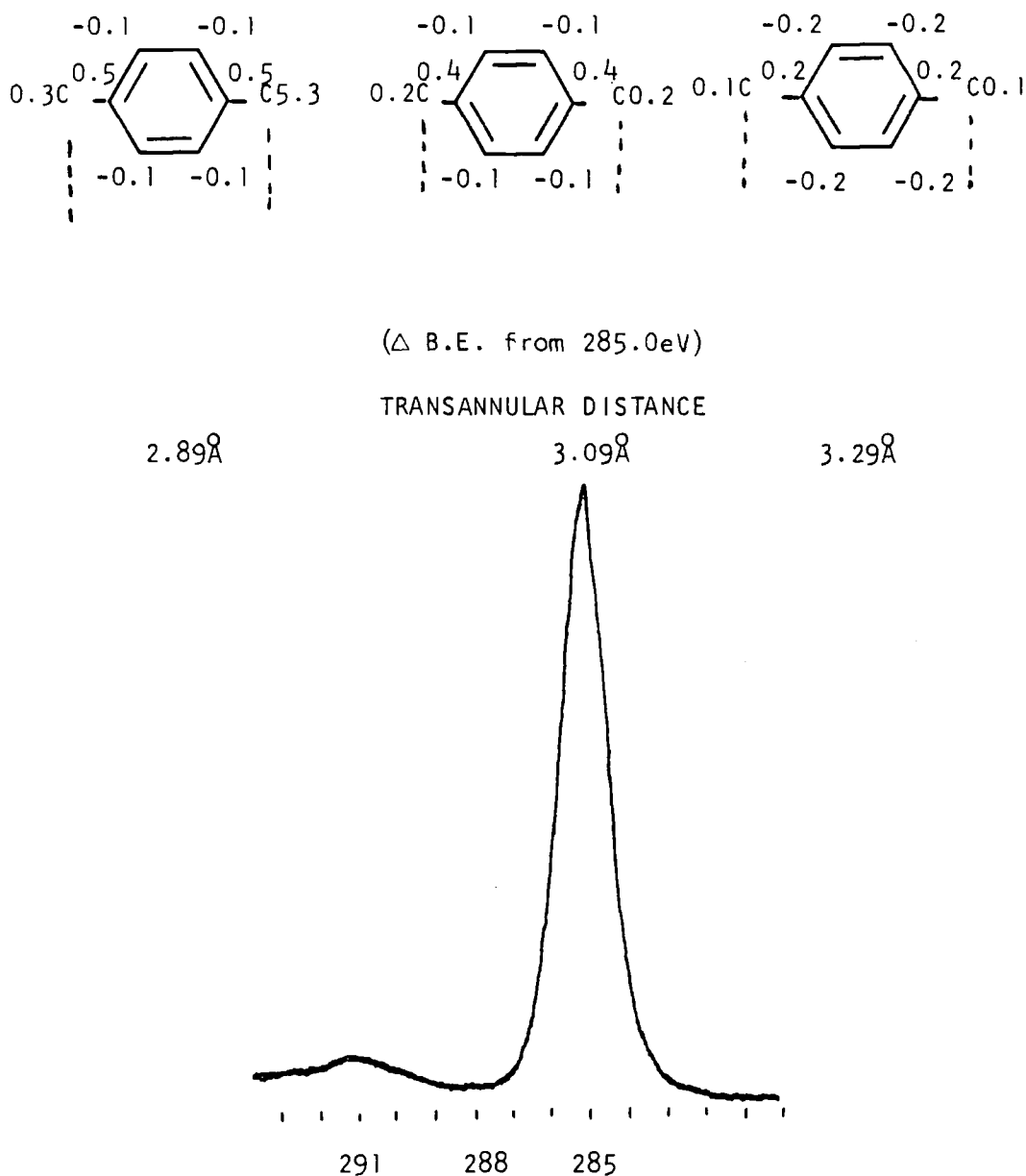


FIGURE 5.3

Effects of variable transannular distances calculated from the GPM compared with experimentally determined C_{1s} core level spectrum for unsubstituted [2.2] paracyclophane

(0.1eV) differences in calculated C_{1s} B. E.'s in going from the 2.89Å to 3.29Å transannular distances cannot be resolved with the present instrumentation. We might, however, expect there to be somewhat larger identifiable differences in the $\pi \rightarrow \pi^*$ relative intensity ratios when compared to the primary photoionization peak and the calculations for determining the shake-up intensities, described elsewhere^{58, 140}, revealed a trend in the total probabilities for the $\pi \rightarrow \pi^*$ transitions in the order as expected, namely 8.08, 7.73 and 7.43% for transannular distances of 2.89Å, 3.09Å and 3.29Å, respectively. This $\pi \rightarrow \pi^*$ transition can be seen in Fig. 5.3 (expanded by a factor of 10) and area ratios measured as accurately as possible indicate an 8.2% $\pi \rightarrow \pi^*$ transition relative to the primary photoionization peak. Previously reported results indicate that trends for shake-up phenomenon in similar compounds can be predicted^{38, 140} using the CNDO/2 model, however, absolute intensities are somewhat determined by the particular parameterization. That the shake-up intensity predicted for the smallest transannular distance of 2.89Å agrees quite well with the CNDO/2 prediction is almost certainly fortuitous. It is, however, gratifying that the values are as close as they are. Concluding this section, it would appear that if there is some deviations from the transannular distance reported in the literature for the unsubstituted [2.2] PCP, it would be very difficult to detect it by the difference in the C_{1s} core level spectrum.

b) Substituted [2.2] PCP's

When considering the theoretical models to predict the C_{1s} core level B.E.'s the substituted compounds can be divided into two distinct classes when considering the di- and tetra-substituted models, and these are depicted in Fig. 5.4, the single and double ring substitution.

Considering firstly the dichloro [2.2] PCP, calculations within the GPM were carried out on the seven possible isomers and the results of the predicted C_{1s} B.E.'s are displayed in Fig. 5.5 along with the synthesized C_{1s} core level spectra predicted by the GPM and the experimentally determined spectrum. It is quite apparent that difficulties would be encountered in distinguishing any of the pseudo-isomers (double ring substitution), however, not only are the single ring isomers distinguishable from each other, they are also distinguishable from the pseudo-isomers. Comparing the experimentally determined spectra with the calculated spectra, it is readily apparent that a number of the isomers can be eliminated based upon lineshape comparison. (The

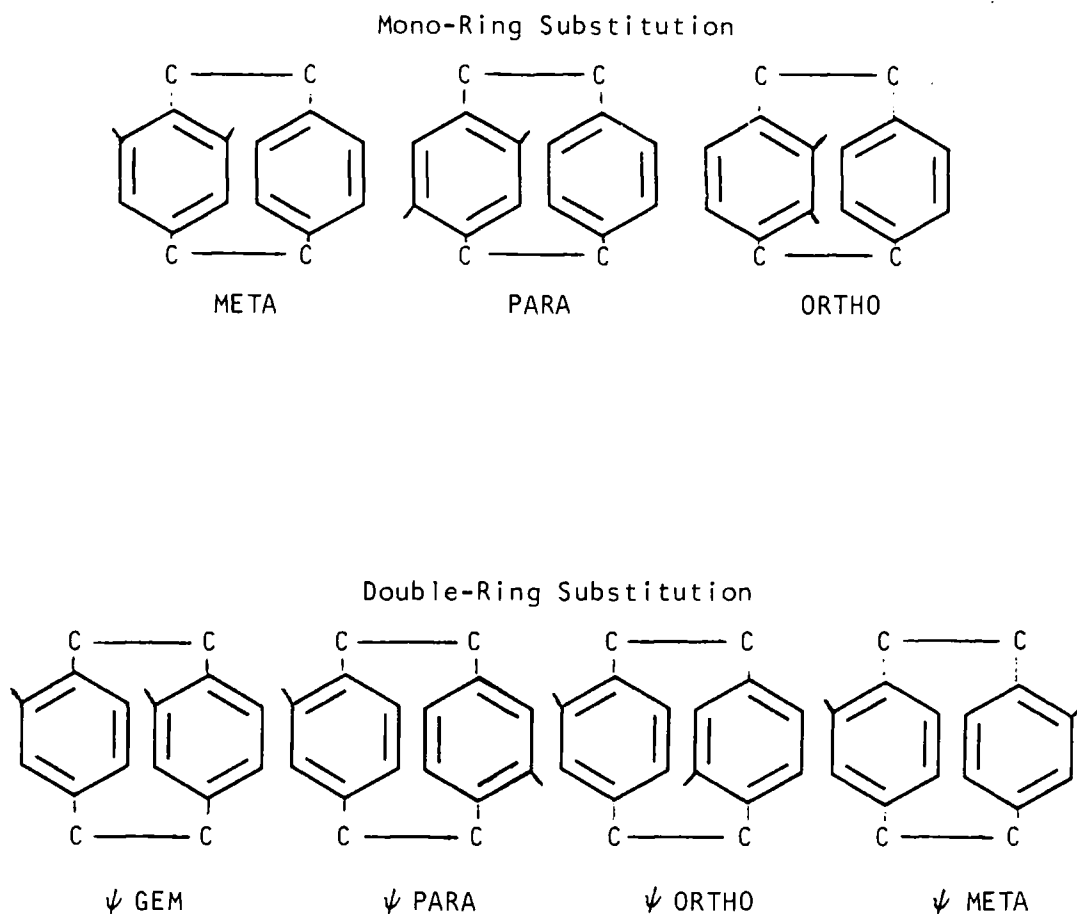


FIGURE 5.4

Isomeric model nomenclature for substituted [2.2] paracyclophane

dotted lines appearing on the synthesized curves reflect the experimental line shape difference to the high B.E. side of the peak). Although poor comparisons are drawn between most of the calculated isomers, when compared with the experimental spectrum a close fit is found for the pseudo-para isomer and an excellent fit for the single ring substituted para isomer. Assuming a linewidth of approximately 1.4 eV for the C_{1s} line (normally found for our instrument) the para isomer fits more closely with the experimental data than the pseudo-para isomers in that the chemical shifts calculated for the pseudo-para isomer would require a linewidth of ~ 1.2 eV to fit the data, which is quite narrow for a powder sample commonly experienced with our instrument. The ESCA data

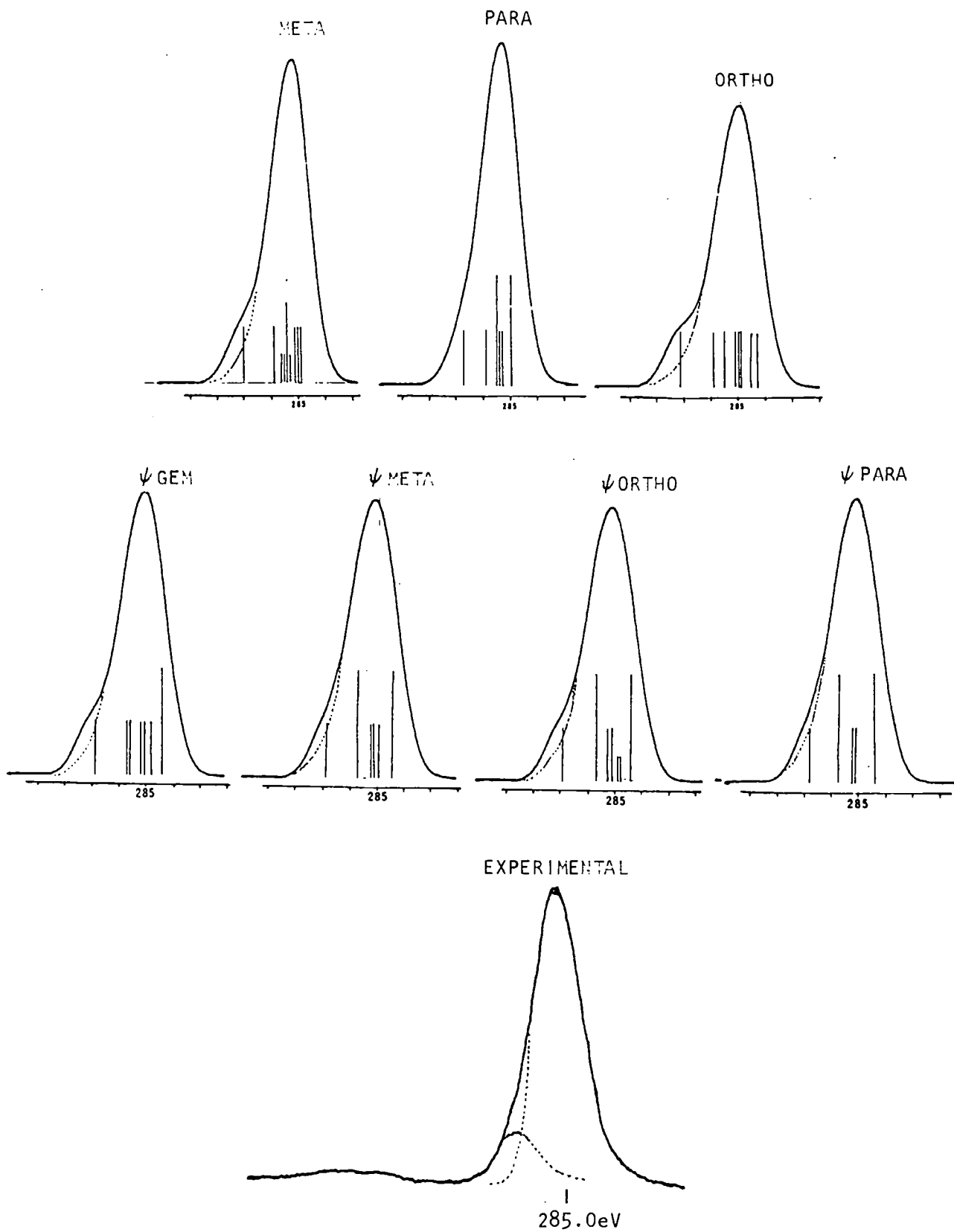


FIGURE 5.5

Theoretical calculations within the GPM, synthesized C_{1s} core level spectrum and experimentally determined C_{1s} core level spectrum for dichloro [2.2] paracyclophane

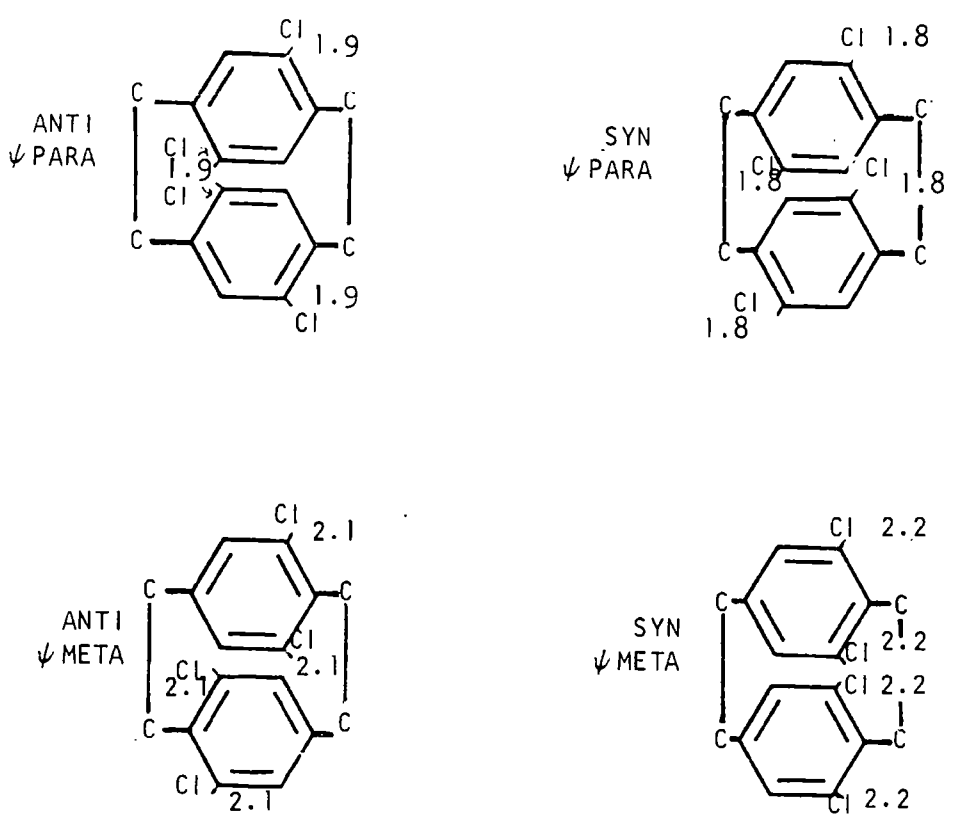
would, therefore, favor the para isomer when compared to the theoretical calculation. The CL_{2p} to C_{1s} intensity ratios confirm a dichloro derivative.

Calculations on the tetrachloro [2.2] PCP reveal a more complicated isomeric possibility in that not only can we have pseudo isomers, but we can have them in anti- and syn-configurations. Because of steric hindrance considerations, it is unlikely to have all four chlorines substitute on the same ring, therefore, calculations were carried out on the double ring substituted derivatives with only one for single ring substitution and these are shown in Fig. 5.6. Without synthesizing calculated spectra, the carbon $_{1s}$ B.E.'s shown on the figure resolve into spectra indicating that the ortho (both anti- and syn-), tri-single and tetra-single substitution are unlikely isomers and that based upon the calculated lineshapes the para and meta isomers for both the anti- and syn- are indistinguishable.

These conclusions appear reasonable based upon the results of the dichloro derivative previously discussed. The CL_{2p} to C_{1s} relative intensity ratio are consistent with a tetra substituted isomer.

The theoretical calculations on the pseudo-isomers for the dimethyl [2.2] PCP reveal very little difference in the C_{1s} B.E.'s for the ortho, meta, para and gem isomers and a representative calculation (for the pseudo-para) along with the experimental spectrum is shown in Fig. 5.7. The $\pi \rightarrow \pi^*$ intensity ratio to the primary peak is consistent with the structure.

The remaining disubstituted derivative, dibromo [2.2] PCP was not evaluated from a theoretical standpoint considering that little difference is expected between the bromo and the chloro derivatives. The experimental spectra for the C_{1s} and Br_{3d} levels are also shown in Fig. 5.7. In comparing the spectra for the unsubstituted, chloro and bromo substituted dimers with the spectra from the experimental work in Chapter 4 on electron mean free paths, it is apparent that ESCA is sampling the repeat unit of the polymer in that identical spectra are observed for both the paracyclophane and the poly-p-xylylenes. To further confirm this evidence the B. E.'s for the model compound for the unsubstituted polymer, 1,2-di-p-tolyethane, were calculated and the results, along with the experimental spectrum, are shown in Fig. 5.8. Excellent agreement is demonstrated between the calculated B. E.'s for the model and the experimental B. E.'s for the 1, 2-di-p-tolyethane and the poly-p-xylylene.



(ALL Δ B.E. from 285.0eV)

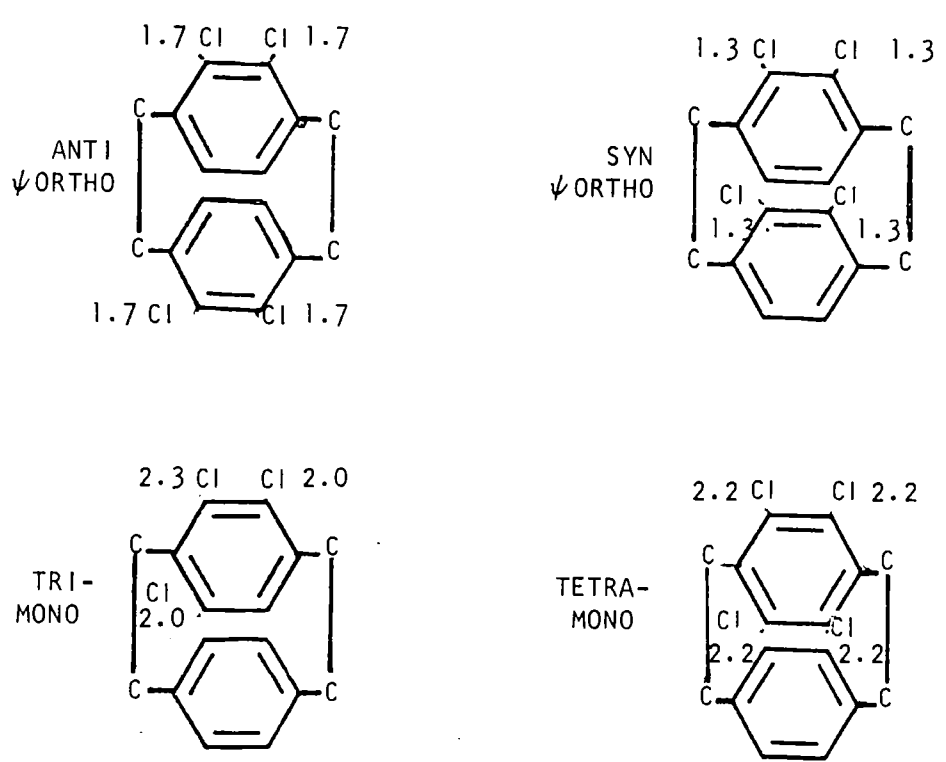
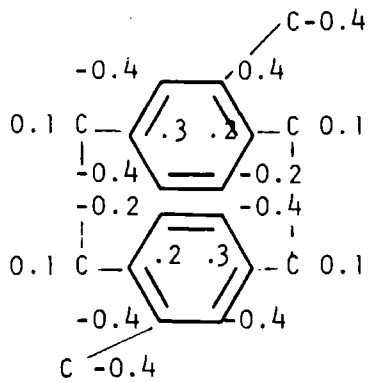


FIGURE 5.6

Theoretically calculated B.E.'s (within the GPM) for a series of tetra-substituted chloro [2.2] paracyclophanes and the experimentally determined C_{1s} core level spectrum



(Δ B.E. from 285.0eV)

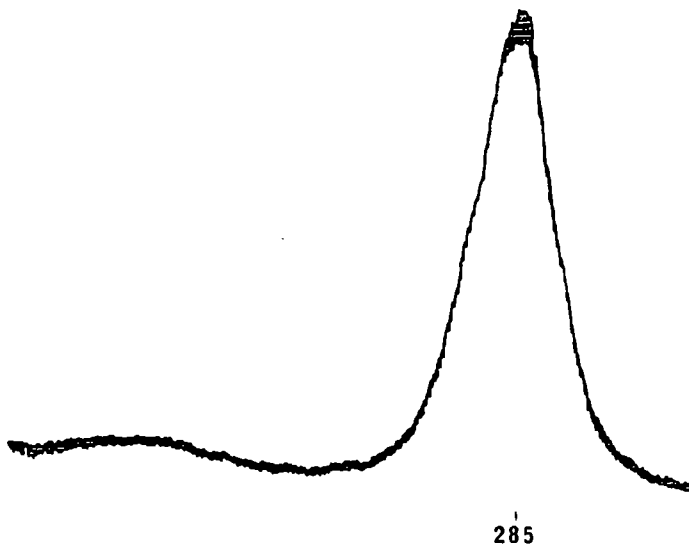
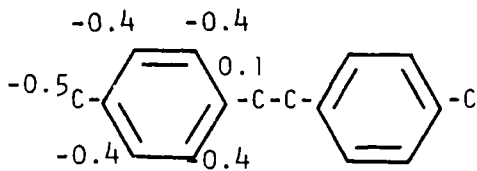


FIGURE 5.7

Theoretically derived B.E.'s (within the GPM) for pseudo-para dimethyl [2.2] paracyclophane and the experimentally determined

C_{1s} core level spectra



(Δ B.E. from 285.0eV)

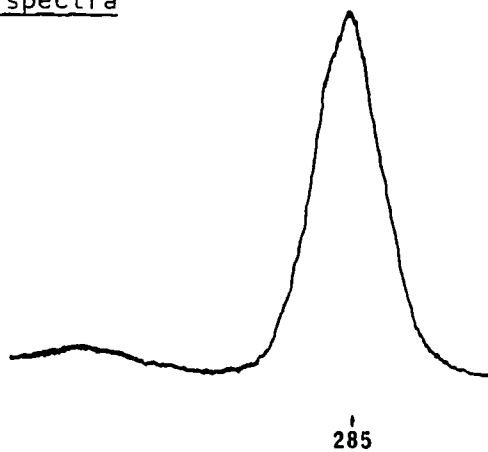


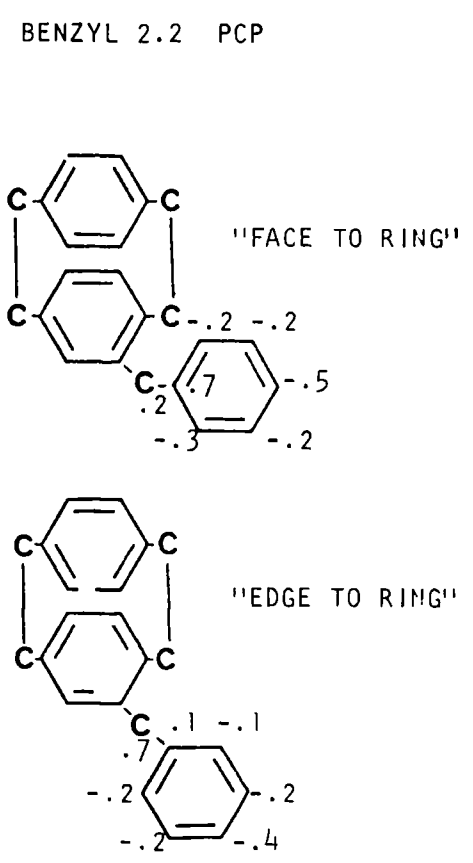
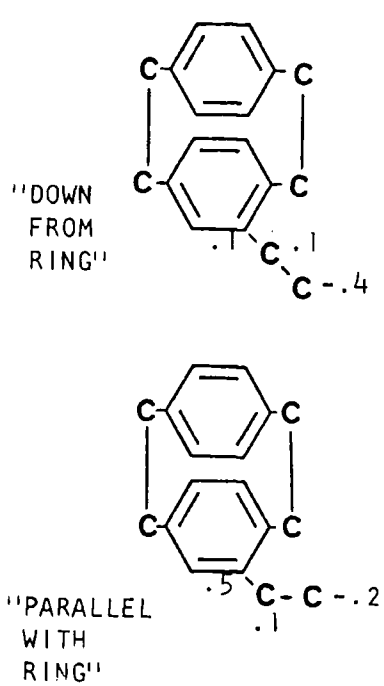
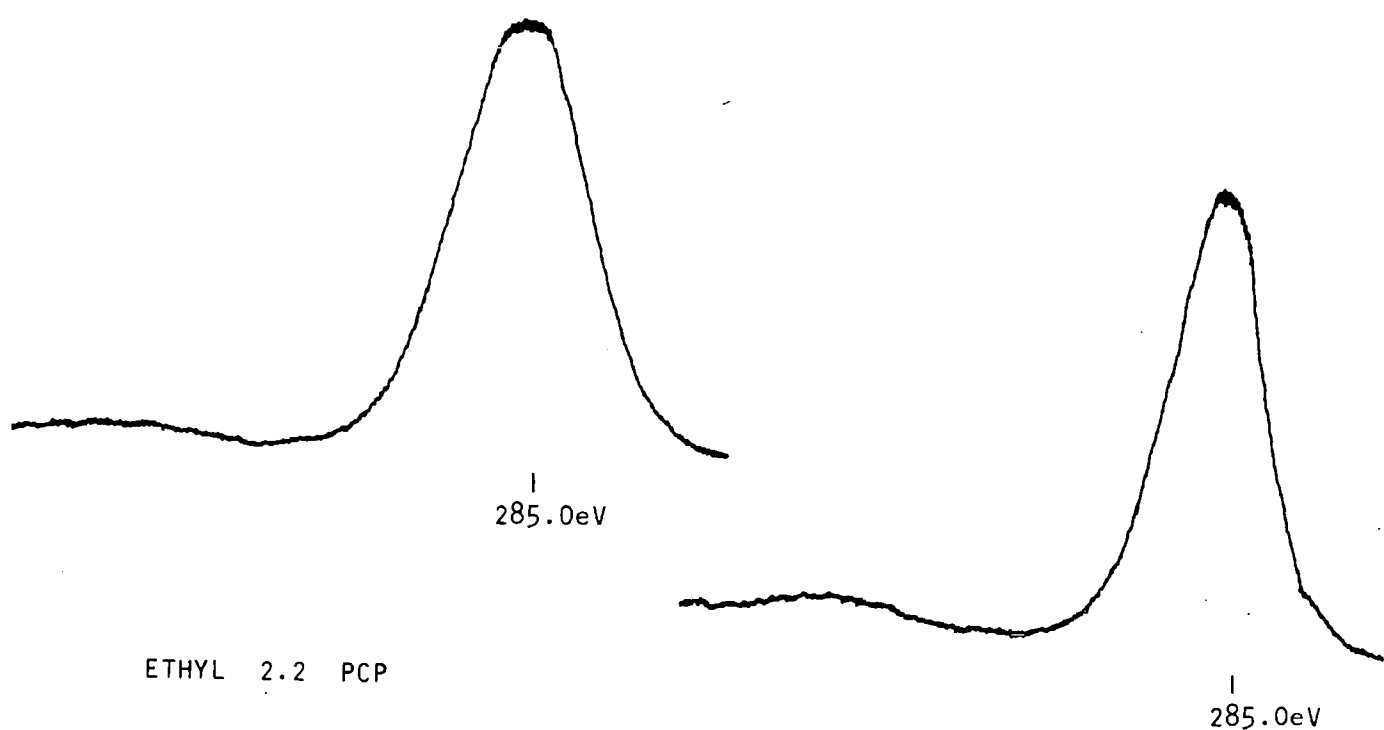
FIGURE 5.8

Theoretically derived B.E.'s (within the GPM) for 1,2-di-p-tolyethane and the experimentally determined C_{1s} core level spectrum

For the remaining mono-substituted derivatives, the theoretical calculations, along with spectra for the ethyl and benzyl derivatives, are shown in Fig. 5.9. Calculations were carried out with the substituents rotated throughout different angles with respect to the paracyclophane benzene rings and for the ethyl and benzyl derivatives, the predicted C_{1s} core level B. E.'s were not changed regardless of the configuration. However, for the acetyl derivative, slight differences were observed when the carbonyl group was rotated to be either in the plane of the benzene ring or perpendicular to it. The results are displayed in Fig. 5.10 and although these differences were calculated and the experimental data best fits the derivative where the carbonyl group is perpendicular to the ring, the differences are so marginal that the configuration determined by ESCA would be questionable.

In conclusion, the study of these isomeric conformations of the substituted [2.2] paracyclophanes has revealed that in some cases (namely the dichloro and acetyl) ESCA, along with the appropriate GPM's can predict the lineshape of particular isomers and with more detailed investigations of shake-up phenomenon in these systems, along with the use of monochromatized X-ray source, one might be able to identify particular isomers in systems such as these.

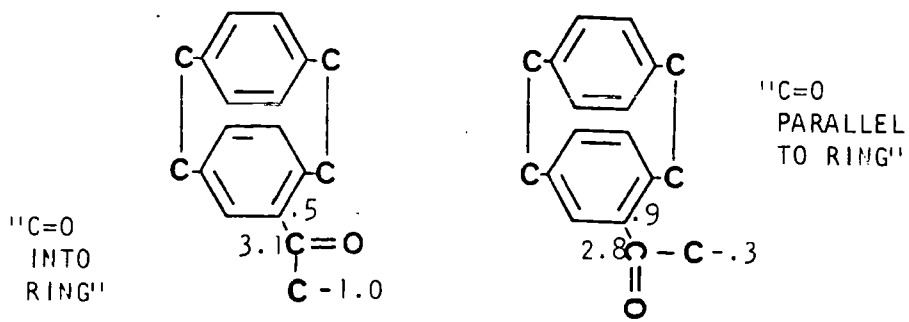
The data also provides a firm basis for investigating the internal consistency of the data for the thin films employed in the investigation of mean free paths as a function of kinetic energy.



(Δ B.E. from 285.0 eV)

FIGURE 5.9

Theoretically calculated B.E.'s for isomers of ethyl and benzyl [2.2] paracyclophane and their experimentally determined C_{1s} core level spectra



(Δ B.E. from 285.0 eV)

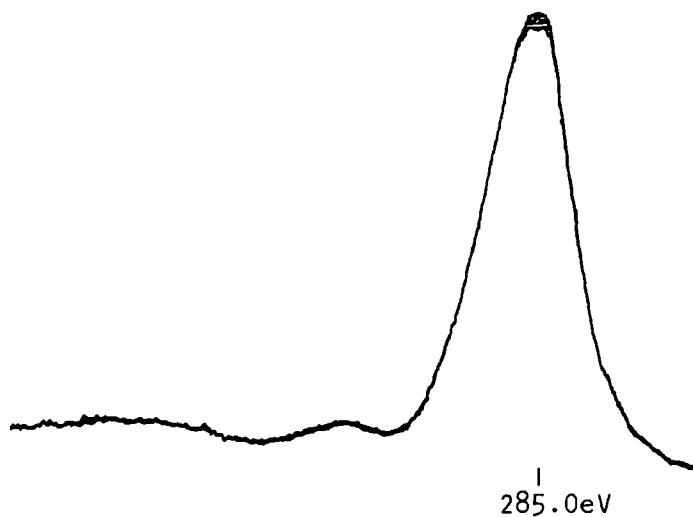


FIGURE 5.10

Theoretically calculated B.E.'s for isomers of acetyl [2.2] paracyclophane and the experimental C_{1s} and O_{1s} core level spectra

CHAPTER 6

An Investigation into Sample Charging Phenomena

CHAPTER 6

An Investigation into Sample Charging Phenomena

i) Introduction

The problems associated with sample charging in the ESCA examination of thick insulating samples was recognized and diagnosed at an early stage of development of the technique of Siegbahn and co-workers¹⁸. Indeed, the suggested use of the characteristic signal arising from contaminant hydrocarbon films originating in the extraneous atmosphere of the spectrometer as a convenient energy reference derives from those pioneering studies and to this date offers with due care and attention a convenient and reliable means of correcting for sample charging^{18,128}. In the intervening decade, various aspects of sample charging phenomena have been studied in some detail^{29,194,235-238}, however, as a recent ASTM report²³⁹ affirms, sample charging and its correction is still a source of error in attempting to set up calibration standards for insulators and, indeed, the prevailing climate would seem to be that the phenomena encompassed by sample charging is a nuisance which practicing spectroscopists must learn to live with. Through extensive investigations on polymeric systems we have come to appreciate the potential source of information which may be derived from the direct study of sample charging and which has largely been overlooked in the past^{127,142}. It is the purpose of this chapter to illustrate this theme by consideration of sample charging phenomena for both metal and polymer samples and it will be shown that the equilibrium static charge built up on a sample is characteristic of structure and bonding in the outermost few tens of Angstroms.

The experiments described in this work fall into three categories. In the first category a series of polymer films and gold were mounted on the sample probe such that they were effectively electrically isolated, although in 'intimate contact' with the probe tip. Measurements were then made of the static equilibrium charge for each sample as evidenced by the shift in core level spectra from the binding energies appropriate to samples ideally in electrical contact with the spectrometer. The second series of experiments involved the monitoring of the time dependent nature of the sample charging under a given set of experimental conditions as a function of hydrocarbon contamination which was allowed to

accumulate on the sample surfaces. The final series of experiments consisted in attaching polymer films ($\sim 50\mu$ thick) to the spectrometer probe such that only 'spotted contact' was made, and monitoring the time dependence of the initial charging phenomena, as well as that associated with deliberate hydrocarbon contamination.

ii) Experimental

a) Samples

The polymers used in this study are listed in Table 6.1,

List of materials used in this study and the physical form studied in the ESCA experiment

<u>Material</u>	<u>Designation for Script</u>	<u>Form</u>
Polyethylene (high density)	PE	Film(F)
Polyvinyl Fluoride	PVF	F, Powder(F)
Polyvinylidene Fluoride	PVF ₂	F
Polytetrafluoroethylene	PTFE	P, F
Polyhexafluoropropene	PHFP	P
Ethylene-Tetrafluoroethylene Copolymer	E-TE	F
Poly-n-butyl Methacrylate	PBMA	F, P
Polyethylene Terephthalate	PET	F
Polycaprolactam (Nylon 6)	N6	F
Polyvinyl Chloride	PVC	P
Gold	Au	F (Sheet)

TABLE 6.1

and were used directly in preparing samples for the ESCA investigations.

All polymers, except for the E-TE copolymer, were obtained from Cellomer Associates, In., Webster, N.Y. 14580, U.S.A., and were used as received.

The ethylene-tetrafluoroethylene copolymer (E-TE) included in this work has previously been subject of an ESCA investigation¹⁴². The structure of the copolymer (52% tetrafluoroethylene) is known to be largely alternating and, therefore, is closely similar in composition and structure to polyvinylidene fluoride (PVF₂).

The polymers were studied as either fine powders (P) coated onto doublesided 'Scotch' tape (3M Company, Tape No. 75, a thermosetting silicone based adhesive on polyester film) directly attached to the spectrometer probe tip, or as films (F) attached by either of two methods: 1) films mounted in what is referred to as 'intimate contact' were attached directly to the probe tip with double-sided 'Scotch' tape, and pressed in place, 2) films mounted in what is henceforth referred to as 'spotted contact' were wrapped over the probe tip and taped to the opposite side. These two methods of attaching the films to the probe tip provided two distinct situations. The first being a composite of conductor (probe tip at ground potential)/dielectric ('Scotch' tape)/and film sample; the second being a conductor/vacuum and point contact of film and probe tip.

The gold (Johnson Matthey Chemicals Ltd., Grade I, London) samples were mounted directly onto the probe tip with 'Scotch' tape.

In the hydrocarbon contamination study involving biasing of a gold sample, the experimental procedure was as follows. Two samples were mounted side-by-side on double-sided tape where one sample was in electrical contact with the spectrometer (grounded) and one sample connected to a D.C. supply, variable from +20 to -20 Volts. Under these experimental conditions two peaks are observed in the spectra of the particular core levels being investigated associated with the two samples separated by the applied bias.

In all cases, except the biasing experiment, sample sizes were 7 x 18 mm., whereas in the biasing experiment each sample approximated half that value.

b) Instrumentation

Spectra were recorded with an A.E.I. ES200 AA spectrometer using $Mg_{K\alpha_{1,2}}$ exciting radiation.

The X-ray gun is of the 'hidden filament or Henke' type design¹⁰⁰ in which the filament is not directly in front of the target. The power source to the gun consists of a Marconi-Elliott Type GX5 high voltage generator that may be operated in the vacuum region of $\sim 10^{-5}$ torr. The target can be operated at a power of up to 500 watts and both voltage and current supplies are stabilized to 0.1% which produces photon fluxes in the region of ~ 0.1 millirad per second. Both voltage and current are dial up facilities in which

integral values in the range 2-15 kv and 2-20 mA were available.

Typical operating conditions were: X-ray gun, 12 kv, 15 mA; pressure in the sample chamber, $\sim 10^{-8}$ torr. Under the experimental conditions employed, the gold $4f_{7/2}$ level at 84 eV used for calibration of the energy scale, had a full width at half maximum (FWHM) of 1.2 eV. No evidence was obtained for radiation damage to the samples during the typical time scale involved in these measurements. All spectra taken in this study were recorded at a fixed angle of 45° with respect to the X-ray photon source and the focusing lens to the analyzer. Spectra were recorded in the fixed retardation ratio mode.

c) Sample Charge Measurement and Time Dependent Studies

The charge on the sample was determined as the difference between the measured kinetic energy of a photoemitted electron from a specific core level and the kinetic energy approximate to a sample ideally in electrical contact with the spectrometer. The latter is taken as the kinetic energy appropriate to the absolute binding energy as previously determined for these systems, on the same calibration scale (cf. Chapter 3)

It was observed for all of the samples in this investigation that the charge was time dependent, therefore, spectra were recorded immediately upon irradiation (taken as $T=0$) and subsequently every five minutes. The equilibrium charge is taken as the maximum observable shift obtained from a contamination free sample.

For the particular cases of polytetrafluoroethylene and gold, the equilibrium sample charge was measured as a function of the applied potential (kv) and the filament emission current (mA) to the X-ray source.

(iii) Results and Discussion

a) Equilibrium Charging of Polymers

Over a period of years it has become increasingly evident from extensive investigations of a wide range of polymeric materials¹²⁵⁻¹³⁰, that sample charging is dependent on electronic structure. The initial experiments in this work involved a systematic investigation of the sample charging characteristic of a series of polymers ($\sim 50\mu$ in thickness) studied under identical instrumental conditions, (unmonochromatized $Mg_{K\alpha_{1,2}}$ X-ray source 12 kv, 15 mA with a fixed electron take-off angle of 45°). In these initial experiments samples were mounted in intimate contact with the copper probe tip (spectrometer probe grounded)

by means of double-sided 'Scotch' tape as outlined above. With this configuration, it was established that the equilibrium shift in kinetic energy scale arising from sample charging was rapidly established (at least as far as the typical time scale taken to record spectra are concerned). Repeat measurements established that the sample charging was typically reproducible to $\pm 10\%$ even in comparing powdered samples with films.

That the shifts are characteristic of the polymer system is readily apparent if we consider the data for three typical samples viz. PE, PVF₂ and PHFP. The corresponding shifts in kinetic scale δ are ~ 3.4 eV, ~ 7.5 eV and ~ 10 eV. It should be emphasized that these values pertain specifically to the experimental arrangement described above. To shed further light on the relationship between sample charging and electronic structure, investigations were also made on gold sheet (ultra high purity ~ 0.3 mm. thick) mounted on double-sided 'Scotch' tape. The equilibrium static charge in this case amounted to ~ 13.5 eV.

Under identical instrumental conditions it seems that the surface charge acquired by a sample must be a function of the total photoionization cross section and to investigate this in some detail we may consider appropriate relative theoretical cross sections for each material. As a starting point, the recently published data of Schofield²⁰⁶ have been employed to compute cross sections for both the gold and polymer surfaces and for convenience in discussing this data, this has been normalized to a unit surface area. Knowing typical covalent radii for gold²⁴⁰ and as a first approximation taking representative bond lengths and angles¹⁴¹ for extended chains of the polymers together with appropriate interchain spacings²⁴¹, it is possible to compute relative photoionization cross sections per unit area for the polymer and gold surfaces*. The correlation between equilibrium charge, as measured as a shift (δ) in kinetic energy scale; and total theoretical cross section for photoionization is shown in Fig. 6.1. The exhibited trend of larger shift being

*Gold was chosen for this particular study both because of its chemical inertness (and, hence, reproducible character of the surface) and for the high cross section for photoionization. In addition, gold still serves as a primary source for the energy referencing of spectrometers^{18,128}.

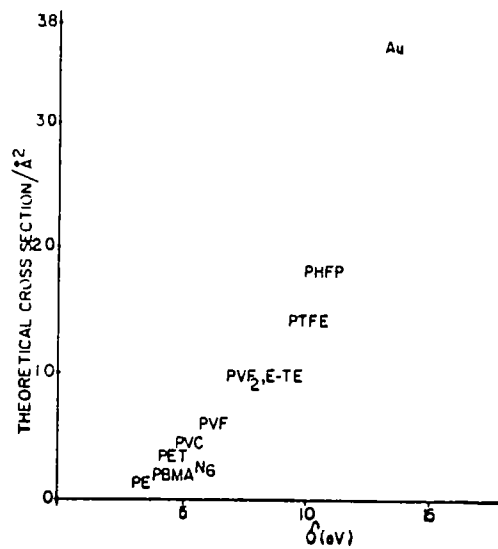


FIGURE 6.1

Calculated total theoretical cross sections for normalized unit areas for various polymers and gold, versus, experimentally determined equilibrium charging shift (δ) for samples irradiated with a $\text{Mg}_{K\alpha_{1,2}}$ X-ray photon source (12 kv, 15 mA) and electrically isolated from the spectrometer

associated with higher cross section is particularly striking and although the absolute magnitude of sample charging as such represents a convolution of many contributing factors, such a correlation underscores the structural dependence of such phenomena. It is of a particular interest to note that polyvinylidene fluoride (PVF_2) exhibits the same charging characteristics as a ethylene/tetrafluoroethylene copolymer (E-TE in Fig. 6.1) of essentially identical overall composition. This again illustrates the characteristic nature of sample charging phenomena since it is known that the structure of this copolymer is largely alternating and, hence, has a close correspondence with PVF_2 . Having outlined the characteristic nature of the sample charging phenomena and having intimated that this depends strongly on structure and bonding in the surface regions, we now describe a series of experiments which amply demonstrate the surface sensitivity of the phenomena.

b) Surface Sensitivity of Sample Charging

In Chapter 3 a method was outlined which allows a convenient means of both obviating and selectively controlling hydrocarbon contamination of surfaces. We have, therefore, systematically investigated sample charging as a function of hydrocarbon contamination of the surface for both gold and the polymer samples. The objective of this investigation is twofold; first, to investigate the sensitivity of sample charging phenomena to surface contamination and second, to provide a more detailed study than has hereto been available on the reliability of establishing absolute binding energies by reference to hydrocarbon contamination samples.

Spectra were, therefore, recorded under conditions in which hydrocarbon contamination built up over a convenient time period of ~100 minutes. Since the features which emerge from this investigation are common to all of the systems studied, we confine our detailed attention to gold, PTFE and PVF₂ which together with PE encompass the spectrum of sample charging observed for the complete series. Considering firstly gold, Fig. 6.2 shows a plot of the

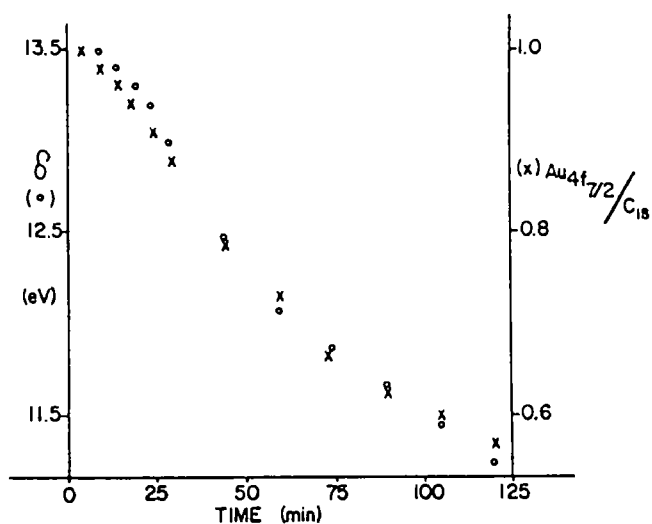


FIGURE 6.2

Change in sample charging (δ), versus, hydrocarbon contamination calculated from peak area intensity ratios $Au_{4f_{7/2}}/C_{1s}$ for a gold

sample electrically isolated from the spectrometer

change in sample charging as a function of hydrocarbon build up. From the relative intensity ratios of the core level spectra it may readily be shown (cf. Chapter 4) that the initial gold sample to which the equilibrium static charge in Fig. 6.1 pertains corresponds to a gold surface with hydrocarbon coverage corresponding to a monolayer ($\sim 5\text{\AA}$). The correlation between decrease in surface charging and increase in thickness of the hydrocarbon contaminant layer provides a straightforward pictorial representation of the surface sensitivity of sample charging. With a knowledge of electron mean free paths as a function of kinetic energy it is a straightforward matter to estimate the thickness of the hydrocarbon film (cf. Chapter 4). (In this connection it should be noted that the independent estimates based on the signal attenuations for the $\text{Au}_{4f_{7/2}}$ and C_{1s} levels give essentially the same result.) For a decrease in sample charging of 2 eV, the corresponding increase in thickness of the hydrocarbon overlayer is $\sim 8\text{\AA}$. The form of the curve relating sample charging to the thickness of contaminant film would suggest that a completely clean surface studied under identical conditions would have a slightly larger shift (probably of the order of a few eV) the net effect being to displace the data point for gold indicated in Fig. 6.1 to the right. If for a sample of essentially zero total cross section, the sample charging were zero, the data points relating to sample charge (δ) to cross section would then fit a smooth curve. These experiments, therefore, suggest that charging for samples which are insulated from the spectrometer probe depend on structure and bonding on a depth scale of the same order of magnitude as electron mean free paths.

The deliberate surface contamination of samples with hydrocarbon* has been advocated¹²⁷ as one of the most routinely reliable and reproducible means of establishing the energy reference for insulating samples. In this connection, therefore, it is of interest to consider the shift in binding energy between the $\text{Au}_{4f_{7/2}}$ and C_{1s} levels as a function of overall sample charging. This is shown in Fig. 6.3.

*As we have previously emphasized, separate experiments must be carried out to fully characterize this hydrocarbon contamination which, in our particular spectrometer, has a binding energy of 285 eV (reference $\text{Au}_{4f_{7/2}}$ 84 eV).

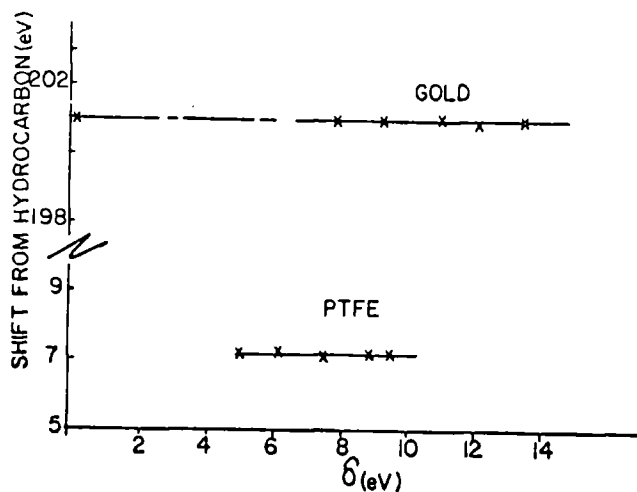


FIGURE 6.3

Absolute shift in kinetic energy between the $Au_{4f_{7/2}}$ and C_{1s} core levels, versus, overall sample charging (δ)

Considering the extremes, of zero sample charging (gold in electrical contact with spectrometer) and the maximum in sample charging (~ 13.5 eV), the shift in energy between the core levels of substrate (Au) and overlayer (hydrocarbon) is exactly the same within very small error limits ~ 0.1 eV. Since for most polymeric systems (for which we have previously advocated the use of this technique for energy calibration), the span in sample charging is substantially smaller, the accuracy of the method is extremely good.

The corresponding data for PTFE, PVF_2 and PE are shown in Fig. 6.4. The decrease in sample charging as a function of hydrocarbon deposited on the surface is clearly evident in the particular cases of PTFE and PVF_2 . However, the closely similar chemical nature of the polymer surface and contaminant film ensure that for PE the sample charging remains essentially constant. Since the overall integrated intensity of the C_{1s} levels for the latter do not change with time, there is not direct evidence from this source alone that hydrocarbon contamination of PE itself occurs. The fact that it does, however, may readily be demonstrated by investigating samples with submonolayer extents of surface oxidation. Such low levels of oxidation do not of themselves alter the overall sample charging, however, they do provide

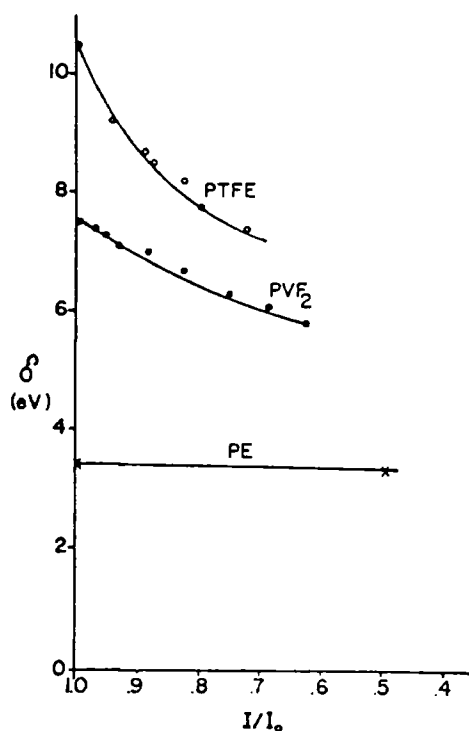


FIGURE 6.4

Decrease in sample charging (δ), versus, hydrocarbon contamination

a valuable 'marker' in the O_{1s} levels. By monitoring the decrease in intensity as a function of time it may thus be readily demonstrated that hydrocarbon contamination also occurs for PE.

The rate of build up of hydrocarbon is a convolution of several factors including the partial pressure of extraneous hydrocarbon in the vicinity of the sample surface*. The single most important sample dependent factor will be the sticking probability for hydrocarbon at the polymer surface which will be related to surface free energy. On this

*We have previously discussed (Chapter 3) that in our particular spectrometer configuration hydrocarbon contamination is attributable to desorption from the end cap of the horizontally mounted X-ray gun of Henke design. These experiments show that the contamination is 'line of sight' as might have been anticipated from typical mean free paths in the pressure range to which the experiments pertain ($\sim 10^{-8}$ torr). Such contamination may readily be obviated by cooling the end cap and thus adventitously it is possible to selectively contaminate surface.

basis we might anticipate that under comparable experimental conditions, rates of hydrocarbon contamination should reflect this. By monitoring the decrease in C_{1s} intensity appropriate characteristic peaks for PHFP, PTFE, PVF_2 , E-TE and PVF, films attributable to hydrocarbon contamination as a function of time this may readily be demonstrated. Thus, the time taken for the signal to decrease by 1/eth of its original value in a particular series of experiments in which hydrocarbon contamination was deliberately accelerated was 280, 120, 84, 90, and 80 minutes, respectively, for PHFP, PTFE, PVF_2 , E-TE and PVF. Since each polymer system has a characteristic equilibrium charging shift, we might also anticipate that the change in this shift as a function of surface contamination should also be characteristic of the sample. This may readily be shown by considering the change in equilibrium charging shift for PHFP, PTFE, PVF_2 , E-TE and PVF when the contaminant film is such that the characteristic C_{1s} levels for these systems has again decreased by 1/eth of its original value. The corresponding shifts for this series of polymers are 3.5, 3.3, 1.5, 1.8 and 1.2 eV, respectively.

It should be noted that in these experiments it is also possible to monitor the shift between the C_{1s} signal of the hydrocarbon contaminant and the peaks of characteristic binding energy for the fluoropolymers. As in the case of gold, discussed above, the shift is independent of sample charging within very narrow limits confirming our previously developed thesis that hydrocarbon contamination is an excellent technique for energy referencing. (The data for PTFE being a representative sample is shown in Fig. 6.3.) In the particular case of PE, the rate of build up of hydrocarbon may be monitored by following the decrease in intensity of the extraneous O_{1s} signal. For gold, as we have previously noted, the original sample has approximately a monolayer of hydrocarbon contamination already present and we might, therefore, anticipate that the rate of build up of hydrocarbon contamination of both the PE and gold samples would be somewhat similar. That this is the case may readily be demonstrated by following the decrease in intensity of the gold $4f$ levels. When due allowance is taken of the differing electron mean free paths corresponding to electrons photomeitted from the O_{1s} and Au_{4f} levels, the comparable rates put onto a similar basis as those of the other samples gives a time scale of ~50 minutes which is entirely reasonable on the basis

of the higher surface free energy.

One question which immediately springs to mind on the basis of the data presented this far is, "do rates of hydrocarbon contamination themselves depend on the absolute magnitude of surface charge?" The crucial issue embodied in this question is whether sticking probabilities are in any way substantially altered compared with the neutral system if the sample carries a surface charge. To investigate this possibility experiments were carried out in which gold sample, either insulated from or in electrical contact with the spectrometer, were studied simultaneously and the rates of hydrocarbon contamination monitored as a function of charging shift between them. Experiments corresponding to overall positive and negative charging shifts were carried out and revealed that for charging shifts ranging from +19v to -10v the rates of hydrocarbon build up were identical to that of the gold sample in electrical contact with the spectrometer. The sticking probabilities under the conditions of these experiments, therefore, directly reflect structure and bonding of the sample surface.

To summarize the data presented to this point, it is clear that sample charging under a given set of conditions is characteristic of a sample and depends on structure and bonding on a similar depth scale to that appropriate to typical electron mean free paths.

c) Sample Charging as a Function of the Operating Parameters of the X-ray Source.

As the logical next stage in the investigation, therefore, we have studied sample charging as a function of the operating parameters of the X-ray source. As a reasonable overall compromise in terms of signal intensity, signal/background, signal/noise, time scale for generating spectra, minimizing radiation damage, etc., the most usual operating conditions using an unmonochromatized $Mg_{K\alpha_{1,2}}$ X-ray source

is 12 kv and 15 mA. We have, therefore, investigated sample charging for gold mounted insulated from the spectrometer probe and the results are displayed in Fig. 6.5. Considering firstly sample charging as a function of current in the X-ray tube at a fixed voltage (12 kv) it is clear that in the range 6-20 mA sample charging remains essentially constant. Below 6 mA there is a gradual increase such that at 2 mA the sample charge has changed by ~ 0.2 eV (viz. $\sim 1.4\%$ change in sample

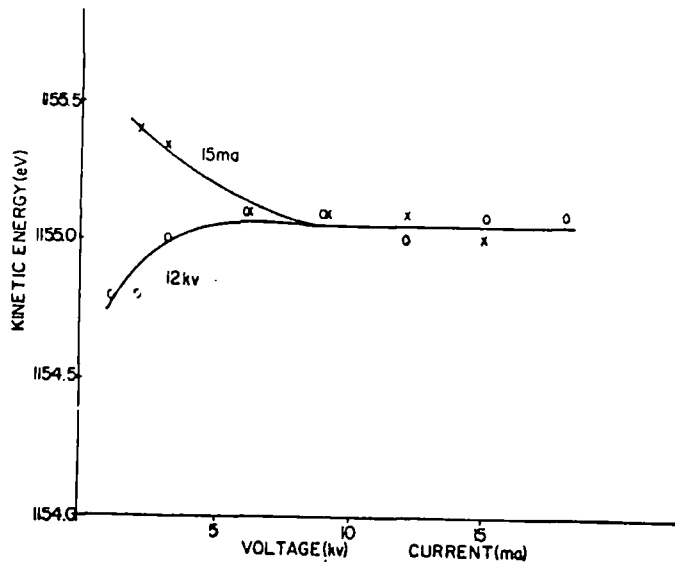


FIGURE 6.5

Overall sample charging (δ), as a function of fixed voltage (12 kv) and variable current (6-20 mA) and fixed current (15 mA) and variable voltage (2-15 kv) for a gold sample electrically isolated from the spectrometer

charging for an order of magnitude decrease in current). Also shown is the change in sample charging for a fixed operating current of 15 mA and varying the voltage in the range of 2 kv-15 kv. In the region 6-15 kv which spans the normal operating region for all commercially available spectrometers, the sample charging is constant within very narrow limits. Below 6 kv there is a tendency for sample charging to decrease, however, the effect is again small such that at 2 kv the sample charging differs by only ~ 0.3 eV from the equilibrium charge under normal operating conditions. These experiments, therefore; amply demonstrate that under the conditions employed in this work, the equilibrium charge acquired by a sample is essentially constant over a wide range of operating conditions encompassing power loadings in the range 12 watts - 225 watts. Furthermore, it may readily be shown that with samples directly mounted onto the probe with double-sided 'Scotch' insulating tape that the time scale to establish equilibrium charge is rapid compared with the typical time scale required to record the data. Essentially identical data are, therefore, obtained if equilibrium charge is studied by successively

increasing or decreasing either the voltage or current in the X-ray tube, viz. the data displayed in Fig. 6.5 exhibit no hysteresis effects. To demonstrate that the phenomena illustrated in Fig. 6.5 are entirely representative of samples in general comparable studies have also been carried out on PTFE and again in the operating range 6-15 kv and 4-20 mA equilibrium charge remains constant.

d) Time Dependent Studies of Sample Charging

Although, as we have indicated for sample mounted on double-sided 'Scotch' insulating tape the equilibrium for a given sample is rapidly established, this is not generally the case for polymer films which are directly attached to the spectrometer probe either by locating screws or by insulating tape located on the reverse side of the probe tip. In the case of sample mounted on 'Scotch' tape the adhesive bonding at the tape/probe and polymer/tape interface ensures intimate contact and the composite, therefore, behaves as a capacitor of layered dielectric composition. For samples mounted directly on the probe, however, the polymer-probe contact on a macroscopic scale is 'spotted' and the situation is much more complex.

In this section, therefore, we describe the time dependence of sample charging phenomena for polymer films mounted directly in contact with the spectrometer probe.

Three systems were chosen for detailed investigation, namely, PTFE, E-TE and PE. Considering firstly the data (Fig. 6.6) for PE, the initially measured shift for the 50μ film (identical to that used for the investigation described in section 3b), corresponds closely to that for films mounted on 'Scotch' tape, however, over a period of ~ 25 minutes the charging shift increases until an equilibrium value of ~ 5 eV is attained. Both PTFE and the E-TE copolymer exhibit similar, but somewhat larger increases in sample charging with respect to the initial values which again correspond closely to those measured for sample mounted on insulating tape. The maximum in charging shift relative to that measured for samples mounted on tape increases in going from PE to PTFE. For PTFE and E-TE polymer films the decrease in sample charging is attributable to hydrocarbon contamination as is clearly evidenced by the core level spectra. Although the sticking probability for hydrocarbon on the PTFE surface is lower than for the E-TE copolymer the decrease in shift onsets after a shorter period since the difference in cross sections between

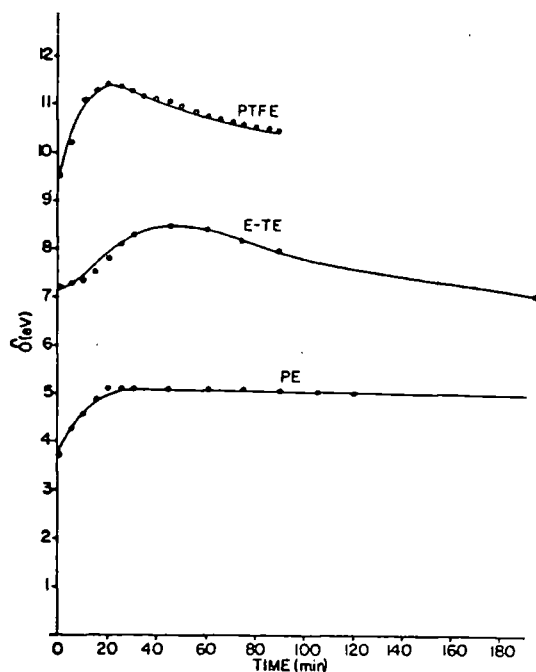


FIGURE 6.6

Sample charging of PTFE, E-TE and PE mounted directly in contact with the probe tip ('spotted contact') versus time

a hydrocarbon overlayer and polymer are somewhat larger in the case of PTFE (cf. Fig. 6.1). The data displayed in Fig. 6.6 are representative of that obtained for a number of repeat experiments. Since it is unlikely that the polymer-probe interface was exactly the same in this series of experiments, and since the extraneous hydrocarbon partial pressure was also allowed to vary, we would not expect to exactly reproduce the data for a given sample. The broad features in each case, however, follow the trends discussed above. Namely, that the initial charge showed a close similarity to that for samples mounted directly on 'Scotch' tape and that the shift first increased and then decreased as a function of time, the decrease being associated with hydrocarbon contamination. For films studied in this manner, therefore, (spotted contact), even in the absence of hydrocarbon contamination there is a distinctive time dependence for the sample charging and clearly the accurate measurement of absolute binding energies requires that such films be studied when equilibrium has been established. If measurements are being made over extensive energy ranges and which require considerable

time spans, then it becomes imperative to take such factors into account. Such a situation exists in generating valence band spectra where the low photoionization cross sections for soft X-ray sources often entails experiments on an extended time scale¹²⁷. Hydrocarbon contamination which needs to be taken into account in measuring absolute and relative binding energies must also be considered from the point of view of the shifts in sample charging which may arise consequent upon its build up at sample surface. Although, therefore, even for polymer samples mounted directly on to the spectrometer probe, sample charging is characteristic of the polymer, the convolution of factors contributing to the time dependence of such charging considerably complicates matters and in the extreme could lead to artificially narrowed or broadened peaks, skewed line shapes and incorrect energy referencing. It is clear, therefore, that if use is to be made of the structural dependence of sample charging then samples must be studied under conditions in which the equilibrium charge is rapidly attained and hydrocarbon contamination (which provides an extremely convenient and reliable energy reference) must also be closely controlled.

e) Sample Charging as a Function of Surface Modification

One of the most important attributes of ESCA as a spectroscopic tool in the study of polymeric system, is the capability of elaborating features of structure and bonding pertaining to the surface and sub-surface and hence, effecting a depth profile¹²⁷. The information levels which have been employed in this regard hinge on the absolute magnitude and differences in magnitude of electron mean free paths as a function of kinetic energy. Thus, from the relative intensities of core level spectra corresponding to differing escape depths and from the angular dependence both of intensity ratios for individual core levels and for the component peaks of a given core level it is possible to investigate structure and bonding in inhomogeneous surface regions. A particularly important area of application of the technique is in the elaboration of surface modification of polymers which encompasses many important commercial processes such as improvement of adhesive bonding, printability, wettability, barrier coatings, etc.

Clark and Dilks have demonstrated the great utility of ESCA in such areas in recent papers detailing the kinetic and mechanism of both direct and radiative energy transfer process involved in the modification of polymers by interaction with inductively coupled RF

plasma excited in inert gases^{142,243}. The surface sensitivity of the sample charging phenomena suggests that the major changes in surface structure associated with such treatments would readily be monitored by this means and we have previously indicated that this is indeed the case in a preliminary form¹⁴². As a particular apposite example of the information available from the direct investigation of sample charging we therefore, consider how the phenomenon provides a straightforward means of monitoring the interaction of an E-TE copolymer with plasma excited in argon at power loading of 0.5 and 5.0 W¹⁴².

The copolymer of essentially the same composition as PVF₂ has a closely similar equilibrium charging shift of 7.5 eV when studied under standard operating conditions (sample mounted on double-sided 'Scotch' tape). The detailed analysis of both the core and valence level spectra for the system as a function of reaction time with plasma excited under given conditions reveals that the surface modification is dominated by a direct energy transfer mechanism involving inert gas ions and metastables and which involves the production of a surface which has a greatly reduced fluorine content^{142,243}. Since the charging characteristic of the copolymer and of a solely hydrocarbon based polymer such as PE are so different, it might be anticipated that changes in equilibrium charge would provide a sensitive monitor for changes in surface composition. That this is indeed the case is amply illustrated by the data in Fig. 6.7.

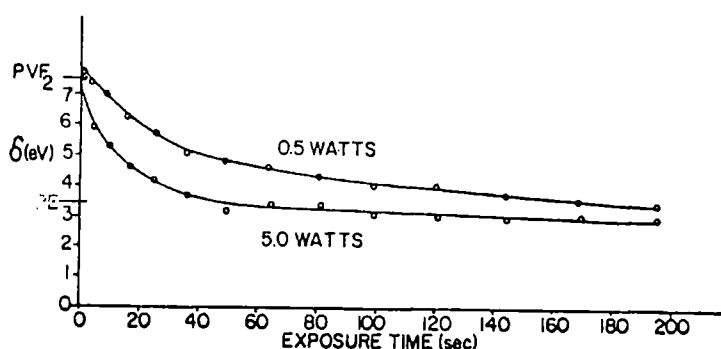


FIGURE 6.7

Sample charging of E-TE (δ) as a function of time of exposure to plasmas excited in argon at power loadings of 0.5 and 5.0 watts

In all cases the equilibrium charge for extended reaction time approaches that of PE and, indeed, with a knowledge of electron mean free paths as a function of kinetic energy it is possible to estimate the thickness of the surface layer at which this situation obtains. In each case the estimate suggests a depth of ~ 3 monolayers which is entirely reasonable in the light of the data previously presented in section b. Thus, for effectively monolayer hydrocarbon coverage of the E-TE copolymer the sample charging decreases by ~ 1.8 eV which is roughly half of the total decrease in shift for the discharge treated samples. From a detailed analysis of the reaction kinetics it may readily be shown that under a given set of experimental conditions, the rate of surface reaction increases in the order $0.5 \text{ w.} < 5.0 \text{ w.}$ and the sample charging data alone illustrate this most convincingly. Thus, the rate of decrease of sample charging which reflects the decreased fluorine content of the surface region also falls in the same order. It is clear, therefore, that sample charging phenomena can add an extra dimension to such investigations and is eminently worthwhile studying in its own right.

CHAPTER 7

An ESCA Investigation into a Series of Aliphatic, Aromatic
and Fluorine Containing Polycarbonates

CHAPTER 7

An ESCA Investigation into a Series of Aliphatic, Aromatic and Fluorine Containing Polycarbonates

i) Introduction

A systematic ESCA study on a large number of homopolymers of simple monomeric systems was presented in Chapter 3. The compilation of substituent effects on C_{1s} , O_{1s} , Cl_{2p} , Si_{2p} , F_{1s} , S_{2s} and Br_{3d} core levels illustrates the characteristic nature of the effects and suggests that they may be used as a 'fingerprint' analytical tool for the characterization of polymeric surfaces. The determination of the absolute and relative binding energies and the relative peak intensities for the various polymer systems enables a comparison to be drawn with data pertaining to the surface composition with that of the bulk^{21,125,127}. With this extensive tabulation of data on polymer systems, more detailed investigations on particular polymer systems can readily be accomplished with ESCA.

In this chapter, a study has been made on a series of aliphatic, aromatic and fluorine containing polycarbonates which includes data pertaining to the absolute and relative binding energies for C_{1s} , O_{1s} and F_{1s} core levels, degree of polymerization (D.P.) for low MW polyfluorocarbonates, confirmation of the core level assignments by comparison with model compounds and theoretical calculations (within the CNDO/2 SCF formalism utilizing the groundstate potential model) and the compositions of these selected polymers as determined by ESCA.

ii) Experimental

a) Samples

The model compounds and polycarbonates, listed in Table 7.1, were obtained from the following sources: the model compounds were obtained as reagent-grade materials which were shown by GLC to be $\geq 98\%$ purity, the aromatic polycarbonates (of bisphenol A type) of the various MW 's listed were obtained from Cellomer Associates, Inc. (P.O. Box 311, Webster, N.Y., U.S.A.) and were used directly in preparing samples for the ESCA investigation. The remaining aliphatic, glycol and fluorine containing polycarbonates were specially prepared polymers and their synthesis and characterization is described elsewhere²⁴⁴.

Model Compounds and Polycarbonates Studied

<u>Model Compounds</u>	<u>Form</u>
$\phi - \overset{\text{O}}{\parallel} \text{C} - \text{O} - \phi$	(SP)
$\left[\text{CF}_3 \text{CH}_2 \text{O} \right]_2 \overset{\text{O}}{\parallel} \text{C}$	(CV)
$\phi - \overset{\text{O}}{\parallel} \text{C} - \text{O} - \text{CH}_2 (\text{CF}_2)_3 \text{CH}_2 \overset{\text{O}}{\parallel} \text{C} - \text{O} - \phi$	(SP)
 <u>Polymers</u>	
$\text{CF}_3 \text{CH}_2 \text{O} \left[\overset{\text{O}}{\parallel} \text{C} - \text{OCH}_2 (\text{CF}_2)_3 \text{CH}_2 \text{O} \right]_x \overset{\text{O}}{\parallel} \text{C} - \text{OCH}_2 \text{CF}_3 \quad x \sim 2-18$	(N)
$\left[\overset{\text{O}}{\parallel} \text{C} - \text{O} (\text{CH}_2)_x \right]_n$	x = 4, 5, 6, 10 (P)
$\left[\overset{\text{O}}{\parallel} \text{C} - \text{O} (\text{CH}_2)_2 \right]_n$	x = 2, 3, 4 (P)
$\left[\phi - \overset{\text{C}}{\underset{\text{C}}{\parallel}} - \phi \overset{\text{O}}{\parallel} \text{C} - \text{O} \right]_n$	MW = 33, 50 and 95K (CF)

TABLE 7.1

b) Sample Preparation

The three model compounds were studied in the form of thin films condensed onto a cooled gold substrate (~ -170°C) directly in the spectrometer source. To accomplish this, the liquid sample (CV)

$(\text{CF}_3 \text{CH}_2 \text{O})_2 \overset{\text{O}}{\parallel} \text{C}$ was injected (~0.1 ul) into a reservoir shaft (2500 cm³ in volume) which was attached to the source region of the spectrometer by means of an insertion lock system. The sample was leaked through a Metrosil plug in the reservoir shaft and the directed jet of vapor impinged onto the cooled gold substrate mounted onto a sample probe. The reservoir temperature was typically ca. 30°C and that of the cooled probe tip ca. -170°C. The remaining model compounds, in the form of powders (SP), were introduced into the spectrometer in fine capillary tubes and the compounds sublimed onto the cooled probe tip as described above for the liquid compound. By studying these samples as thin films on gold, sufficient charge carriers are available such that sample charging is obviated,

allowing for direct calibration of the energy scale (cf. Chapter 6).

The polymers were studied as either fine powders (P) coated onto double-sided 'Scotch' tape directly attached to the spectrometer probe, as neat films (N) where a small sample was spread on gold and the gold attached to the probe by double-sided 'Scotch' tape, or as thin films (CF), cast from methylene chloride (spectroscopic grade) onto gold substrates attached to the probe as described above. Due care was taken to avoid contamination of the polymers during preparation for the ESCA studies, although the commercial aromatic polymers were used as received with no further purification.

c) Instrumentation

The instrumentation used for the recording of ESCA spectra and the deconvolution of overlapping peaks has been described in Chapter 3 under (c) Instrumentation.

iii) Theoretical

The data pertaining to model compounds for monomeric systems with respect to the C_{1s}, O_{1s} and F_{1s} core levels have been described elsewhere^{1,21,125,127,137}. These data include the determination of absolute and relative binding energies for similar systems, although further investigations were performed on three additional model compounds in this study. For the larger polymer model systems, calculations were carried out within the all valence electron CNDO/2 SCF MO formalism⁷⁰ employing the charge potential model¹⁸ within the ground state configuration (GPM), described in detail in Chapter 3, in the section on 'Model Compounds'.

iv) Results and Discussion

a) Model Compounds

1) Experimental

The primary sources of ESCA data which have been utilized to date are the relative and absolute binding energies and relative peak intensities of core levels^{1,21,125,127,137}. As a preliminary to the detailed investigation of the polycarbonates, therefore, a study was made on simple model compounds which contained chemical functionalities which have not been investigated in detail previous to this work. This absolute and relative binding energy data, in addition to that previously established for similar (cf. Chapter 3), but not identical systems, provides a firm foundation for the interpretation of the polymer data.

The ESCA spectra for the C_{1s} and O_{1s} core levels for the model compounds are shown in Fig. 7.1. Direct measurement of the relative

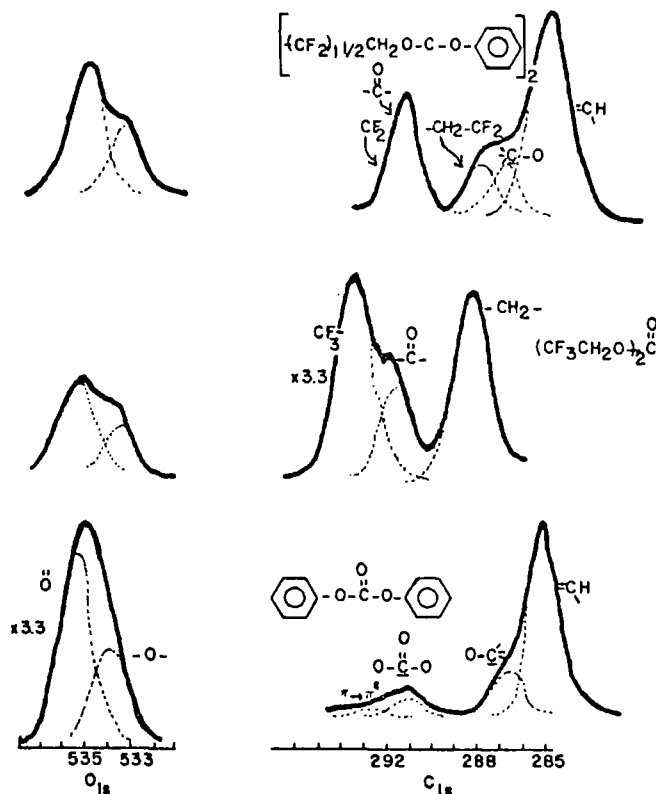


FIGURE 7.1

C_{1s} and O_{1s} core level spectra for model compounds

area ratios for the C_{1s} and O_{1s} levels when used in conjunction with the required sensitivity factors previously determined for Carbon and oxygen stoichiometric ratios for the model compounds. Having determined on the ESCA depth profiling scale that the model compounds are homogeneous and the peak areas representative of the stoichiometry of the compounds, a discussion on the relative and absolute binding energies for the various structural features relevant to the investigation of the polycarbonates follows. Well resolved spectra were obtained in all cases and by careful calibration of the line widths (FWHM) and line shapes, incompletely resolved peaks could be unambiguously deconvoluted within narrow error limits (± 0.2 eV) and the relevant data is shown in Table 7.2.

Experimentally Determined Binding Energies for Model Compounds

Compound	<u>Experimental B.E.'s in eV</u>					
	1s levels					
	C-O-	C=O	$\begin{array}{c} \text{O} \\ \parallel \\ \text{O}=\text{C}=\text{O} \end{array}$	C=O	CF ₃	CF ₂
$\phi-\overset{\text{O}}{\parallel}{\text{C}}-\text{O}-\phi$	535.3	533.9	290.9	286.6		
$\left[\text{CF}_3\text{CH}_2\text{O} \right]_2\overset{\text{O}}{\parallel}{\text{C}}$	535.9	534.1	291.6	288.2	293.5	
$\phi\overset{\text{O}}{\parallel}{\text{C}}-\text{OCH}_2(\text{CF}_2)_3\text{CH}_2\overset{\text{O}}{\parallel}{\text{C}}-\text{O}\phi$	535.5	533.7	291.5	287.2		288.2

TABLE 7.2

As in the cases for other systems previously studied (cf. Chapter 3), the core levels corresponding to carbon atoms not directly bonded to oxygen or fluorine had binding energies centered around 285.0 eV and have been omitted from Table 7.2. In the case where there were no carbon atoms not directly bonded to either oxygen or other carbon atoms containing fluorine e.g. $(\text{CF}_3\text{CH}_2\text{O})_2\overset{\text{O}}{\parallel}{\text{C}}$ hydrocarbon build-up on the sample surface allowed for accurate determination of the reference energy^{1,125,127}. As has been previously noted in Chapter 3, the shift in binding energy for a particular carbon core level is characteristic of the chemical environment^{1,125}. For carbon atoms singly bonded to oxygen, the binding energies fall in the range of 286.6 eV with shifts of 1.6 eV and are characteristic of these type carbons previously determined in other studies¹³⁷. The carbon atoms doubly bonded to oxygen atoms in these models follow the additive rules, discussed in Chapter 2, in that the binding energy is higher than that for ester type carbon atoms doubly bonded to oxygen due to the additional oxygen atom attached in the carbonate group, the B.E. being 291.3 ± 3 eV. This large shift in B.E. for the carbonate type carbon (e.g. ~ 6.3 eV) allows for ready identification of this particular feature. The carbons directly attached to fluorine follow the shifts in binding energies previously established in the extensive studies by Clark and coworkers on other fluoropolymer systems^{125,127,128,130,135}. Carbon atoms with two fluorines attached ($-\text{CF}_2-$) being shifted by ~ 6.0 eV and those with three fluorines attached shifted by ~ 8.5 eV.

It is worthwhile to note that several subtleties exist in the absolute B.E.'s for the carbon core levels. The chemical shift for a carbon attached to the carbonate group ($-O-\overset{O}{\underset{||}{C}}-O-$) is within experimental error identical to that appropriate to a carbon attached to two fluorines, although two different chemical environments exist for the $-CF_2-$ groups in this work. From previous studies^{1,130,135}, it can be shown that secondary substituent effects are such that for $-CF_2-$ groups the binding energy appropriate to $-CF_2-CF_2-CH_2-$ environments is slightly less than for $-CF_2-CF_2-CF_2-$ environments, the B.E.'s being ~ 290.8 eV and ~ 292.2 eV, respectively. This near coincidence of the absolute B.E.'s for the carbons in different chemical environments manifests itself as an envelope containing these particular structural features for the systems studied.

It is important also to note that the $\pi \rightarrow \pi^*$ shake-up satellite overlaps the centroid of the high binding energy component for the aromatic model system ($\phi-\overset{O}{\underset{||}{C}}-\phi$) as might have been anticipated from previously published data^{58,140}.

Low energy $\pi \rightarrow \pi^*$ shake-up transitions for the aromatic residue is within 1.5 eV of the C_{1s} level for the carbonate group and which, therefore, manifests itself as a broad peak, which may readily be deconvoluted, however, to obtain the components.

To conclude the C_{1s} core level assignments the $-CH_2-$ functional group with adjacent $-O-$ and a CF_3 structural feature adjacent ($(CF_3-CH_2-O)_2C$ model) result in a chemical shift for the $-CH_2-$ group of ~ 3.2 eV which is closely similar to that observed for a $-CH_2-$ group with adjacent $-CF_2-CF_2-$ and $-O-$ groups in the $\phi-\overset{O}{\underset{||}{C}}-OCH_2-(CF_2)_3-CH_2-\overset{O}{\underset{||}{C}}-\phi$ model compounds. For the O_{1s} levels the binding energies for the singly and doubly bonded oxygens exhibit the same chemical shifts (~ 1.2 eV $\pm .2$ eV) as that found for the oxygens in an ester type environment¹³⁷. Previous theoretical studies¹³⁷ have unambiguously assigned the higher binding energy component as arising from the singly bonded oxygen and this can also be observed from the O_{1s} core level spectra in Fig. 7.1, manifesting itself in the 2:1 intensity ratio for the ester and carbonyl oxygen, respectively, in these carbonate systems.

2) Theoretical

It has previously been shown in Chapter 3 that with careful calibration, with respect to simple model systems, it is possible to quantitatively describe both relative and absolute binding energies for polymer systems. The analysis is based on the charge potential

model¹⁸, which, as previously discussed, can be formally derived¹ from Koopman's Theorem⁴⁷ in the zero differential overlap approximation, (e.g. CNDO/2 formalism)⁷⁰.

As a necessary prerequisite in the application of this model to the discussion of data pertaining to the polycarbonates, three simple model compounds have been studied experimentally, as we have already noted, and we now consider the theoretical analysis. The charge potential parameters, E^0 and k , for the ground state potential model (GPM), discussed in Chapter 3, for O_{1s} and C_{1s} core levels have previously been determined by analysis of a series of simple model compounds¹³⁷. These values of E^0 and k for each core level were determined as the intercept and slope, respectively, by plotting $E_i - \sum \frac{q_j}{r_{ij}}$ versus the charge, q_i , on atom i from the CNDO/2 calculations^{1,137}. The values obtained for the C_{1s} and O_{1s} model systems, from a least-squares analysis of the data, yielded values of 284.6 eV and 25.2 for E^0 and k , respectively, for the C_{1s} core levels and 534.6 eV and 16.7 for E^0 and k , respectively, for the O_{1s} core levels¹³⁷. Although the correlation coefficient for the C_{1s} is excellent (0.99), the relatively small range of binding energies for the O_{1s} core levels leads to a considerable scatter in the data for the O_{1s} levels, and, therefore, the correlation coefficient is somewhat lower (0.76). Nonetheless, the concomitant error limits still lead to an unambiguous assignment of the O_{1s} core levels, and this has been checked by carrying out detailed nonempirical LCAO SCF MO calculations¹³⁷ of absolute binding energies from computations on the neutral molecules and the relevant hole states.

Fig. 7.2 shows the calculated absolute binding energies for the three model compounds investigated within the GPM formalism, (cf. Chapter 3), using the values of E^0 and k for the C_{1s} and O_{1s} core levels given above. These absolute binding energies taken in conjunction with those developed from previous studies^{125,127,128} on carbon, oxygen and fluorine containing systems allows for detailed assignments of experimental data. It is apparent that the theoretically calculated B.E.'s from Fig. 7.2 are in excellent agreement with the experimentally determined values for the particular core level functionality when compared with Table 7.2.

b) Aliphatic Polycarbonates

The core level spectra for the aliphatic polycarbonates are

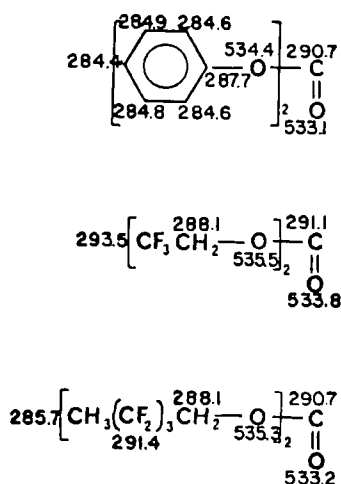


FIGURE 7.2

Calculated B.E.'s from CNDO/2 within the GPM formalism for
the model compounds

shown in Fig. 7.3. If we consider first the simplest of the series, namely the repeat unit containing $x = 4$, the C_{1s} spectrum consists of a doublet with the main photoionization envelope deconvoluted into two equal intensity peaks separated by ~ 1.6 eV. The peak to the higher binding energy in the envelope corresponding to the ester type carbon, of which there are two in the repeat unit and the lower binding energy peak corresponding to the remaining two center carbons. These chemical data are in excellent agreement with the data from the model compounds. The peak at ~ 290 eV can be recognized as the carbonate carbon ($-\text{O}-\overset{\text{O}}{\underset{\text{O}}{\text{C}}}-\text{O}-$) and its relative intensity ratio and absolute binding energy yield structural sampling of the repeat unit where $x = 4$ for the polymer system in Fig. 7.3. As the alkyl group increases in length from $x = 4$ to $x = 10$, the shoulder arising from the carbon atoms directly bonded to ester oxygens becomes less well resolved, but is still quite apparent for the $x = 10$ system. The relative intensity ratio of the central carbons to ester type carbons is in excellent agreement with the proposed structures.

In observing the O_{1s} core levels for the polymer systems it is apparent that the overall band profiles arise from the two peaks of

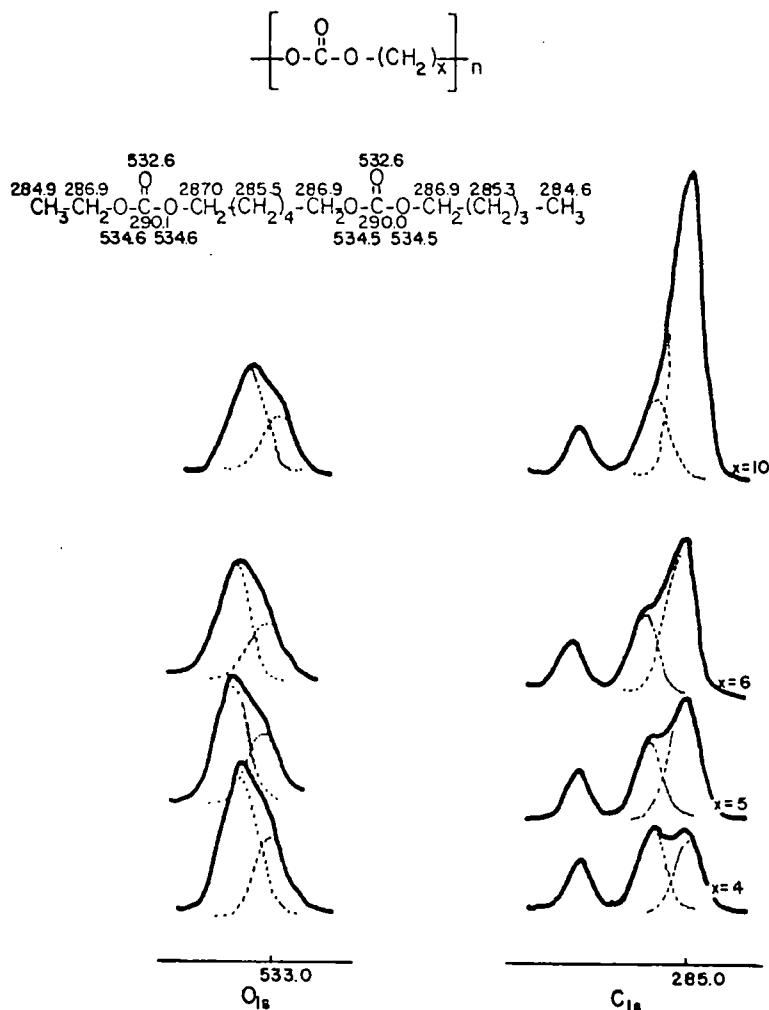


FIGURE 7.3

C_{1s} and O_{1s} core level spectra for the aliphatic polycarbonates

unequal intensity assigned to the carbonyl and ester oxygens, separated by ~ 1.5 eV. The absolute and relative binding energies are in excellent agreement with those of simple model systems from Table 7.2. In comparing the relative intensity ratios of the O_{1s} and C_{1s} core levels, with the appropriate sensitivity factors described in Chapter 3 for the core levels it can be shown that the core level spectra depicted in Fig. 7.3 are highly representative of the proposed structure for the aliphatic polycarbonate series. Also shown in Fig. 7.3 is the theoretical model used for the determination of absolute B.E.'s within the GPM formalism¹. The B.E.'s indicated on the model for the polymer system is further confirmation of the assignments given to the core level spectra for the polymers.

An interesting comparison can be made between an aliphatic and an aromatic polycarbonate and the core level spectra are shown in Fig. 7.4.

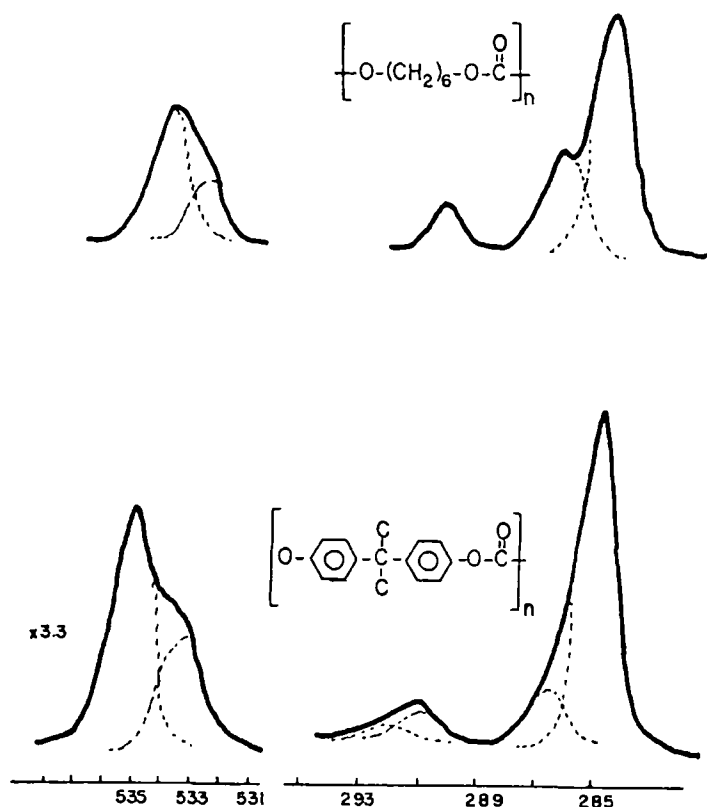


FIGURE 7.4

Core level spectra for a comparison of a typical aliphatic and aromatic polycarbonate

The C_{1s} spectrum of one of the poly (bisphenol A) carbonate samples shows, in addition to the characteristic peaks arising from the chemically shifted structural features, a low intensity peak to which the binding energy side of the main spectrum arising from the $\pi \rightarrow \pi^*$ transitions accompanying core ionizations in the aromatic systems. These shake-up transitions have centroids shifted ~ 7 eV from the primary photoionization peak^{58c,d,140} and, consequently, as a result of the carbonate type carbon being shifted by ~ 6 eV, an envelope appears in the spectra containing the two peaks. Based upon experimentally determined intensity ratios and binding energies for the $\pi \rightarrow \pi^*$ transitions relative to the primary photoionization peaks

in a number of aromatic systems^{58,140} an excellent assignment can be given to the spectra in Fig. 7.4. The observation of shake-up phenomena, therefore, gives a straightforward means of distinguishing between aliphatic and aromatic polycarbonates, and this unique use of shake-up phenomena has also been applied to other systems^{58,140}.

c) Polyglycolcarbonates

In Fig. 7.5 is shown the C_{1s} and O_{1s} core level spectra of a

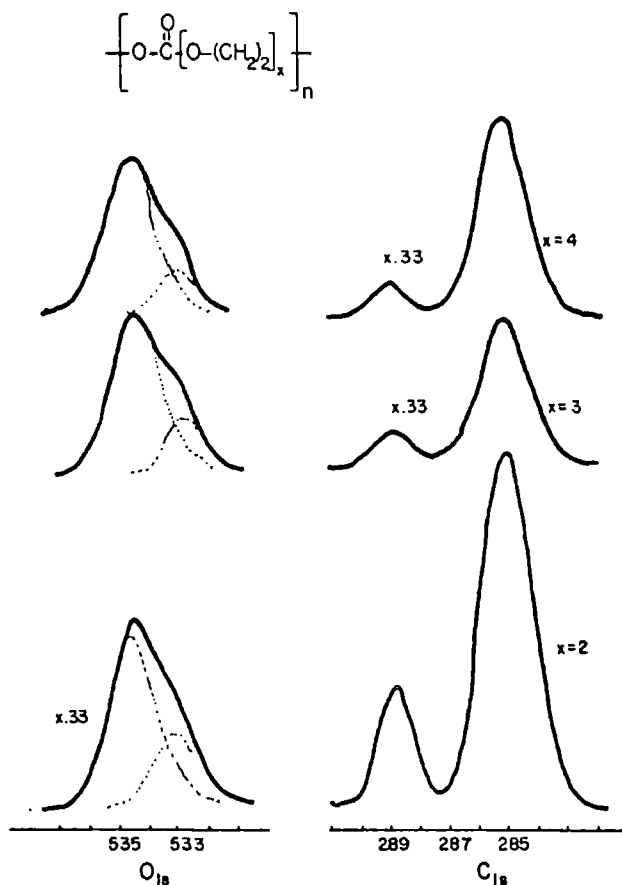


FIGURE 7.5

C_{1s} and O_{1s} core level spectra of polyglycolcarbonates

series of polyglycol carbonates where x is 2, 3 and 4. Similar arguments apply in the discussion of these core level spectra as to the aliphatic polycarbonates. The major difference of course, being that the intensity ratios of the ester type carbons to the carbonate type carbons is the only measure of the stoichiometry of the carbon system, since the repeat unit consists of $-\text{O}-\text{C}-\text{C}-\text{O}-$ centroid units

and these carbons all fall within a narrow absolute binding energy range and appear as a single peak in the spectrum. A comparison of the relative intensity ratio of the carbonate to ester type carbons in Fig. 7.5 reveals ratios in agreement with the proposed repeat units where $x = 2, 3$ and 4 , and absolute binding energies in agreement with simple model systems for the C_{1s} core levels.

The overall band profiles for the O_{1s} core levels follow identical agreements to those of the aliphatic polycarbonates, and a comparison of the O_{1s} to C_{1s} relative intensity ratios together with the appropriate sensitivity factors (cf. Chapter 3) reveal a statistically sampled polymer repeat unit corresponding to the proposed structures given in Fig. 7.5.

The theoretical models developed for the confirmation of binding energy assignments within the GPM formalism are shown in Fig. 7.6, and it is readily seen that the experimental data and

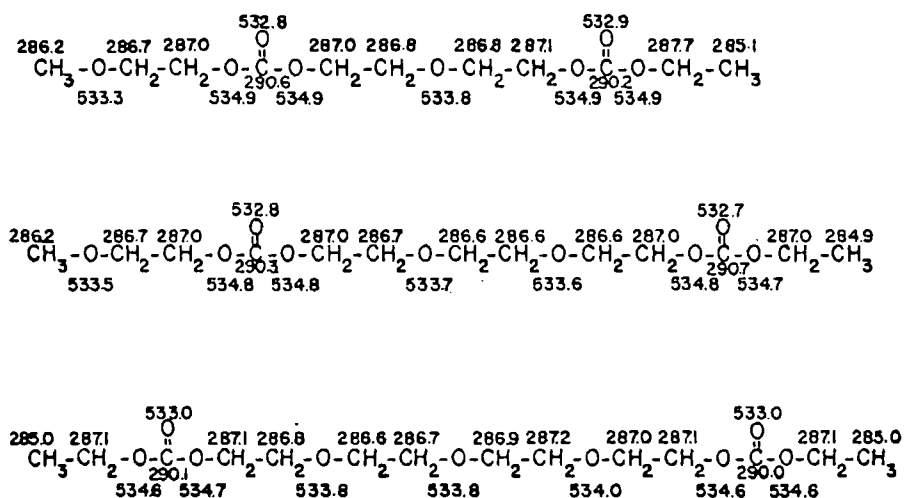


FIGURE 7.6

Calculated B.E.'s from CNDO/2 within GPM formalism
for polyglycolcarbonates

the theoretical models are in good agreement.

d) Fluorocarbonate Polymers

It is often the case that particular structural features may be characteristic of the end groups of a given polymer system. The

direct detection of such end groups by means of their characteristic binding energies provides a convenient means of establishing the degree of polymerization (DP) in low molecular weight material. (It is important to emphasize that the determination of the DP in polymer systems is highly dependent upon the polymer being investigated. For instance, the core level spectra for the three aromatic polycarbonates of differing \overline{MW} 's reveal no information with regard to the DP's.) However, a particularly favorable situation arises for systems in which the terminal groups involve CF_3 - residues where the chemical shift of the carbon is significantly higher in binding energy than other functional groups, e.g. $\sim 293.5 \text{ eV}^1$. If due care is taken to ensure that ESCA statistically samples the repeat unit (by, for example, considering the relative intensities of the same element with differing escape depth dependencies)^{125,127,137}, then the comparison of the area ratios for chemically shifted components of a given core level may be used to straightforwardly estimate the DP's. As an example, in Fig. 7.7 is shown the C_{1s} core level spectra for a series of low \overline{MW} fluorocarbonate polymers, of the general formulae indicated in the Figure. It has been shown by the appropriate model systems in Fig. 7.2 that the $-O-\overset{O}{C}-O-$ and $-CF_2-$ carbon $1s$ levels occur at approximately the same binding energy. The C_{1s} levels for the series of low \overline{MW} materials in Fig. 7.7 fall into three distinct regions and with the appropriate calibration of linewidths and lineshapes for the individual components from the model compounds, the analysis produces that, indicated by the dotted curves. From the relative areas of the CF_3 - component carbons to the $-CF_2-$ and $O-\overset{O}{C}-O$ carbon peaks the DP's may be calculated as shown in Fig. 7.8.

The two methods of comparing relative area ratios give slightly different results which may be due to specific orientation effects, however, the two methods are within $\sim 10\%$ and shown an excellent correlation with DP's determined on these materials by vapor pressure osmometry as indicated in Fig. 7.9. By contrast, the DP's as determined by ^{19}F NMR do not, however, agree with those determined by these two techniques, although the reason for the discrepancy is unclear.

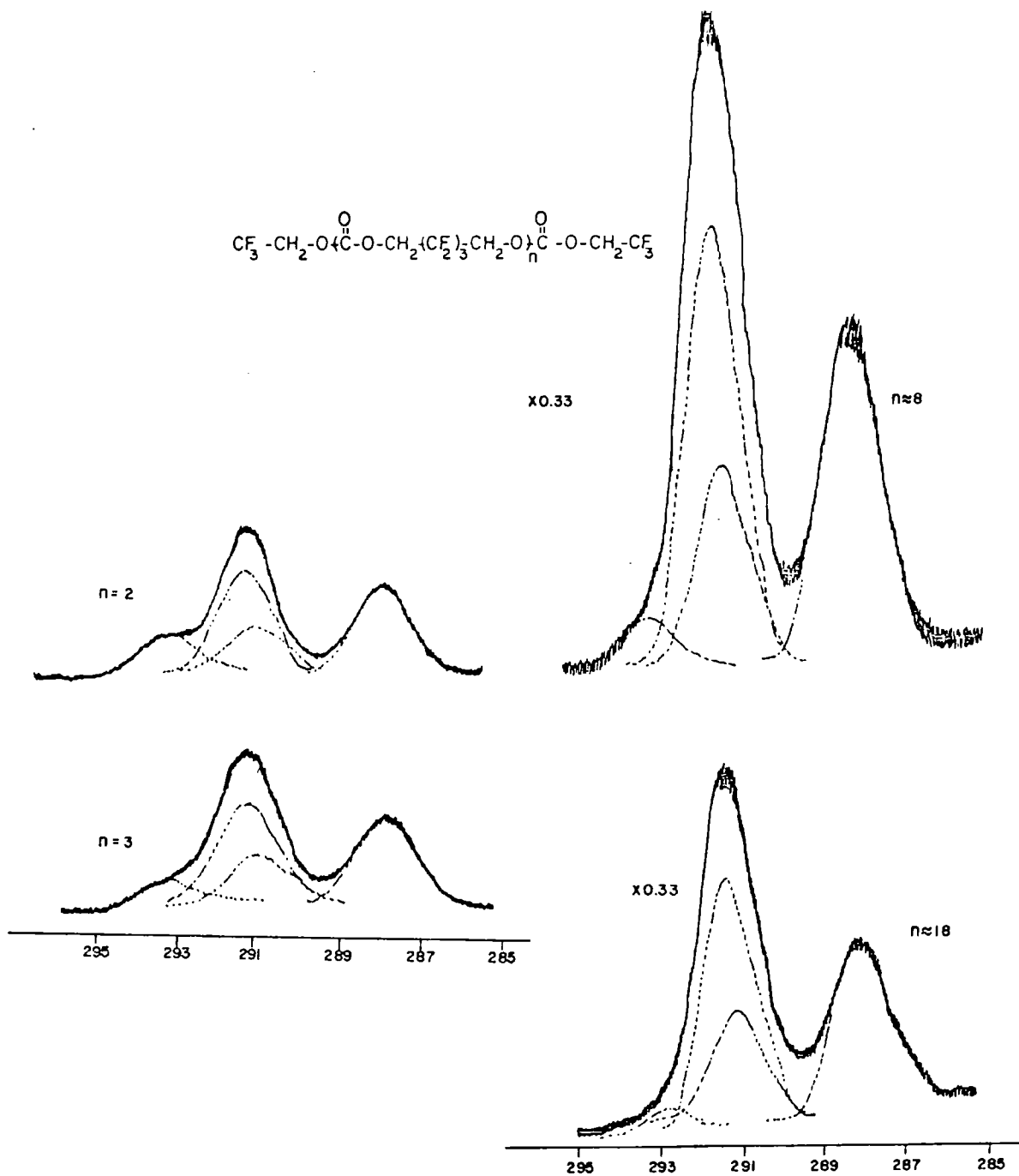


FIGURE 7.7

C_{1s} core level spectra for the series of low MW
fluorocarbonate polymers

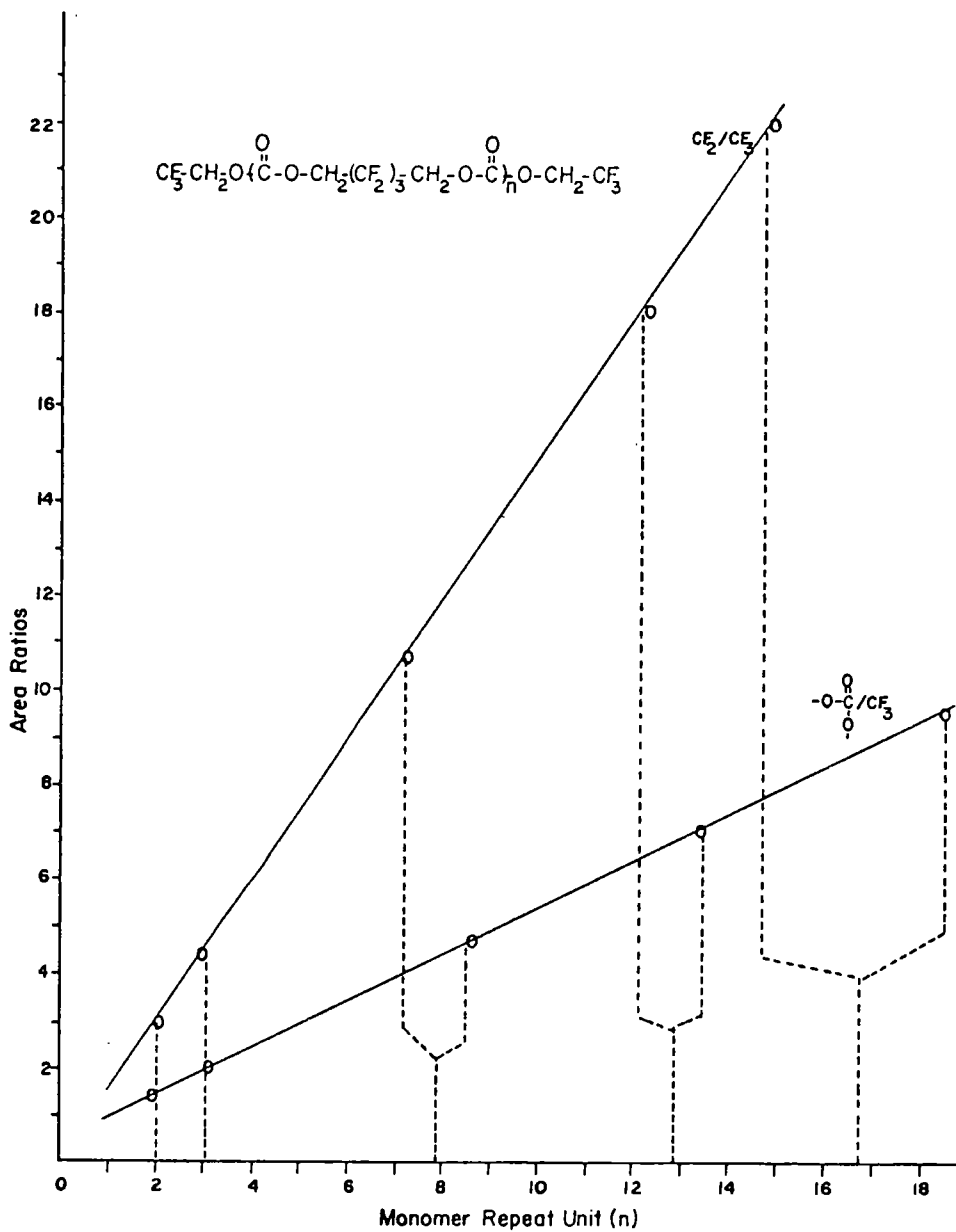


FIGURE 7.8

D.P.'s for low \bar{M}_w fluorocarbonates from area ratio
in the C_{1s} spectrum

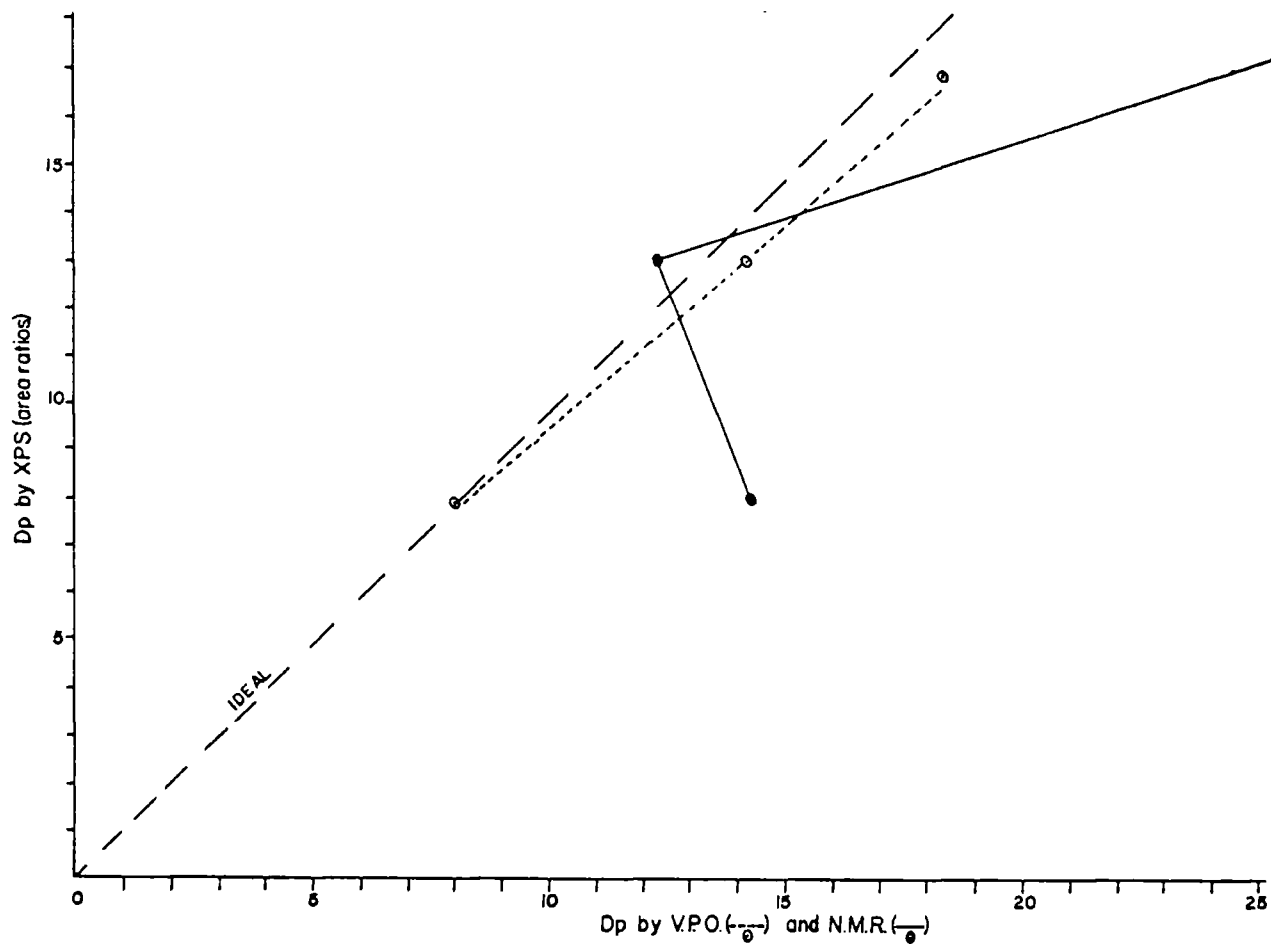


FIGURE 7.9
A comparison of the D.P.'s of the low \bar{M}_w
fluorocarbonates determined by ESCA, NMR and VPO

CHAPTER 8

An ESCA Investigation of Polymer-Metal Interfaces

CHAPTER 8

An ESCA Investigation of Polymer-Metal Interfaces

i) Introduction

In the preceding chapters, details have been presented on how ESCA may be addressed to the investigation of structure, bonding and reactivity in polymers. The radio-frequency plasma (RF plasma) treatment and oxidation of polymers and solids in general has been the subject of considerable research interest, both academically and industrially over the past decade (cf. reference 142). The surface properties of such modification make it difficult to employ conventional analytical techniques for understanding the processes which occur during surface modification by means of plasmas excited in a variety of gases. The great surface sensitivity of ESCA as a spectroscopic tool in this important area is clearly demonstrated by the fact that modifications effected under conditions of extremely low power loadings are detectable on time scales of the order of seconds^{127,142}. In appropriate cases where the core levels involved span a substantial range in kinetic energy for the photoemitted electrons, it is possible to derive considerable information concerning structure and bonding in the modified regions from an investigation of the primary sources of information provided by relative peak areas and absolute and relative binding energies^{1,127,128}. Thus, RF plasmas excited in oxygen at relatively high powers have routinely been used to selectively remove an organic phase so that the inorganic component in composites may be studied in the so-called plasma ashing procedure²⁴⁵. A similar technique has been used to prepare thin samples for investigation by electron spectroscopy²⁴⁵. It is clear that ESCA should have a considerable role to play in these types of surface studies and this chapter illustrates the potential of the technique for selective removal of an organic overlayer on a series of transition metals (Nb, Mo, W and Zr) by means of RF plasmas excited in argon and oxygen to enable direct studies to be made of the interface.

ii) Background

In many 'real life' situations it is often necessary to investigate metals with a contaminant overlayer which may be polymeric

in nature. For most metals used in typical working environments the systems to be investigated are quite complex, usually consisting of a metal/metal oxide system together with the overlayer. As we have pointed out in Chapter 4, electron mean free paths are extremely short and an overlayer of, say $\sim 100\text{\AA}$, would effectively obscure the core level spectra for the metal/metal oxide system which is often the focus of attention. The study of polymer/metal interfaces may, therefore, be approached by a technique which involves selective removal of the organic phase to a level where it is possible to 'see through' to the interface. The flexibility of RF plasmas excited in inert gases and oxygen in terms of instrumentation and close control of important variables (power, pressure, reaction time, etc.) facilitates the ESCA investigation of interfaces to obtain information on structure and bonding at the interface, the prime focus of attention being the metal core levels. Since the phenomenon of multiplet splittings in paramagnetic systems is inextricably linked with shake-up phenomenon, it should be stated, at the outset, that any study inevitably involves investigation of absolute and relative binding energies in addition to multiplet and shake-up fine structure. Over the past few years, studies of well characterized transition metal systems (mostly first row) has yielded valuable information on multiplet splittings and shake-up processes such that major areas of application of data derived from such studies (e.g. determining spin states, stereochemistry, electronic environment) can be delineated. The theoretical interpretation of such data is at a qualitative level with most of the broad features being understood^{152,246-249}. The obvious problems in taking advantage of these information levels in many real life situations arises from the overlayers that are generally present on the average commercial metal sample. The short mean free paths for the photoemitted electrons, therefore, obviates the possibility of using the information levels in principle available from the study of multiplet and shake-up phenomena in such systems. It is clear that with the background already available, the real problem in this area is a means of effectively cleaning the samples without chemically modifying the features of interest as far as the metal surface is concerned. In simple terms, if data of adequate signal/noise ratio and intensity can be obtained for the relevant metal core levels, the

currently available background on multiplet effects, shake-up phenomena and chemical shifts will be sufficient to derive the information on spin state, stereochemistry, etc. which one might hope to gain from the ESCA experiment. This data is not usually accessible from commercially produced surfaces because they are extensively contaminated.

The major research problem then resolves itself into developing a general method of removing most of this contamination without chemically disturbing the interface (i.e. you need to be sure that you are looking at the transition metal in its original state rather than that produced by the cleaning process). The obvious methods of solvent and degreasing treatments are known from previous work to be either unsuccessful or to lead to chemical modification of the surface to be studied. A further possibility is to use an argon ion gun and etch the surface, although this technique has problems since with the normal arrangement, any organic film is rapidly etched and selective sputtering of the underlying surface makes it difficult to control¹. In the work detailed in this chapter it is shown how controlled removal of contaminant films, to such a level that the metal/metal-oxide/contaminant interface may be directly investigated by ESCA, can be accomplished by use of low powered inductively coupled RF plasmas excited in oxygen and argon.

We can divide the mechanisms for removal of the contaminant overlayers into two distinct categories, 1) those exposed to an inert gas plasma where the overlayer is removed by 'ablation' and 2) those exposed to an oxygen plasma where the overlayer is removed by oxidation or 'ashing'; although at high power loadings ablation may also contribute. Considering firstly the features of inert gas plasmas at power loadings of 0.05 to 100 watts, and pressure ranges of 0.1 to 1.0 torr; the electron distribution may be approximated by a Maxwellian function which, in the pressure range of interest, peaks typically in the region of 0-10 eV¹⁴². The average electron energy is a function of the power and pressure and has been shown to increase with increasing ionization potential of the sustaining gas, while electron concentrations vary in the opposite sense¹⁴². While electrons play a dominant role in the plasma itself, in the interaction of a plasma, with a polymer they play a secondary role. Although there have been no definitive studies on the mean free paths

of electrons in the energy range of 0-10 eV in polymers, the generalized form of the mean free path as a function of kinetic energy (cf. Chapter 4) for most materials which have been studied in detail suggest mean free paths of hundreds of angstroms for near zero kinetic energy electrons. With these relatively long mean free paths, the direct energy transfer in the surface region of the overlayer is likely to be relatively small and dominated by phonon excitations. This, of course, lends itself nicely to a gentle technique for removing organic overlayers from metals. The ionization potentials and metastable energies of argon are 15.76, 15.94 and 11.55 and 11.72 eV, respectively, and although the positive ions and neutral species in the RF plasma have mean ambient kinetic energy, the ions and metastables have sufficient energy to cause ionization of the organic overlayer through ion neutralization²⁵⁰ and Penning ionization²⁵¹ processes, respectively. All of the energies given above are sufficiently large to ionize most polymers and organic overlayers. Although no attempt has been made here to distinguish between the mechanisms or to determine the kinetics of the RF plasma overlayer interaction, recent work of the effects on polymers of RF plasmas excited in inert gases has significantly enlarged the depth of understanding of these systems^{127, 142, 252-253}. In general, the authors have pointed out that valence ionization of the polymers is energetically feasible by direct interaction with the inert gas ions or metastables while for short wavelength vacuum U.V. radiation the largest contribution to the attenuation coefficient is undoubtedly from photoionization and from transitions to diffuse Rydberg states, which in the solid closely approximate, in properties, the ionized states²⁵²⁻²⁵³.

The RF plasmas excited in oxygen, however, have been studied in detail with respect to the composition and mechanism of atom formation by several authors²⁴⁵. The primary reactive species have been found to be $O_2^1\Delta_g$ molecules and O^3P oxygen atoms; their individual concentration ranging from 10 to 20% depending on the experimental conditions, including wall and other catalytic effects. Both the atoms and excited molecules react with the organic overlayers and numerous papers have appeared on these reactions. The mechanisms of reaction of oxygen atoms and its excited electronic states with other gas phase species comprise a number of exhaustive kinetic investigations, and in some cases activation parameters and rate constants

have been determined with a reasonable degree of accuracy (cf. 245 and references therein). However, in heterogeneous systems, the mechanistic data for the RF plasmas excited in oxygen cannot be interpreted easily and the oxidation for these systems is quite complex.

The interpretation of the ESCA spectra of the hydrocarbon and polymer overlayers with respect to the absolute and relative binding energies and the relative peak intensities corresponding to the appropriate core levels under investigation can be based on the extensive studies on organic systems detailed in Chapter 2 through 4. Chemical shifts in the carbon core levels corresponding to carbon attached to oxygens in different chemical environments are well understood and tabulated both experimentally and theoretically (cf. Chapter 3).

The model systems chosen for study were molybdenum, tungsten, niobium and zirconium. All of these metals, as normally investigated, have a hydrocarbon contaminant film and metal oxide system in the outermost few tens of angstroms. Molybdenum and tungsten are widely used in alloys and have very high cross sections for photoemission from the preferred core levels with the photoemitted electrons having considerable mean free paths. (Both of these features contrast strongly with the situation that exists for elements in the first transition series.) A further feature which distinguishes these systems is the complexity of the oxide formulations which nonetheless are fairly well characterized and provide a useful introduction to the use of line shape analysis procedures. The variety of available oxidation states for molybdenum, for example, provide a fine probe for following the removal of an overlayer since when the reactive species of the plasma reach the interface there are dramatic changes in the molybdenum core levels. Zirconium and niobium are included as examples of much simpler oxide systems and the choice of all these systems, in general, is based upon considerations of the metal/metal-oxide systems, of lattice energetics for the systems, particularly with regard to oxidation and reduction by species present in a typical 'cool' inductively coupled RF plasma excited in inert gases and oxygen.

iii) Experimental

The study of polymer/metal interfaces by the plasma ashing technique has led to the development of a particular reactor configuration which allows considerable flexibility in terms of sample handling and the investigation of the pressure and power dependence

of the surface modifications. The reactor employed in this study, shown schematically in Fig. 8.1, was mounted directly onto the insertion port of the ESCA spectrometer and pumped by a 50 liter/minute

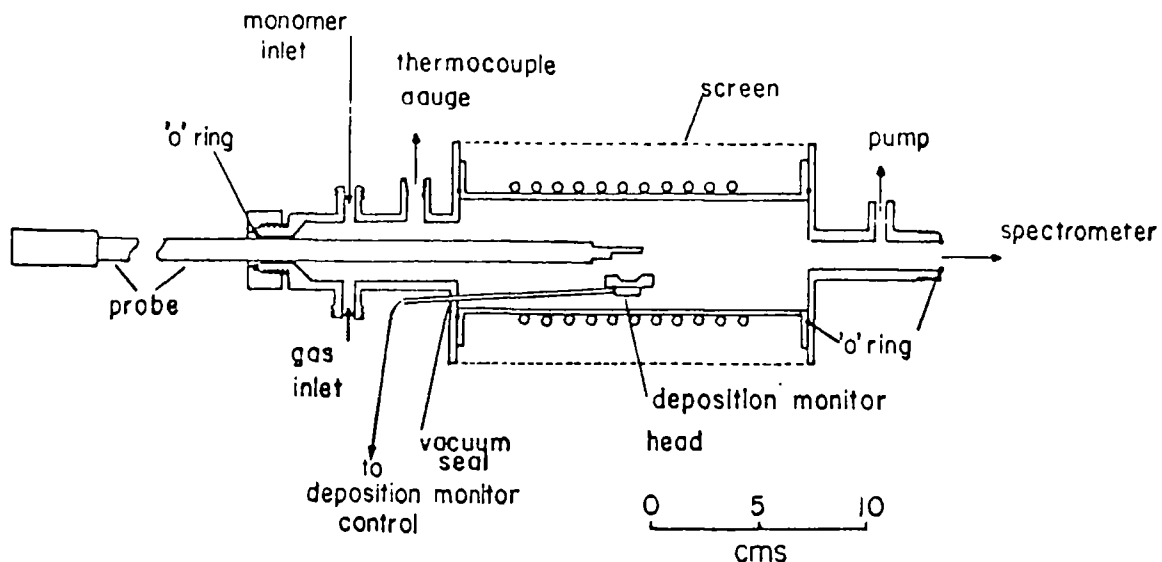


FIGURE 8.1

The plasma reactor and sample mounting

rotary vacuum pump system via a 1/2" copper tube. Pressures were recorded using a thermocouple vacuum gauge. The reactor consisted of a Pyrex tube 16 cm. long and 5 cm. diameter sandwiched between stainless steel flanges by Viton 'O' ring seals and enclosed in a copper mesh screen to prevent RF interference with the electronics of the spectrometer. The discharge was excited by a 4 μ H, 14 turn copper coil wound centrally on the Pyrex tube. Samples were mounted (by means of double-sided Scotch tape) on a 1/2" stainless steel probe, 60 cm. long which was capable of passing through the reactor on 'O' ring seals and into the spectrometer for analysis of the samples without being exposed to the atmosphere.

Plasmas were excited, in all cases, using a Tegal Corporation RF Generator capable of delivering a power output from 0.05 watts to 100 watts, continuously variable. A pulsing facility was used at

lower power levels, giving greater stability to the plasma. Tuning of the RF power was achieved by an L-C matching network and monitored by the standing wave ratio using a Heathkit HM102 RF power meter.

Research grade argon was used and purified by a sorption train (Hydro-Purge, Coast Engineering Laboratories, California, and Dow Gas Purifier, Dow Chemical Company, Midland Michigan) which removed hydrocarbons, water, carbon dioxide and oxygen. The oxygen was research grade and was used with no further purification. To maintain reproducibility from run to run flow rates were measured by monitoring the initial rise in pressure as a function of time when the reactor was isolated from the pumping system.

Spectra of the samples were recorded on an AEI ES200 B spectrometer using $Mg_{K\alpha_{1,2}}$ radiation and under the conditions employed in this investigation the $Au_{4f_{7/2}}$ level at 84.0 eV binding energy, used for calibration purposes, had a full width at half maximum of 1.15 eV.

Spectra were integrated by means of a DuPont 310 curve resolver. In all cases the measured binding energies are quoted with a precision of ± 0.1 eV and area ratios $\pm 5\%$, although these may be slightly generous limits for some of the samples, treated for long periods in the plasma, where the core level spectra exhibited fairly complex line shapes.

For each plasma run described in this chapter the cycle of operation was the same. The probe was first inserted into the reactor without a sample so that the tip was at a fixed geometry with respect to the reactor. The pressure was adjusted to that required for the particular run to be performed and the system allowed to purge for approximately half an hour before striking the glow and adjusting the power rating to that required. The probe was then withdrawn and a sample mounted, on the probe tip by means of Scotch tape ensuring that no tape was exposed. On replacing the probe the pressure was re-adjusted before each discharge period and the system purged for half an hour before the first and 5 minutes before subsequent periods. The time intervals of the discharge periods were such that the total treatment time increased as discussed in the next section. After each discharge the probe tip was advanced into the spectrometer, via the 'O' ring seals and a gate valve, for analysis of the sample. Spectra were recorded as fast as possible (~ 3 minutes) to minimize hydrocarbon

contamination from the spectrometer onto the sample.

The transition metals selected for this study were studied as received without rigorous pretreatment to prepare the surface. The polymer overlayer, applied directly to the molybdenum surface was polychloro-p-xylylene and the procedure of the vapor phase polymerization onto the transition metals was described thoroughly in Chapter 4. Hydrocarbon contamination build-up on the surface was accomplished by allowing the X-ray cap to heat in the spectrometer with the sample in close proximity. Details of this technique are described in Chapter 3 under the heading, "Energy Referencing".

iv) Results and Discussion

As representative examples of a complex and simple metal/metal oxide system we consider in detail the results for molybdenum and zirconium, respectively. Metal surfaces generally involve a combination metal/metal oxide surface both of which may readily be characterized by their respective core level spectra. If we take molybdenum, for example, a considerable amount of data has been tabulated in the literature²⁵⁴⁻²⁵⁷ on the absolute binding energies for the relevant core levels on the complex metal/metal oxide surface. The binding energies for the $MO_{3d}^{5/7,7/2}$ core levels, which have the highest cross-section for the $Mg_{K\alpha_{1,2}}$ photon source, are shown in Table 8.1, along with the binding energy for the O_{1s} levels.

<u>Molybdenum/Molybdenum Oxide System</u>					
(BE in eV)					
	MoO_3	MoO_x	MoO_2	Mo	O_{1s}
MO $3d\ 5/2$	232.2	231.2	229.3	228.0	530.5
$3d\ 7/2$	235.5	234.2	232.4	231.2	
FWHM	1.4 ± 0.2	2.1 ± 0.2	1.6 ± 0.2	1.3 ± 0.3	

TABLE 8.1

From the table it is apparent that the different oxidation states for the metal oxides are sufficiently shifted for analysis and identification by ESCA and whilst the FWHM for the Mo_{3d} levels associated with the Mo, MoO_2 and MoO_3 structures are closely similar, those for the MoO_x oxide phase where $2 < x < 3$ are considerably broader. This has been

attributed to some seven oxide phases intermediate between MoO_2 and MoO_3 ²⁵⁸. The O_{1s} levels appropriate to the metal oxides appear as a relatively broad peak centered at ~ 530.5 eV, which is conveniently removed to lower binding energy with respect to oxygens attached to carbons in the contaminant layer or for hydrogen bonded water. It is important to note that with a knowledge of spin-orbit coupling, FWHM and chemical shifts in binding energy it is relatively straightforward to analyze the complex lineshapes which arise for typical metal/metal oxide systems to obtain the components. For a study such as this, where we are essentially monitoring the metal core levels to establish the point at which the polymer/metal or contaminant/metal interface becomes exposed during the overlayer removal step, a knowledge of the various factors described above is essential.

To illustrate the controlled nature of the overlayer removal step, Fig. 8.2 shows the core level spectra for the initial sample of

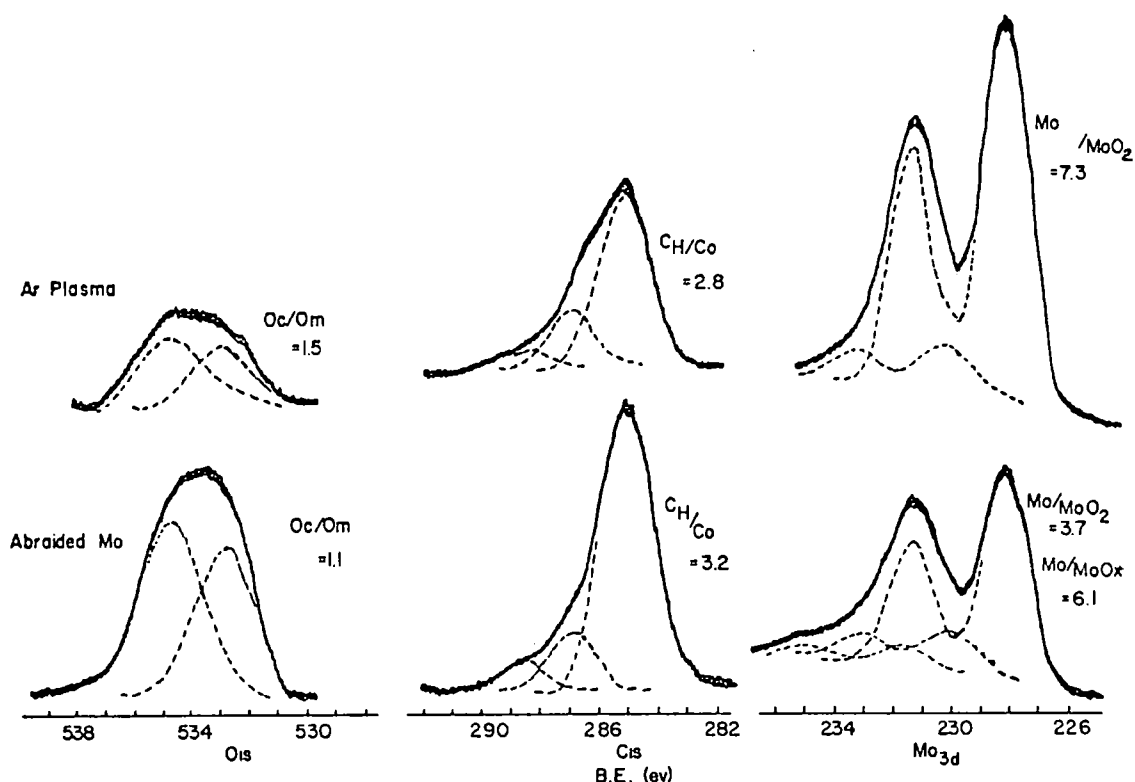


FIGURE 8.2

Core level spectra for molybdenum sample treated in an argon plasma

abraded molybdenum (a) and that treated in an industrially coupled RF plasma excited in argon (10 watts, 100 μ , 45 minutes) (b). Considering first the abraded molybdenum sample, an analysis of the Mo_{3d} core levels indicates that the metal contains an oxide layer comprised of MoO_2 and MoO_x phases and based upon the relative intensities of the oxides to the metal levels, this is comparatively thin. The C_{1s} spectrum, when deconvoluted into three components corresponding to COOH, C=O and CH structural features in going from high to low binding energy, reveals the nature of the contaminant overlayer. The O_{1s} core levels may be similarly deconvoluted into two components corresponding to oxygens involved in the inorganic oxide phase (low binding energy component) and organic overlayer (high binding energy component). It is worthwhile at this point, before proceeding to the discussion on the argon plasma treatment, to demonstrate the inhomogeneous nature of the composite metal/metal oxide/contaminant overlayer system in the results of an angular dependent study shown in Fig. 8.3. At a high take-off angle for the photoemitted electrons (going towards grazing exit) the surface features are enhanced (as discussed in Chapters 1 & 4) and it is readily apparent that the organic material is present as an overlayer on the metal/metal oxide surface. The relative intensity ratios for the carbon and oxygen core levels indicate that the oxidized component of the organic phase is at the metal oxide interface.

The argon plasma treatment (Fig. 8.2b) of the abraded molybdenum surface reduces the MoO_x phases and the relative intensity ratios of the Mo/MoO_2 increases from 3.7 to 7.3 in going from the abraded to argon plasma treated samples. The relative intensity ratios of the Mo metal to the carbon and oxygen contaminant layer also increased quite substantially which is readily apparent in Fig. 8.2. It is interesting to note that even after the argon plasma treatment for 45 minutes that the organic overlayer contaminant phase is still apparent in the spectra and this can be attributed to two effects. Firstly, the ions and metastables present in the RF plasma tend to cause predominantly crosslinking to occur within the organic phase in addition to gentle ablation. It could be anticipated that even considering the gentle ablation, that the crosslinked film may be relatively resistant to ablation. Secondly, although for typical organic polymer and hydrocarbon contaminated metal surfaces, the sticking coefficient for extraneous hydrocarbon in the spectrometer source is extremely low^{1,127}, this is certainly not the

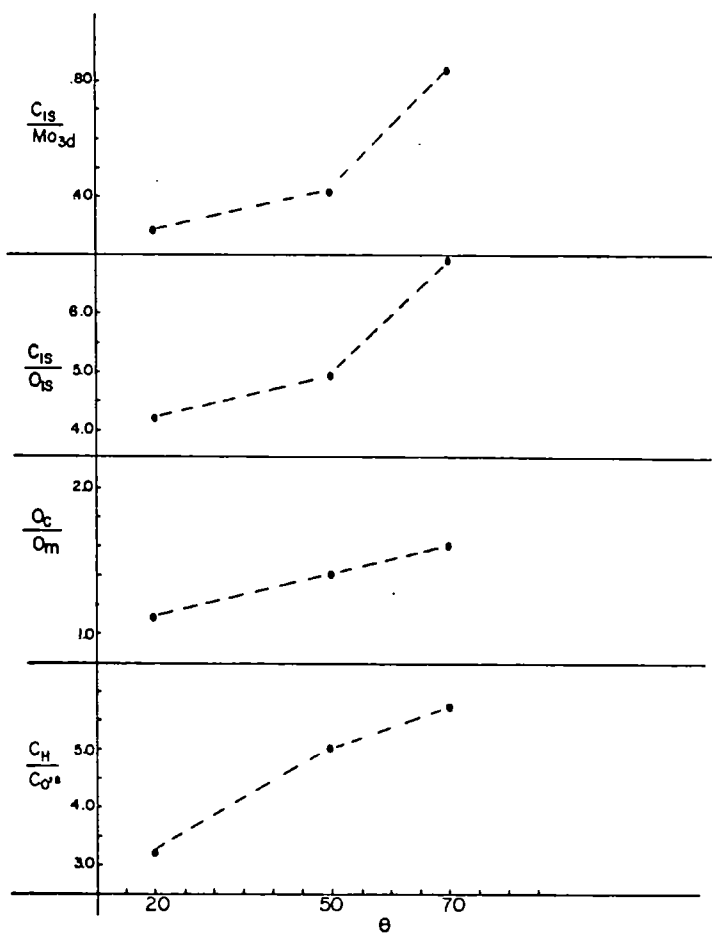


FIGURE 8.3

Angular study on abraded molybdenum sample

case for the catalytically active 'clean' metal/metal oxide surface. At a typical base pressure of 10^{-8} torr, therefore, the argon plasma ablated metal/metal oxide surface has an extremely high sticking probability and the major contribution to the low binding energy component in the C_{1s} spectrum of the plasma treated sample, therefore, can be attributed to extraneous hydrocarbon scavenged from the residual spectrometer atmosphere. This is an important point since it is possible for sticking coefficients to differ by four or five orders of magnitude from the initial 'contaminated' surface to the final 'clean' surface²⁵⁶⁻²⁵⁷.

Now considering a different sample of abraided molybdenum, Fig. 8.4 shows the effects of two successive treatments with plasmas excited

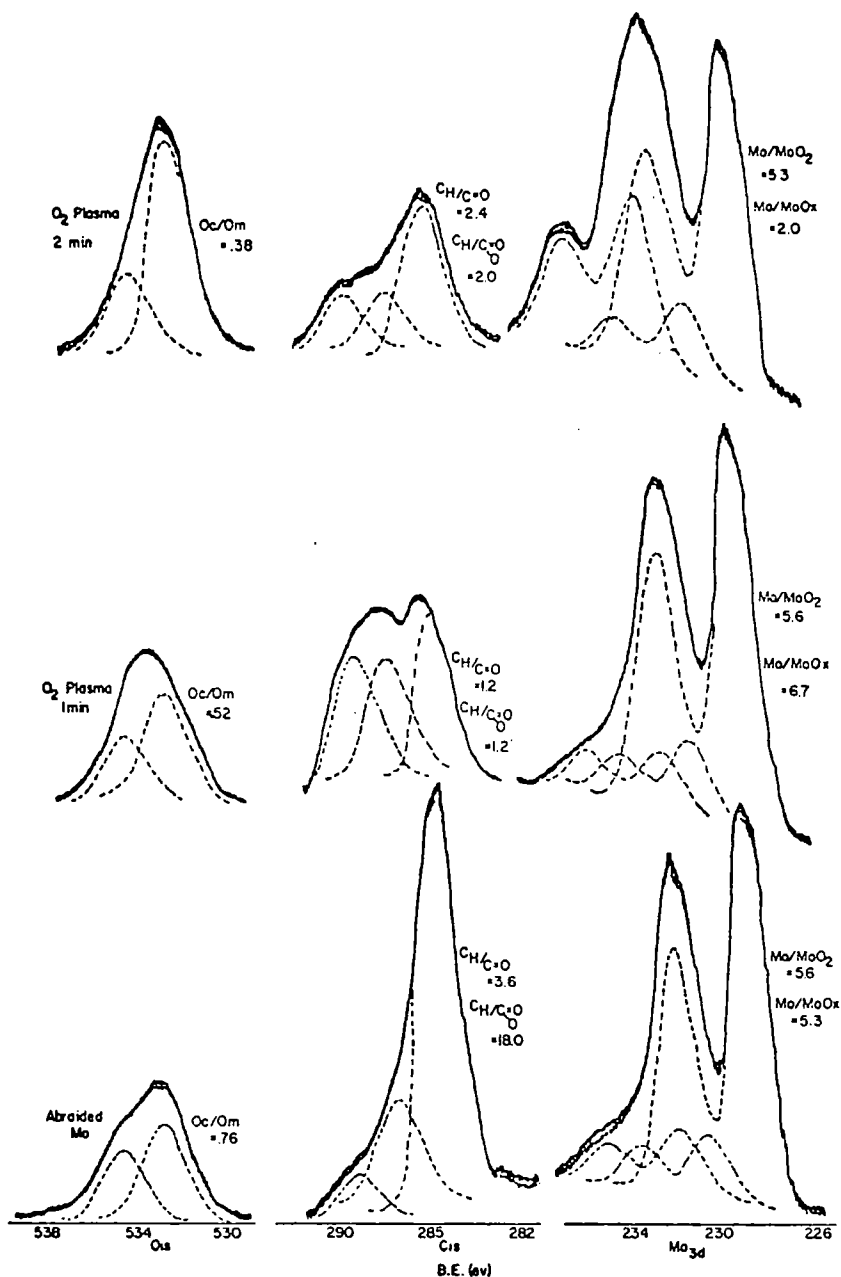


FIGURE 8.4

Core level spectra for molybdenum sample treated in an oxygen plasma for successive one-minute exposures

in oxygen for one-minute periods each (at 100 μ and 25 watts). In core level spectra for the abraided molybdenum sample are shown in Fig. 8.4(a) and although there are subtle differences in the spectra relative to the abraided sample shown in Fig. 8.2 (a), in general the surfaces constitute

similar chemical structure. After the first one minute period of exposure to the oxygen plasma (Fig. 8.4 (b)) it is clear that the interface remains intact since the metal core levels remain essentially unchanged. The form of the C_{1s} and O_{1s} core levels, however, change quite drastically as the hydrocarbon overlayer is oxidized. A reduction in the $-CH-$ type core levels and an increase in the oxidized carbon levels is consistent with an oxidation of the hydrocarbon overlayer. After a further one minute exposure (Fig. 8.4 c), however, the Mo_{3d} levels is significantly modified as the interface is reached. The O_{1s} core levels also manifest this in that the ratio of the metal bonded oxygens (O_m) increase significantly with respect to the carbon bonded oxygens (O_c). It is again interesting to note that the low binding energy component of the C_{1s} levels is still apparent and this may be rationalized along the same lines as presented above. However, the fact that the dominant effect is the conversion of the MoO_2 oxide phase to the MoO_x phases and of the Mo metal to MoO_2 without the production of significant quantities of MoO_3 indicates the selective nature of the oxygen plasma treatment.

In a further series of experiments, an abraided sample of molybdenum was deliberately contaminated in the spectrometer source such that a hydrocarbon contaminant film several monolayers thick was produced. The results of successive oxygen plasma treatments for periods of a minute on the Mo_{3d} levels are shown in Fig. 8.5, along with a plot of

the rapid removal of hydrocarbon ($C_{1s}(1-\frac{I_0}{I_\infty})$ -vs-time) superimposed over the spectra. The removal of the hydrocarbon contaminant overlayer to reach the metal interface is clearly evident in Fig. 8.5 at power loadings of 20 watts at 100μ . As the hydrocarbon overlayer is removed, the extent of oxidation rapidly increases. The rapid change in the metal core level spectra as the interface is reached provides a very convenient indicator for control of the system and this will generally be the case for metal/metal oxide/overlayer systems. It should be noted that the C_{1s} core level spectra are also highly diagnostic at the stage just prior to reaching the interface and are characterized by two components of equal intensity, ~ 289 eV and ~ 287.5 eV associated with the $-C_{OH}^0$ and $\dot{C} = 0$ carbon components, respectively, and a lower binding energy component centered at ~ 285 eV attributable to extraneous hydrocarbon material scavenged by the metal/metal oxide surface.

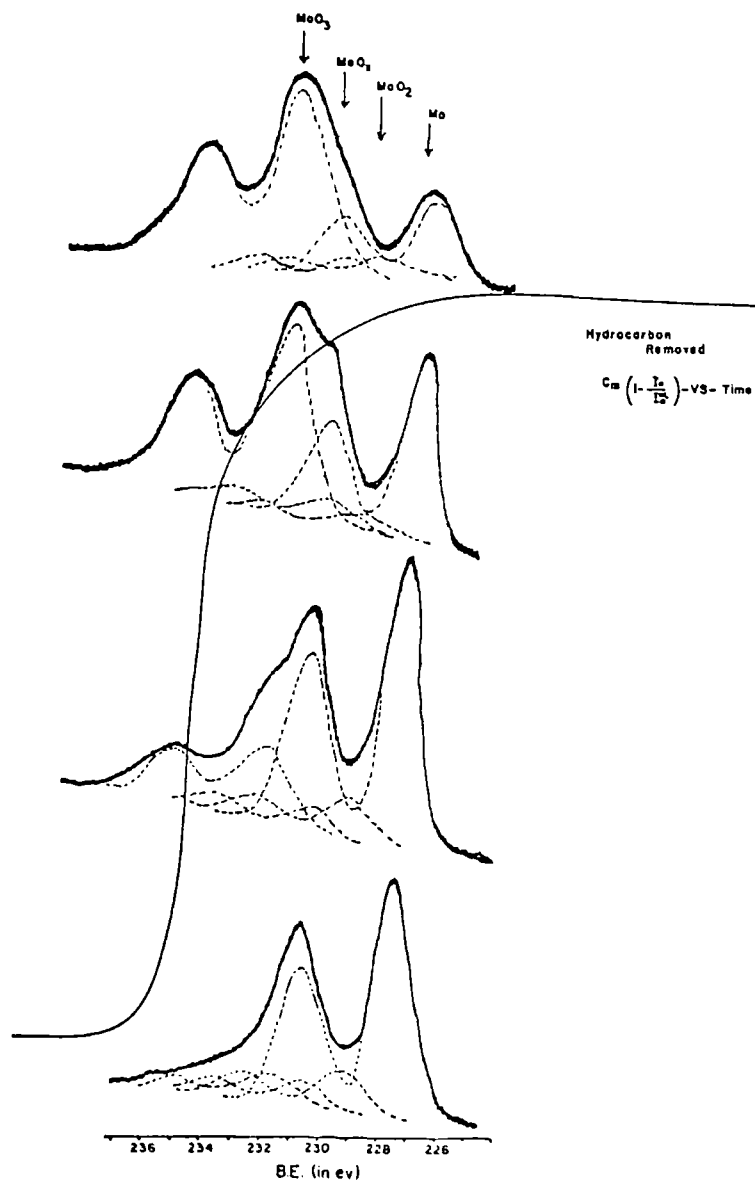


FIGURE 8.5

Molybdenum 3d core levels upon successive oxygen plasma exposure,

plot of $(1 - \frac{I_0}{I_\infty})_{C_{1s}}$ overlayer -vs- time superimposed on spectra

Having established that the plasma treatment is sufficiently selective to allow the direct investigation of interfaces, thin polymer films of known thickness were prepared by in-situ polymerization of the pyrolysis product of [2.2] paracyclophane as described in Chapter 4. The chloro derivative, Dichloro [2.2] paracyclophane, was chosen for a variety of

reasons, the primary one being the ease of control of generating thin films on metal/metal oxide substrates. With the use of a quartz crystal microbalance it was possible to deposit films of known thickness directly onto the abraded molybdenum substrates. Preliminary experiments demonstrated that the oxidation of the polychloro-p-xylylene overlayer proceeded at a much faster rate than for the typical hydrocarbon contamination and at a power loading of 10 watts a 300Å polymer film was removed in about 20 minutes. In Fig. 8.6 are shown the successive oxygen plasma

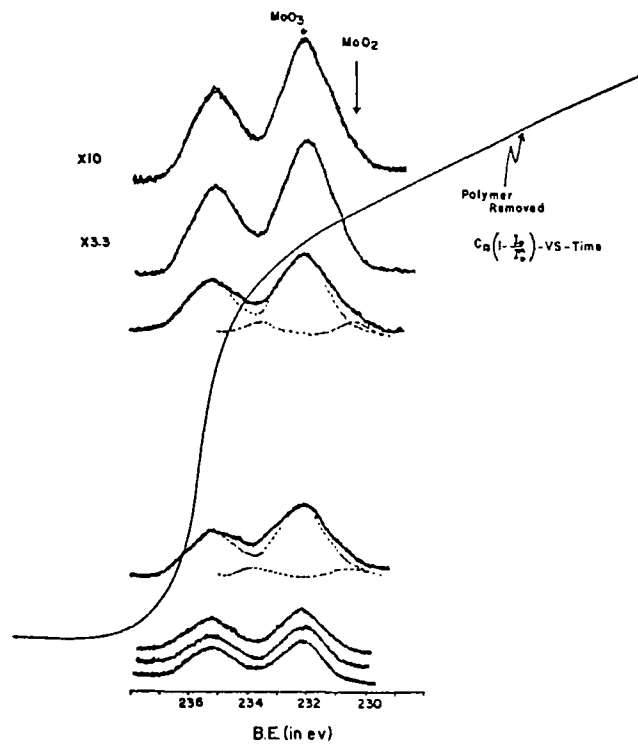


FIGURE 8.6

Molybdenum 3d core levels upon successive oxygen plasma exposure

to the polymer overlayer, plot of $(1 - \frac{I_o}{I_o})_{C_{1s}}$ polymer overlayer

-vs- time superimposed on spectra

treatments of the polymer coated molybdenum substrate and the very rapid removal of the polymer overlayer with time. It should be noted that the

C_{1s} core levels reveal essentially complete removal of the polymer film as shown in Fig. 8.7 after a seven minute exposure.

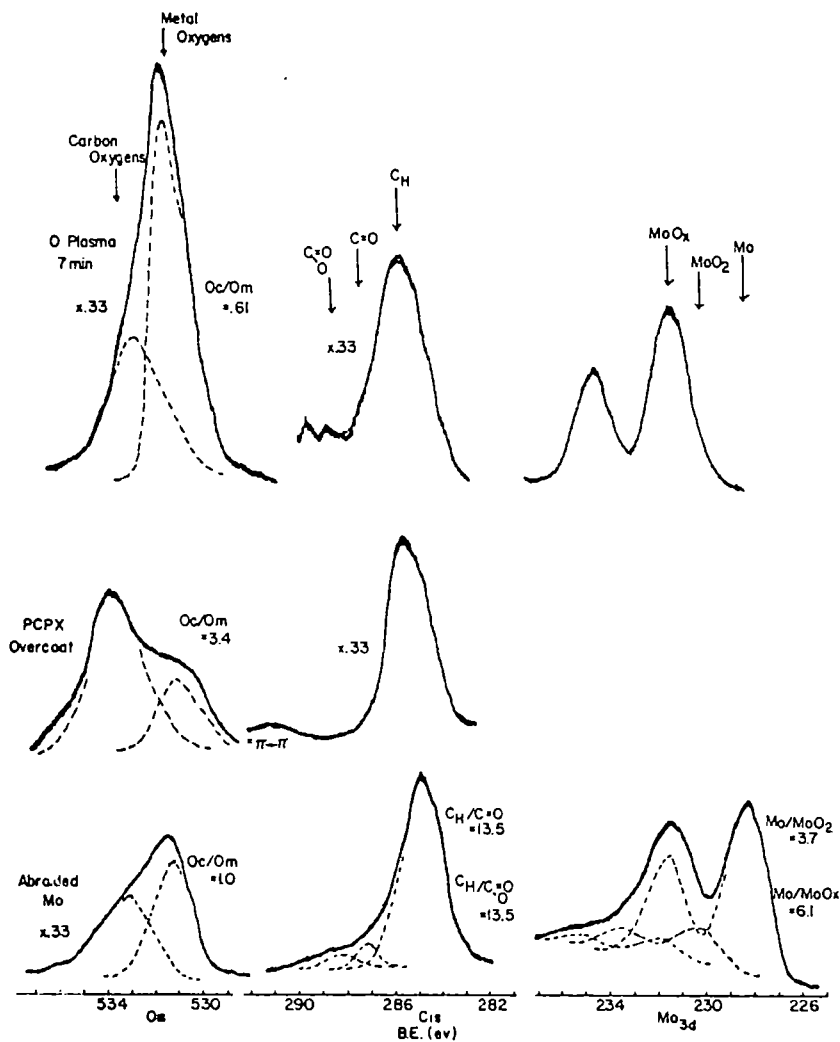


FIGURE 8.7

Core level spectra for molybdenum overcoated with polyparaxylylene and exposed to an oxygen plasma

With these two quite different results in the removal of the organic overlayer from the molybdenum substrate competitive experiments were carried out with a polymer overlayer of about 30\AA (at which level the substrate Mo_{3d} levels are observed at relatively low attenuation) and a hydrocarbon overlayer of about 15\AA thick, a level reached in a

reasonable time (3-4 hours) in the spectrometer. It again was a straightforward matter to monitor the increase in intensity of the substrate core levels as the over layers were removed, before the oxygen plasma modified the interface itself. That the rate of removal of the hydrocarbon overlayer is slower than that of the polychloro-p-xylylene is evident from the data in Fig. 8.8. It should also be noted that the induction period

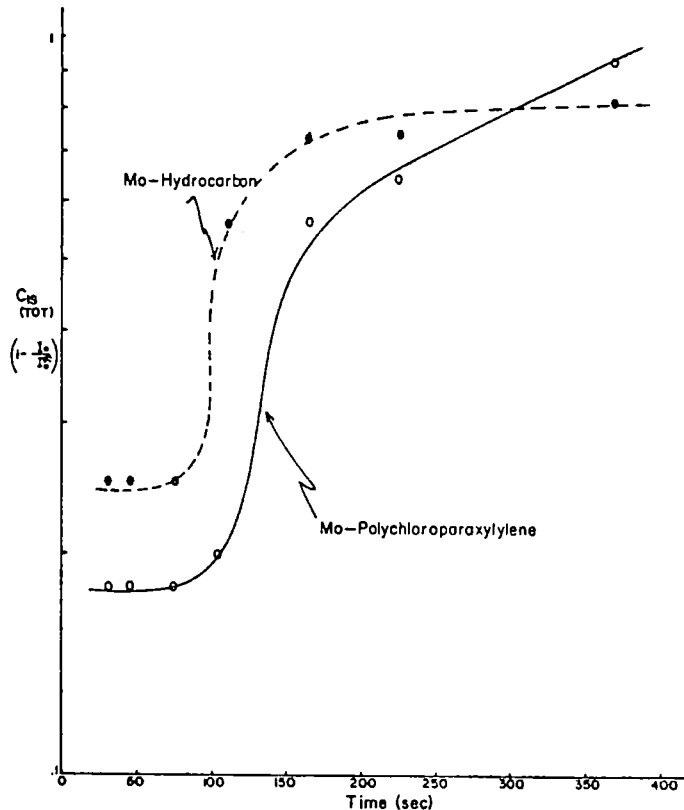


FIGURE 8.8

Absolute intensity ratios for hydrocarbon and polymeric overlayers on molybdenum exposed to an oxygen plasma

of approximately 50 - 100 seconds is associated with the generations of $\text{-C}=\text{O}$ and $\text{-C}=\text{O}$ structural features in the organic phase before a significant removal of organic material takes place. There is some evidence that at the very interface, the oxidized organic phase is strongly bound to the inorganic phase and that it is somewhat dependent upon the structure of the initial system. It should be noted in Fig. 8.8 that the curve for the polymer overcoating approaches unity (an arbitrary value

where all the overlayer is removed), whereas for the hydrocarbon overlayer the curve levels out at about .8 and under the conditions employed for the oxygen plasma, did not show any marked decrease in the overlayer with time. The generation of polyfunctional low molecular weight materials at the interface which can behave as good ligands, might well form the basis for this observation. It should also be noted that the sticking probability for the extraneous hydrocarbon depends markedly on the surface structure produced during the plasma modified surfaces.

For zirconium, an example of a simpler metal/metal oxide system, a similar picture emerges for that found in the molybdenum system as shown in Fig. 8.9 on the angular dependent study on an abraided zirconium sample. The core level spectra for the zirconium sample exposed

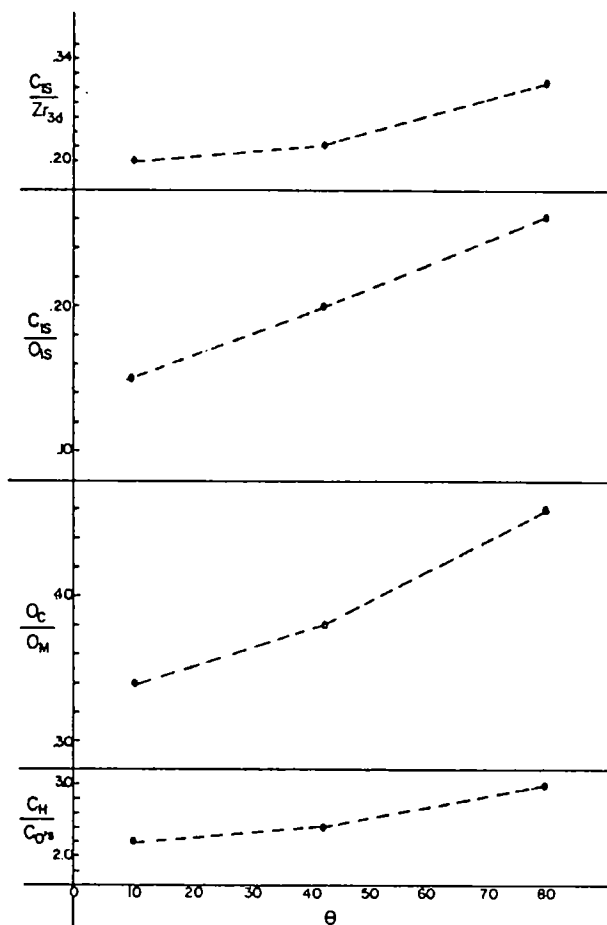


FIGURE 8.9

Angular study on abraided zirconium sample

to an oxygen excited plasma are shown in Fig. 8.10 and again the most interesting feature is the controlled removal of the hydrocarbon overlayer until the interface is reached when the low molecular weight

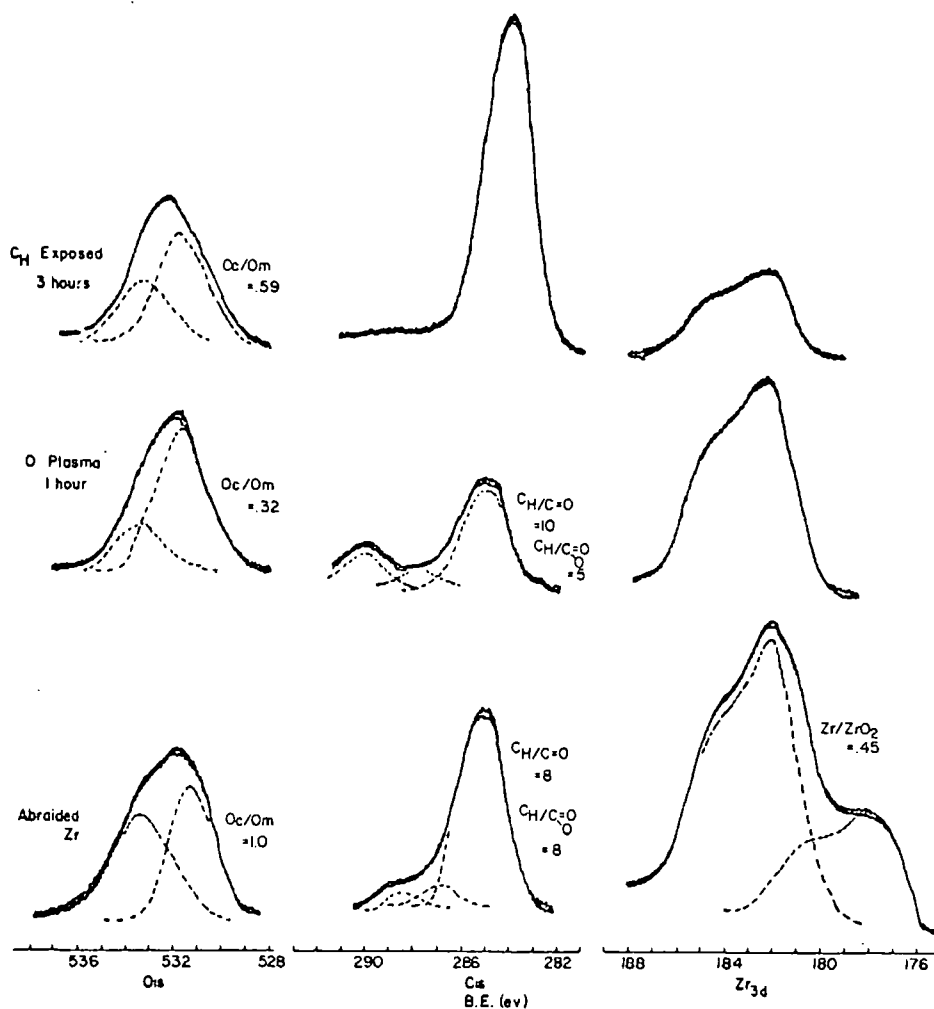


FIGURE 8.10

Core level spectra for zirconium sample treated in an oxygen plasma for 1 hour and exposed to hydrocarbon

oxidized material interacts strongly with the metal/metal oxide system and is, therefore, not readily removed. The high sticking probability for extraneous hydrocarbon manifest for the molybdenum system previously discussed, is also apparent for the zirconium active surface. In this case, however, the oxide system is basically very much simpler,

consisting of essentially a ZrO_2 phase²⁵⁵. Again, it can be readily shown that the contaminant overlayer may be selectively removed to such a level that the substrate core levels for the metal/metal oxide may be investigated at a good signal/noise ratio.

Similar results were obtained for the niobium and tungsten surfaces and the results of the studies on all the systems are displayed in Fig. 8.11. The basic trends on the selective removal of the contaminant

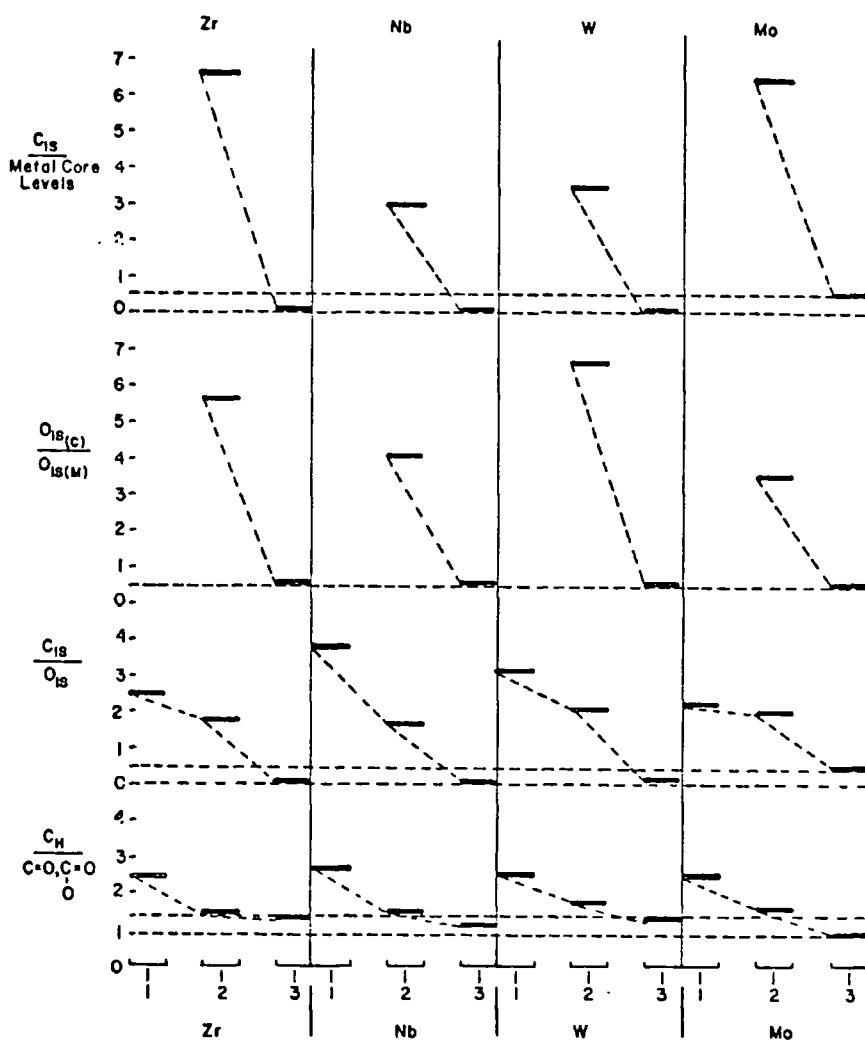


FIGURE 8.11

Comparison of the changes in the relative intensity ratios for carbon, oxygen and metal core levels when exposed to successive oxygen plasma treatments

overlayers are displayed revealing the similarity in studying substrate core levels on intact systems. By studying appropriate model systems it should be possible to establish the 'etching rates' for organic contaminant overlayers, enabling closer control of the approach to the interface and the determination of the thickness of the overlayer. The flexibility of the RF plasma instrumentation would allow convenient 'etching rates' in the thickness ranges from a few to several thousand angstroms.

CHAPTER 9

The Application of ESCA to the Structural Determination
of a Fluoropolymer

CHAPTER 9

The Application of ESCA to the Structural Determination of a Fluoropolymer

i) Introduction

We have discussed in the previous eight chapters the application of ESCA in the determination of structure, bonding and morphology of surfaces in general with particular emphasis on polymeric surfaces. In the experimental chapters from three to eight, we have developed the usefulness of ESCA in the investigation of well characterized materials to define parameters such as absolute and relative binding energies, relative intensity ratios for specific core levels, electron mean free paths, etc. These studies have not only added to the accumulation of an ESCA data bank on polymers of which Clark and co-workers (cf. reference 1, 127, 128) have already contributed a substantial portion, in fact, except for a few isolated publications, nearly all), but now enable us to progress, with the aid of all the data, to examine systems that have heretofore eluded other analytical techniques because of experimental difficulties. In this chapter we present such a system; a polymeric material, hereafter referred to as PP-9, which forms a substantial part of the by-product in the catalytic fluorination route to polyfluorobenzene from Imperial Smelting Corporation (a subsidiary of Rio Tinto Zinc). This material is highly insoluble in the common solvents used in standard polymer analytical techniques, lending itself to ESCA investigation very nicely.

ii) Experimental

The material, PP-9, as received from Imperial Smelting Corporation, had an apparently low T_g at room temperature, was glassy and cold-flowed reasonably rapid (for instance, a coating one inch long on the inside of a glass tube would flow to the bottom of the tube in approximately two hours at room temperature). Several attempts at recrystallization of the PP-9 from various aliphatic and aromatic solvents was unsuccessful, due to the insolubility of PP-9. However, two fluorinated solvents, namely $CFCl_3$ and 1,1,1,3,3,3-Hexafluoroisopropanol (Pierce Chemical Company) were found to be reasonable solvents for PP-9 at elevated temperature, with the former the superior of the two.

Therefore, the following samples were prepared for analysis by ESCA:

- 1) Neat PP-9, as received, designated PP-9n
- 2) PP-9 solubilized in boiling CFCl_3 and recrystallized by allowing to stand at room temperature overnight, designated PP-9c
- 3) PP-9 solubilized in boiling CFCl_3 and precipitated into hot benzene and allowed to stand overnight at room temperature. This system was divided into two samples (a) the material that precipitated out of solution overnight, designated PP-9p and (b) the material remaining in the supernate which was coated onto gold by solution casting and allowing the solvent to evaporate, designated PP-9s.

All solid samples were coated onto a gold substrate and heated slightly ($\sim 30\text{-}40^\circ\text{C}$) to form a thin film for ESCA analysis.

The ESCA instrumentation has been described in previous chapters (3-8) and the deconvolution of the core level spectra was accomplished with the Dupont 310 curve resolver, described in previous chapters.

iii) Discussion of Results

A wide scan of the neat PP-9n revealed only carbon and fluorine elements present (although hydrogen cannot be identified with ESCA, cf. Chapter 1) and, therefore, high resolution narrow scans of the C_{1s} and F_{1s} core levels were made to determine the relative ratios of carbon and fluorine and the particular features of the C_{1s} core level spectra, and these are shown in Fig. 9.1. The C_{1s} core level spectrum revealed a rather complicated envelope and in order to establish a reference binding energy, hydrocarbon contamination was allowed to build up on the sample over a period of five (5) hours, (cf. Chapter 1 for the rationale of using hydrocarbon contamination for a reference binding of 285 eV). The C_{1s} core level spectra for the 0, 2 and 5 hour data points are shown in Fig. 9.2. Although the F_{1s} core level spectra are not shown for these samples, the binding energy was not shifted during hydrocarbon build-up and only the intensity decreased, as would be expected. Using the hydrocarbon reference line at 285.0 eV, a deconvolution of the envelope was made with assignments of absolute binding energies for the respective peaks, including the F_{1s} core levels and F_{2s} core-like levels and these are shown in Fig. 9.3.

Firstly, the absolute binding energy assignments for the F_{1s} and F_{2s} core levels as indicated in Fig. 9.3 are in excellent agreement with those found by Clark and co-workers on a sampling of a large number of fluoropolymer systems^{1,126,127,128}, namely F_{1s} (690.1 eV) and F_{2s} (33.3 eV). It is especially interesting to note that for the F_{1s} levels the

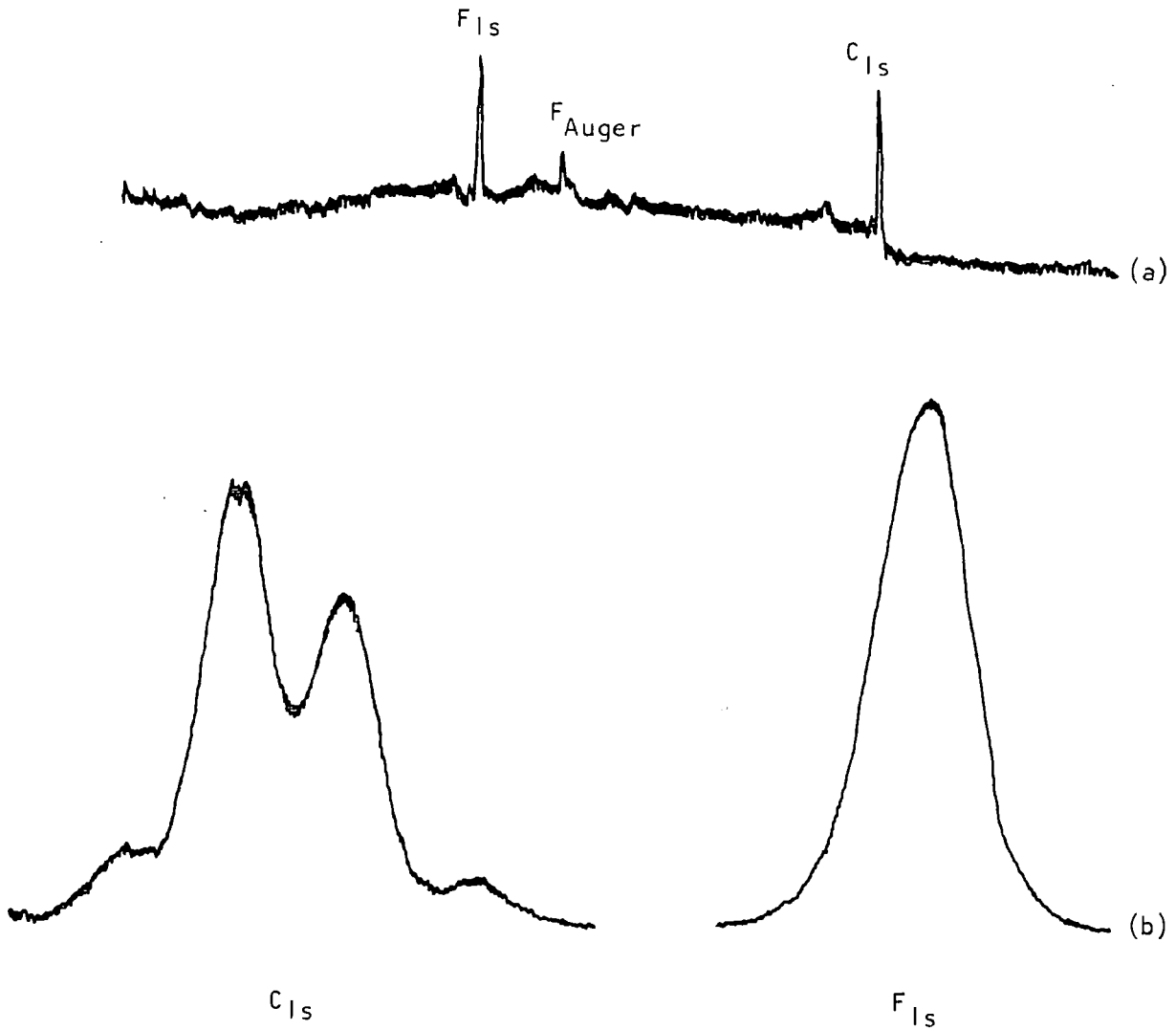


FIGURE 9.1

A wide scan of PP-9n indicating the elemental composition (9.1a), and high resolution scans of the C_{1s} and F_{1s} core levels (9.1b) for fine details

peak B.E. at 690.1 eV is indicative of a fluoropolymer system with a high degree of fluorination whereas a low degree of fluorination results in a F_{1s} B.E. of 689.3 eV¹. A comparison of the relative intensity ratios of the F_{1s} to C_{1s} core levels from Fig. 9.3 indicates a ratio of approximately 1.5/1, respectively and a relative intensity ratio of F_{1s}/F_{2s} of 1.05 (after the necessary cross section and sensitivity corrections). These latter results indicate a homogeneous

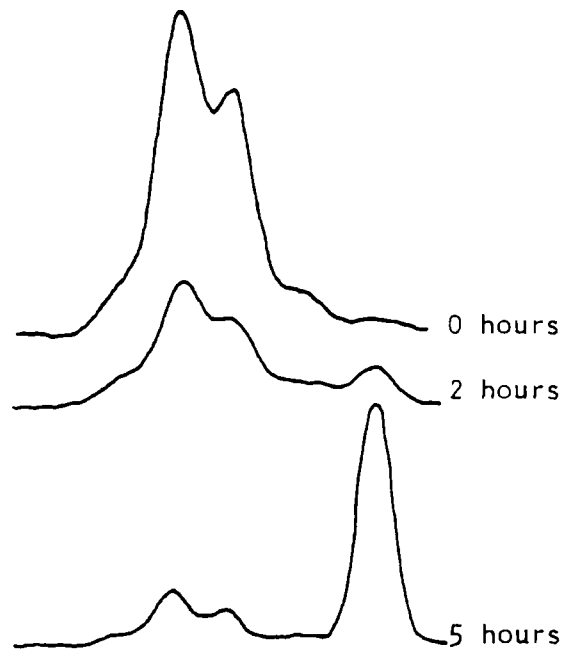


FIGURE 9.2

C_{1s} core level spectra of PP-9n at 0, 2 and 5 hours, allowing hydrocarbon contamination to build-up on sample surface to establish reference binding energy

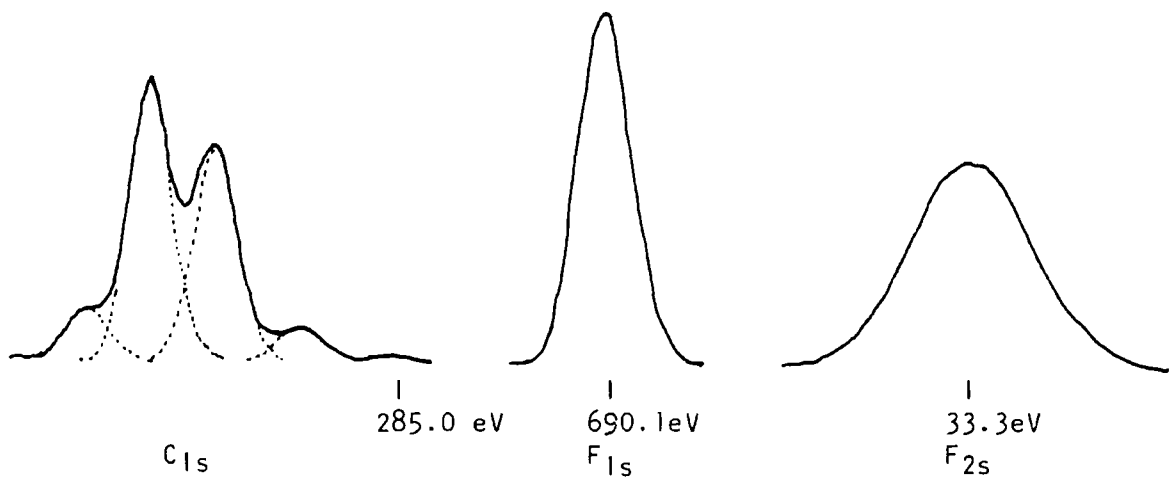


FIGURE 9.3

Deconvolution of C_{1s} core level spectrum of uncontaminated PP-9n and assignments for absolute peak binding energies for the C_{1s}, F_{1s} and F_{2s} core levels using the hydrocarbon contaminant level assigned to 285.0 eV

sample on the ESCA depth profiling scale which would appear reasonable. Therefore, since we appear to have a rather homogeneous material and the relative intensity ratio for the F_{1s} and F_{2s} are in the proper ratios for a homogeneous sample, a study was made to obtain the purest PP-9 for the ESCA study.

The polymer was found to be quite soluble in boiling $CFCl_3$ and when precipitated into benzene at elevated temperatures and allowed to stand for ~ 24 hours, some precipitate was able to be filtered from the solvent mixture. In Fig. 9.4 is shown the C_{1s} core level spectra for

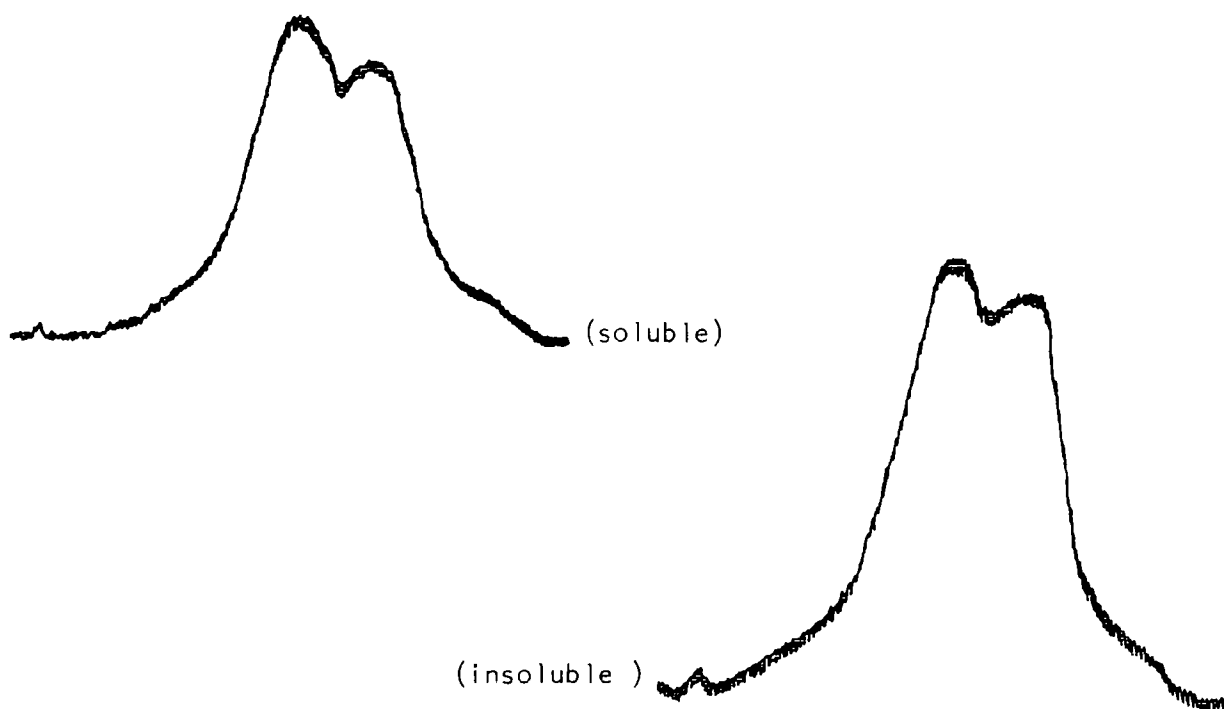


FIGURE 9.4

C_{1s} core level spectra of soluble and insoluble portions of PP-9n
polymer precipitated from $CFCl_3$ into benzene

for the precipitated material, PP-9p, and the soluble material from the solvent mixture cast onto gold, PP-9s. On close examination of the core level spectra, we can see very little difference in the overall and the deconvoluted envelopes, which would lead us to believe that the soluble portion (PP-9s) of the PP-9n most likely differs from the precipitated portion, PP-9p, in molecular weight and not composition, the lower \overline{MW} being soluble in the solvent mixture. On the hypothesis that this low

\overline{MW} material may be somewhat volatile, PP-9n was cast neat onto a gold substrate and an investigation of the effects on the C_{1s} core levels of heating the sample in the spectrometer is shown in Fig. 9.5. Although

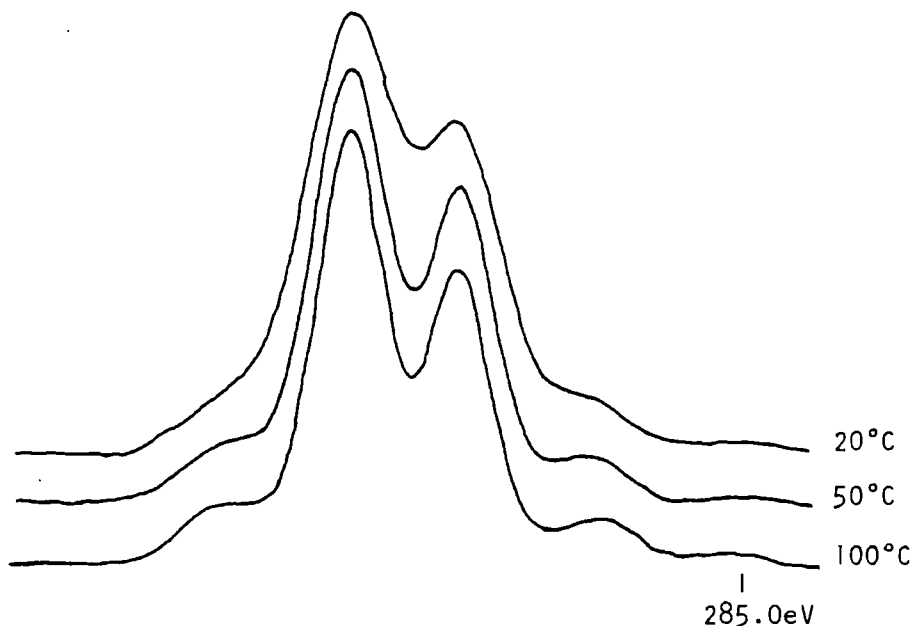


FIGURE 9.5

Effects on C_{1s} core level spectrum of heating PP-9n

the evidence is not conclusive, in progressing from the sample at 20°C to the sample at 100°C we can see an orderly increased resolution in the fine structure of the C_{1s} core level envelope, and we also note that an increase in the pressure in the source region of the spectrometer was experienced. The combination of the increased resolution and increase in pressure would be indicative of a low \overline{MW} volatile component; which would lead to a smearing-out of the spectrum envelope.

Further study of the PP-9n in $CFCl_3$ revealed that upon dissolution at reflux and allowing the sample to stand overnight, small crystals of material were formed. Separation of these crystals (PP-9c) by filtration and subsequent examination by ESCA, revealed the core level spectra shown in Fig. 9.6. Fig. 9.6(a) shows the crystal material melted onto a gold substrate and Fig. 9.6(b) shows a valence band study. It is obvious that little difference is seen in this C_{1s}

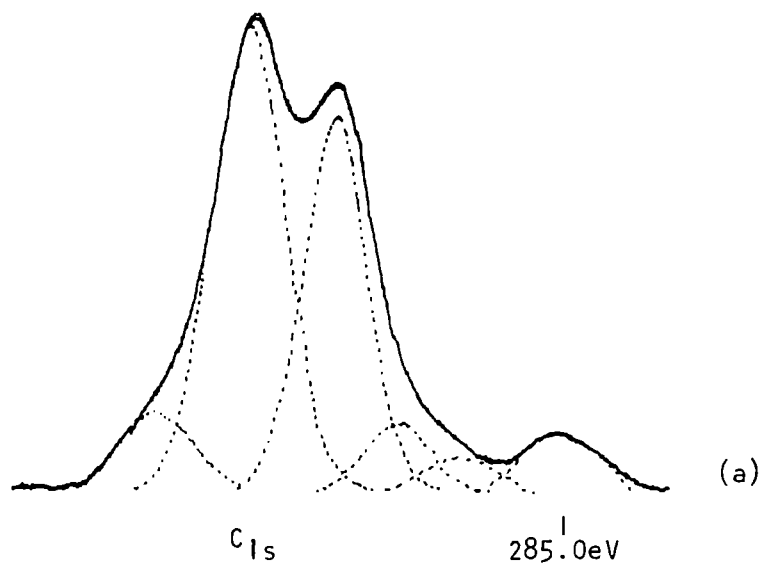
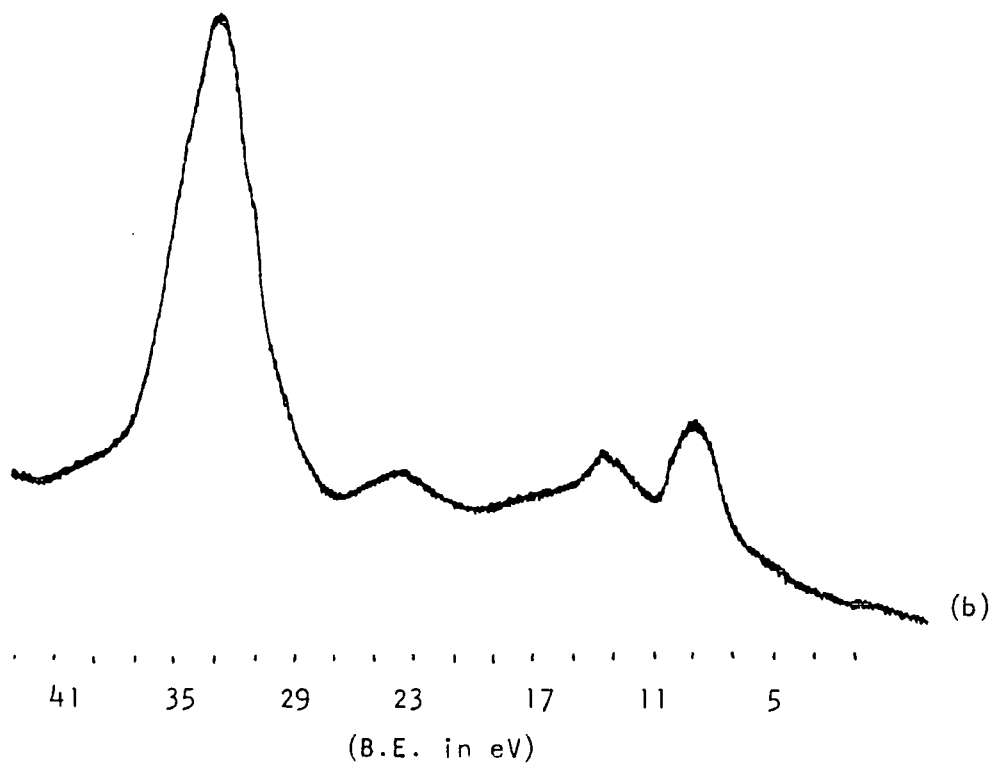


FIGURE 9.6

Spectra for purified PP-9c (a) C_{1s} core levels, (b) valence band

spectra when compared to previous figures and even when compared to the 'unpurified' PP-9n envelope (Fig. 9.1), there appears only subtle differences. D.S.C. indicated a large transition zone extending from -50 to 20°C, probably resulting from gross mixtures of different \overline{M}_w materials, however, similar in structure as evidenced by ESCA.

The detailed deconvolution of the C_{1s} spectrum in Fig. 9.6(a) results in the relative intensity ratios and absolute B.E.'s found in Table 9.1 for the C_{1s} and F_{1s} core levels based upon the previous work on fluoropolymers (cf. Chapter 3, ref. 1, 126, 127 and 128).

Experimental data for PP-9c for C_{1s} and F_{1s} core levels

a) Relative Area Ratios

C ₁	C ₂	C ₃	C ₄	C ₅	C _{CH}
1.75	11	7.5	1.25	1	1

b) Absolute B. E.'s

C ₁	C ₂	C ₃	C ₄	C ₅	C _{CH}
293.7	291.8	290.0	288.6	287.3	285.0

c) Group Assignments (most probable)

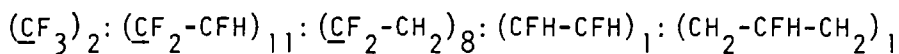
C ₁	C ₂	C ₃	C ₄	C ₅	C _{CH}
<u>CF</u> ₃ -	<u>CF</u> ₂ -CFH	<u>CF</u> ₂ -CH ₂	<u>CFH</u> -CFH	CH ₂ - <u>CFH</u> -CH ₂	-CH ₂ -CH ₂ -

d) F_{1s} B.E. - 690.7 eV

F_{1s}/C_{1s} Relative Area Ratio 1.5/1

TABLE 9.1

From the individual component peaks in the C_{1s} core level spectrum a good estimate of the overall computed stoichiometry reveals the general system given below:



An analysis of this system, based upon previous work on the fluorination dynamics of aliphatic systems²⁵⁹⁻²⁶¹ and the work of Clark and co-workers¹³⁰ on the fluorination of polyethylene, reveals those to be logical ratios for the group assignments. A microanalysis of the purified PP-9c confirmed the overall ratio of F/C obtained by ESCA (see Table 9.1), and the apparent lack of a shake-up satellite in the spectrum confirms the existence of an aliphatic system.

The valence band spectrum (Fig. 9.6b) is entirely consistent with a system containing fluorine and carbon and although the resolution is much poorer in this region than UPS data, we can observe

contributions from the carbon 2s and 2p levels at lower binding.

In conclusion, considering prior to this work virtually nothing was known of this material due to its insolubility in common solvents used in typical polymer analysis, ESCA has been useful in determining the overall elemental ratios present (excluding hydrogen) and has contributed to a considerable understanding of the structure and bonding in this unique polymer system.

REFERENCES

1. D. T. Clark, 'Chemical Aspects of ESCA' in 'Electron Emission Spectroscopy', W. Dekeyser and D. Reidel (Eds.), D. Reidel Publishing Company, Dordrecht-Holland, 373 (1973)
2. H. Robinson and W. F. Rawlinson, *Phil. Mag.*, 28, 277 (1914)
3. H. Robinson, *Proc. Roy. Soc. A*, 104, 455 (1923)
4. H. Robinson, *Phil. Mag.*, 50, 241 (1925)
5. M. DeBroglie, *Compt. Rend.*, 172, 274 (1921)
6. J. A. VanAkker and E. C. Watson, *Phys. Rev.* 37, 1631 (1931)
7. M. Farence, Jr., *Phys. Rev.* 51, 720 (1937)
8. A. Bazin, *Zhurnal Eksperimental'noi i Teoreticheskoi Fiziki*, 14, 23 (1944)
9. R.G. Steinhardt, Jr., F. A. D. Granados and G. I. Post. *Anal. Chem.*, 27, 1046 (1955)
10. B. L. Henke, Tech. Report No. 6, Contract No. AF49 (638)-394, Air Force Office of Scientific Research (1962)
11. K. Siegbahn and K. Edvarsson, *Nucl. Phys.*, 1, 137 (1956)
12. C. Nordling, E. Sokolowski and K. Siegbahn, *Phys. Rev.* 105, 1676 (1957)
13. A. M. Lindh, 'Handbuch der Experimentalphysik', Bd. 24 Teil 4, ed. W. Wien and F. Harnes, Leipzig (1930)
14. H. W. B. Skinner and J. E. Johnson, *Proc. Roy. Soc. A*, 161, 420 (1937)
15. C. Nordling, E. Sokolowski and K. Siegbahn, *Arkiv. Fys.* 13, 483 (1958)
16. S. Hagstrom, C. Nordling and K. Siegbahn, *Phys. Lett.*, 9, 235 (1964)
17. C. Nordling, S. Hagstrom and K. Siegbahn, *Z. Physik*, 178, 433 (1964)
18. K. Siegbahn, C. Nordling, A. Fahlman, R. Nordberg, K. Hamrin, J. Hedman, G. Johansson, T. Berkmark, S. E. Karlsson, I. Lidgren and B. Lindberg, 'ESCA, Atomic, Molecular and Solid State Structure Studied by Means of Electron Spectroscopy', Almquist and Wiksells, Uppsala (1967)

19. K. Siegbahn, C. Nordling, G. Johansson, J. Hedman, P. F. Heden, K. Hamrin, U. Gelius, T. Berkmark, L. D. Werme, R. Manne and Y. Baer, 'ESCA Applied to Free Molecules', North-Holland Publ. Co., Amsterdam (1969)
20. C. D. Wagner, *Fara. Disc.*, 60 306 (1975)
21. D. T. Clark, 'Structure and Bonding in Polymers as Revealed by ESCA' in 'Electronic Structure of Polymers and Molecular Crystals', Ed. J. Lodik and J. M. Andre, Plenum Press, New York (1975) (NATO Summer School Lectures, Namur, September 1974)
22. U. Gelius, E. Basilier, S. Swensson, T. Berkmark and K. Siegbahn, *J. Elect. Spect.* 2, 405 (1974)
23. K. Siegbahn, *Conference Proceedings, Namur 1974: J Elect. Spect.* 5, 3 (1974)
24. U. Gelius, S. Swensson, H. Siegbahn, E. Basilier, A. Farälv and K. Siegbahn, *Chem. Phys. Lett.*, 28, 1 (1974)
25. (a) cf. D. W. Turner, A. D. Baker, C. Baker and C. R. Brundle, 'Molecular Photoelectron Spectroscopy', Wiley, New York, (1970)
 (b) L. Åsbrink and J. W. Kabalais, *Chem. Phys. Lett.*, 12, 182 (1972)
26. L. Åsbrink, *Chem. Phys. Lett.* 7, 549 (1970)
27. J. F. McGilp and I. G. Main, *J. Elect. Spect.*, 6, 397 (1975)
28. P. Ascarelli and G. Missoni, *Faraday Disc.* 54 (1972)
29. G. Johansson, J. Hedman, A. Berndtson, M. Klasson and R. Nilsson, *J. Elect. Spect.*, 2, 295 (1973)
30. (a) P. Auger, *J. Phys. Radium*, 6, 205 (1925)
 (b) P. Auger, *Compt. Rend.* 65, 180 (1925)
 (c) J. J. Lander, *Phys. Rev.* 91, 1382 (1953)
 (d) cf. T. A. Carlson, 'Photoelectron and Auger Spectroscopy'
 (e) D. Coster and R. de L. Kronig, *Physica* 2, 13 (1935)
 (f) E. H. S. Burhop 'The Auger Effect and Other Radiationless Transitions', Cambridge University Press, (1952)
31. C. D. Wagner and P. Biloen, *Surface Sci.*, 35, 82 (1973)

32. C. D. Wagner, *Anal. Chem.*, 44, 967 (1972)
33. C. C. Chang, *Surface Sci.*, 25, 53 (1971)
34. J. P. Coad, M. Gettings and J. C. R. Riviere, *Fara. Disc.*, 60, 269 (1975)
35. A. E. Sandström, in S. Flügge, *Handbook of Physics*, VOL. XXX, X-rays, P. 164 (Springer-Verlag, Berlin, 1957)
36. A. Rosen and I. Lindgren, *Phys. Rev.* 176, 114 (1968)
37. P. S. Bagus, *Phys. Rev.* 139A, 619 (1965)
38. D. A. Shirley, in 'Advances in Chemical Physics', VOL. 23, 85, eds. I. Prigogine and S. A. Rice (Wiley, New York, 1973)
39. U. Gelius and K. Siegbahn, *Fara. Disc.*, 54, 257 (1972)
40. L. C. Snyder, *J. Chem. Phys.*, 55, 95 (1971)
41. D. B. Adams and D. T. Clark, *Theoret. Chim. Acta.* 31, 171 (1973)
42. M. F. Guest, I. H. Hillier, V. R. Saunders and M. H. Wood, *Proc. Roy. Soc. A333*, 201 (1973)
43. D. T. Clark, I. Scanlan, J. Muller, *Theoret. Chim. Acta*, (Berl.), 35, 341 (1974)
44. E. Clementi, H. Popkie, *J. Am. Chem. Soc.* 94, 4057 (1972)
45. W. Meyer, *J. Chem. Phys.* 58, 1017 (1973)
46. B. Levy, P. H. Millie, J. Ridard and J. Vinh, *J. Elect. Spect.* 4, 13 (1974)
47. T. A. Koopmans, *Physica*, 1, 104 (1933)
48. D. B. Adams and D. T. Clark, *Theoret. Chim. Acta (Berl.)*, 31, 171 (1973)
49. H. Hartman and E. Clementi, *Phys. Rev. A*, 133, 1295 (1964)
50. C. W. Scherr, J. N. Siverman and F. A. Matsen, *Phys. Rev.* 127, 830 (1962)
51. C. S. Fadley, S. B. M. Hagstrom, M. P. Klein and D. A. Shirley, *J. Chem. Phys.* 48, 3779 (1968)
52. L. C. Snyder and H. Basch, *J. Amer. Chem. Soc.* 91, 2189 (1969)
53. D. T. Clark and I. W. Scanlan, *J. Chem. Soc. Trans Fara II* 70, 1222 (1974)

54. D. T. Clark, I. W. Scanlan and J. Muller, *Theoret. Chim. Acta*, 35, 341 (1974)
55. D. T. Clark and J. Muller, *Theoret. Chim. Acta (Berl.)*, 41, 193 (1976)
56. D. T. Clark, 'ESCA Applied to Polymers' in 'Advances in Polymer Science', Springer-Verlag, (1977) (in Press)
57. D. T. Clark in 'Progress in Theoretical Organic Chemistry', VOL. 2, Ed. I. G. Csizmadia, Elsevier 1976 (in Press)
58. cf. (a) D. T. Clark, D. B. Adams, I. W. Scanlan and J. S. Woolsey, *Chem. Phys. Letters*, 25, 263 (1974)
(b) D. T. Clark and D. B. Adams, *J. Elect. Spect.* 7, 401 (1975)
(c) D. T. Clark, A. Dilks, J. Peeling and H. R. Thomas, *Faraday Soc. Disc.* 60, 183 (1975)
(d) D. T. Clark, D. B. Adams, A. Dilks, J. Peeling and H. R. Thomas, *J. Elect. Spect.* 8, 51 (1976)
59. R. Manne and T. Åberg, *Chem. Phys. Letters*, 7, 282 (1970)
60. J. N. Murrell and B. J. Ralston, *J. Chem. Soc. Faraday II*, 68, 1393 (1972)
61. M. E. Schwartz, *Chem. Phys. Lett.* 6, 631 (1970)
62. D. A. Shirley, *Chem. Phys. Lett.* 15, 325 (1972)
63. W. L. Jolly and D. N. Hendrickson, *J. Am. Chem. Soc.* 92, 1863 (1970)
64. J. M. Hollander and W. L. Jolly, *Acc. Chem. Res.* 3, 193 (1970)
65. D. T. Clark and D. B. Adams, *J. Chem. Soc., F and Trans II*, 68, 1819 (1972)
66. D. B. Adams and D. T. Clark, *J. Elect. Spect.* 2, 201 (1973)
67. W. J. Hehre, R. F. Stewart and J. A. Pople, *J. Chem. Phys.* 51, 2657 (1969)
68. R. Ditchfield, W. J. Hehre and J. A. Pople, *J. Chem. Phys.* 54, 724 (1971)
69. L. G. Parrat, *Rev. Mod. Phys.* 31, 616 (1959)
71. R. E. Watson and A. J. Freeman, *Hyperfine Interactions*, (Eds. A. J. Freeman and R. B. Frankel), Academic Press, New York, (1967)

72. C. S. Fadley, D. A. Shirley, A. J. Freeman, P. S. Bagus and J. V. Mallow, *Phys. Rev. Lett.* 23, 1397 (1969)
73. J. H. Van Vleck, *Phys. Rev. Lett.* 45, 405 (1934)
74. C. S. Fadley, *Electron Spectroscopy*, Ed., D. A. Shirley, 781, North Holland (1972)
75. D. W. Davis and D. A. Shirley, *J. Chem. Phys.* 56, 669 (1972)
76. J. C. Carver, C. A. Thomas, L. C. Cain and G. K. Schweitzer, *Electron Spectroscopy*, Ed., D. A. Shirley, 803, North Holland (1972)
77. cf. P. W. Atkins, 'Molecular Quantum Mechanics', Oxford University Press, London (1970)
78. cf. F. A. Cotton and G. Wilkinson, 'Advanced Inorganic Chemistry', John Wiley, New York (1972)
79. T. Novakov and J. M. Hollander, *Bull. Am. Phys. Soc.*, 14, 524 (1961)
80. T. Novakov and J. M. Hollander, *Phys. Rev. Lett.*, 21, 1133, (1968)
81. G. K. Wertheim, 'Mossbauer Effect: Principles and Applications', Academic Press (1964)
82. T. Novakov, Ref. 26 of C. S. Fadley, 'Electron Spectroscopy', Ed. D. A. Shirley, North Holland (1972)
83. R. P. Gupta and S. K. Sen, *Phys. Rev. Lett.*, 28, 1311 (1972)
84. G. M. Bancroft, I. Adams, H. Lampe and T. K. Sham, *Chem. Phys. Lett.*, 32, 173 (1975)
85. J. M. Andre, J. Delhalle, S. Delhalle, R. Caudano, J. J. Pireaux and J. J. Verbist, *Chem. Phys. Letts.*, 23, 206 (1973)
86. J. Delhalle, J. M. Andre, S. Delhalle, J. J. Pireaux, R. Caudano and J. J. Verbist, *J. Chem. Phys.*, 60, 595 (1974)
87. J. J. Pireaux, J. Riga, R. Caudano, J. J. Verbist, J. M. Andre, J. Delhalle and S. Delhalle, *J. Elect. Spect.*, 5, 531 (1974)
88. J. Delhalle, *Chem. Phys.*, 5, 306 (1974)
89. J. M. Andre, J. Delhalle, *Chem. Phys. Lett.*, 17, 145 (1972)
90. P. Ascarelli and G. Missoni, *J. Elect. Spect.*, 5, 417 (1974)
91. G. Johansson, J. Hedman, A. Berndtsson, M. Klasson and R. Nilsson, *J. Elect. Spect.*, 2, 295 (1973)
92. D. S. Urch and M. Webber, *J. Elect. Spect.*, 5, 791 (1974)

93. D. Betteridge, J. C. Carver and D. M. Hercules, *J. Elect. Spect.*, 2, 327 (1973)
94. C. R. Ginnard and W. M. Riggs, *Anal. Chem.*, 46(9), 1306 (1974)
95. D. T. Clark in "Handbook of Electron Spectroscopy", Ed. O. Briggs, Heyden & Sons (1976)
96. D. A. Huchital and R. T. McKeon, *Appl. Phys. Lett.* 20, 158 (1972)
97. D. T. Clark, H. R. Thomas and A. Dilks, *J. Elect. Spect.*, 1977 (to be submitted)
98. C. S. Fadley, R. J. Baird, W. Siekhaus, T. Novakov and S. Å. L. Beigstrom, *J. Elect. Spect.*, 4, 93 (1974)
99. T. A. Carlson and G. E. McGuire, *J. Elect. Spect.*, 1, 161 (1972)
100. B. L. Henke, *Adv. X-ray Analysis*, 13, 1 (1976)
101. B. L. Henke, *J. Phys. (Paris)*, C4, 115 (1971)
102. J. H. Scofield, Lawrence Livermore Laboratory, Report No. UCRL-51326, Jan. (1973)
103. D. R. Penn, *J. Elect. Spect.*, 9, 29 (1976)
104. J. J. Huang, J. W. Rabalais and F. D. Ellison, *J. Elect. Spect.*, 6, 85 (1975)
105. D. T. Clark and A. Dilks, *J. Polymer Sci., Poly. Sci. Edition*, (1977) (in Press)
106. N. Beatham and A. F. Orchard, *J. Elect. Spect.* 9, 129 (1976)
107. A. T. Giese and C. S. French, *Appl. Spectr.* 9, 78 (1955)
108. J. M. Vanderbuilt and C. Heinrich, *Appl. Spectr.* 7, 171 (1953)
109. E. Gunders and B. Kaplan, *J. Opt. Soc. Amer.* 55(9), 1094 (1965)
110. A. E. Martin, *Nature (London)*, 180, 211 (1957)
111. H. F. Smith, P-E, UV-FL Prod. Dept. Tech Memo No. 34 (1970)
112. G. L. Green and T. C. O'Haver, *Anal. Chem.* 46(14), 2191 (1974)
113. C. A. Evoms, Jr., *Anal. Chem.* 47(9), 855A (1975)
114. I. W. Drummond, G. A. Errock, J. M. Watson, *GEC J. of Sci. and Tech.*, 41 (2 & 3), 94 (1974)
115. H. Hori, N. Maeda, N. Kobayashi and M. Sakisaka, *Nucl. Inst. and Meth.*, 130, 135 (1975)

116. C. R. Brundle, M. W. Roberts, D. Latham and K. Yates, *J. of Elect. Spect.*, 3, 241 (1974)
117. C. R. Brundle, *Appl. Spectr.*, 25(1), 8 (1971)
118. D. M. Hercules, *Anal. Chem.*, 48(5), 294R (1976)
119. J. P. Allen, Jr., J. D. Durham, G. K. Schweitzer and W. E. Deeds, *J. of Elect. Spect.*, 8, 395 (1976)
120. B. L. Henke, *Phys. Rev. A*6, 94 (1972)
121. R. M. Eisenberg, 'Fundamentals of Modern Physics, Ch. 14, John Wiley and Sons, New York (1961)
122. U. Geluis, E. Basilier, S. Svensson, T. Berkmark and K. Siegbahn, *J. Elect. Spect.*, 2, 405 (1973)
123. E. M. Purcell, *Phys. Rev.*, 54, 818 (1938)
124. J. C. Helmer and N. H. Weichert, *Appl. Phys. Lett.*, 13, 268 (1968)
125. D. T. Clark, plenary lectures ACS Symposium, 'Advances in Polymer Friction and Wear', Los Angeles, March 1974, Ed. C. H. Lee, 5A, Plenum Press, New York (1975)
126. D. T. Clark and W. J. Feast, *J. Macromol. Sci. Reviews in Macromol. Chem.*, C12, 191 (1975)
127. D. T. Clark, 'ESCA Applied to Polymers', in 'Advances in Polymer Science', Springer-Verlag (in Press)
128. D. T. Clark in 'Structural Studies of Macromolecules by Spectroscopic Methods', Chapter 9, Ed. K. Ivin, J. Wiley & Sons, London (1976)
129. J. L. Kardos, *J. Polym. Sci., Polym. Letters Ed.*, 12, 161 (1974)
130. D. T. Clark, W. J. Feast, W. K. R. Musgrave and I. Ritchie, *J. Polym. Sci., Polym. Chem. Ed.*, 13, 857 (1975)
131. B. D. Washo, *J. Macromol. Sci., Chem. A*10(3), 559 (1976)
132. M. M. Millard and A. E. Pavlath, *J. Macromol. Sci., -Chem. A*10 (3), 579 (1976)
133. D. W. Rice and D. F. O'Kane, *J. Electro. Soc.*, 123(9), 1308 (1976)
134. D. T. Clark and D. Shuttleworth, *J. Polym. Sci., Polym. Chem. Ed.* (to be submitted)

135. D. T. Clark, W. J. Feast, I. Ritchie and W. K. R. Musgrave, *J. Polym. Sci., Polym. Chem. Ed.*, 12, 1049 (1974)
136. D. T. Clark, J. Peeling and J. M. O'Malley, *J. Polym. Sci., Polym. Chem. Ed.*, 14, 543 (1976)
137. D. T. Clark and H. R. Thomas, *J. Polym. Sci., Polym. Chem. Ed.*, 14, 1671 (1976)
138. A. W. Potts, T. A. Williams and W. C. Price, *Disc. Faraday Soc.*, 54, 182 (1972)
139. D. T. Clark, D. Kilcast, W. J. Feast and W. K. R. Musgrave, *J. Polym. Sci., Polym. Chem. Ed.* 10, 1637 (1972)
140. D. T. Clark and A. Dilks, *J. Polym. Sci., Polym. Chem. Ed.*, 14, 533 (1976)
141. L. E. Sutton, "Tables of Interatomic Distances" (Chemical Society, Special Publication, No. 18) Chemical Society, London (1965)
142. D. T. Clark and A. Dilks, A. C. S. Centennial Meeting, New York, April 1976 "International Symposium on Advances in Characterization of Polymer - Metal Surfaces" Ed. L. H. Lee, Academic Press (1976)
143. K. Nakaniishi, "Infrared Absorption Spectroscopy", Holden-Day, San Francisco (1964)
144. D. T. Clark, D. Kilcast, W. J. Feast and W. K. R. Musgrave, *J. Polym. Sci., Polym. Chem. Ed.*, 11, 389 (1973)
145. W. L. Jolly, *Trans. Faraday Soc., Faraday Disc.*, 54, 13 (1972)
146. J. Peeling, D. T. Clark, I. M. Evans and D. Boulter, *J. Sci. Ed. Agric.*, 27, 331 (1976)
147. D. T. Clark, D. Kilcast and D. B. Adams, *Fara. Disc. Chem. Soc.*, 54, 182 (1972)
148. G. Howat and O. Goscinski, *Chem. Phys. Lett.* 30, 87 (1975)
149. D. W. Davis and D. A. Shirley, *J. Elect. Spect.*, 3, 137 (1974)
150. D. L. Liberman, *Bull. Amer. Phys. Soc.* 9, 1336 (1969)
151. cf. R. S. Swingle II and W. M. Riggs, *C. R. C. Crit. Rev. Anal. Chem.*, 5, 267 (1975) C. R. C. Press, Cleveland
152. cf. T. A. Carlson, et al, in R. Caudano and J. Verlist (Eds.) *Namur Conference Proceedings, J. Elect. Spect.*, 5 (1974)

153. M. Barber and D. T. Clark, Chem. Comm., 22 (1970)
154. D. T. Clark and D. Kilcast, J. Chem. Soc. A, 3286 (1971)
155. D. T. Clark, D. Kilcast, D. B. Adams and W. K. R. Musgrave, J. Elect. Spect., 6, 117 (1975)
156. D. T. Clark, R. D. Chambers, D. Kilcast and W. K. R. Musgrave, J. Chem. Soc., Faraday Trans. 11, 69, 309 (1972)
157. J. M. Hill, D. G. Royce, C. S. Fadley, L. F. Wagner and F. J. Grunthaner, Chem. Phys Lett. (1976)(in Press)
158. B. J. Lindberg, J. Elect. Spect. 5, 149 (1974)
159. D. T. Clark, D. Kilcast and D. H. Reid, J. Chem. Soc. D, 638 (1971)
160. D. T. Clark and D. M. J. Lilley, Chem. Phys. Lett. 9, 234 (1971)
161. I. W. Scanlan, Ph. D. Thesis, Durham University, U. K. (1974)
162. J. J. Quinn, Phys. Rev. 126, 1453 (1962)
163. G. A. Katrich and O. G. Sarbei, Sov. Phys. Solid State, 3, 1181 (1961)
164. H. Kanter, Phys. Rev. B1, 522 (1970)
165. H. Kanter, Appl. Phys. Lett., 10, 73 (1967)
166. W. F. Krolikowski and W. E. Spicer, Phys. Rev. B1, 478 (1970)
167. D. E. Eastman, Solid State Comm. 8, 41 (1970)
168. P. Neilson
169. E. R. Jones, J. T. McGinney and M. B. Webb, Phys. Rev., 151, 476 (1966)
170. M. P. Seah, J. Phys, F3, 1538 (1973)
171. M. Mehta and C. S. Fadley, Phys. Rev. Lett., 55A, 59 (1975)
172. M. P. Seah, Sur. Sci., 32, 703 (1972)
173. (a) P. W. Palmberg and T. N. Rhodin, J. of Appl. Phys. 39, 2425 (1968)
(b) J. M. Morabito, Sur. Sci., 49, 318 (1975)
174. J. W. T. Ridgeway and D. Haneman, Sur. Sci., 24, 451 (1971)
175. J. W. T. Ridgeway and D. Haneman, Sur. Sci., 26, 683 (1971)

176. F. L. Battye, J. G. Jenkin, J. Liesegang and R. C. G. Leckey, *Phys. Rev.* B9, 2887 (1974)
177. S. Thomas and T. W. Haas, *J. Voc. Sci. Technol.*, 10, 380 (1973)
178. C. J. Todd and R. Heckingbottom, *Phys. Lett.* 42A, 455 (1973)
179. K. Jacobi and J. Halzl, *J. Sur. Sci.*, 26, 54 (1971)
180. M. Klasson, A. Berndtsson, J. Hedman, R. Nilsson, R. Nyholm and C. Nordling, *J. of Elect. Spect.*, 3, 427 (1974)
181. P. B. Needham, T. J. Dricoll, *J. Voc. Sci. Technol.*, 11, 278 (1974)
182. J. D. Andrade, M. S. Hall and G. Iwanoto, A. C. S. Centennial Meeting, New York, April 1976. 'International Symposium on Advances in Characterization of Polymer Surfaces; Ed. L. H. Lee, VOL. Z, Academic Press (1976)
183. D. J. Jackson, T. E. Gallon and A. Chambers, *Sur. Sci.* 36, 381 (1973)
184. C. R. Brundle, M. W. Roberts, *Chem. Phys. Lett.*, 18, 380 (1973)
185. R. G. Steinhardt, J. Hurdis and M. L. Palman, in *Electron Spectroscopy Proceedings of an International Conference, Asilomar, Calif. 7-10 Sept. 1970*, Ed. D. A. Shirley, North Holland Publ. Co. (1972)
186. W. A. Frazer, J. V. Floris, W. N. Delgass and W. P. Robertson, *Sur. Sci.*, 36, 661 (1973)
187. M. Klasson, J. Hedman, A. Bendtsson, R. Nilsson, C. Nordling and P. Melnik, *Physica Scripta*, 5, 93 (1972)
188. M. L. Tarny and G. K. Wehner, *J. Appl. Phys.* 44, 1534 (1973)
189. H. Kanter, *Phys. Rev.* B1, 2357 (1970)
190. Y. Baer, P. F. Heden, J. Hedman, M. Klasson and C. Nordling, *Solid State Comm.* 8, 1479 (1970)
191. K. Larsson, C. Nordling, K. Siegbahn and E. Stenhagen, *Acta. Chem. Scand.*, 20, 2880 (1966)
192. R. M. Stern and S. Sinharoy, *Sur. Sci.*, 33, 131 (1972)
193. P. Cadman, S. Evans, J. D. Scott and J. M. Thomas, *J. C. S. Faraday II*, 71, 1777 (1975)

194. T. Dickinson, A. F. Povey and P. M. A. Sherwood, J. C. S. Faraday Trans. 1, 72, 686 (1976)
195. I. Lindau and W. E. Spicer, J. Elect. Spect. 3, 409 (1974)
196. J. C. Tracy, J. Vacuum Sci. and Technol., 11, 280 (1974)
197. C. J. Powell, Sur. Sci. 44, 29 (1974)
198. D. T. Clark and J. Peeling, J. of Polym. Sci., Polym. Chem. Ed., 14, 2941, (1976)
199. D. T. Clark, Disc Faraday Soc., 60, 198 (1975)
200. K. B. Blodgett, J. Amer. Chem. Soc., 57, 1007 (1935)
201. H. Kuhn, D. Moebius and H. Buchev in "Physical Methods of Chemistry", A. Weissberger and B. Rossiter, Eds. (1972)
202. J. F. Stephens, J. Coll. Interface Sci., 38, 557 (1972)
203. R. S. Swingle, II and W. M. Riggs, CRC Crit. Rev., Anal. Chem. 5, 267 (1975)
J. M. Hill, D. G. Royce, C. S. Fadley, L. F. Wagner and F. J. Grunthaner, Chem. Phys. Lett. (1977) (in Press)
204. S. Evans, Disc. Faraday Soc., 60, 199 (1975)
205. F. M. Chapman and L. L. Lohr, J. Amer. Chem. Soc. 96, 4731 (1974)
206. J. H. Scofield, J. Elect. Spect. 8, 129 (1976)
207. (a) W. F. Gorham, J. Polym. Sci. A4 (1966)
(b) W. F. Gorham in "Ency. of Polymer Sci. and Technol.", VOL. 15 (1971)
(c) W. F. Gorham, U. S. Patent 3, 342, 754 Sept., 1976
208. D. J. Cram and H. Steinberg, J. Amer. Chem. Soc., 73, 5691 (1951)
209. (a) W. D. Niegisch, J. Polym. Sci. B4 (1966); J. Appl. Phys. 37, 4041 (1966)
(b) S. Kubo and B. Wunderlick, J. Appl. Phys. 42, 4558 (1971); J. Appl. Phys., 42, 4565 (1971)
210. Kronos, Inc. Torance, California, Technical Note NO. 002, Dec., 1971
211. K. H. Behindt, J. Vac. Sci. and Technol. 8, 5 (1971)
212. M. Szwarc, Nature, 160, 403 (1947)
213. C. J. Brown and A. C. Farthing, Nature, 164, 915 (1949)

214. K. Lonsdale, H. H. Milledge and K. V. K. Rao, Proc. Roy. Soc. A255, 82 (1960)
215. K. N. Trueblood, Air Force Research Grant AF-AFOSR-240-63
216. L. L. Ingraham, J. of Chem. Phys., 27, 1228 (1957)
217. R. C. Helgeson and D. J. Cram, J. of Amer. Chem. Soc. 88:3, 509 (1966)
218. D. J. Cram, J. of Amer. Chem. Soc., 81, 5977 (1959)
219. A. Ron and O. Schnepf, J. Chem. Phys. 37, 2540 (1962)
220. A. Ron and O. Schnepf, J. Chem. Phys. 44, 19 (1966)
221. M. A. El-Sayed, Nature, 197, 481 (1963)
222. M. T. Valta, J. Haebig and S. A. Rice, J. Chem. Phys. 43, 886 (1965)
223. D. J. Wilson, V. Boekelheide and R. W. Griffin, Jr., J. Amer. Chem. Soc. 82, 6302 (1960)
224. J. S. Waugh, R. W. Fessenden, J. Amer. Chem. Soc., 79, 846 (1957)
225. R. H. Boyd, J. Chem. Phys., 49, 2574 (1968)
226. J. T. S. Andrews and E. F. Westrum, Jr., J. Phys. Chem. 74, 2170 (1970)
227. R. H. Boyd, Tetrahedron, 22, 119 (1966)
228. D. J. Cram and H. J. Riech, J. Amer. Chem. Soc. 91, 3517 (1969)
229. H. E. Winberg, F. S. Fawcett, W. E. Mochel and C. W. Theobald, J. Amer. Chem. Soc. 82, 1428 (1960)
230. F. D. Marsh and T. E. Young, cited in reference 229
231. G. W. Brown and F. Sondheimer, J. Amer. Chem. Soc. 89, 7116 (1967)
232. H. Hopf, Angew. Chem., 84, 471 (1972)
233. D. F. Pollart, U. S. Patent 3,149,175
234. D. F. Pollart, Div. Petroleum Chemistry, ACS, Atlantic City Meeting, Sept. 12-17 (1965)
235. D. J. Hnatowick, J. Hudis, M. L. Perlman and R. C. Razaini, J. Appl. Phys. 42, 4883 (1971)
236. C. K. Jorgensen and H. Berthon, Chem. Phys. Lett. 31, 416 (1975)

237. J. R. McCreary and R. J. Thorn, *J. Elect. Spect.* 8, 425 (1976)
238. M. F. Ebel and H. Ebel, *J. Elect. Spect.* 3, 169 (1974)
239. T. E. Madley, C. D. Wagner and A. Joshi, *J. Elect. Spect.* (1977) (in Press)
240. *Internat. Tables for X-ray Crystallography*, VOL. III, Eds. C. H. Macgillary, G. D. Rich and K. Lonsdale, the Kynoch Press, Birmingham (1962)
241. B. Wunderlich, "Macromolecular Physics", VOL. 1, Academic Press, New York (1973)
242. D. T. Clark, H. R. Thomas, A. Dilks and D. Shuttleworth, *J. Elect. Spect.*, 10, 455 (1977)
243. A. Dilks, Ph. D. Thesis, Durham University, U. K. (1977)
244. D. T. Clark, W. J. Feast, H. R. Thomas and P. Tweedale, *J. Polym. Sci., Polym. Chem. Ed.* (to be submitted)
245. cf. "Techniques and Applications of Plasma Chemistry", Ed. J. R. Hollahan and A. T. Bell, J. Wiley and Sons, New York (1974)
246. T. A. Carlson, *Ann. Rev. Phys. Chem.*, 26, 211 (1975)
247. T. A. Carlson, J. C. Carver and G. A. Vernon, *J. Chem. Phys.*, 62, 932 (1975)
248. R. P. Gupta and S. K. Sen, *Phys. Rev.*, B10, 71 (1974)
249. T. A. Carlson, *Disc. Faraday Soc.* 60, 30 (1975) and references therein
250. H. D. Hagstrom in "Techniques of Metals Research", Ed. R. F. Bunshak, J. Wiley and Sons, New York (1972)
251. E. E. Muschlitz, Jr., *Science*, 159, 599 (1968)
252. D. T. Clark and A. Dilks, Part XV, *J. Polym. Sci., Polym. Chem. Ed.* (1972) (in Press)
253. D. T. Clark and A. Dilks, Part XVIII, *J. Polym. Sci., Polym. Chem. Ed.* (1977) (in Press)
254. K. S. Kim, W. E. Baitinger, J. W. Amy and N. Winograd, *J. Elect. Spect.* 5, 351 (1974)

255. R. Holm and S. Strop, Appl. Phys. 9, 217 (1976)
256. C. B. Brundle, J. Elect. Spect. 5, 291 (1974)
257. A. Barrie and C. R. Brundle, J. Elect. Spect., 5, 321 (1974)
258. L. Kihlberg, Acta Chem. Scand., 13 954 (1959)
259. R. A. Pasternak, M. V. Christensen and J. Heller, Macromolecules, 3, 366 (1970)
260. R. A. Pasternak, G. L. Burns and J. Heller, Macromolecules, 4, 470 (1971)
261. R. G. Gerritse, J. Chromatog., 77, 406 (1973)

